University of Alberta

Regional Controls on the Stratigraphic and Diagenetic Evolution of Woodbend Group Carbonates, North-central Alberta, Canada.

by

Harald Huebscher ©

A thesis submitted to the Faculty of Graduate Studies and Research in partial fulfillment of the requirements for the degree of Doctor of Philosophy.

Department of Earth and Atmospheric Sciences

Edmonton, Alberta
Fall 1996

National Library
of Canada

Acquisitions and
Bibliographic Services Branch

395 Wellington Street
Ottawa, Ontario
K1A 0N4

Bibliothèque nationale
du Canada

Direction des acquisitions et
des services bibliographiques

395, rue Wellington
Ottawa (Ontario)
K1A 0N4

Your file Votre référence

Our file Notre référence

The author has granted an irrevocable non-exclusive licence allowing the National Library of Canada to reproduce, loan, distribute or sell copies of his/her thesis by any means and in any form or format, making this thesis available to interested persons.

L'auteur a accordé une licence irrévocable et non exclusive permettant à la Bibliothèque nationale du Canada de reproduire, prêter, distribuer ou vendre des copies de sa thèse de quelque manière et sous quelque forme que ce soit pour mettre des exemplaires de cette thèse à la disposition des personnes intéressées.

The author retains ownership of the copyright in his/her thesis. Neither the thesis nor substantial extracts from it may be printed or otherwise reproduced without his/her permission.

L'auteur conserve la propriété du droit d'auteur qui protège sa thèse. Ni la thèse ni des extraits substantiels de celle-ci ne doivent être imprimés ou autrement reproduits sans son autorisation.

ISBN 0-612-18045-X

Canada

University of Alberta

Library Release Form

Name of Author: **Harald Huebscher**

Title of Thesis: **Regional Controls on the Stratigraphic and Diagenetic Evolution of Woodbend Group Carbonates, North-central Alberta, Canada**

Degree: **Doctor of Philosophy**

Year this Degree Granted: **1996**

Permission is hereby granted to the University of Alberta Library to reproduce single copies of this thesis and to lend or sell such copies for private, scholarly, or scientific research purposes only.

The author reserves all other publication and other rights in association with the copyright in the thesis, and except as hereinbefore provided, neither the thesis nor any substantial portion thereof may be printed or otherwise reproduced in any material form whatever without the author's prior written permission.

Harald Huebscher
11247 76 Avenue
Edmonton, Alberta
Canada T6G 0K2

Date: Oct. 04, 1996

University of Alberta

Faculty of Graduate Studies and Research

The undersigned certify that they have read, and recommend to the Faculty of Graduate Studies and Research for acceptance, a thesis entitled **"Regional Controls on the Stratigraphic and Diagenetic Evolution of Woodbend Group Carbonates, North-central Alberta, Canada"** by **Harald Huebscher**, in partial fulfillment of the requirements for the degree of **Doctor of Philosophy**.

Hans-G. Machel

Dr. H.G. Machel

Dr. B. Jones

Dr. K. Muehlenbachs

Dr. C.H. Moore

M E Evans

Dr. M.E. Evans

H. Baadsgaard

Dr. H. Baadsgaard

Date: 13/09/96

ABSTRACT

The Upper Devonian (Frasnian) Woodbend Group of north-central Alberta consists of a lower, transgressive part, represented by the Cooking Lake platform, overlying carbonate buildups and interfingering basin-fill successions, and an upper, regressive part, represented by the Grosmont carbonate platform. Carbonate complexes of the Woodbend Group, i.e. the Rimbey-Meadowbrook reef trend and the overlying Grosmont platform, contain prolific hydrocarbon reservoirs.

Depositional architecture reflects the effects of antecedent shelf topography, eustasy, clastic input and varying carbonate production on the stratigraphic evolution of the Woodbend Group. A combined approach of log marker stratigraphy and lithofacies analysis reveals that Woodbend shelf development proceeded in six phases. Phase 1 is characterized by a rapid sea level rise that caused backstepping of carbonate complexes. Strong clastic input during phase 2 produced a shallow shelf which acted as nucleus for the Grosmont carbonate platform (phase 3). Due to a large subtidal carbonate factory, platform progradation progressed rapidly during phase 4. A prolonged sea level stillstand (phase 5) caused progradation of tidal flats resulting in decreased carbonate production and termination of platform growth due to 'clastic pollution' (phase 6).

Reservoir quality in Woodbend Group carbonates is greatly influenced by their diagenetic history. Dolomitization and karstification are recognized as the two most important processes that preserved and/or enhanced reservoir porosity and permeability. Three diagenetic reservoir classes were defined, (1) limestones (Φ=1 to 5%), (2) dolostones (Φ=5 to 25%), and (3) karsted dolostones (Φ=25 to 40%).

A detailed study of the texture, geochemistry and distribution of Woodbend replacement dolomites shows that these dolomites originated from two different fluid types. Grosmont dolomites formed from evaporated seawater and were modified by descending marine (?) fluids. Leduc dolomites likely formed from warm, basinal fluids. These basinal fluids ascended through the Rimbey-Meadowbrook reef trend into the Grosmont platform resulting in further alteration of Grosmont dolomites.

An extensive data base of cores, thin sections and wireline logs was used to investigate the physical evidence for karst as well as the distribution of karst features in the giant Grosmont heavy-oil reservoir. The Grosmont paleokarst concentrated along traceable levels that run approximately parallel to Early Cretaceous paleo-elevation levels. Karst levels cross-cut Devonian strata, including carbonate reservoir units and shaly intervals used to contain steam during bitumen recovery tests. These results can be used to locate possible seal breaches and better sites for future enhanced recovery projects.

ACKNOWLEDGEMENTS

This thesis was financially supported by funds from a Natural Science and Engineering Research Council (NSERC) strategic grant to Eric W. Mountjoy (McGill University) and Hans G. Machel (University of Alberta) that has been supplemented by funds from Amoco Canada Petroleum Company Ltd., Chevron Canada Resources Ltd., Home Oil Company Ltd., Imperial Oil Resources Ltd., Norcen Energy Resources Ltd., Pan Canadian Petroleum Ltd., and Shell Canada Ltd. Further financial support was provided by an NSERC operating grant to Hans G. Machel and by a grant from the Alberta Oil Sands Technology and Research Authority (AOSTRA, Agreement # 800) to Hans G. Machel. The author, furthermore, gratefully acknowledges two Amoco Graduate Fellowships in Geology.

Thanks go to Hans Machel and Pat Cavell for all the editorial work that hopefully greatly improved the final version of this thesis. The occasional discussions with Lawrence Bernstein, Paul Blanchon, Pat Cavell, Eugene Dembicki, Mark Hearn, Chris Holmden, Ping Luo, Kim Manzano, Leo Piccoli, Ning Qiang, Mike Ranger, Ben Rostron and Jack Wendte provided many helpful insights and ideas. Technical assistance was provided by Diane Caird (XRD analyses), Olga Levner (stable isotope analyses), Don Resultay (special thanks for all those ultra-thin sections) and Paul Wagner (electron microprobe).

I give my warmest thank you to my parents for their moral as well as monetary support. Last but not least, I like to thank my wife Ruth for her love, support, great food and all those damn fine haircuts.

TABLE OF CONTENTS

CHAPTER 1

INTRODUCTION 1

References 7

CHAPTER 2

STRATIGRAPHIC EVOLUTION OF THE WOODBEND GROUP IN NORTH-CENTRAL ALBERTA 9

Introduction 9

Geologic setting 11

Log marker stratigraphy 15

Lithofacies associations 19

Stratigraphic and regional trends 41

Stages of shelf development 48

Controls on shelf development 59

Conclusions 63

References 64

CHAPTER 3

PETROGRAPHY, DIAGENESIS AND POROSITY EVOLUTION OF UPPER DEVONIAN WOODBEND GROUP CARBONATES, NORTH-CENTRAL ALBERTA 69

Introduction 69

Geologic setting 72

Methods 74

Diagenetic processes and products 77

Paragenetic sequence 116

Diagenetic reservoir classes 117

Summary and conclusions 121

References 122

CHAPTER 4

DOLOMITIZATION AND DOLOMITE MODIFICATION IN THE WOODBEND GROUP OF NORTH-CENTRAL ALBERTA, CANADA 128

Introduction 128

Geologic setting 130

Database and methods 135

Petrography 136

Regional distribution 142

Geochemistry 145

Discussion 160

Conclusions 177

References 178

CHAPTER 5

DEVELOPMENT AND DISTRIBUTION OF PALEOKARST IN THE GROSMONT HEAVY-OIL RESERVOIR, NORTH-EASTERN ALBERTA 185
Introduction 185
Geologic setting 186
Petrography 190
Topography of the Grosmont paleokarst 202
Paleokarst distribution 207
Karst interpretation 217
Effects on reservoir properties 221
Conclusions 222
References 223

CHAPTER 6

CONCLUSIONS 228

LIST OF TABLES

CHAPTER 2

Table 2.1: Lithofacies characteristics 20

CHAPTER 3

Table 3.1: Calcite stable isotope data 75
Table 3.2: Relative abundance of diagenetic phases 118

CHAPTER 4

Table 4.1: Geochemistry of Woodbend dolomites 148
Table 4.2: Dolomite stable isotope data 149
Table 4.3: Estimated geochemical composition of Late Devonian seawater, marine dolomites and evaporitive dolomites, and measured values of Woodbend replacement dolomites 152

LIST OF FIGURES

CHAPTER 1

Figure 1.1: Location of study area 2

CHAPTER 2

Figure 2.1: Location of study area 10
Figure 2.2: Well and core control map 13
Figure 2.3: Stratigraphic nomenclature and log marker stratigraphy 14
Figure 2.4: Woodbend Group log marker subdivision 17
Figure 2.5: Photographs of subtidal facies types I 23
Figure 2.6: Photographs of subtidal facies types II 25
Figure 2.7: Photographs of peritidal facies types I 30
Figure 2.8: Photographs of peritidal (II) and basinal (I) facies types 35
Figure 2.9: Photographs of basinal facies types II 38
Figure 2.10: Woodbend Group platform cycles 42
Figure 2.11: Legend for stratigraphic cross-sections 44
Figure 2.12: N-S stratigraphic cross-section A-A' 45
Figure 2.13: N-S stratigraphic cross-section (along reef trend) B-B' 46
Figure 2.14: Lithofacies maps of Woodbend Group I: LCL 1 (lower Cooking Lake); UCL/ML 2 (upper Cooking Lake/Majeaux Lake) 49
Figure 2.15: Lithofacies maps of Woodbend Group II: L 3 (Leduc); LI 4 (lower Ireton) 50
Figure 2.16: Lithofacies maps of Woodbend Group III: LG 5 (lower Grosmont); UG 6 (upper Grosmont 1) 53
Figure 2.17: Lithofacies maps of Woodbend Group IV: UG 7 (upper Grosmont 2); UG 8 (upper Grosmont 3a) 54
Figure 2.18: Lithofacies maps of Woodbend Group V: UG 9 (upper Grosmont 3b); UI 10 (upper Ireton) 56
Figure 2.19: E-W stratigraphic cross-section C-C' 57
Figure 2.20: Eustatic sea level curve for Upper Devonian of Euramerica (modified after Johnson et al., 1985) 60

CHAPTER 3

Figure 3.1: Location of study area 70
Figure 3.2: Core control map and location of hydrocarbon reservoirs 71
Figure 3.3: Stratigraphic nomenclature 73
Figure 3.4: Paragenetic sequence, burial history and porosity development 79
Figure 3.5: N-S stratigraphic cross-section showing distribution of main lithologies 80
Figure 3.6: Photomicrographs of diagenetic phases I (calcite cements) 82
Figure 3.7: Calcite cement types 84
Figure 3.8: Carbon-oxygen isotope plot of calcite samples 87
Figure 3.9: Dolomite types 92
Figure 3.10: Photomicrographs of paragenetic phases II (dolomites) 95

Figure 3.11: N-S stratigraphic cross-section showing distribution of replacement dolomite types 96
Figure 3.12: Photomicrographs of diagenetic phases III (dolomites) 98
Figure 3.13: Photomicrographs of diagenetic phases IV (various) 100
Figure 3.14: N-S stratigraphic cross-section showing distribution of anhydrites 104
Figure 3.15: Photomicrographs of diagenetic phases V (sulfates) 106
Figure 3.16: Photomicrographs of diagenetic phases VI (fractures) 110
Figure 3.17: Pathways for creation and destruction of bioclast molds 111

CHAPTER 4

Figure 4.1: Location of study area and core control map 131
Figure 4.2: Stratigraphic nomenclature 132
Figure 4.3: Isopach map of lower Ireton Fm. aquitard 134
Figure 4.4: Photomicrographs of replacement dolomites I 139
Figure 4.5: Photomicrographs of replacement dolomites II 141
Figure 4.6: Photomicrographs of replacement dolomites III 143
Figure 4.7: N-S stratigraphic cross-section showing distribution of replacement dolomite types 144
Figure 4.8: Distribution of lithologies in the LGM 146
Figure 4.9: Crystal size vs. element concentrations in replacement dolomites 153
Figure 4.10: Stable isotope composition of replacement dolomites 155
Figure 4.11: δ^{18}O vs. crystal size in replacement dolomites 156
Figure 4.12: δ^{18}O vs. element concentrations in replacement dolomites 157
Figure 4.13: δ^{18}O vs. present structural elevation of replacement dolomites 159
Figure 4.14: Stable isotope composition of replacement dolomites vs. depth 162
Figure 4.15: Mole % $MgCO_3$ vs. Sr content in replacement dolomites 166
Figure 4.16: Burial history plot of Woodbend Group 171
Figure 4.17: Temperature vs. δ^{13}C composition of dissolved HCO_3^- in water 174

CHAPTER 5

Figure 5.1: Location of study area 187
Figure 5.2: Stratigraphic nomenclature 189
Figure 5.3: Photomicrographs of microscopic karst fabrics and cements 192
Figure 5.4: Schemeatic representation of breccia types 196
Figure 5.5: Photographs of macroscopic karst fabrics 198
Figure 5.6: Simplified core log of paleosol deposit 201
Figure 5.7: Lower Cretaceous paleogeography of Alberta 203
Figure 5.8: Paleotopography of the sub-Cretaceous unconformity (modified after Ranger, 1994) 205
Figure 5.9: Subcrop map of Devonian strata 206
Figure 5.10: Core log and well log response of Grosmont plaeokarst I 208
Figure 5.11: Core log and well log response of Grosmont paleokarst II 209
Figure 5.12: Core log and well log response of Grosmont paleokarst III 210
Figure 5.13: Location map of paleokarst and paleosols 211

Figure 5.14: Number of karstified intervals as a function of present structural elevation, and depth below the sub-Cretaceous unconformity and top of the Lower Mannville Group 213
Figure 5.15: Number of karstified intervals vs. depth below the top of the Lower Mannville Group in the study area (total), the Grosmont High, lowlands (total), the Wabasca Sub-Basin, and the McMurray Sub-Basin 214
Figure 5.16: N-S cross-section A-A' across the Grosmont High 216
Figure 5.17: E-W cross section B-B' 219

CHAPTER 1

INTRODUCTION

Ever since the discovery of the Leduc oil field in 1947, the first major oil discovery in central Alberta, Canada, the Upper Devonian (Frasnian) Woodbend Group has received much attention from geologists. The Energy Resources Conservation Board of Alberta (ERCB, 1993) estimated that the Woodbend Group held about 32 % of the established initial reserves of conventional oil and associated gas contained within Paleozoic strata of the Alberta portion of the Western Canada Sedimentary Basin. In addition, giant reserves of heavy-oil and bitumen (315 billion bbl; ERCB, 1993) and associated gas are trapped along the Woodbend subcrop edge beneath the giant Athabasca oil sand deposits.

Much of the work done on the Woodbend Group has focussed on the stratigraphy, facies, paleontology and, to a lesser degree, diagenesis of individual carbonate reef complexes because they contain the vast majority of hydrocarbon pools. Few attempts have been made to study the Woodbend Group on a regional or basin-wide scale, and all published regional studies have dealt solely with aspects of stratigraphy, depositional history and paleogeography. The overall paleogeographic outline of Woodbend carbonate complexes and of the adjacent shale basins (Fig. 1.1) was established by Belyea (1964). The stratigraphy of basin-filling sediments and the controls on basin-fill sedimentation, with strong emphasis on the shale basins in central Alberta, were discussed by Stoakes (1980, 1992a). More recently, several studies have attempted to analyze the stratigraphy and depositional patterns of the Woodbend Group from a sequence stratigraphic point of view. Stoakes (1992b) characterized Woodbend Group deposits as a transgressive-regressive unit (Woodbend mega-sequence). Building on these results, Switzer et al. (1994) described the paleogeographical evolution and mapped the overall lithofacies distribution of Woodbend Group deposits. Despite these studies, there still remains a great deal of uncertainty regarding the factors that control Woodbend shelf development,

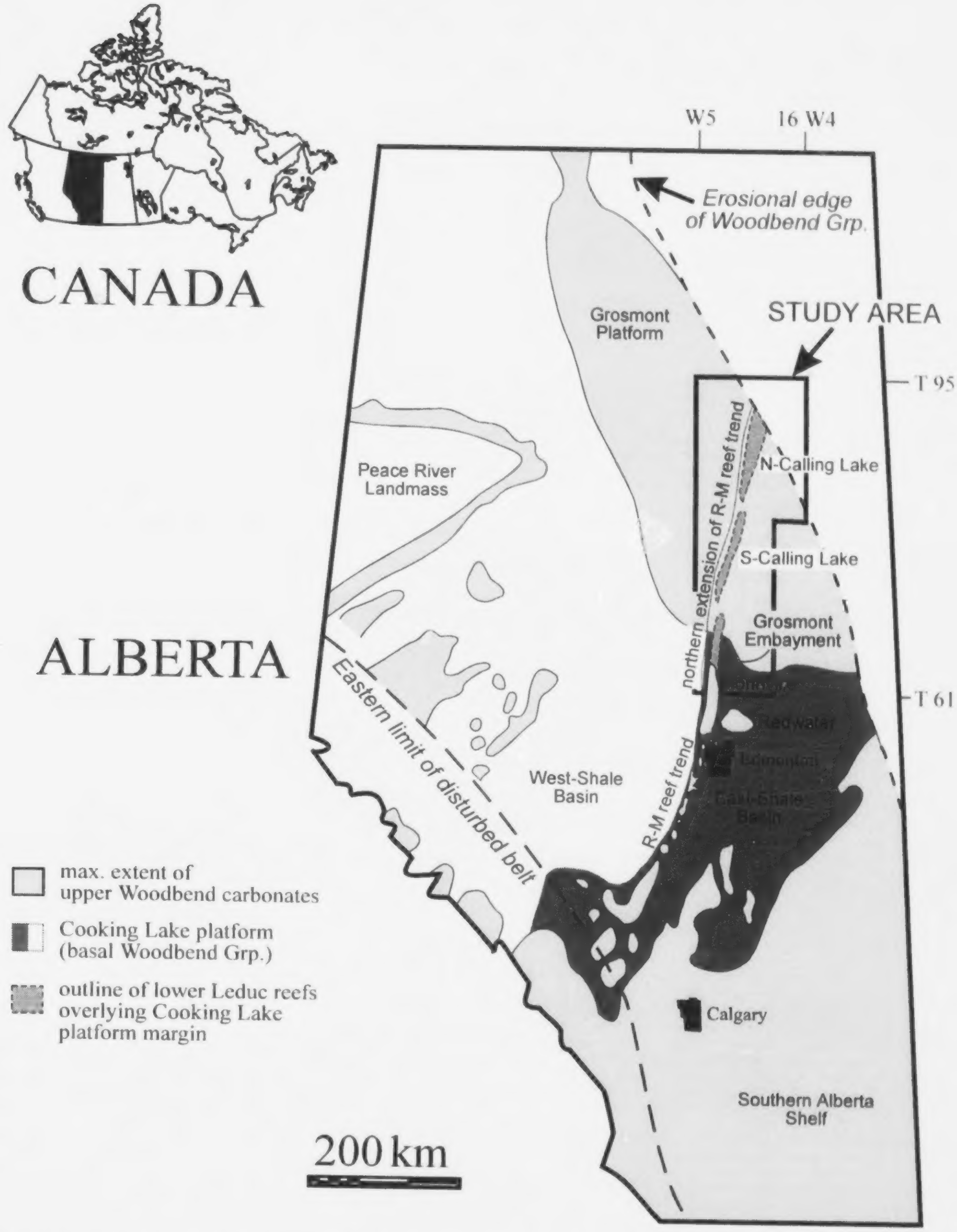
CANADA
ALBERTA
W5
16 W4
Erosional edge of Woodbend Grp.
STUDY AREA
T 95
T 61
Grosmont Platform
Peace River Landmass
N-Calling Lake
S-Calling Lake
northern extension of R-M reef trend
Grosmont Embayment
Redwater
Edmonton
East-Shale Basin
West-Shale Basin
R-M reef trend
Eastern limit of disturbed belt
Calgary
Southern Alberta Shelf
200 km
max. extent of upper Woodbend carbonates
Cooking Lake platform (basal Woodbend Grp.)
outline of lower Leduc reefs overlying Cooking Lake platform margin

Fig. 1.1: Simplified distribution of platform and reef carbonates of the Late Devonian Woodbend Group (modified after Switzer et al., 1994) and location of the study area in Alberta. Shown are the aerial extent of the Cooking Lake platform (basal Woodbend Grp.), of overlying lower Leduc reefs (northern extension of R-M reef trend), and of platform and reef carbonates of the upper Woodbend Group. R-M reef trend = Rimbey-Meadowbrook reef trend.

especially with respect to the interaction between carbonate platform, reef trend and basin filling (siliciclastic) sediments.

Few studies have been published on the diagenesis of Woodbend Group carbonates on scales exceeding that of a single hydrocarbon pool. This is surprising, considering that the diagenetic evolution of Woodbend carbonates was accompanied by profound changes in reservoir characteristics, a fact that has major economic implications for the Alberta oil industry. Dolomitization in particular, has created reservoirs with, compared to limestones, favourable porosity and permeability characteristics (Wardlaw, 1979; Luo and Machel, 1995). In addition, dolomitized platform margins (i.e. the Cooking Lake platform margin; Fig 1.1) are thought to have acted as regional migration pathways for hydrocarbons and/or formation fluids (e.g. Gussow, 1954; Machel and Mountjoy, 1987). In spite of the importance of dolomitization, few studies attempted to document regional patterns of dolomitization, although regional-scale mechanisms are thought to have controlled dolomitization of Woodbend and other Devonian carbonates of the Western Canada Sedimentary Basin. Based on petrographical and geochemical data Machel and Mountjoy (1987) and Amthor et al. (1993) interpreted regional scale flow of burial fluids along ancient platform margins to have controlled dolomitization of Woodbend reef trends, e.g. the Rimbey-Meadowbrook reef trend of central Alberta (Fig. 1.1). More recently, Shields and Brady (1995) claimed that, on the basis of regional and stratigraphic distribution of dolomite, "regional scale reflux dolomitization accounts for the majority of dolostones in the Western Canada Sedimentary Basin". This claim, however, has not been substantiated by petrographic and/or geochemical data.

This dissertation deals with the Woodbend Group in north-central Alberta (Fig. 1.1) in a series of four papers/chapters. The study area stretches from the regional and stratigraphic junction of the Grosmont platform with the Rimbey-Meadowbrook reef trend and interfingering basin-fill sediments to the Woodbend subcrop edge in northeastern Alberta (Fig. 1.1), following the course of the northern Rimbey-Meadowbrook reef trend and its northern extension which underlies the Grosmont platform. This part of the basin contains the only documented example of a prograding carbonate platform complex, i.e. the Grosmont platform, in the Upper Devonian Woodbend Group. In other words, it is the only place in Alberta where the regressive portion of the Woodbend cycle resulted in carbonate platform progradation as compared to the commonly observed siliciclastic basin-fill (Stoakes, 1980; 1992a). The particular setting of the study area provides an excellent opportunity to explore controls on platform development as well as interactions between carbonate platforms, reef trends and siliciclastic basin-fill sediments.

The architecture of the Woodbend Group in north-central Alberta not only presents special challenges for stratigraphic studies but also offers unique opportunities for diagenetic studies. Dolomitization is regionally pervasive in the Rimbey-Meadowbrook reef trend and its northern extension as well as in the Grosmont platform. However, two genetically different dolomite types appear to be present. Dolomites in the Rimbey-Meadowbrook reef trend have been interpreted to be of burial origin (Machel and Mountjoy, 1987; Amthor et al., 1993), whereas Grosmont dolomites are thought to be of early, evaporitive origin (Theriault and Hutcheon, 1987). Considering that these two dolomite types are representative of the two proposed regional dolomitization mechanisms (see above), this area provides a unique opportunity to (1) directly compare adjacent dolomite occurrences of proposed different origin, (2) to determine the regional distribution of these dolomite types, and, therefore, (3) the regional extent of burial vs. reflux (evaporitive) dolomitization. In addition, the stratigraphic architecture of the Woodbend Group in the study area may have allowed interactions between the two dolomitization realms. In north-central Alberta, the Woodbend Group comprises two distinct aquifers (Bachu and Underschultz, 1993), the Grosmont and the Cooking Lake/Leduc aquifers, which are generally separated by a regionally extensive, thick aquitard consisting of basin-fill sediments. In the study area, however, hydraulic continuity between the two aquifers occurs at a few sites along the top of the northern extension of the Rimbey-Meadowbrook reef trend where the intervening, shaly aquitard is thin or missing. It is conceivable that different dolomitizing fluids, either burial fluids, evaporated seawater, or both, gained access to both aquifers through these sites of hydraulic communication. Hence, this particular setting of two distinct Woodbend aquifers that are locally in hydraulic communication allows testing of the different dolomitization mechanisms as well as the study of their regional extent, importance and of the potential cross-formational (between aquifers) migration of dolomitizing fluids.

In addition, Woodbend reservoir development in northeastern Alberta has been greatly influenced by subaerial exposure and resulting karstification along the Woodbend subcrop (Fig 1.1) (Luo et al., 1994; Luo and Machel, 1995; Dembicki and Machel, 1996). In fact the giant Grosmont heavy-oil reservoir is the only confirmed paleokarst reservoir in Devonian carbonates of Alberta. However, little is known about the distribution of karst and the controls on karstification in this reservoir.

The main objective of the first paper (*Chapter 2*) is to characterize the stratigraphic and paleogeographic evolution of the Woodbend Group in the study area. Wireline log marker stratigraphy was used in combination with lithofacies data from core to delineate, in greater detail than previously published (Cutler, 1983; Switzer et al., 1994), the sequential evolution of the Woodbend shelf in north-central Alberta. In addition, the presence of backstepping and prograding carbonate platform deposits, the proximity to postulated Upper Devonian clastic sources (Stoakes, 1980), and the availability of a well established eustatic sea level curve for the Devonian of the Western Canada Sedimentary Basin (Johnson, 1985) made this area an ideal candidate to examine controls on Woodbend shelf development. The results of this chapter suggest that localization and development of carbonate platforms and reefs was influenced by a combination of clastic input and carbonate production, in addition to the established controls of eustasy and antecedent shelf topography (Wendte, 1992).

Different aspects of the diagenetic evolution of Woodbend Group carbonates are the topic of *Chapters 3, 4* and *5*. A general descriptive framework of the diagenetic history and the distribution of diagenetic phases is provided in *Chapter 3*. Special emphasis was placed on the regional distribution of major pore creating and pore occluding phases, the knowledge of which has great potential in delineating reservoir heterogeneity and possible pathways and barriers for fluid flow.

Differences in petrography, geochemistry and, therefore, origin and modification of replacement dolomites in the Rimbey-Meadowbrook reef trend and the Grosmont platform are the topic of *Chapter 4*. Whereas replacement dolomitization of the Rimbey-Meadowbrook reef trend has been attributed to burial fluids (Machel and Mountjoy, 1987; Amthor et al., 1993), dolomitization of the Grosmont platform was interpreted to have occurred early during diagenetic history by hypersaline fluids (Theriault and Hutcheon, 1987; Luo et al., 1994). Based on textural, stable isotope, major element and trace element data, this chapter presents new constraints on the origin of these replacement dolomites. It is demonstrated that early, texturally and chemically unstable Grosmont replacement dolomites were diagenetically modified to more stable dolomites. This study is, therefore, another example of stabilization of early dolomites during diagenesis (cf. Land, 1985; Mazzullo, 1992). The recognition of dolomite diagenesis has important implications with respect to the reliability of geochemical data as indicators for environments and mechanisms of dolomitization. It is also shown that burial fluids inferred to be responsible for dolomitization of the Rimbey-Meadowbrook reef trend ascended into the Grosmont platform, resulting in further alteration of Grosmont replacement dolomites. In addition, it is demonstrated that reefal buildups may act as fluid pathways between two aquifers, and that such cross-formational fluid flow has potential implications on carbonate diagenesis.

In *Chapter 5* a compilation of the physical evidence for karstification and a reevaluation of the distribution patterns of paleokarst fabrics in the Grosmont Formation is presented. The Grosmont paleokarst is of great economic concern because it controls much of the porosity and permeability characteristics of the giant Grosmont heavy-oil reservoir (Luo et al., 1994; Luo and Machel, 1995). Reservoir heterogeneity that resulted from paleokarst was likely responsible for the varying success of steam stimulation projects during the early 1980's (Harrison, 1982). By combining an extensive data base of cores and wireline logs, this chapter documents that the Grosmont paleokarst is concentrated along traceable levels that run approximately parallel to Early Cretaceous paleo-elevation levels. The results of this chapter have direct implications for locating possible seal breaches and, as a result, aid in choosing better sites for future recovery projects because paleokarst levels breach shaly intervals that were used to contain steam during previous recovery tests.

REFERENCES

Amthor, J.E., Mountjoy, E.W., and Machel, H.G., 1993, Subsurface dolomites in Upper Devonian Leduc buildups, central part of Rimbey-Meadowbrook reef trend, Alberta, Canada. Bulletin of Canadian Petroleum Geology, v. 41, p. 164-185.

Bachu, S., and Underschultz, J.R., 1993, Hydrogeology of formation waters, northeastern Alberta, American Association of Petroleum Geologists Bulletin, v. 77, p. 1745-1768.

Belyea, H.R., 1964, Upper Devonian, Part II - Woodbend, Winterburn and Wabamun Groups. In: McCrossan, R.G., and Glaister, R.P., eds., Geological history of western Canada, Alberta Society of Petroleum Geologists, v. 77, p. 1745-1768.

Cutler, W.G., 1983, Stratigraphy and sedimentology of The Upper Devonian Grosmont Formation, Alberta, Canada. Bulletin of Canadian Petroleum Geology, v. 31, p. 282-325.

Dembicki, E.A., and Machel, H.G., 1996, Recognition and delineation of paleokarst zones by the use of wireline logs in the bitumen-saturated Upper Devonian Grosmont Formation of northeastern Alberta, Canada. American Association of Petroleum Geologists Bulletin, v. 80, p. 695-712.

Energy Resources Conservation Board of Alberta, 1993, Alberta's reserves of crude oil, gas, natural gas liquids and sulphur. Energy Resources Conservation Board, Report ST 94-18, Calgary.

Gussow, W.C., 1954, Differential entrapment of oil and gas: a fundamental principle. American Association of Petroleum Geologists Bulletin, v. 38, p. 816-853.

Harrison, R.S., 1982, Geology and production history of the Grosmont carbonate pilot project, Alberta, Canada. In: Meyer, R.F., Wynn, J.C., and Olson, J.C., eds., The future of heavy crude and tar sands. Second International Conference on heavy crude and tar sands, Caracas, Venezuela, February 7-17, 1982, v.1, p. 199-204.

Johnson, J.G., Klapper, G., and Sandberg, C.A., 1985, Devonian eustatic fluctuations in Euramerica. Geological Society of America Bulletin, v. 96, p. 567-587.

Land, L.S., 1985, The origin of massive dolomite. Journal of Geological Education, v. 33, p. 112-125.

Luo, P., and Machel, H.G., 1995, Pore size and pore throat types in a heterogeneous dolostone reservoir, Devonian Grosmont Formation, Western Canada Sedimentary Basin. American Association of Petroleum Geologists Bulletin, v. 79, p. 1698-1720.

Luo, P., Machel, H.G., and Shaw, J., 1994, Petrophysical properties of matrix blocks of a hetrogeneous dolostone reservoir - the Upper Devonian Grosmont Formation, Alberta, Canada. Bulletin of Canadian Petroleum Geology, v. 42, p. 465-481.

Machel, H.G., and Mountjoy, E.W., 1987, General constraints on extensive pervasive dolomitization - and their application to the Devonian carbonates of western Canada. Bulletin of Canadian Petroleum Geology, v. 35, p. 143-158.

Mazzullo, S.J., 1992, Geochemical and neomorphic alteration of dolomite: a review. Carbonates and Evaporites, v. 7, p. 21-37.

Stoakes, F.A., 1980, Nature and control of shale basin fill and its effect on reef growth and termination: Upper Devonian Duvernay and Ireton Formations of Alberta, Canada. Bulletin of Canadian Petroleum Geology, v. 28, p. 345-410.

Stoakes, F.A., 1992a, Nature and succession of basin fill strata. In: Wendte, J.C., Stoakes, F.A., and Clarence, C.V., Devonian-Early Mississippian carbonates of the Western Canada Sedimentary Basin: a sequence stratigraphic framework. Society for Sedimentary Geology (SEPM) Short Course No. 28, p. 127-144.

Stoakes, F.A., 1992b, Woodbend megasequence. In: Wendte, J.C., Stoakes, F.A., and Clarence, C.V., Devonian-Early Mississippian carbonates of the Western Canada Sedimentary Basin: a sequence stratigraphic framework. Society for Sedimentary Geology (SEPM) Short Course No. 28, p. 183-206.

Switzer, S.B., Holland, W.G., Christie, D.S., Graf, G.C., Hedinger, A.S., McAuley, R.J., Wierzbicki, R.A., and Packard, J.J., 1994, Devonian Woodbend - Winterburn strata of the Western Canada Sedimentary Basin. In: Mossop, G.D., and Shetsen, I., comps., Geological Atlas of the Western Canada Sedimentary Basin. Canadian Society of Petroleum Geologists and Alberta Research Counsil, p. 165-202.

Theriault, F., and Hutcheon, I., 1987, Dolomitization and calcitization of the Devonian Grosmont Formation, northern Alberta. Journal of Sedimentary Petrology, v. 57, p. 955-966.

Wardlaw, N.C., 1979, Pore systems in carbonate rocks and their influence on hydrocarbon reservoir efficiency. In: Geology of carbonate porosity, American Association of Petroleum Geologists Continuing Education Course Note Series 11, p. E1-E24.

Wendte, J.C., 1992, Platform evolution and its control on reef inception and localization. In: Wendte, J.C., Stoakes, F.A., and Clarence, C.V., Devonian-Early Mississippian carbonates of the Western Canada Sedimentary Basin: a sequence stratigraphic framework. Society for Sedimentary Geology (SEPM) Short Course No. 28, p. 41-87.

CHAPTER 2

STRATIGRAPHIC EVOLUTION OF THE WOODBEND GROUP IN NORTH-CENTRAL ALBERTA

INTRODUCTION

The Woodbend Group in Alberta, Canada, contains classic examples of Upper Devonian (Frasnian) deposits. Numerous studies have dealt with the Woodbend Group, both in outcrop in the Canadian Rocky Mountains as well as in the subsurface of the Western Canada Sedimentary Basin. Woodbend Group deposits have received great attention because they are of considerable economic interest as hydrocarbon reservoirs. This is especially true for the carbonate buildups of the Rimbey-Meadowbrook reef trend (Fig. 2.1), the so-called "Golden Trend", which contain the first oil reservoirs found in central Alberta.

The composition of the Woodbend Group in Alberta ranges from limestones, dolostones and anhydrites to shales, minor siltstones and sandstones, including various mixtures between siliciclastics, carbonates and anhydrites. Overall, there appears to be a clear distinction between carbonate dominated shallow, inner shelf and shale dominated deeper, outer shelf deposits (Wilson, 1975). After an initial sea-level rise and drowning of carbonate complexes of the lowermost Woodbend Group, the general outline and position of these inner and outer shelf deposits remained relatively unchanged in most of Alberta throughout Woodbend Group deposition (Stoakes, 1992; Switzer et al., 1994). In north-central Alberta, however, the character of the Woodbend Group is different, in that it contains prograding clastic wedges and carbonate platforms. These deposits bury earlier stratigraphic and paleogeographic elements, such as the Rimbey-Meadowbrook reef trend and its northern extension, and document a general regression that occurred much later in other areas.

Although a stratigraphic framework was developed early on (Belyea, 1952; Andrichuk, 1958), the Woodbend Group in north-central Alberta received relatively minor

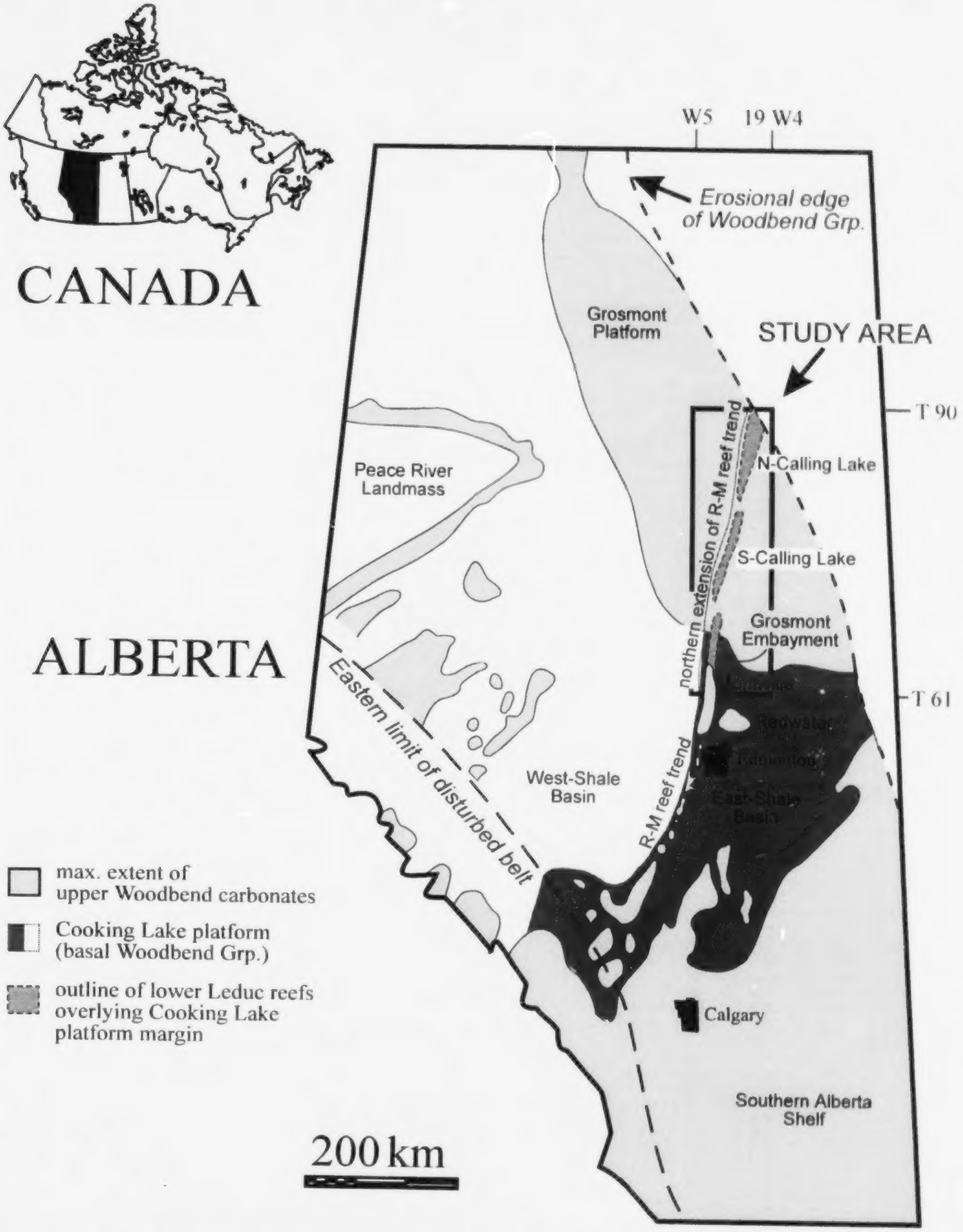
CANADA
ALBERTA
W5
19 W4
Erosional edge of Woodbend Grp.
Grosmont Platform
STUDY AREA
T 90
N-Calling Lake
northern extension of R-M reef trend
S-Calling Lake
Grosmont Embayment
T 61
Peace River Landmass
Redwater
Edmonton
East-Shale Basin
West-Shale Basin
R-M reef trend
Eastern limit of disturbed belt
Calgary
Southern Alberta Shelf
200 km
max. extent of upper Woodbend carbonates
Cooking Lake platform (basal Woodbend Grp.)
outline of lower Leduc reefs overlying Cooking Lake platform margin

Fig. 2.1: Simplified distribution of platform and reef carbonates of the Late Devonian Woodbend Group (modified after Switzer et al., 1994) and location of the study area in Alberta. Shown are the aerial extent of the Cooking Lake platform (basal Woodbend Grp.), of overlying lower Leduc reefs (northern extension of R-M reef trend), and of platform and reef carbonates of the upper Woodbend Group. R-M reef trend = Rimbey-Meadowbrook reef trend.

attention. With the exception of a general synopsis given by Switzer et al. (1994), previous stratigraphic studies in this area did not deal with the entire Woodbend Group. Only the stratigraphy of the upper Woodbend Group (i.e. the stratigraphy of the Grosmont platform) has been studied in greater detail (Harrison and McIntyre, 1981; Harrison, 1982; 1984; Cutler, 1983; Theriault, 1988; Dembicki, 1994).

This study examines 1) lithostratigraphy, 2) depositional facies, and 3) stratigraphic and spatial distribution of Woodbend Group lithofacies units. Wireline log marker stratigraphy is used to correlate Woodbend Group deposits in north-central Alberta and in central Alberta. Emphasized are the stratigraphic and spatial relationships between 1) prograding clastic wedge and carbonate platform deposits and 2) the Rimbey-Meadowbrook reef trend. Lithofacies and stratigraphic data are combined to document different developmental stages in the evolution of the Woodbend Group in north-central Alberta. Furthermore, the unique evolution of the Woodbend Group in the study area, its proximity to postulated Upper Devonian clastic sources (Stoakes, 1980), and the availability of data on the eustatic history (Johnson et al., 1985) make this area an excellent candidate to examine the importance of controls other than relative sea level changes on Woodbend shelf development.

GEOLOGIC SETTING

Upper Devonian (Frasnian) successions in north-central Alberta were deposited in a shallow epeiric sea that bordered the Canadian Shield to the northeast. During the beginning of the Frasnian stage this area was the site of a major marine transgression that had begun during the Givetian stage. This transgression resulted in breakup (into isolated reefal buildups), backstepping and landward retreat of carbonate platforms. Deeper, more basinal areas which also formed as a result of the transgression were covered by argillaceous sediments. During the end of the Frasnian stage a major marine regression started resulting in progradation of carbonate platforms which again covered the western Canadian shelf in Alberta by early Famennian time.

Successions deposited during the above described transgressive-regressive cycle form the so-called Beaverhill-Saskatchewan (second order) sequence (Moore, 1989). In terms of the stratigraphic nomenclature used in central Alberta this sequence includes, in ascending order, the Beaverhill Lake, Woodbend and Winterburn Groups. Each of these groups roughly correlates to one or several third order transgressive-regressive (T-R) cycles (Johnson et al., 1985). The Woodbend Group, which is the topic of this study, corresponds to the Devonian T-R cycle IIc (Johnson et al., 1985), during which the Devonian sea transgressed farthest onto the western Canadian shelf (Moore, 1989).

Five formations constitute the Woodbend Group in the study area, which is located in north-central Alberta between townships 61 and 90 and between the fifth meridian and range 19 west of the fourth meridian (Figs. 2.1 and 2.2). The stratigraphic relationships of these formations are schematically shown in Fig. 2.3a. The Cooking Lake Formation consists of carbonate platform deposits overlying the Beaverhill Lake Group. Wendte (1974, 1992) divided the Cooking Lake Formation into upper, middle and lower members. Basinal lithologies, i.e., bituminous limestones and shales that correspond to the Cooking Lake carbonate platform deposits, are referred to as the Majeaux Lake Member of the Cooking Lake Formation (cf. Switzer et al., 1994). The Leduc Formation constitutes reefal carbonate buildups that developed above the Cooking Lake platform margin, forming the Rimbey-Meadowbrook reef trend and its northern extension in the study area. This formation is very differently developed in southern and northern portions of the study area. Whereas in the south the Leduc Formation (Morinville reef; Figs. 2.1 and 2.2) has a maximum thickness of 220 m, it reaches only a thickness of 60 m in the north (Northern and Southern Calling Lake reef; Figs. 2.1 and 2.2). The Grosmont Formation constitutes carbonate platform deposits that extend from central Alberta to the Northwest Territories (Belyea, 1952). The Grosmont Formation can be divided into five informal units (Harrison and McIntyre, 1981; Harrison, 1982; 1984), i.e., the lower Grosmont (LGM) and upper Grosmont 1, 2, 3a and 3b (UGM 1, UGM 2, UGM 3a, and UGM 3b, respectively) (Fig. 2.3a), which are separated by thin shale or marl beds, the so-called Grosmont shale breaks. The post-Cooking Lake basinal succession, which interfingers with the Leduc and Grosmont Formations, consists of bituminous limestones and shales of the Duvernay Formation and of shales to argillaceous carbonates of the Ireton Formation (Fig. 2.3a). In the northern part of the study area, where the Grosmont

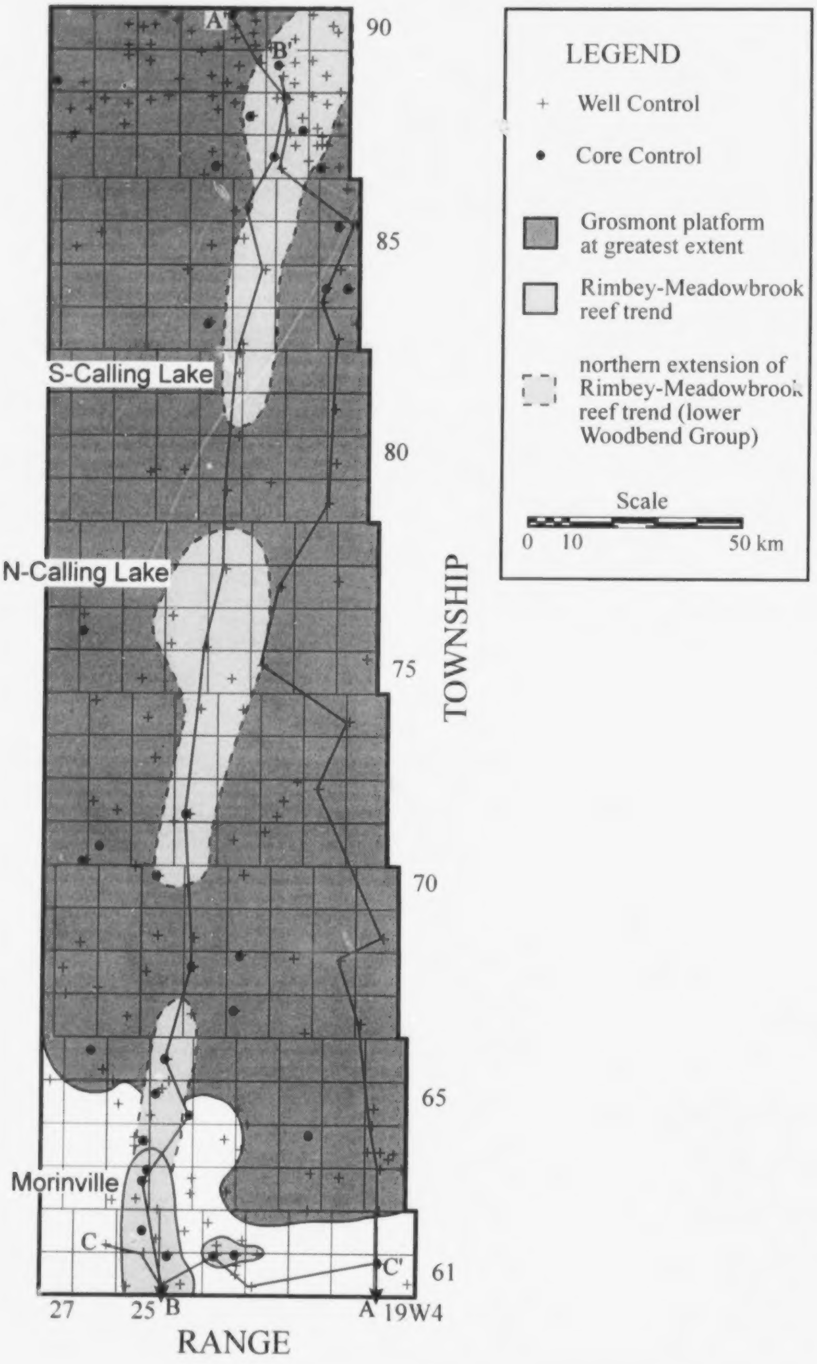
A'
B'
90
85
80
75
70
65
61
TOWNSHIP
S-Calling Lake
N-Calling Lake
Morinville
C
C'
27
25
B
A
19W4
RANGE
LEGEND
Well Control
Core Control
Grosmont platform at greatest extent
Rimbey-Meadowbrook reef trend
northern extension of Rimbey-Meadowbrook reef trend (lower Woodbend Group)
Scale
0
10
50 km

Fig 2.2: Well and core control map and location of cross-sections in the study area. The map also shows the Grosmont Formation at its maximum extent as well as the location of Leduc reefs adjacent to and underlying the Grosmont platform.

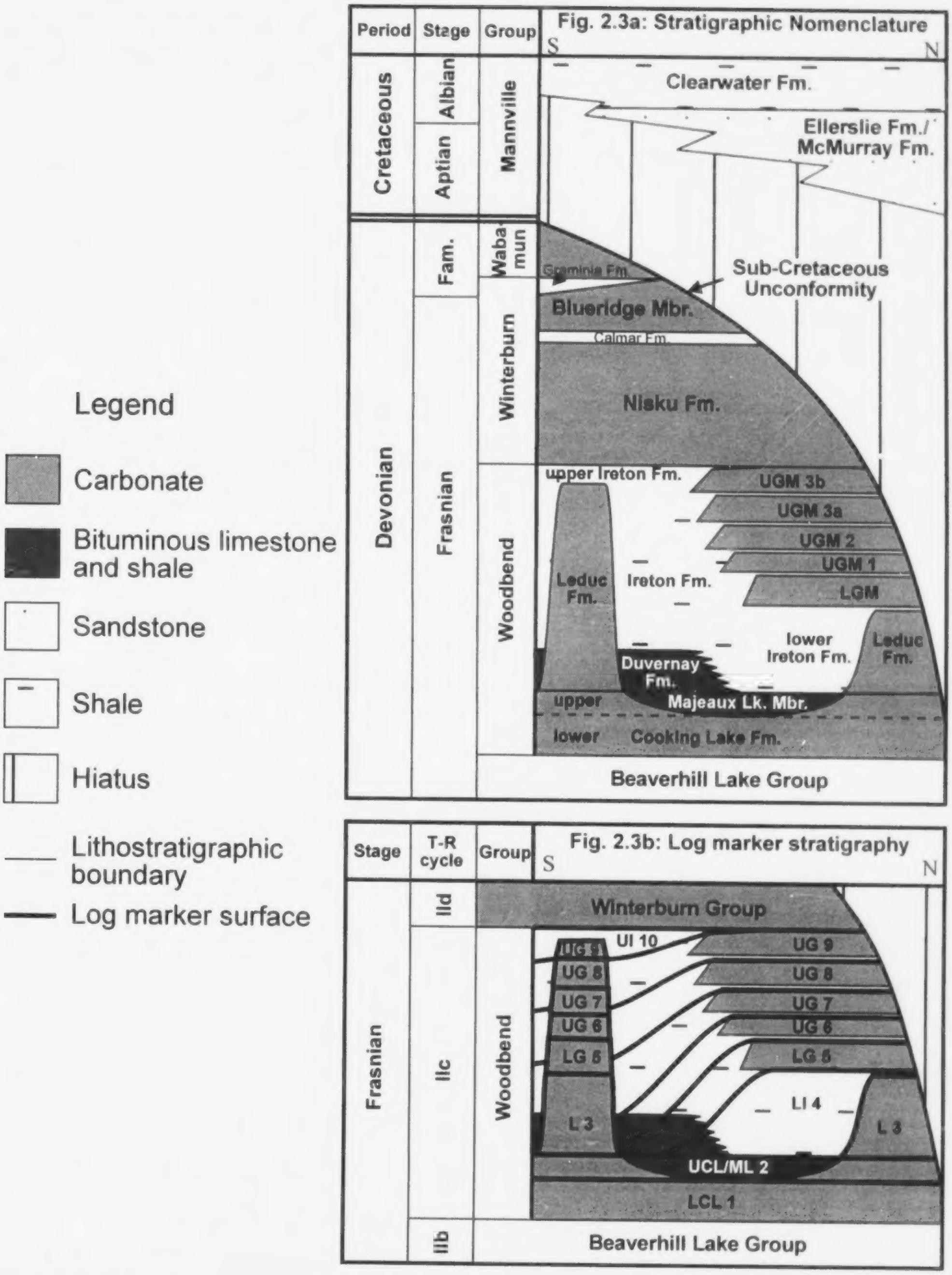
Legend
Carbonate
Bituminous limestone and shale
Sandstone
Shale
Hiatus
Lithostratigraphic boundary
Log marker surface
Period
Stage
Group
Fig. 2.3a: Stratigraphic Nomenclature
S
N
Cretaceous
Albian
Aptian
Mannville
Clearwater Fm.
Ellerslie Fm./ McMurray Fm.
Devonian
Fam.
Frasnian
Wabamun
Winterburn
Woodbend
Graminia Fm.
Sub-Cretaceous Unconformity
Blueridge Mbr.
Calmar Fm.
Nisku Fm.
upper Ireton Fm.
UGM 3b
UGM 3a
UGM 2
UGM 1
LGM
Leduc Fm.
Ireton Fm.
lower Ireton Fm.
Leduc Fm.
Duvernay Fm.
upper
Majeaux Lk. Mbr.
lower
Cooking Lake Fm.
Beaverhill Lake Group
Stage
T-R cycle
Group
Fig. 2.3b: Log marker stratigraphy
S
N
Frasnian
IId
IIc
IIb
Woodbend
Winterburn Group
UI 10
UG 9
UG 8
UG 7
UG 6
LG 5
LI 4
L 3
UCL/ML 2
LCL 1
Beaverhill Lake Group

Fig. 2.3a: Lithostratigraphic nomenclature of the principal Upper Devonian and Lower Cretaceous units in the study area. General Devonian stratigraphic nomenclature follows the definitions used in Switzer et al. (1994). Grosmont subdivisions follow the informal nomenclature of Harrison (1982; 1984).

Fig. 2.3b: Log marker stratigraphy and inferred, allostratigraphic units of the Woodbend Group in the study area. See text for more detailed explanations.

Formation is developed, the Ireton Formation is informally divided into lower (below the Grosmont Formation) and upper (above the Grosmont Formation) Ireton Formation (cf. Cutler, 1983). Some authors who studied the stratigraphy of the Grosmont Formation (Theriault, 1988; Luo et al., 1992; Luo et al., 1993; Dembicki, 1994) have used the term "Upper Ireton" for silty carbonates of the UGM 3b. In this study the term upper Ireton Formation is only applied to argillaceous deeper water carbonates developed above the Grosmont Formation.

In the study area, which is located in an area of the Western Canada Sedimentary Basin that was not disturbed by tectonic faulting, the Woodbend Group dips to the southwest at approximately 5.5 m per kilometer. The Woodbend Group is overlain by the Upper Devonian (Frasnian) Winterburn Group. In the northeastern corner of the study area, however, the Woodbend Group is truncated by the sub-Cretaceous unconformity, which is a regional erosional surface that resulted from prolonged subaerial exposure and partial to complete erosion of Paleozoic strata. In areas of truncation by the sub-Cretaceous unconformity the Woodbend Group is overlain by the Lower Cretaceous Mannville Group (Fig. 2.3a).

LOG MARKER STRATIGRAPHY

Wireline log marker stratigraphy (database = log suites from 211 wells; Fig. 2.2) was used in order to establish correlations between the formations of the platform and basin settings and to define approximate allostratigraphic units. These allostratigraphic units were later used to map the distribution of facies associations during several stages of development (= "time" slices) of the Woodbend Group.

The usage and interpretation of log marker stratigraphy in this study follows the principles that were defined and established by a number of authors who studied the Woodbend Group in central Alberta (McCrossan, 1961; Oliver and Cowper, 1963; Stoakes, 1980; Cutler, 1983; Switzer et al., 1994; Wendte et al., 1995). Log markers are defined as patterns or shifts in electrical or gamma-ray wireline log responses that can be widely correlated over several hundreds of kilometers. These log markers have been interpreted to reflect depositional shelf bathymetry as well as to approximate allostratigraphic markers (cf. Oliver and Cowper, 1963; Stoakes, 1980). This interpretation is based on observations that log markers cross-cut formations (McCrossan, 1961) and that log markers and corresponding lithological differences and surfaces in core accurately reflect facies changes and depositional bathymetry along a shelf profile (Stoakes, 1980).

Stratigraphic studies of basin-fill successions (Oliver and Cowper, 1963; Stoakes, 1980) defined log marker horizons along hardground surfaces and calciturbidite deposits. These surfaces and deposits are interpreted to represent changes of environmental factors, such as fluctuations in sea level and/or changes in the amount and type of sediment influx which temporarily overprinted normal basin sedimentation. Stratigraphic studies of carbonate platform deposits, i.e. the Grosmont Formation, used widely correlatable shale beds, the so-called shale breaks (Fig. 2.4), as log markers (Harrison, 1982; 1984; Cutler, 1983; Theriault, 1988; Machel and Hawlader, 1990; Luo et al., 1992; Luo et al., 1993; Dembicki, 1994; Switzer et al., 1994). Analogous to hardground surfaces in the basin-fill successions, the base of each platform shale marker is interpreted to approximate an allostratigraphic surface. Platform shale markers comprise the basal layer of platform shallowing upward cycles with evidence for significant increase in water depth at the cycle break. The base of a platform shale marker is, therefore, interpreted to represent a major marine flooding surface (Van Wagoner et al., 1987). Cutler (1983) interpreted shale marker formation to be the result of sea level rises which briefly shut off carbonate production. During this interruption in carbonate deposition a layer of clastic material was deposited from background sedimentation, separating individual depositional (shallowing upward) cycles.

In this study individual allostratigraphic units were defined based on log marker stratigraphy in the Grosmont platform area (northern part of the study area). This area was chosen because it allows for the most unambiguous recognition of wireline log markers and because the definition of lithological units and formations coincides with the proposed allostratigraphic units, because both are based on and bound by shale marker beds. Based on the log marker stratigraphy in the Grosmont platform area 10 allostratigraphic units were defined and correlated throughout the study area (Fig. 2.3b). To distinguish these allostratigraphic units from lithostratigraphic formations and members each unit has been

WELL 13-6-84-19 W4M

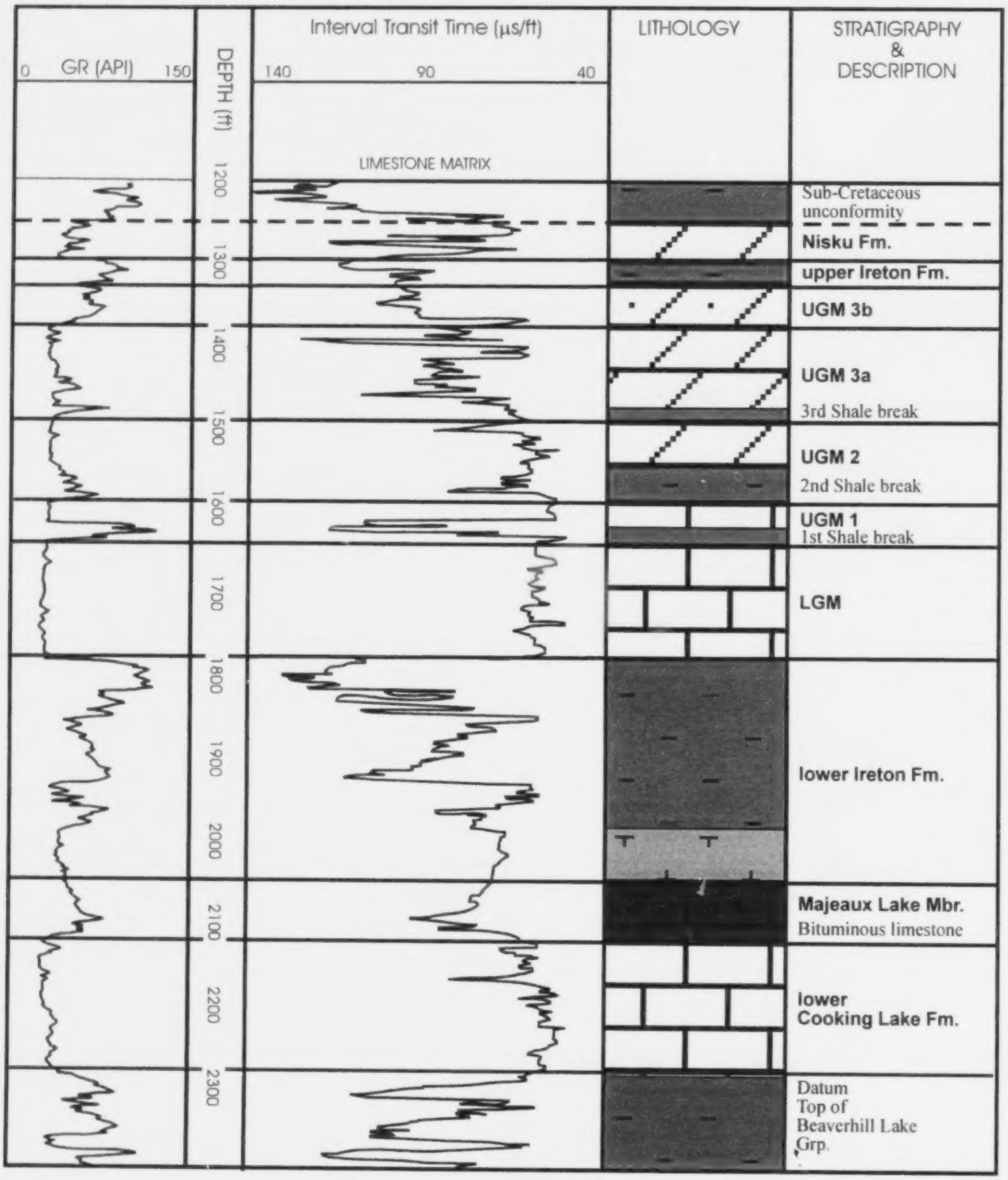

Fig. 2.4: Example of the log marker subdivision of the Woodbend Group in north-central Alberta. Unit tops are based on wireline log picks of marker horizons (e.g. Grosmont shale breaks in the Grosmont Formation). Well 13-6-84-19W4 is an example of a typical Woodbend gamma-ray and sonic response from the northern part of the study area.

designated with the capital letters of the formations they are based on which is followed by a number corresponding to the position of the unit in the Woodbend Group succession (1 = oldest, 10 = youngest). The allostratigraphic units are called in ascending order (names in brackets identify the formations the units are based on), LCL 1 (lower Cooking Lake Formation), UCL/ML 2 (upper Cooking Lake Formation / Majeaux Lake Member), L 3 (Leduc Formation), LI 4 (lower Ireton Formation), LG 5 (LGM), UG 6 (UGM 1), UG 7 (UGM 2), UG 8 (UGM 3a), UG 9 (UGM 3b), and UI 10 (upper Ireton Formation). This nomenclature is used in stratigraphic cross-sections and "time" slice maps. Figures 2.3a and 2.3b show the relationships between lithostratigraphic units and log marker allostratigraphic defined units.

The definition of allostratigraphic units in the regressive portion of the Woodbend Group, i.e. the Grosmont Formation and equivalent basin-fill strata of the Duvernay and Ireton Formations, follows the informal stratigraphic nomenclature introduced by Harrison (1982; 1984) and is based on the correlation of shale markers as discussed above. The contact between individual units was picked at the base of the shale marker beds (Fig. 2.4) emphasizing the onset of clastic dominated sedimentation and the beginning of a new shallowing upward cycle. These shale markers were traced into the basin-fill successions in the southern part of the study area where they correspond to a change from carbonate to shale dominated basinal sedimentation (cf. Cutler, 1983). In core this change correlates to the top of a condensed carbonate section and is marked by a calciturbidite deposit and/or a submarine hardground surface (cf. Stoakes, 1980; Wendte et al., 1995).

The definition of allostratigraphic units in the transgressive portion of the Woodbend Group, which consists of the Cooking Lake and Leduc Formations and equivalent basin-fill successions (Majeaux Lake Member and lower parts of the Duvernay and Ireton Formations), and of the Morinville reef (Leduc Formation) in the southern part of the study area is more problematic. In most cases apparent log markers and/or supporting core control are absent, and divisions of the carbonate successions are based on extrapolated divisions identified in the basin-fill strata. The definition of the LCL 1 and UCL/ML 2 allostratigraphic units is based on the work of Wendte (1974; 1992) who recognized three members (upper, middle, lower) in the Cooking Lake Formation of central Alberta. The upper and middle members, which are present in most of the study area, comprise the LCL 1 unit. The UCL/ML 2 unit consists of the upper member of the Cooking Lake Formation, which is present only in the southernmost portion of the study area and along the Leduc reef trend. This UCL/ML 2 unit correlates to the Majeaux Lake Member in the northern part of the study area. The definition of the L 3 allostratigraphic unit is based on the Leduc Formation as identified in the northern part of the study area. The correlation of the L 3 unit with basin-fill strata and the Leduc Formation of the Morinville reef can only be estimated because of the absence of suitable core intervals (for a definition based on cycle breaks) as well as log markers. The definition of the LI 4 allostratigraphic unit is based on a log marker and a corresponding hardground surface at the contact between the lower Ireton Formation and the LGM member of the Grosmont Formation (Fig. 2.4). This marker can be traced southward into the successions of basin-fill where it divides the lower Ireton Formation and corresponds to a compositional change in basin-filling deposits from shale to more calcareous sediments. The part of the lower Ireton Formation below this hardground marker surface comprises the LI 4 unit. The portion above this hardground marker surface is interpreted as equivalent to carbonate platform deposits of the LGM member of the Grosmont Formation, and, consequently, is part of the LG 5 unit. Whether the lowest portions of the lower Ireton Formation may in fact be basin-fill equivalent strata of the L 3 unit could not be determined because reliable log markers are not present. The boundary between the L 3 and LI 4 units is, therefore, only schematic and does not represent a allostratigraphic surface.

LITHOFACIES ASSOCIATIONS

Thirty three Woodbend Group cores (Fig. 2.2) were measured and logged on a decimeter scale. Related lithofacies types were grouped into three facies associations based on sedimentary structures, characteristic bioclasts and stratigraphic relationships. Raw descriptive data for each lithofacies type are provided in Table 2.1. More extensive descriptions and reviews of individual Woodbend lithofacies types from in and around the study area were published by Klovan (1964), Wendte (1974; 1992), McGillivray and Mountjoy (1975), Stoakes (1980), Cutler (1983), Walls (1983), and Machel and Hunter

Table 2.1: Lithofacies characteristics.

Subtidal facies association

Tabular stromatoporoid floatstone to rudstone (Figs. 2.5a, 2.5c). Medium brown to dark brown, massive beds consisting mainly of tabular to lenticular stromatoporoids at times in original growth position. Minor components include bulbous stromatoporoids, solitary and colonial corals, calcareous algae, calcispheres, brachiopods and crinoids. The matrix consists of coarse grained, skeletal packstones and wackestones.

Bulbous stromatoporoid rudstone to framestone (Figs. 2.5b, 2.5c). Light to dark brown, featureless beds consisting mainly of bulbous stromatoporoids and minor tabular stromatoporoids, solitary and colonial corals, calcareous algae, calcispheres, bryozoans, brachiopods, gastropods, pelecypods, crinoids and ostracods. Matrix composition varies from skeletal wackestone to grainstone. Individual components are commonly reworked, fragmenred and abraded.

Peloid-intraclast packstone to grainstone (Figs. 2.6a, 2.6c). Bedded (cm-scale), cross bedded and bioturbated, light grey to light brown of packstones and well sorted grainstones. Main components are peloids and intraclasts. Minor components are coated grains (oncoids), algal coated aggregate grains, and bioclastic material. Bioclasts are abraded and have a micritic rim.

Bioclast packstone to grainstone (Fig. 2.6b). Bedded (cm to m-scale) and cross-bedded, light brown, moderately to well sorted, packstone to grainstone. Main components are bioclasts derived from brachiopods, gastropods, stromatoporoids and corals. Minor components include intraclasts and aggregate grains. Bioclasts are rounded and may have a micritic rim.

Amphipora floatstone to rudstone (Fig. 2.6d). Bedded (cm-scale) to laminated, light to dark brown floatstone to rudstone consisting mainly of *Amphipora* type stromatoporoids. The matrix consists of wackestones to packstones containing bioclasts (mainly brachiopods, gastropods and calcareous algae), peloids and aggregate grains.

Nodular, argillaceous wackestone (Figs. 2.8c, 2.9b). Greenish brown to medium brown wackestone with nodular fabric. Nodules may be round and separate or may coalesce into continuous, wavy bands. Nodular character is often enhanced by clay seams and low amplitude stylolites. Main components are bioclasts, particularly brachiopods and crinoids.

Peritidal facies association

Algal laminated (dolo)mudstone to packstone. Planar, wavy and crinkly laminated, grey (dolo)mudstone or peloidal packstone. Common sedimentary structures include small, irregular fenestra and mud cracks.

Bioturbated, peloidal packstone (Fig. 2.7b). Planar bedded (cm to m-scale) to laminated (mm-scale) light grey to light brown, mottled (bioturbated), peloidal packstone. Individual laminae may be separated by bituminous material. Common sedimentary structures include mud cracks, contorted beds, birdseye type fenestrae, pseudomorphs after gypsum and halite, and open burrows.

Intraclast breccia (Figs. 2.7a, 2.7c). Light grey, cm to m-sized beds of angular to subrounded, poorly sorted clasts of laminated carbonates and siltstones floating in a silty/argillaceous, fine crystalline dolomitic matrix. Individual clasts are mostly flat; some clasts display bending and folding.

Laminated silty/sandy (dolo)mudstone (Fig. 2.7a). Planar laminated couplets of grey (dolo)mudstone and dark grey siltstone/sandstone. Siltstone layers consist of well sorted quartz, feldspar and carbonate peloids and intraclasts. Mud cracks are common.

Table 2.1(contd.): Lithofacies characteristics.

Laminated argillaceous (dolo)mudstone (Fig. 2.7d). Planar, wavy and crinkly laminated couplets of grey (dolo)mudstone and light green calcareous shale. Argillaceous laminae appear mottled and bioturbated. Mud cracks are common.

Laminated anhydritic (dolo)mudstone (Fig. 2.8a). Planar to wavy laminated couplets of light grey (dolo)mudstone and grey anhydrite. Mudstone layers may have a base of peloids and small intraclasts and commonly display mud cracks and birdseye type fenestrae and contain pseudomorphs after gypsum and halite.

Massive to nodular anhydrite (Fig. 2.8b). Dark grey banded or nodular "chicken-wire" anhydrite. Individual bands or nodules may be surrounded by mudstone rims/layers.

Basinal facies association

Bioturbated, argillaceous wackestone (Fig. 2.8d). Medium brown, mottled wackestone. Burrowing traces are the dominant sedimentary structure. Components include peloids, intraclasts and bioclasts, such as crinoids and brachiopods. Commonly associated with bioclast-lithoclast rudstones; upper contact is often marked by an erosional surface or pyritized hardground surface.

Bioturbated, calcareous shale (Fig. 2.9a). Light green, bedded (m-scale) commonly mottled calcareous shale. Horizontal and vertical burrow traces are common. Components, commonly bioclasts, are sparse.

Bioclast-lithoclast rudstone (Figs. 2.9b, 2.9c). Greenish-brown commonly graded (upward fining) rudstone. Main components are lithoclasts, derived from shallow and deep water facies, and bioclasts, such as stromatoporoids, corals, crinoids and brachiopods. Bioclasts are commonly fragmented and abraded. Matrix composition ranges from skeletal grainstones and packstones to argillaceous wackestone. Scoured, erosional base with infilling of fractures and borings of underlying beds. Upward contact may be gradational (to nodular, argillaceous wackestone) or sharp (erosional contact).

Green, featureless shale. Thick (m-scale) beds of green shale, often finely interlaminated with argillaceous mudstone, less commonly bioturbated. Rare fauna of brachiopods and crinoids. Inclined bedding surfaces, convolute bedding and synsedimentary folding present in some cases. Upper contact may be gradational (to nodular, argillaceous wackestone) or sharp (hardground surface).

Bituminou s(lime)mudstone/wackestone and shale (Fig. 2.9d). Dark grey to black, planar to irregular laminated couplets of shale and carbonate. Individual laminae are separated by bituminous material and by low amplitude stylolites. Laminae drape around occasional large components and carbonate nodules. Carbonate layers consist of dense micrite with some small lithoclasts and bioclasts (ostracods, conodonts). Macrofossils, such as brachiopods, crinoids and cephalopods are extremely rare.

Fig. 2.5a: Stromatoporoid rudstone. Lenticular stromatoporoids, coral and brachiopod fragments are set in a dark wackestone matrix. Coin is 17.5 mm in diameter. Core slab. Well location 3-34-88-20W4, 1324' (Leduc Fm.).

Fig. 2.5b: Bulbous stromatoporoid floatstone. Stromatoporoids are abraded and rotated. Coin is 17.5 mm in diameter. Core slab. Well location 3-28-70-24W4, 3556' (upper Cooking Lake Fm.).

Fig. 2.5c: Tabular stromatoporoid rudstone in bioclast-intraclast grainstone matrix. Stromatoporoids are fractured and abraded. Coin is 17.5 mm in diameter. Core slab. Well location 1-32-61-23W4, 3761' (UGM 3b).

Fig. 2.5d: Stromatoporoid-coral rudstone in bioclast packstone to grainstone matrix. Large colonial coral fragment is abraded and crosscut by stylolites. Coin is 17.5 mm in diameter. Core slab. Well location 1-32-61-23W4, 3803' (UGM 3b).

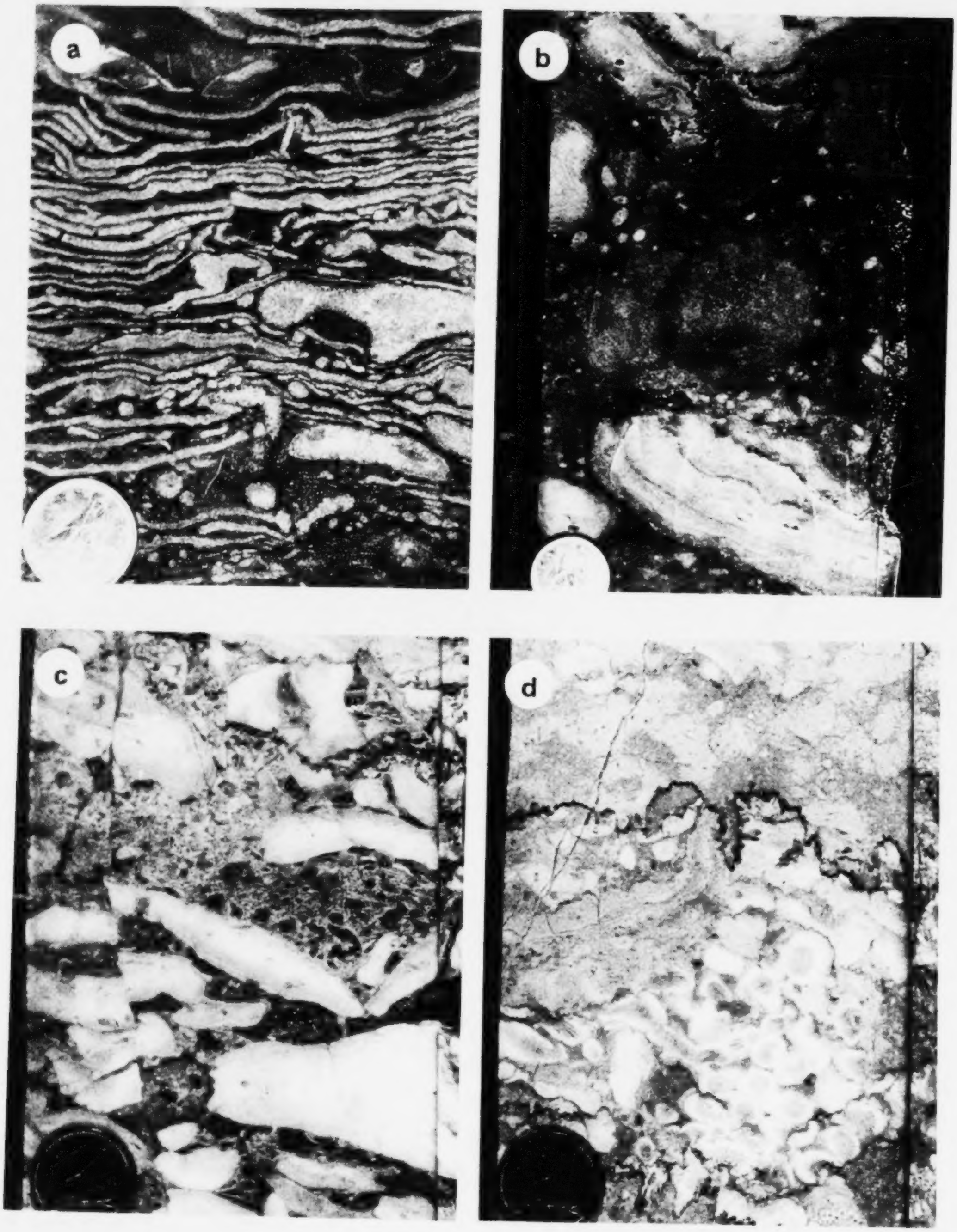
a
b
c
d

Fig. 2.6a: Peloid-intraclast packstone with interbedded mudstone layers. Coin is 17.5 mm in diameter. Core slab. Well location 14-26-64-21W4, 2694' (UGM 3b).

Fig. 2.6b: Intraclast-bioclast grainstone. Note the grain size difference above and below the stylolite. Coin is 17.5 mm in diameter. Core slab. Well location 1-32-61-23W4, 3778 (UGM 3b).

Fig. 2.6c: Peloid-intraclast packstone facies with dominant coated grain content. Components show a dark appearing micritized rim and/or a light colored algal coating. Coin is 17.5 mm in diameter. Core slab. Well location 10-17-84-19W4, 460.5 m (LGM).

Fig. 2.6d: Amphipora floatstone with large, bulbous stromatoporoid fragments. Bulbous stromatoporoids are partially dissolved. Matrix consists of a dark, bituminous wackestone. Coin is 17.5 mm in diameter. Core slab. Well location 3-28-70-24W4, 3557' (upper Cooking Lake Fm.).

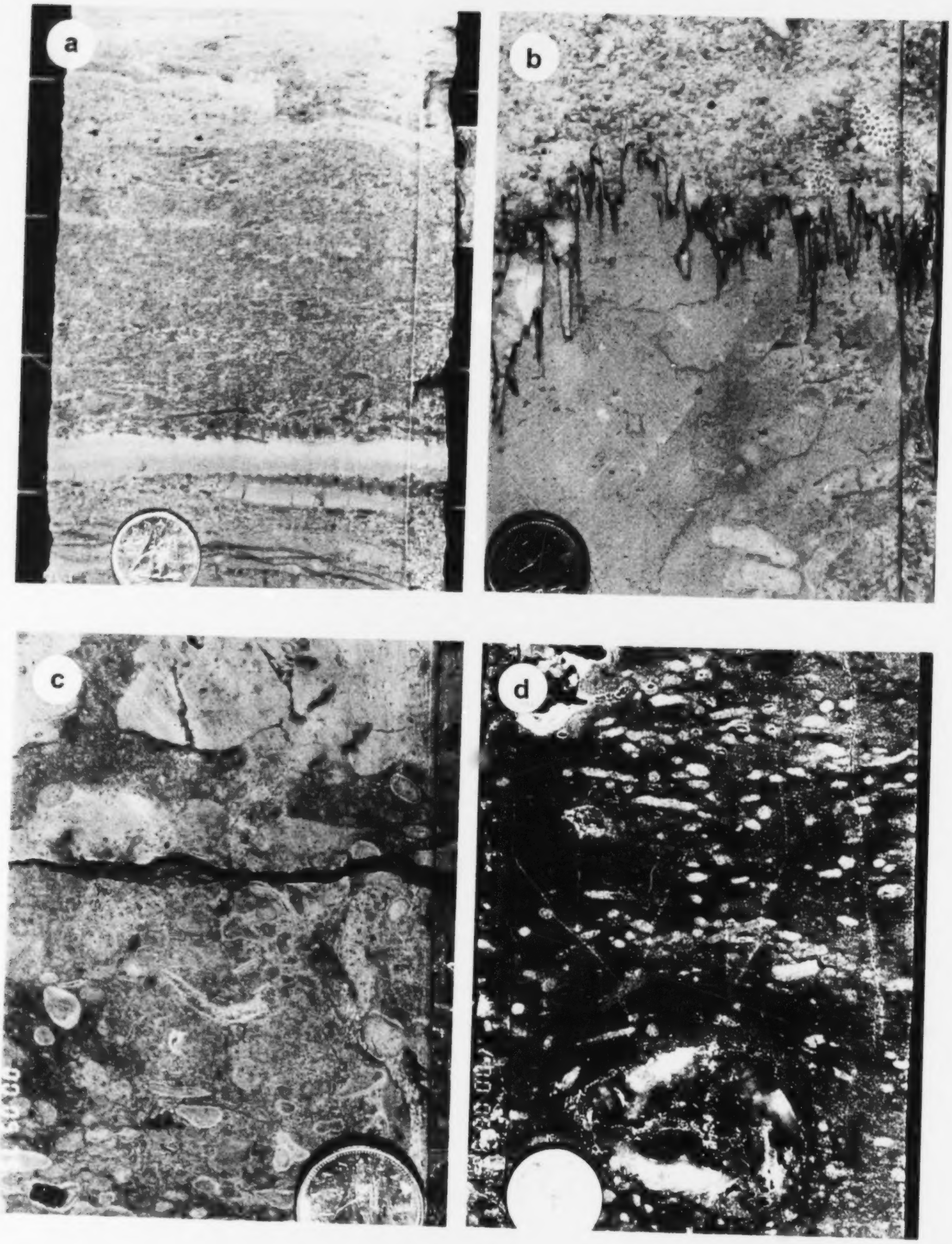
a
b
c
d

(1994). General overviews of Upper Devonian facies types and their bathymetric position were published by Embry and Klovan (1971; 1972) and Wilson (1975). The purpose of the following paragraphs is to infer depositional environments and processes from the observations described in Table 2.1. These facies interpretations in conjunction with the log marker stratigraphy are used to construct stratigraphic cross-sections and maps of individual "time" slices describing the stratigraphic development of the Woodbend Group in the study area.

Subtidal facies association

The subtidal facies association, which forms the lower portion of platform shallowing upward cycles, comprises the majority of Woodbend Group lithofacies in the study area. This lithofacies association dominates shallowing upward cycles in the upper and lower Cooking Lake Formation, the LGM and UGM 1 members of the Grosmont Formation, as well as in Leduc Formation reefs. In the UGM 2, UGM 3a, and UGM 3b members of the Grosmont Formation subtidal deposits are only a minor component of individual shallowing upward cycles. The component lithofacies types (Table 2.1) were deposited in environments ranging from very shallow subtidal to deep subtidal. For mapping purposes the subtidal lithofacies association was further divided on the basis of types of carbonate deposits (reef, platform) and major lithologies such as limestones and dolostones, which are not discussed separately here, and calcareous shales (not labelled differently from calcareous shales of the basinal lithofacies association). The following discussion emphasizes recognition criteria as well as stratigraphic trends of this lithofacies association. Detailed descriptions of individual lithofacies types are listed in Table 2.1.

Platform carbonates.- Subtidal platform carbonates are identified on the basis of sedimentological criteria (texture, components, bioclasts, sedimentary structures), stratigraphic criteria (position on shelf and in shallowing upward cycle) and paleoecological criteria (fossil assemblages). Characteristics of individual facies types vary widely because of the wide spectrum of depositional environments included under the term subtidal platform carbonates. Textures range from matrix supported mudstones and argillaceous mudstones, that were deposited under low water energy conditions commonly beneath the normal wave base, to grain supported textures deposited under high water energy conditions generally above the normal wave base (Wilson, 1975). Grain composition also varies between different facies. Deep subtidal lithofacies contain only few components, commonly small, pelagic bioclasts and intraclasts (Wilson, 1975). Open marine, shallow subtidal facies are generally dominated by bioclastic material and show a great diversity of bioclast types. Very shallow subtidal or restricted marine facies are dominated by one component type, such as a single bioclast type (e.g. *Amphipora* type stromatoporoids, gastropods), peloids, intraclasts and oncoids (Krebs, 1974; Wilson, 1975). Sedimentary structures vary from nodular and irregular banded in argillaceous units, to heavily bioturbated in mud supported and fine grained component supported facies types. Very shallow subtidal lithofacies show planar or low angle cross-bedding indicative of wave or current action.

Reefal carbonates.- The term reefal carbonates, as used in this study, refers to carbonate deposits of small (km-scale), isolated platforms, particularly of the Rimbey-Meadowbrook reef trend and its northern extension, that are rimmed by stromatoporoid-coral reefs (e.g. Klovan, 1964; McGillivray and Mountjoy, 1975; Walls, 1983). Reefal carbonates share many individual lithofacies types with subtidal platform carbonates. However, reefal carbonates are distinct in that they contain a large portion of boundstone lithofacies characteristic of reefal environments. Reefal associations commonly lack deep subtidal, argillaceous mud dominated lithofacies types. Instead deeper subtidal lithofacies are characterized by mud supported wackestones and floatstones that were stabilized by lenticular to platy stromatoporoids, solitary corals and crinoids (Fig. 2.5a) (Embry and Klovan, 1972). This lithofacies corresponds to the colonization stage of James (1984a). The bulk of reefal carbonate association comprises floatstones, rudstones and boundstones containing large fragments of reef building organisms such as tabular and bulbous stromatoporoids as well as solitary and colonial corals. These lithofacies types are interpreted to have formed at or near the location of active reef growth in a shallow, wave agitated, high energy environment above the normal wave base (Embry and Klovan, 1972) and most of them are probably accumulations of eroded reef framework. Other common lithofacies types include bioclastic and peloidal grainstones that are interpreted to have formed under constant wave action on shoals or back reef flats of the reef interior (Walls, 1983).

Calcareous shales.- Calcareous shales are restricted to the basal layer of platform shallowing upward cycles, representing the deepest conditions of individual cycles. They form widely correlatable shale breaks that can be used as marker beds. These shale breaks are interpreted to have formed during a single flooding "event", but not in a single depositional environment. This is evident from observed stratigraphic and cross-platform trends. Stratigraphically, individual shale markers are developed under more shallow conditions in younger platform units, because of the overall shallowing of the Woodbend shelf. Furthermore, each individual shale bed constitutes several distinct lithofacies that are characteristic of different depositional environments and bathymetric positions during deposition. The most shallow endmember of this lithofacies unit are laminated calcareous shales and (lime)mudstones (Fig. 2.7d). This lithofacies type is interpreted to have formed under peritidal to very shallow subtidal conditions because of common mudcracks and reworked horizons. Water energy appears to have been mostly low with occasional higher energy events which caused erosion and reworking. The second lithofacies type are bioturbated calcareous shales. The muddy composition and often excellent preservation of bioturbation features suggest sedimentation under protected, quiet water conditions and/or below the normal wave base. Shales interbedded with nodular, argillaceous carbonates represent open marine, deep subtidal conditions. This interpretation is supported by the observation that this lithofacies type commonly contains macrofossils indicative of open marine conditions such as brachiopods, crinoids and cephalopods (Krebs, 1974; Wilson, 1975).

The formation of shale marker beds in the platform environment has been attributed to relative sea level rises which temporarily shut off carbonate and siliciclastic sedimentation (Stoakes, 1980; Cutler, 1983). During this initial time of low or absent sedimentation erosional surfaces and submarine hardgrounds were formed which often characterize the sharp, lower contact of the shale marker. Deposition of siliciclastics appears to have resumed shortly after each sea level rise causing the formation of widely correlatable shale beds on the platform. Their upper contact is generally gradational due

Fig. 2.7a: Laminated dolomudstone and siltstone. The top dolomudstone and siltstone layers are cracked and are lifted off the rock surface. Lithoclasts derived from laminated dolomudstones and siltstones fill in small depression in the left and upper part of the picture. Coin is 17.5 mm in diameter. Core slab. Well location 4-33-68-22W4, 2625' (UGM 3b).

Fig. 2.7b: Bioturbated dolomudstone. Wispy and irregular structures are probably due to bioturbation. Note vertical compaction fractures (CF) and worm burrows (W). Coin is 17.5 mm in diameter. Core slab. Well location 13-22-83-22W4, 558.0 m (UGM 3a).

Fig. 2.7c: Brecciated dolomudstone. Clasts consist of laminated and massive dolomudstone fragments. Coin is 17.5 mm in diameter. Core slab. Well location 13-22-83-22W4, 564.75 m (UGM 3a).

Fig. 2.7d: Laminated dolomudstone interlayered with calcareous shale. Laminae are often broken due to desiccation and bioturbation and show infilling by the overlying lithology. Coin is 17.5 mm in diameter. Core slab. Well location 10-17-84-19W4, 424.75 m (UGM 3a).

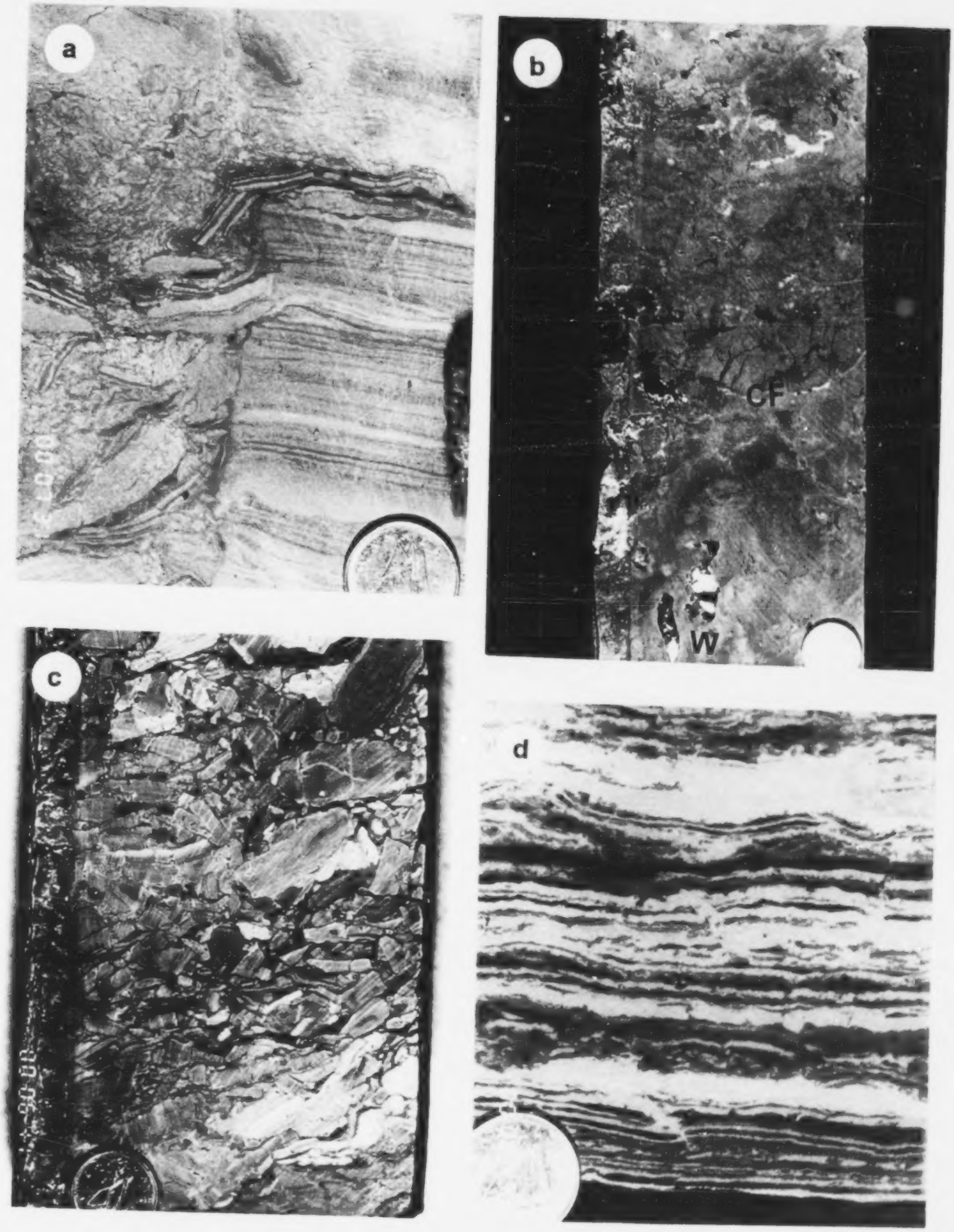
a
b
CF
W
c
d

to the slow reinitiation of carbonate production. How soon carbonate sedimentation resumed is related to the bathymetric position and the distance from the carbonate production area. Outer shelf areas recovered slowly and initial carbonates still contain a significant amount of argillaceous material. Inner shelf areas recovered faster which resulted in the deposition of thin, patchy and calcareous shale markers.

Peritidal facies association

The peritidal facies association is commonly present at the top of each platform shallowing upward cycle. Individual lithofacies types of this association form thin caps on cycles that are dominated by subtidal lithofacies types, i.e. in the upper and lower Cooking Lake Formation, the LGM and UGM 1 members of the Grosmont Formation, as well as in Leduc Formation reefs. Lithofacies types of the peritidal facies association are the dominant component in the UGM 2, UGM 3a, and UGM 3b members of the Grosmont Formation. The component lithofacies types were deposited in environments ranging from supratidal to very shallow subtidal. This discussion focusses on groups of lithofacies types that are used to divide the peritidal facies association into three mappable lithofacies units, silty dolostones, anhydritic dolostones, and (clean peritidal) dolostones. These units are critical to the stratigraphic interpretation and the discussion about controls on platform development following later in the text.

Silty/sandy carbonates.- This lithofacies unit consists of two individual lithofacies types, 1) laminated dolomudstones and siltstone/sandstones, and 2) brecciated dolomudstones (Figs. 2.7a, 2.7b). It represents a mixed carbonate-siliciclastic unit in the strictest sense. Carbonate and clastic material are both, texturally mixed as well as interlaminated. This lithofacies unit caps platform shallowing upward cycles of the UGM 3a and UGM 3b members of the Grosmont Formation in the northern part of the study area.

Laminated dolomudstones and siltstone/sandstones are interpreted to have been deposited on tidal flats as couplets of quartz-muscovite silt and fine sand and peloidal carbonate mud, possibly during storm tides (Hardie and Ginsburg, 1977). The quartz-muscovite silt and fine sand is interpreted to be aeolian in origin and was probably derived from a northeasterly source, either from the Canadian shield or the Ellesmerian orogen (Stoakes, 1980), analogous to the situation of the modern Persian Gulf (Shinn, 1983; 1986). This interpretation is based on the excellent sorting as well as the subangular rounding of quartz silt and sand grains (Mazzullo et al., 1992). It is likely that once the aeolian material was deposited on the tidal flat it was reworked by tidal currents and redeposited as planar laminae and low-angle cross laminae.

Brecciated dolomudstones form layers that range from a few centimeters to several meters in thickness. These beds are often laterally continuous and can be correlated over tens of kilometers in the northern portion of the Grosmont platform (Luo et al., 1992). These breccia layers are significant because they occur near the top of individual shallowing upward cycles as well as at the top of the overall Woodbend transgressive-regressive cycle. Individual clasts are commonly flat, fractured and angular attesting to reworking after initial cementation. Some clasts, however, are bend and folded which is indicative of soft sediment deformation of semi-lithified layers. The breccia matrix consists of fine crystalline dolomites and quartz silt. Breccias may be clast or matrix supported and may have a chaotic to fitted fabric. Based on their stratigraphic position and the abundance of desiccation structures in underlying layers breccia clasts are thought to have formed during exposure and subsequent drying of the peritidal sediment or dissolution of evaporite minerals and metastable carbonates. Breccia clasts are interpreted to have been reworked during storm events and/or subaerial exposure of the tidal flat surface (Assereto and Kendall, 1977; Shinn, 1983; Kendall and Warren, 1987). The formation of several meter thick breccia layers may be the result of accumulation and subsequent preservation of breccias in local depressions.

Anhydritic carbonates.- This lithofacies unit occurs predominantly in the UGM 3a and UGM 3b members of the Grosmont Formation and is especially prominent in the western part of the study area, where anhydritic carbonates dominate the peritidal portion of the platform shallowing upward cycles. The differences between the normal Grosmont succession and this lithofacies unit are distinct enough for some authors to grant this anhydritic succession a separate formation status (Hondo Formation, Cutler, 1983). Anhydritic carbonates consist of interlaminated (mm-scale) to interbedded (cm-scale) layers of dolomudstone, peloidal dolopackstones and anhydrite (Fig. 2.8a) that reach a thickness of several meters. Anhydrite is also present in nodular form with individual nodules ranging from a few millimeters to several centimeters in diameter. Massive to nodular "chicken-wire" anhydrite (Fig. 2.8b) is only a minor component of the Grosmont platform succession. The carbonate portion of the anhydrite carbonate couplets are mostly planar to wavy bedded and have a base of peloidal packstone which grade into dolomudstone. Mud cracks and birdseye type fenestrae are commonly observed sedimentary structures indicative of tidal flat sedimentation (Shinn, 1983). Anhydritic carbonates are commonly underlain by peritidal carbonates and capped by silty/sandy carbonates. Based on this stratigraphic relationship and the observed sedimentary structures anhydritic carbonates are interpreted to have formed in a tidal flat environment.

Clean, peritidal carbonates.- This lithofacies unit characterizes most of the peritidal deposits of the Woodbend Group. It is most prominent in the UGM 2 and UGM 3a members of the Grosmont Formation, but also forms the cap on shallowing upward cycles in more open marine intervals such as the lower and upper Cooking Lake Formation, the LGM and UGM 1 members of the Grosmont Formation as well as in Leduc Formation reefs. The interpretation of this lithofacies unit as peritidal deposits is primarily based on sedimentary structures characteristic of this environment. Commonly observed sedimentary structures include mudcracks and mud diapers, planar and algal lamination, birdseye type and irregular fenestrae, and intraclast layers. This set of sedimentary structures is indicative of processes governing intertidal sedimentation, such as desiccation, storm deposition and reworking, and algal mat formation (Logan, 1974; Shinn, 1983). Intervals containing indicative sedimentary structures are often interbedded with massive dolomudstones. This lithofacies type lacks apparent bedding surfaces and, instead, has a mottled texture that originates most likely from bioturbation.

Basinal facies association

Sediments of the basinal facies association are predominantly present in off-platform settings of the southernmost part of the study area (East and West-Shale Basins; Fig. 2.1). This facies association comprises the Duvernay and Ireton Formations (Fig.

Fig. 2.8a: Laminated dolomudstone and anhydrite. Dolomudstone layers have a light colour and show planar lamination. Thin, dark layers are anhydrite. Anhydrite also fills fractures and small birdseye type vugs in the upper part of the picture. Coin is 17.5 mm in diameter. Core slab. Well location 15-17-71-25W4, 2920' (UGM 3b).

Fig. 2.8b: Massive anhydrite with "chicken-wire" texture. Coin is 17.5 mm in diameter. Core slab. Well location 10-17-84-19W4, 500.5 m (LGM).

Fig. 2.8c: Nodular, argillaceous wackestone. Main components are brachiopod and crinoid fragments. Wispy stylolites are concentrated around carbonate nodules. Coin is 17.5 mm in diameter. Core slab. Well location 14-26-64-21W4, 2633' (upper Ireton Fm.).

Fig. 2.8d: Bioturbated wackestone. Note the abundance of vertical and horizontal bioturbation structures (arrows). Skeletal material consists mainly of small brachiopod and crinoid fragments. Coin is 17.5 mm in diameter. Core slab. Well location 4-33-68-22W4, 3403' (Majeaux Lake Mbr.).

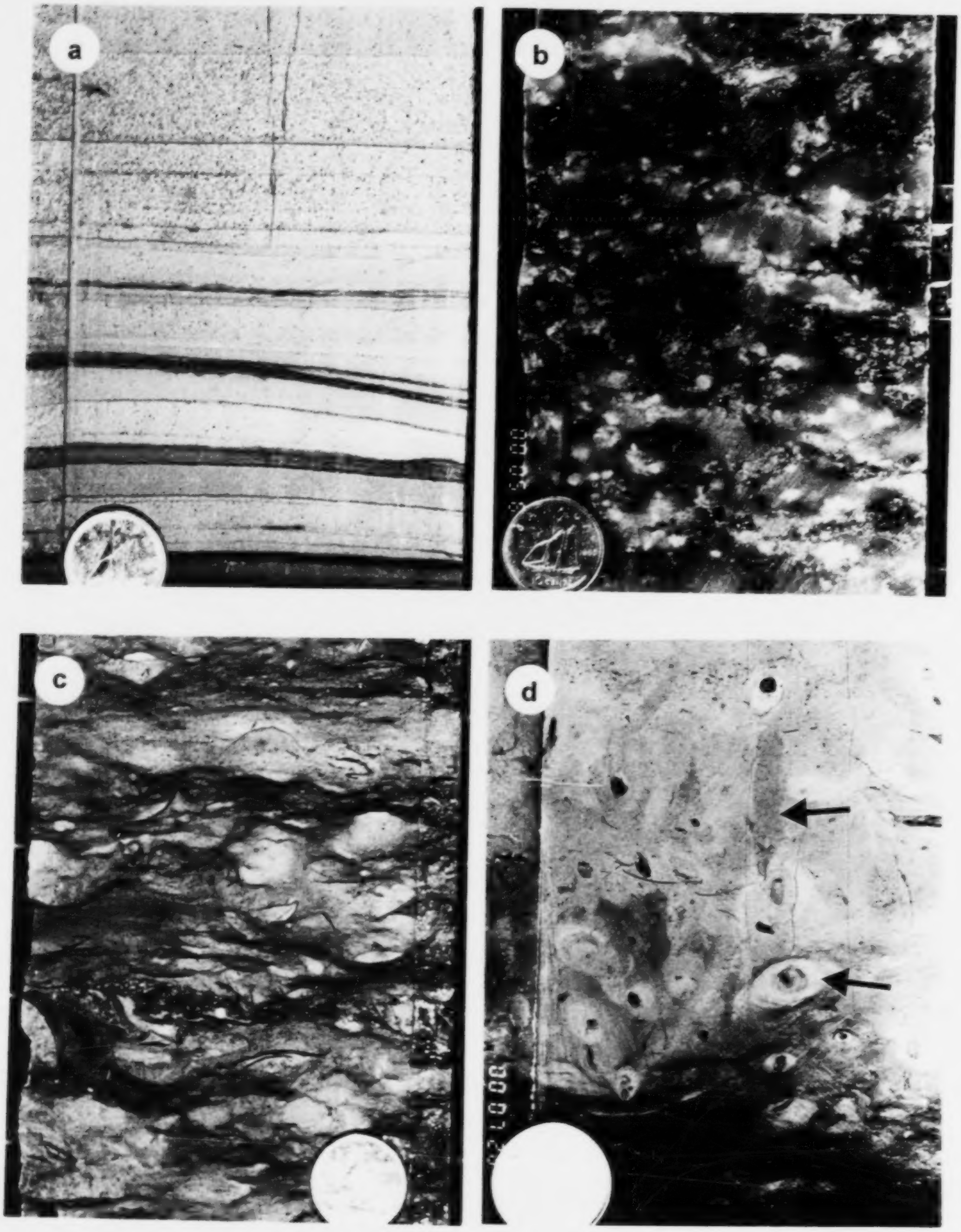
a
b
c
d

2.3a) in this area which consist of bituminous carbonates and shales, and of shales to argillaceous carbonates, respectively. In the rest of the study area the basinal facies association is only present in the lower, transgressive portion of the Woodbend Group, comprising the Majeaux Lake Member, the basinal equivalent of the Cooking Lake Formation, and the lower Ireton Formation (Fig. 2.3a). The component lithofacies types of the basinal facies association were deposited in environments ranging from deep subtidal platform and slope settings to starved basinal settings. Mappable lithofacies units were defined based on the three main lithologies of the basinal lithofacies association, argillaceous carbonates, shales, and bituminous carbonates and shales.

Argillaceous carbonates.- Argillaceous carbonates dominate basinal sedimentation in intervals of the Ireton Formation that are roughly time equivalent to the upper members of the Grosmont Formation. This lithofacies unit consists of three interbedded lithofacies types, 1) bioclast-lithoclast rudstone to floatstone, 2) nodular argillaceous wackestone, and 3) bioturbated argillaceous mudstone to calcareous shale.

Bioclast-lithoclast rudstones to floatstones (Figs. 2.9b, 2.9d) consist mainly of abraded bioclastic material derived from adjacent carbonate platform areas (e.g. corals and stromatoporoids; Fig. 2.9b) which is intermixed with bioclastic material originating from deeper water environments, such as crinoids, thin-shelled brachiopods, tentaculitids and cephalopods (Krebs, 1974). Lithoclasts, the second major component type, were derived from shallow and deep water carbonate lithofacies as well as shale lithofacies types. Individual lithoclasts are rounded, fractured and often show rip up textures and pyrite or Fe-Mn coatings (Fig. 2.9b). The matrix composition ranges from skeletal grainstones and packstones to argillaceous wackestones. Lithoclast-bioclast rudstones and floatstones have a sharp erosional base which commonly shows scouring, reworking and infilling of cracks and borings of underlying beds. Upward grading and fining of individual beds is common, most beds, however, are themselves eroded and have a sharp upper contact. This lithofacies type is interbedded with and grades into either bioturbated mudstones to calcareous shales or nodular argillaceous wackestones.

Nodular argillaceous wackestones as well as bioturbated argillaceous mudstones to calcareous shales (Table 2.1, Figs. 2.8c, 2.8d, 2.9a, 2.9b) are both interpreted to have

Fig. 2.9a: Bioturbated calcareous shale. Coin is 17.5 mm in diameter. Core slab. Well location 10-14-84-19W4, 241.0 m (UGM 2).

Fig. 2.9b: Nodular, argillaceous wackestone overlain by a bioclast-lithoclast floatstone. Crinoids and brachiopods are the main components of the lower lithofacies. An erosional surface truncates the nodular, argillaceous wackestone. The contact is sharp and shows pyrite mineralization (arrow). The bioclast-lithoclast floatstone consists of clasts from the underlying lithology and stromatoporoid fragments from nearby reef complexes. Coin is 17.5 mm in diameter. Core slab. Well location 14-26-64-21W4, 2656' (upper Ireton Fm.).

Fig. 2.9c: Lithoclast-bioclast packstone. Main components are crinoids, brachiopods and lithoclasts. Sample shows weak bedding caused by intercalated calcareous and argillaceous layers. Deposit is interpreted as calciturbidite. Coin is 17.5 mm in diameter. Core slab. Well location 1-32-61-23W4, 3395' (upper Ireton Fm.).

Fig. 2.9d: Basinal argillaceous, bituminous mudstone. Finely laminated mudstones are interlayered with weakly bedded mudstones to wackestones. Coin is 17.5 mm in diameter. Core slab. Well location 4-33-68-22W4, 3455' (Majeaux Lake Mbr.).

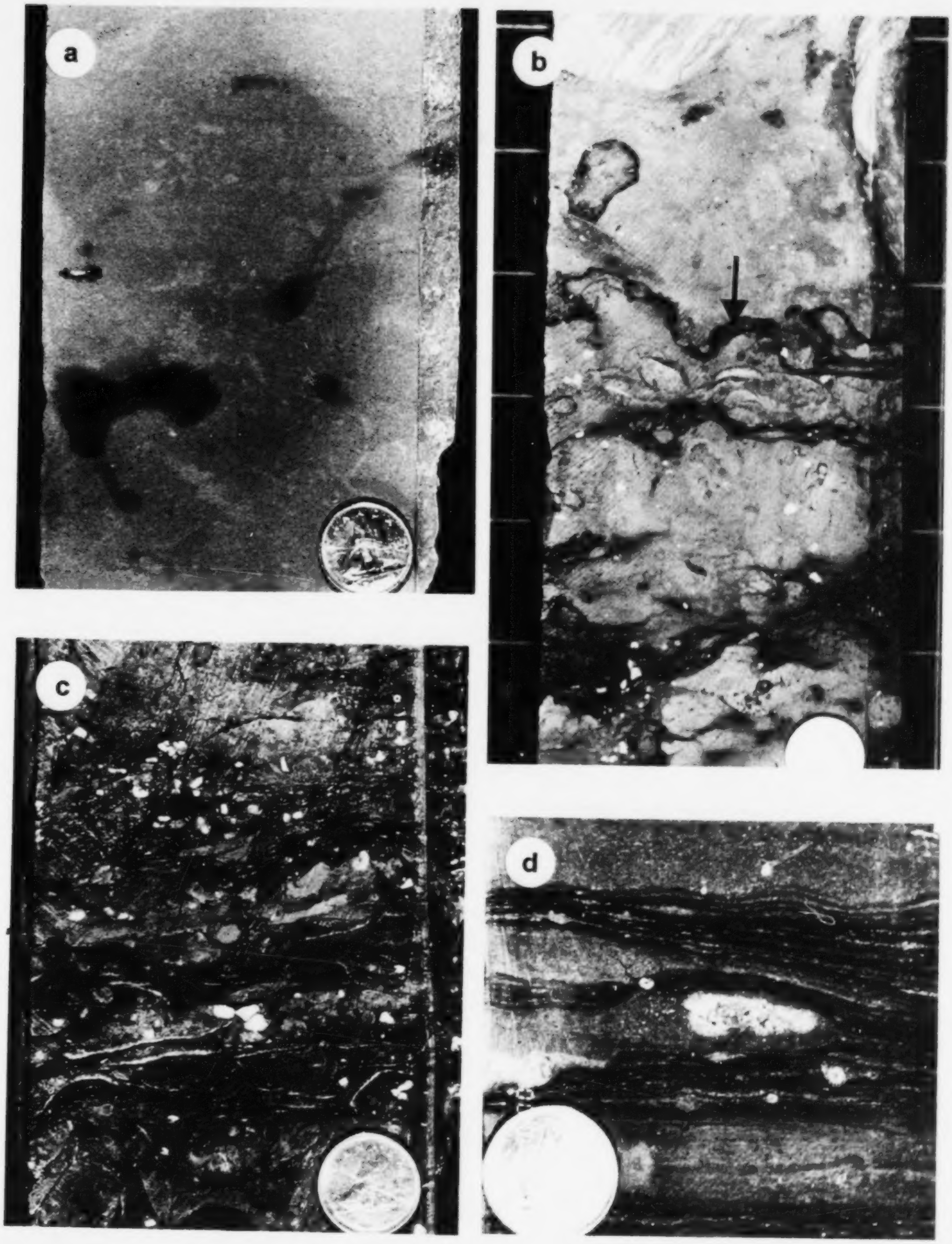
a
b
c
d

been deposited below the normal wave base because of their high content of argillaceous material, fine grain size, mud supported texture, excellent preservation of bioturbation features, and open marine faunal assemblage. Nodular fabrics may be related to multiple hardground surfaces, bioturbation and/or are of diagenetic origin accentuating previously present differences in carbonate content of the original sediment (Scholle et al., 1983). Whereas the lower contact of these lithofacies types to bioclast-lithoclast rudstones to floatstones is generally gradational, their upper contact is commonly marked by a submarine hardground and/or an erosional surface (Fig. 2.9b).

The observed sedimentary structures and sediment composition of bioclast-lithoclast rudstones to floatstones suggest that this lithofacies type is the result of mass transport deposition of platform and reef material (calciturbidites of Stoakes, 1980) into the slope and basin environment. These mass transport deposits are interbedded with argillaceous deposits which represent the basinal background deposition. The high carbonate content of these deposits, compared to the shaly composition of basinal deposits that are age equivalent to the Leduc Formation reefs and LGM platform deposits, is likely related to winnowing of carbonate material from adjacent, extensive carbonate platforms.

Shales.- In the study area shales are the predominant basinal sediment in the lower, transgressive part of the Woodbend Group, i.e. the lower Ireton Formation and intervals of the Ireton Formation that are roughly equivalent to the lower Grosmont Formation. In addition, shales also comprise much of the uppermost Ireton Formation in the southern part of the study area. This succession has been designated as UI 10 unit (upper Ireton "time" slice) in this study.

The shale lithofacies unit consists of thick (up to several meters) beds of massive to fissile green to blue-green shales. At some locations shale layers are interbedded with argillaceous mudstones and calcareous shales. Calcareous layers appear elongate nodular to irregular banded and consist of dense micrite containing a sparse, mainly pelagic fauna of tentaculitids, stylolinids, ostracods and foraminifera (Stoakes, 1980). Some intervals also contain cephalopods, brachiopods and crinoids. Shale as well as carbonate layers are finely laminated and display evidence of horizontal burrowing. Individual laminae drape around carbonate nodules and bioclasts. The sediment composition suggests that this lithofacies unit was deposited under deep-water, low energy conditions representative of a deep platform or slope environment (Krebs, 1974; Wilson, 1975). This interpretation is further supported by the presence of sedimentary structures that are indicative of slumping and other forms of gravity flow, i.e. graded bedding, inclined bedding surfaces, convolute bedding and synsedimentary folding. Accumulated material was probably transported from a northerly source and settled from hemipelagic suspension (Stoakes, 1980). Formation of carbonate nodules and the occasional development of hardgrounds likely occurred during times of low sedimentation rates.

Bituminous carbonates and shales.- Bituminous carbonates and shales are restricted to the basinal member of the Cooking Lake Formation, the Majeaux Lake Member, and the Duvernay Formation (Fig. 2.3a). While this lithofacies covers much of the study area during the transgressive portion of the Woodbend cycle, it retreats southward with the onset of significant clastic input and the inception and progradation of the Grosmont carbonate platform. The Duvernay Formation, which represents this lithofacies unit during the phase of southward retreat, is, in the study area, the condensed, basinal equivalent to a stratigraphic section ranging from the top of the Cooking Lake Formation to the UGM 1 member of the Grosmont Formation. South of the study area the Duvernay Formation is equivalent to even younger platform strata (UGM 2, UGM 3a) (Cutler, 1983; Switzer et al., 1994).

This lithofacies unit consists of grey or black, laminated, bituminous shales which are interbedded with dark brown to dark grey, laminated, bituminous (lime)mudstones (Fig. 2.9d). Lamination is caused by slight changes in the grain size and mineralogy of individual layers and is enhanced by thin bituminous laminae, intercalated calcite cement, low amplitude stylolites or clay seams. Individual laminae are generally planar but drape around occasional large components and carbonate nodules. Carbonate layers consist of dense micrite with some small lithoclasts and microfossils such as stylolinids, tentaculitids, ostracods, conodonts and foraminifers. Macrofossils such as brachiopods and cephalopods are extremely rare. The sparsity of skeletal material consisting of pelagic fauna, the fine grained argillaceous character of the matrix, and the abundance of preserved organic matter suggest deposition under quiet water conditions in a deeper marine, often poorly circulated basinal setting (Embry and Klovan, 1971; Wilson, 1975; Stoakes, 1980; Scholle et al., 1983).

STRATIGRAPHIC AND REGIONAL TRENDS

Trends in platform sedimentation

Idealized shallowing upward cycles from the Woodbend Group in north-central Alberta have been described by various authors (Cutler, 1983; Theriault, 1988; Machel and Hunter, 1994). All of these authors divided idealized platform shallowing upward cycles (Fig. 2.10a) into six to seven members. Idealized platform cycles are characterized by basal deeper water deposits consisting of shale or argillaceous carbonate, the so-called shale break, and nodular (argillaceous) wackestone. These are followed by biostromal, open marine facies (tabular stromatoporoid floatstone to rudstone), marginal marine, lagoonal and shoal deposits (*Amphipora* floatstone to rudstone; peloid, intraclast and/or bioclast packstone to grainstone), and peritidal carbonate facies (laminated, algal-laminated and massive (dolo)mudstone). Brecciated and reworked carbonates (brecciated (dolo)mudstone), indicative of supratidal conditions and subaerial exposure of the carbonate platform, cap the idealized platform cycle.

Actual records of shallowing upward cycles, however, never contain all facies types of the idealized cycle. In many cases the basal shale breaks, peritidal lithofacies or most commonly the brecciated, supratidal cap are missing (Cutler, 1983). Shallowing upward cycles that are closest to the described idealized cycles are present in areas or stratigraphic intervals of carbonate platform successions that are dominated by open marine deposits, i.e. the LCL 1 and UCL 2 units (lower and upper Cooking Lake Formation), the LG 5 unit (LGM member of the Grosmont Formation) and the southern portions of the UG 6 and UG 7 units (UGM 1 and UGM 2 members of the Grosmont Formation). This "open marine" shallowing upward cycle (Fig. 2.10b) ranges between 5 and 20 meters in thickness and is little influenced by siliciclastic input. At the base of each open marine cycle a shale break (shale or argillaceous mudstone) is developed indicating an apparent sea level rise and the temporary suspension of carbonate

Fig. 2.10a: Idealized Woodbend cycle (after Cutler, 1983; Theriault, 1988; and Machel and Hunter, 1994)

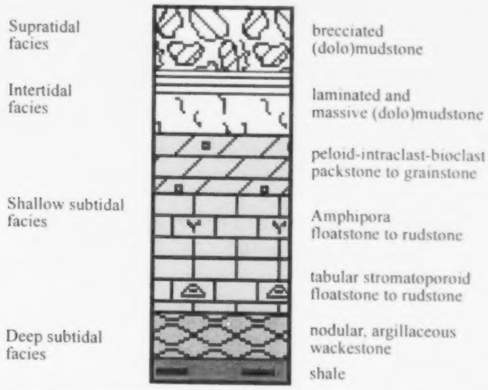
Supratidal facies
Intertidal facies
Shallow subtidal facies
Deep subtidal facies
brecciated (dolo)mudstone
laminated and massive (dolo)mudstone
peloid-intraclast-bioclast packstone to grainstone
Amphipora floatstone to rudstone
tabular stromatoporoid floatstone to rudstone
nodular, argillaceous wackestone
shale

Fig. 2.10b: Open marine platform cycle

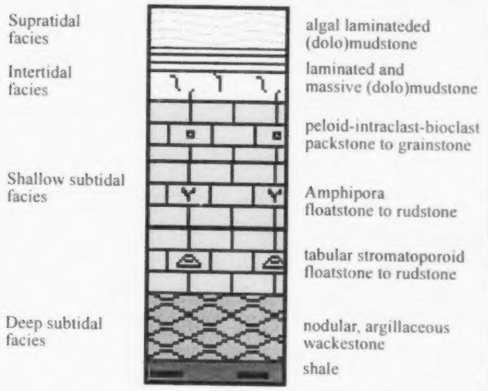
Supratidal facies
Intertidal facies
Shallow subtidal facies
Deep subtidal facies
algal laminateded (dolo)mudstone
laminated and massive (dolo)mudstone
peloid-intraclast-bioclast packstone to grainstone
Amphipora floatstone to rudstone
tabular stromatoporoid floatstone to rudstone
nodular, argillaceous wackestone
shale

Fig. 2.10c: Restricted marine platform cycle

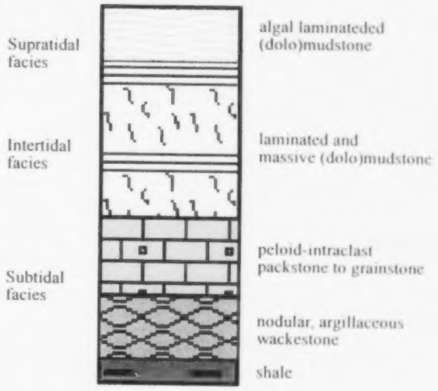
Supratidal facies
Intertidal facies
Subtidal facies
algal laminateded (dolo)mudstone
laminated and massive (dolo)mudstone
peloid-intraclast packstone to grainstone
nodular, argillaceous wackestone
shale

Fig. 2.10d: Anhydritic, restricted marine platform cycle

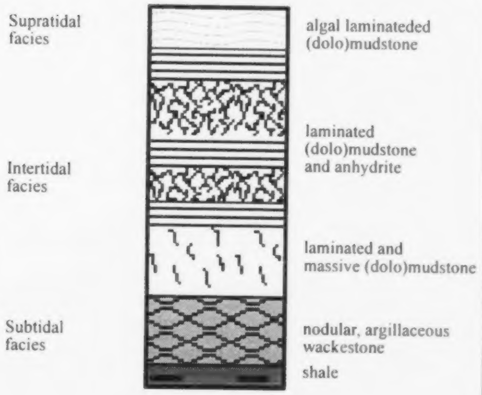
Supratidal facies
Intertidal facies
Subtidal facies
algal laminateded (dolo)mudstone
laminated (dolo)mudstone and anhydrite
laminated and massive (dolo)mudstone
nodular, argillaceous wackestone
shale

Fig. 2.10e: Silty/sandy, restricted marine platform cycle

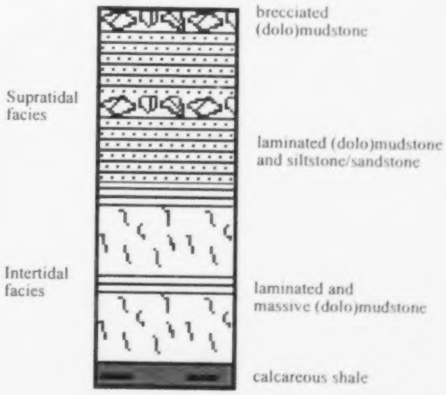
Supratidal facies
Intertidal facies
brecciated (dolo)mudstone
laminated (dolo)mudstone and siltstone/sandstone
laminated and massive (dolo)mudstone
calcareous shale

production. This basal shale is overlain by a thick succession of subtidal platform carbonates (Fig. 2.10b). The top of each cycle is characterized by a thin cap of laminated and/or algal-laminated, intertidal carbonates. Lithofacies suggesting extremely restricted conditions and indicators for subaerial exposure are generally absent.

In the upper members of the Grosmont Formation the character of carbonate platform successions changes progressively from mainly subtidal to predominantly peritidal deposits. This change is documented in shallowing upward cycles which contain progressively less subtidal and more peritidal deposits. Cycles dominated by peritidal deposits range between 5 and 15 meters in thickness and begin with a thin or patchy argillaceous carbonate layer followed by restricted marine, shallow subtidal deposits and a thick peritidal unit. The composition of this peritidal unit changes from clean carbonates (Fig. 2.10c) in the UG 6 (UGM 1) and UG 7 (UGM 2) to anhydritic (Fig. 2.10d) and silty/sandy carbonates (Fig. 2.10e) in the UG 8 (UGM 3a) and UG 9 (UGM 3b).

This progressive shallowing trend of the Woodbend shelf is also evident from the areal distribution of carbonate facies belts. In lower units of the Woodbend Group, i.e. in the LCL 1, UCL 2 and LG 5, carbonate platforms consist exclusively of subtidal realms (Figs. 2.12, 2.13, legend Fig. 2.11). Carbonate platforms of the upper Grosmont Formation (UG 6, UG 7, UG 8, UG 9), however, are characterized by the progressively increasing extent of southward prograding tidal flats (Figs. 2.12, 2.13). This trend culminates in the UG 9 (UGM 3b) with tidal flats covering almost the entire carbonate platform and subtidal conditions being restricted to the platform margin. The extent of evaporitive conditions and influence of terrigeneous siliciclastics also increases progressively in the upper Grosmont Formation, reaching their greatest extent on the UG 9 (UGM 3b) tidal flats (Figs. 2.12, 2.13). Brecciated carbonates, interpreted as exposure breccias, occur frequently in this unit (Luo et al., 1992), but are generally absent in older units.

The above described general shallowing trend of the Woodbend shelf ends above the UG 9 (UGM 3b) unit. Platform-wide peritidal deposition is abruptly terminated across a single surface that separates peritidal deposits of the UG 9 (UGM 3b) from deep subtidal, argillaceous deposits of the UI 10 (upper Ireton Formation). This surface as well as argillaceous deposits of the UI 10, however, are commonly missing in the northern part

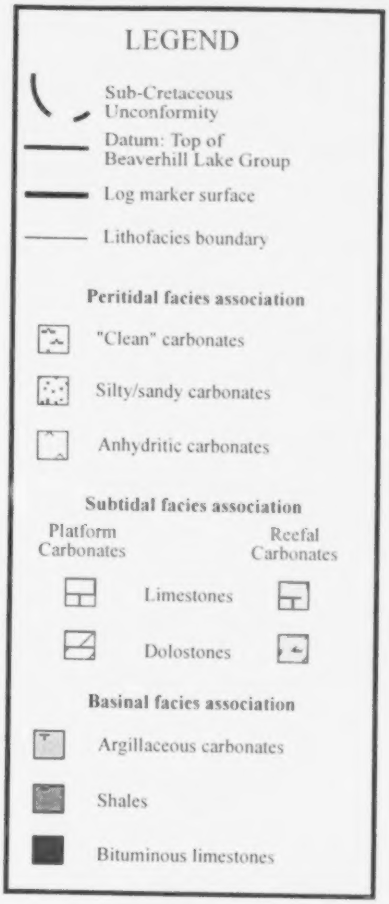
LEGEND
Sub-Cretaceous Unconformity
Datum: Top of Beaverhill Lake Group
Log marker surface
Lithofacies boundary
Peritidal facies association
"Clean" carbonates
Silty/sandy carbonates
Anhydritic carbonates
Subtidal facies association
Platform Carbonates
Reefal Carbonates
Limestones
Dolostones
Basinal facies association
Argillaceous carbonates
Shales
Bituminous limestones

Fig. 2.11: Legend for stratigraphic cross-section A-A' (Fig. 2.12, and B-B' (Fig. 2.13).

Fig. 2.12 (opposite page)**:** North-south gamma ray cross section through the Woodbend Group of north-central Alberta. This cross section follows approximately the eastern edge of the study area. For location of cross section A-A' see Fig. 2.2.

Fig. 2.13 (page 46)**:** North-south gamma ray cross section through the Woodbend Group in north-central Alberta. This section follows the northern extension of the Rimbey-Meadowbrook reef trend from the northern edge of the study area to the Morinville reef in the south. For location of cross section B-B' see Fig. 2.2.

Fig. 2.12: Stratigraphic N-S cross section A-A'

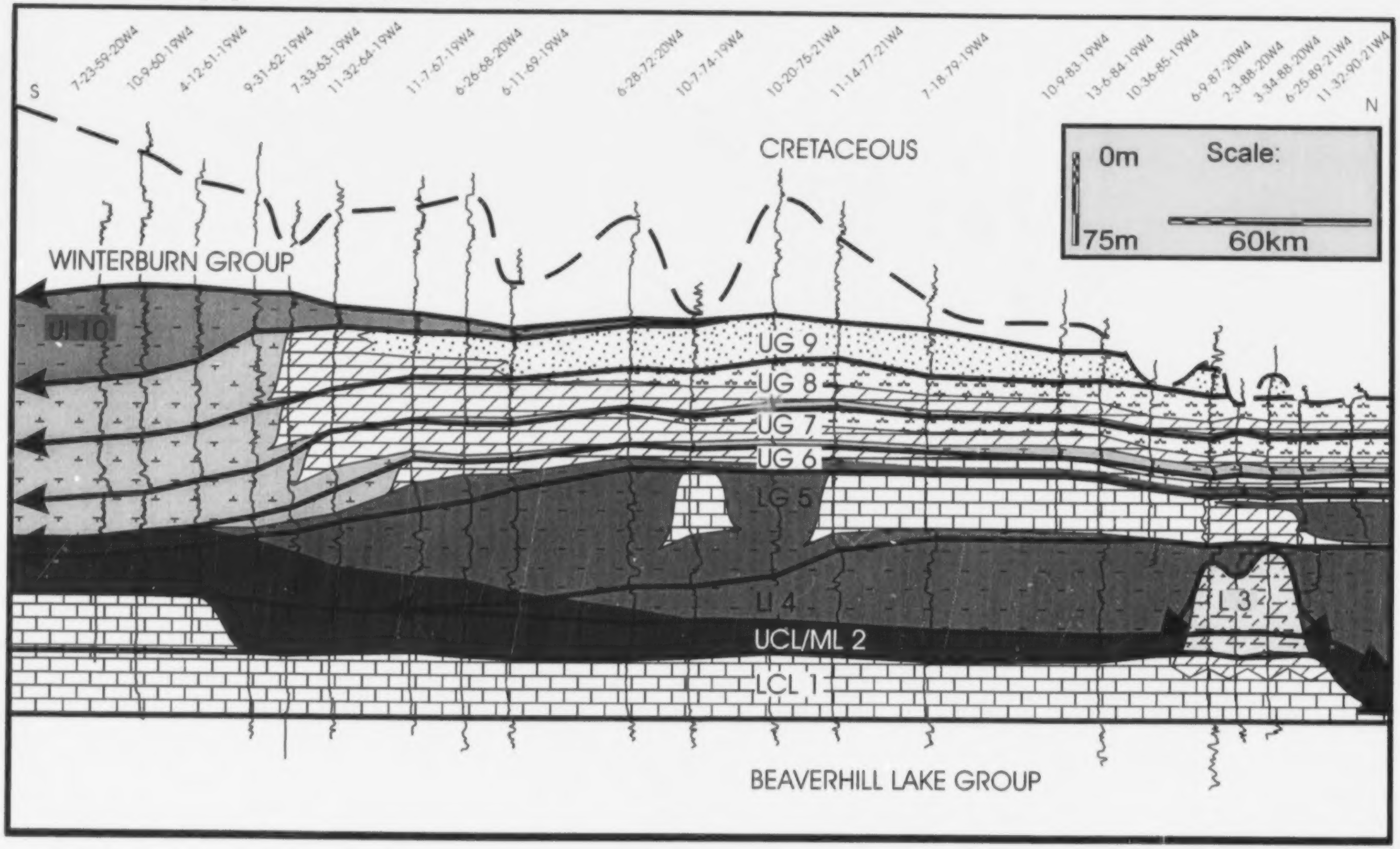
S
7-23-59-20W4
10-9-60-19W4
4-12-61-19W4
9-31-62-19W4
7-33-63-19W4
11-32-64-19W4
11-7-67-19W4
6-26-68-20W4
6-11-69-19W4
6-28-72-20W4
10-7-74-19W4
10-20-75-21W4
11-14-77-21W4
7-18-79-19W4
10-9-83-19W4
13-6-84-19W4
10-36-85-19W4
6-9-87-20W4
2-3-88-20W4
3-34-88-20W4
6-25-89-21W4
11-32-90-21W4
N
CRETACEOUS
Scale:
0m
75m
60km
WINTERBURN GROUP
UI 10
UG 9
UG 8
UG 7
UG 6
LG 5
LI 4
L 3
UCL/ML 2
LCL 1
BEAVERHILL LAKE GROUP

Fig. 2.13: Stratigraphic N-S cross section B-B'

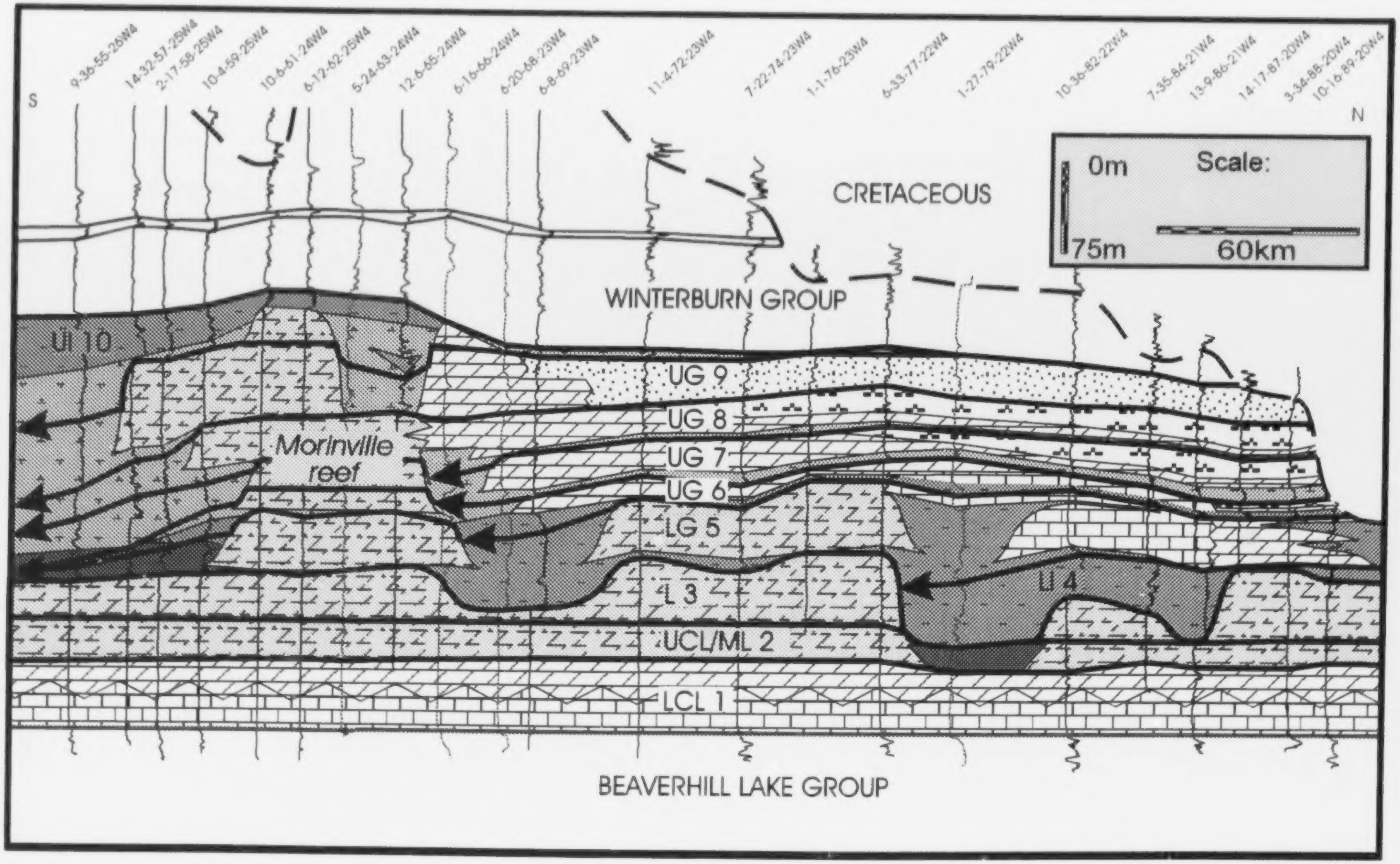
S
N
9-36-55-26W4
14-32-57-25W4
2-17-58-25W4
10-4-59-25W4
10-6-61-24W4
6-12-62-25W4
5-24-63-24W4
12-5-65-24W4
6-16-66-24W4
6-20-68-23W4
6-8-69-23W4
11-4-72-23W4
7-22-74-23W4
1-1-76-23W4
6-33-77-22W4
1-27-79-22W4
10-36-82-22W4
7-35-84-21W4
13-9-86-21W4
14-17-87-20W4
3-34-88-20W4
10-16-89-20W4
0m
Scale:
75m
60km
CRETACEOUS
WINTERBURN GROUP
UI 10
UG 9
UG 8
UG 7
UG 6
LG 5
Morinville reef
L 3
UI 4
UCL/ML 2
LCL 1
BEAVERHILL LAKE GROUP

of the study area (Figs 2.12, 2.13). Instead, the UG 9 (UGM 3b) is directly overlain by shallow water carbonates of the Nisku Formation (Winterburn Group).

Trends in basinal sedimentation

Basinal deposits of the Woodbend Group in the study area display both, a general shallowing trend of the Woodbend shelf as well as several changes in the lithological composition of basinal deposits. Basinal deposits of the lowermost Woodbend Group, the Majeaux Lake Member of the Cooking Lake Formation (LCL 1 and UCL/ML 2) consist of basinal limestones and bituminous limestones (Figs. 2.12, 2.13) that contain only small amounts of argillaceous material.

This pattern of basinal sedimentation, which can be characterized as starved basin sedimentation, changes with the influx of large amounts of argillaceous material of the lower Ireton Formation (Figs. 2.12, 2.13). Green shales are the dominant lithology of this formation (basinal lithofacies of the L 3 (?), LI 4, and LG 5 units). The generally low (<10 %) carbonate content is likely related to the lack or small size of adjacent carbonate producing areas (L 3 and LI 4 units) and/or to a lack of carbonate sediment transported off the platform (LG 5 unit). The introduction of clastic material onto the Woodbend shelf had several drastic implications. Shale deposits formed a southward prograding clastic wedge that pushed the realm of starved basin sedimentation southward (Fig. 2.13) and covered the northern Leduc reefs, essentially eliminating carbonate production in the northern part of the study area. The formation of a clastic wedge also changed the general shelf bathymetry, creating a northern shallow shelf area while the southern part remained basinal. In the northern part of the study area shale deposition is abruptly terminated across a single hardground surface that separates lower Ireton shales from LGM carbonates. In the southern part of the study area shale deposition continued.

Successions of basin-filling sediments equivalent to the upper members of the Grosmont Formation (basinal lithofacies of the UG 6, UG 7, UG 8 and UG 9 units; Figs. 2.12, 2.13) gradually change from shales to calcareous shales and argillaceous carbonates (carbonate content >30%). The carbonate material in these basinal sediments was likely derived from the adjacent Grosmont platform. Carbonates appear to have been introduced into the basinal environment as fine carbonate suspension (Stoakes, 1980; Cutler, 1983) and as coarser material during gravity flows (calciturbidites of Stoakes, 1980) or storm events. In the uppermost Woodbend Group (UI 10 unit) the carbonate content of basinal deposits gradually decreases again (Figs. 2.12, 2.13), probably as a result of reduced carbonate production on the Grosmont platform.

STAGES OF SHELF DEVELOPMENT

Stage 1.- Carbonate platform backstepping

This stage describes the transgressive phase of the Woodbend Group in north-central Alberta. It includes the lowermost three units, i.e. the LCL 1 (lower Cooking Lake; Fig. 2.14a), the UCL/ML 2 (upper Cooking Lake/Majeaux Lake; Fig. 2.14b) and the L 3 (Leduc; Fig. 2.15a). These periods are characterized by several relative sea level rises that interrupt sedimentation and cause widespread backstepping of carbonate platforms.

The beginning of the LCL 1 unit was characterized by a relative sea level fall (Wendte, 1992) that established an open marine carbonate platform on top of the argillaceous sediments of the Waterways Formation (Beaverhill Lake Group). During the subsequent relative sea level rise the Cooking Lake platform prograded and reached its maximum extent covering much of the area that was formerly occupied by the Waterways ramp. The lower Cooking Lake platform, which includes two shallowing upward cycles (Wendte, 1974), consists of clean, open marine, shallow water carbonates. Intertidal conditions, however, were rare throughout the platform area. The western part of the study area is occupied by bituminous deep water limestones. Argillaceous sediments are nearly absent.

During the deposition of the LCL/ML 2 unit the relative rise in sea level outpaced carbonate production in most of the study area. Only the southernmost portion underwent continuous platform development. Along the former western margin of the lower Cooking Lake platform carbonate sedimentation continued and established the string of shoals and stromatoporoid biostromes of the northern Rimbey-Meadowbrook reef trend. Basinal areas east and west of the reef trend are occupied by dark, bioturbated to laminated, bituminous,

Fig. 2.14a: Lithofacies map of LCL 1 unit

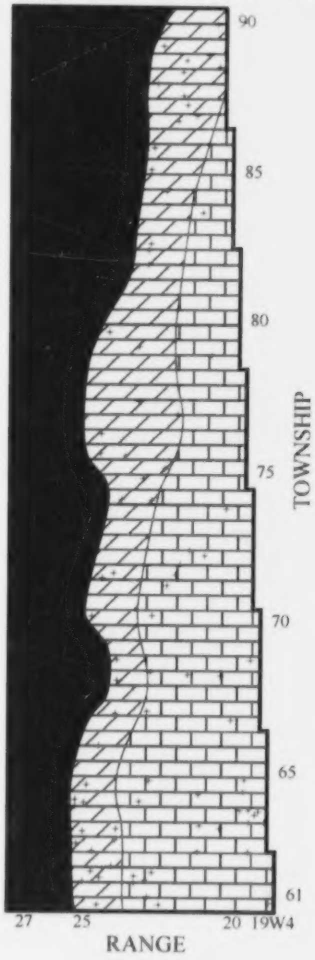
90
85
80
75
70
65
61
TOWNSHIP
27
25
20
19W4
RANGE

Fig. 2.14b: Lithofacies map of UCL/ML 2 unit

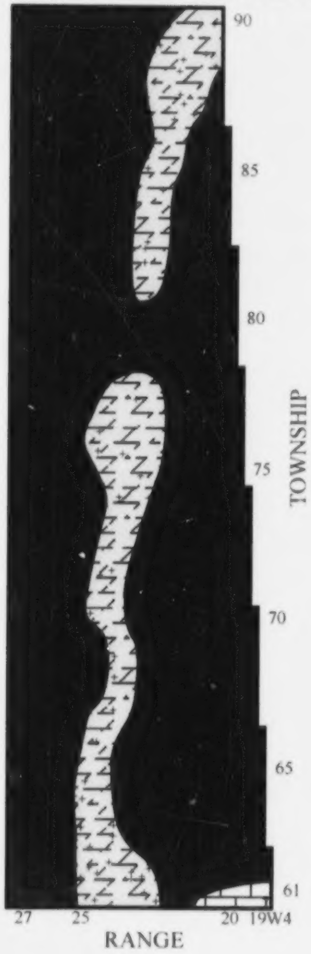
90
85
80
75
70
65
61
TOWNSHIP
27
25
20
19W4
RANGE

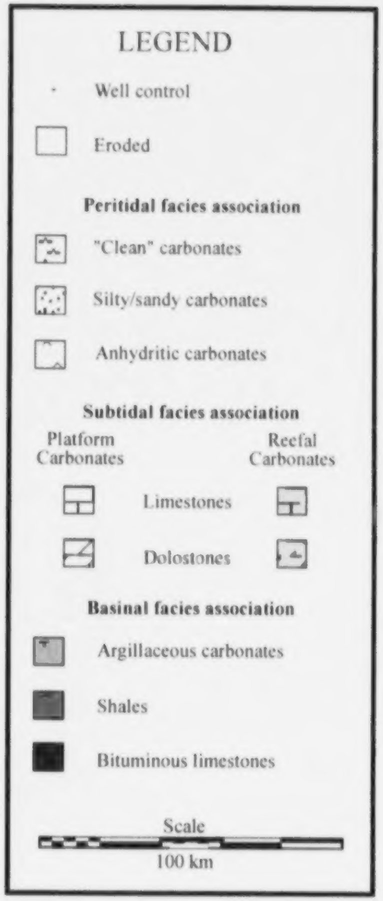
LEGEND
Well control
Eroded
Peritidal facies association
"Clean" carbonates
Silty/sandy carbonates
Anhydritic carbonates
Subtidal facies association
Platform Carbonates
Reefal Carbonates
Limestones
Dolostones
Basinal facies association
Argillaceous carbonates
Shales
Bituminous limestones
Scale
100 km

Fig. 2.15a: Lithofacies map of L 3 unit

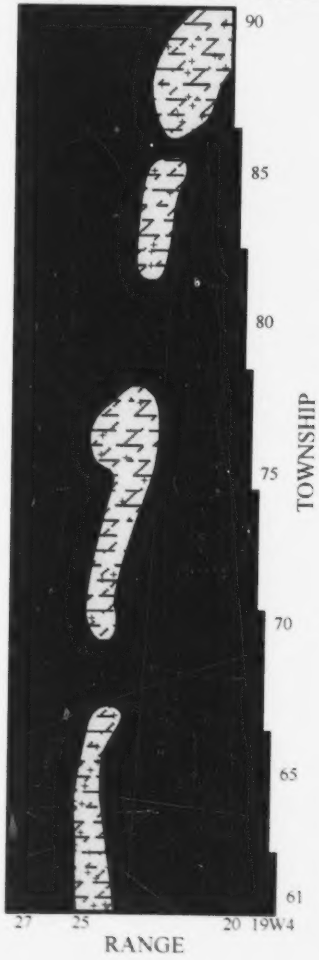
90
85
80
75
70
65
61
TOWNSHIP
27
25
20
19W4
RANGE

Fig. 2.15b: Lithofacies map of LI 4 unit

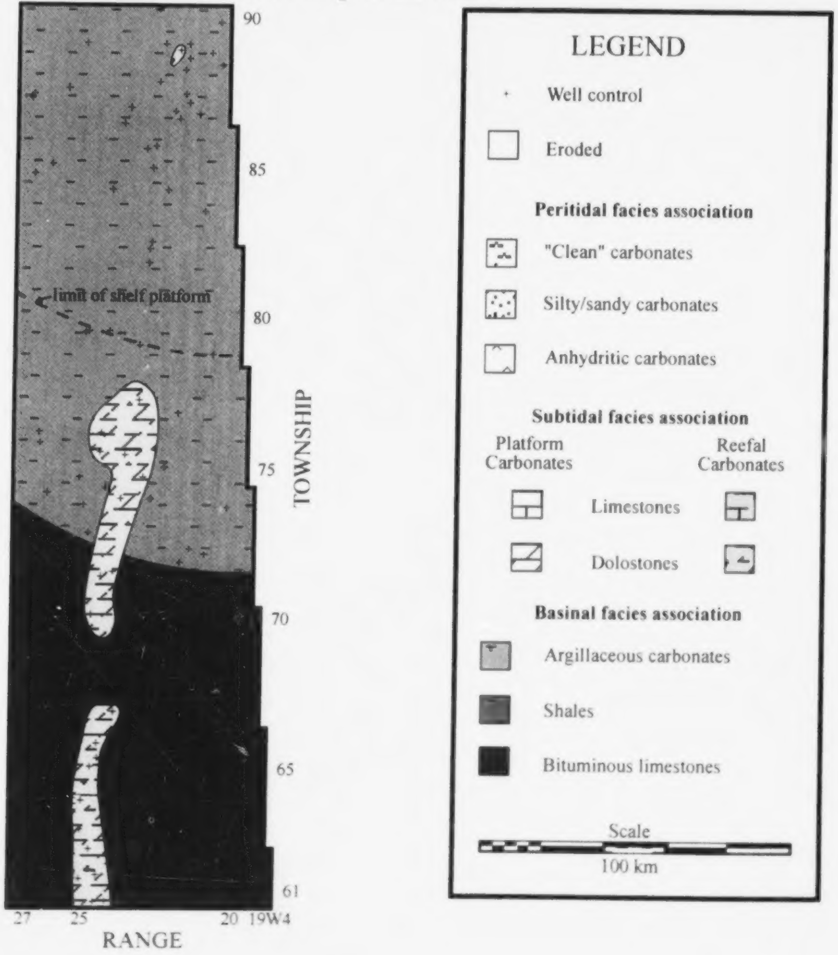
limit of shelf platform
90
85
80
75
70
65
61
TOWNSHIP
27
25
20
19W4
RANGE
LEGEND
Well control
Eroded
Peritidal facies association
"Clean" carbonates
Silty/sandy carbonates
Anhydritic carbonates
Subtidal facies association
Platform Carbonates
Reefal Carbonates
Limestones
Dolostones
Basinal facies association
Argillaceous carbonates
Shales
Bituminous limestones
Scale
100 km

deep water limestones and minor shales of the Majeaux Lake Member.

Further rapid rise of relative sea level caused termination of Cooking Lake platform growth throughout the study area. This so-called L 3 unit marks the furthest incursion of open marine conditions and the greatest relief difference between carbonate banks and basin deposits during Woodbend deposition. Carbonate sedimentation only continued along the former platform margin and above shoals in what used to be the interior platform. These locations underwent stabilization and colonization by crinoids, stromatoporoids and corals and were the nuclei for reef growth during the Woodbend cycle. At the same time basinal sedimentation appears to have remained very slow and only a condensed section of dark, bituminous limestones and minor shales accumulated.

Phase 2.- Initiation of clastic sedimentation

This stage, which consists of the LI 4 (lower Ireton) unit, is characterized by an abrupt change in sedimentation patterns, possibly as a result of e drop in sea level or due to increased clastic input. Large amounts of green shales were introduced from northerly sources and began to infill the northern portions of the Woodbend shelf. The northern half of the study area which was occupied by deep water limestones was subsequently covered by shales (Fig. 2.15b). Shale sedimentation resulted in gradual shallowing and eliminated the previous basinal topography in this area. Furthermore, it caused termination of reef growth and effectively blanketed most of the Leduc reefs north of township 78. At the end of this stage shale sedimentation appears to have been interrupted, possibly as a result of a sea level rise and resulting shut-off of clastic input, resulting in the development of a hardground surface that can be widely traced throughout the study area. Towards the south the effect of clastic input decreases. Lower Ireton shales thin out and grade into bituminous, deep water shales and limestones of the Duvernay Formation. Southern Leduc reefs also remained unaffected.

Phase 3.- Initiation and catch-up of carbonate platform sedimentation

Infill and shallowing of the Woodbend shelf by shales brought much of the northern shelf back into the carbonate production zone. Carbonate platforms were initiated in the shallowest part of the siliciclastic shelf and over several Leduc reefs. It was during the deposition of LG 5 (LGM) unit (Fig. 2.16a) that the familiar Woodbend sedimentation pattern was initiated.

The shallow water platform is characterized by mainly open marine carbonates and argillaceous carbonates that were deposited during three shallowing upward cycles. The LGM platform consists of carbonate muds, sands and reefal deposits that display an abundance of marine biota. Restricted and evaporitic conditions were confined to the uppermost portion of each shallowing upward cycle and to the northeastern part of the platform. Towards the south where the basinal relief was still prominent platform sedimentation was absent and pure carbonate production was restricted to the Rimbey-Meadowbrook reef trend. Shale deposition continued on the platform slope and in former shelf depressions which form the so-called shale embayments (Fig. 2.16a). Deep basinal settings are characterized by sediment starvation and the resulting deposition of bituminous limestones and shales.

Phase 4.- Carbonate platform progradation

This phase in shelf development constitutes the UG 6 (UGM 1), UG 7 (UGM 2) and UG 8 (UGM 3a) units. It was characterized by periodic, moderate, relative sea level rises as well as rapid outward progradation and shallowing of the carbonate platform.

During deposition of the UG 6 (UGM 1) all depressions in the lower Grosmont platform were levelled and carbonates prograded rapidly towards the south and west (Fig. 2.16b). Conditions on the platform appear to have been semi-restricted, i.e. evaporitic conditions were absent but the diversity of platform biota and the number of patch reefs decreased considerably.

Fully restricted conditions, however, dominated most of the carbonate platform during the deposition of the UG 7 (UGM 2) and UG 8 (UGM 3a) units (Figs. 2.17a, 2.17b). Platform progradation slowed down and instead carbonates and shales were transported off the platform into adjacent basinal areas. This outward transport was responsible for the increased infill of the Woodbend shale basins and the retreat of starved, basinal conditions to the southernmost part of the study area and eventually into central Alberta. Sediment input from the platform into the southern basin may also account for the termination of Leduc reefs that are encountered during platform

Fig. 2.16a: Lithofacies map of LG 5 unit

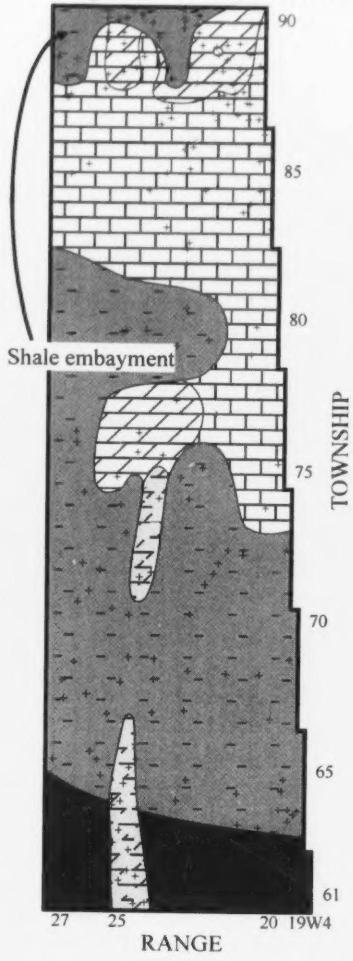
90
85
80
75
70
65
61
TOWNSHIP
27
25
20
19W4
RANGE
Shale embayment

Fig. 2.16b: Lithofacies map of UG 6 unit

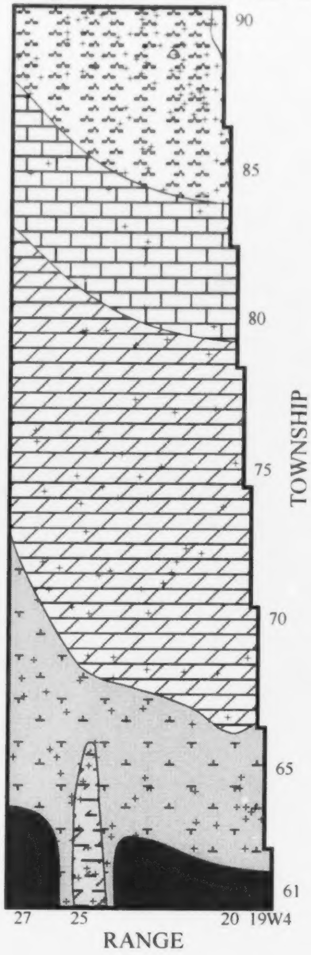
90
85
80
75
70
65
61
TOWNSHIP
27
25
20
19W4
RANGE

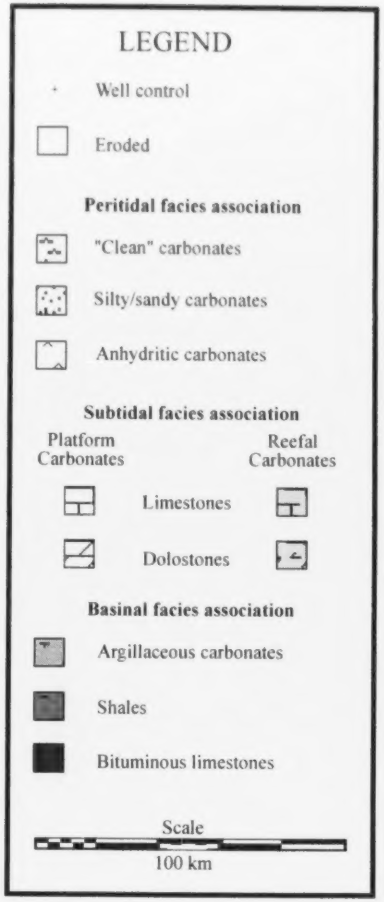
LEGEND
Well control
Eroded
Peritidal facies association
"Clean" carbonates
Silty/sandy carbonates
Anhydritic carbonates
Subtidal facies association
Platform Carbonates
Reefal Carbonates
Limestones
Dolostones
Basinal facies association
Argillaceous carbonates
Shales
Bituminous limestones
Scale
100 km

Fig. 2.17a: Lithofacies map of UG 7 unit

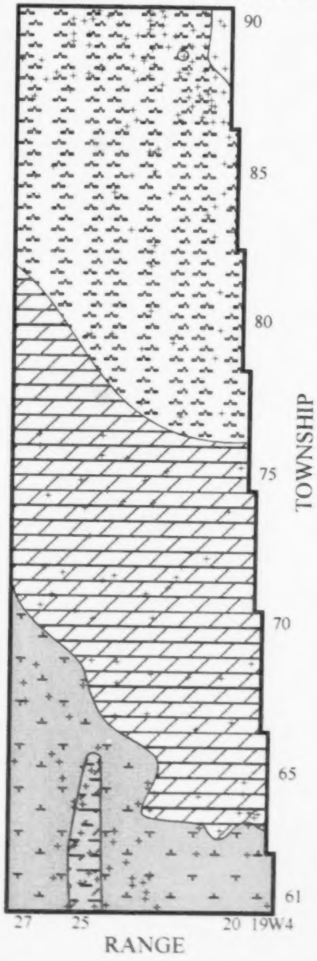

90
85
80
75
70
65
61
TOWNSHIP
27
25
20
19W4
RANGE

Fig. 2.17b: Lithofacies map of UG 8 unit

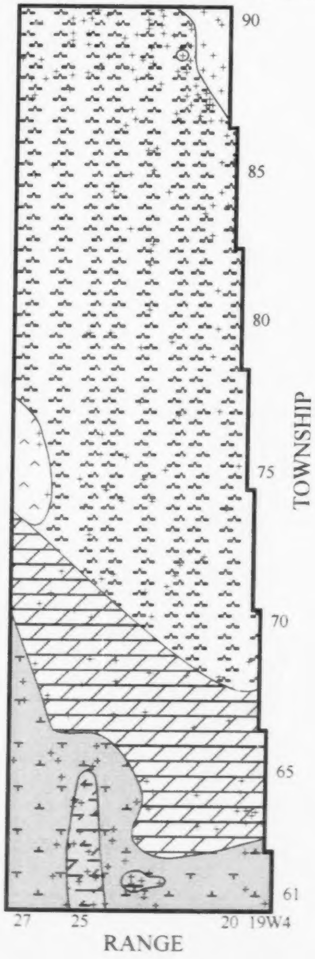

90
85
80
75
70
65
61
TOWNSHIP
27
25
20
19W4
RANGE

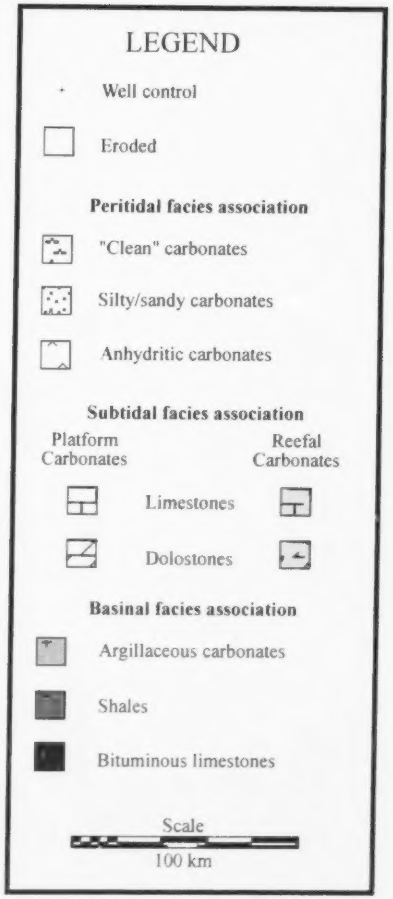

LEGEND
Well control
Eroded
Peritidal facies association
"Clean" carbonates
Silty/sandy carbonates
Anhydritic carbonates
Subtidal facies association
Platform Carbonates
Reefal Carbonates
Limestones
Dolostones
Basinal facies association
Argillaceous carbonates
Shales
Bituminous limestones
Scale
100 km

progradation and the maintenance of a "shale" gap between the Grosmont platform and the Rimbey-Meadowbrook reef trend. Basin infill also had immediate effects on the reef growth of adjacent Leduc buildups such as the Redwater and Morinville reefs. Because of the shallowing of the outer shelf, areas surrounding reefs entered the carbonate production zone which in turn initiated progradation of these isolated carbonate buildups. Conditions also appear to have been shallow enough or otherwise more suitable for autochthonous carbonate production allowing initiation of a small, isolated reef south of the Grosmont platform (Figs. 2.17b, 2.18a and 2.19). A second possible interpretation of the available core and well log data is that a narrow bridge between the Grosmont platform and the Morinville reef existed. The isolated reef interpretation, however, is favored because both the main platform and the reef trend are pervasively dolomitized, whereas reefal carbonates in the Grosmont embayment remained limestones. This situation may, therefore, be analogous to isolated reefs such as Golden Spike and Redwater (Andrichuk, 1958; Illing, 1959).

Phase 5.- Mixed carbonate-siliciclastic deposition

During this stage, which consists of the UG 9 (UGM 3b) unit, the Grosmont platform reached its maximum extent (Fig. 2.18a) and the remarkably uniform carbonate platform of the UG 6 (UGM 2) and UG 7 (UGM 3a) disintegrated into several distinct depositional realms. The central and northern parts of the study area were dominated by peritidal carbonates and interbedded aeolian siltstones and sandstones, which display abundant evidence for subaerial exposure and reworking of platform sediments. The western portion of the shelf is covered by anhydritic carbonates. Cutler (1983) suggested that these anhydritic carbonates originated in a shallow-subaqueous environment that underwent occasional subaerial exposure. This evaporitic setting may have extended further east. Abundant collapse breccias and the abrupt thinning of the UGM 3 (a and b) towards east suggest that evaporites were removed from that area. The southern portion of the Grosmont platform is covered by bioturbated, argillaceous carbonates which display a low faunal diversity and are interpreted to have a restricted, lagoonal origin. Clean carbonates were only deposited along the platform margins. Although cores from this zone do not exist the clean gamma ray signature of the platform margin and abundant

Fig. 2.18a: Lithofacies map of UG 9 unit

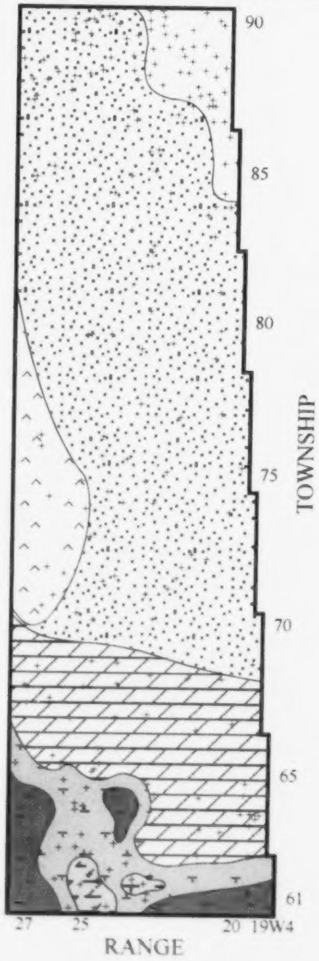
90
85
80
75
70
65
61
TOWNSHIP
27
25
20
19W4
RANGE

Fig. 2.18b: Lithofacies map of UI 10 unit

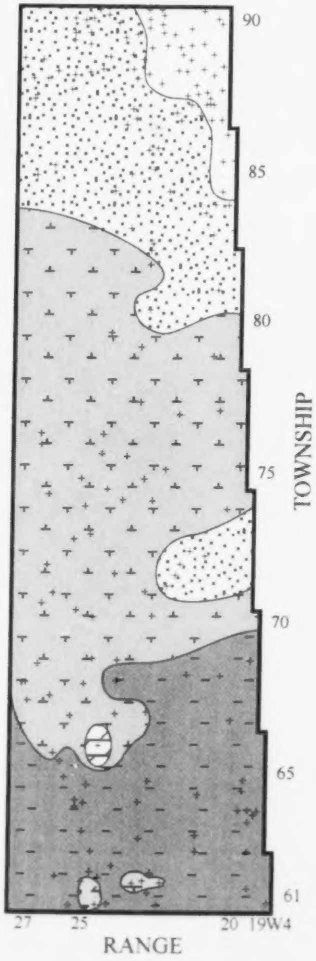
90
85
80
75
70
65
61
TOWNSHIP
27
25
20
19W4
RANGE

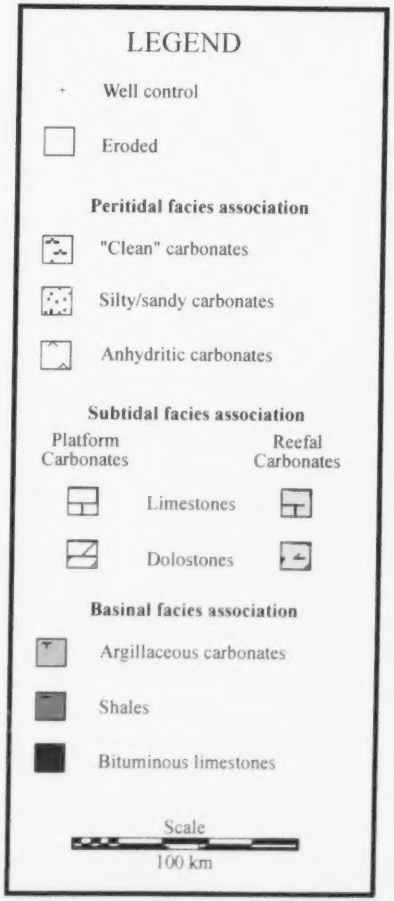
LEGEND
Well control
Eroded
Peritidal facies association
"Clean" carbonates
Silty/sandy carbonates
Anhydritic carbonates
Subtidal facies association
Platform Carbonates
Reefal Carbonates
Limestones
Dolostones
Basinal facies association
Argillaceous carbonates
Shales
Bituminous limestones
Scale
100 km

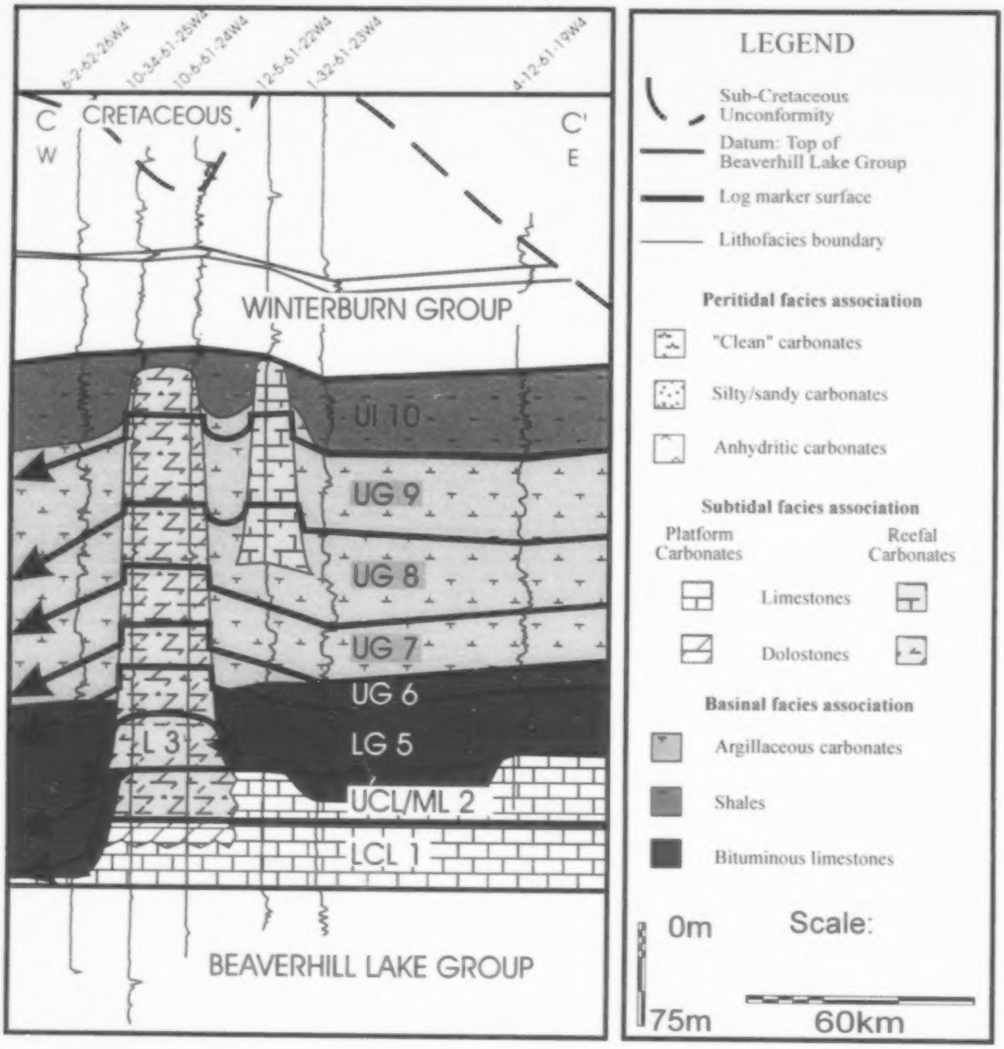
6-2-62-26W4
10-34-61-25W4
10-6-61-24W4
12-5-61-22W4
1-32-61-23W4
4-12-61-19W4
C
W
C'
E
CRETACEOUS
WINTERBURN GROUP
UI 10
UG 9
UG 8
UG 7
UG 6
LG 5
L 3
UCL/ML 2
LCL 1
BEAVERHILL LAKE GROUP
LEGEND
Sub-Cretaceous Unconformity
Datum: Top of Beaverhill Lake Group
Log marker surface
Lithofacies boundary
Peritidal facies association
"Clean" carbonates
Silty/sandy carbonates
Anhydritic carbonates
Subtidal facies association
Platform Carbonates
Reefal Carbonates
Limestones
Dolostones
Basinal facies association
Argillaceous carbonates
Shales
Bituminous limestones
0m
75m
Scale:
60km

Fig. 2.19: East-west cross section of the Woodbend shelf along the southern edge of the study area (Fig. 2.2). Shown are the mainly basinal areas and two reef bodies. The main dolostone reef in the east, sitting directly on the Cooking Lake platform is the Morinville buildup. The smaller limestone buildup in the west is the reef at the south entrance of the Grosmont embayment (Fig. 2.17b, 2.18a). This cross section interprets the limestone reef to be an isolated carbonate buildup which was incepted during UG 8 (UGM 3a) deposition.

stromatoporoids and corals found in gravity flow deposits (Fig. 2.9b) of neighboring wells suggest the presence of a (reefal ?) platform rim.

In the basinal areas calcareous shale deposition and the subsequent shallowing of the East-Shale Basin continued during this period. The Grosmont platform engulfed the northern part of the Morinville reef forming the so called Grosmont embayment. Argillaceous sediments covered parts of the Morinville reef causing termination of reef growth in its northern section. At the same time the Morinville reef resumed its southward progradation (Figs. 2.12, 2.13). The southward shift of carbonate deposition also prompted the "shale" gap or embayment between the Grosmont platform and the Morinville reef to move. For the most part, this embayment is characterized by calcareous shale and calciturbidite deposition and deeper water conditions prevailed throughout this period.

Phase 6.- Siliciclastic basin-fill

This last phase of Woodbend Group sedimentation, which this study refers to as UI 10 unit (upper Ireton; Fig. 2.18b), is characterized by siliciclastic infill of much of the shale basins. Throughout the study area and the rest of the Woodbend basin in Alberta carbonate production and deposition was at first restricted to small areas and then completely terminated. Carbonate platforms and reefs undergo backstepping and were finally covered by Ireton Formation shales.

On the Grosmont platform, especially north of township 75, upper Ireton sediments are thin, patchy or completely missing. On the other hand the overlying Nisku Formation increases in thickness from 40 to 50 meters in the central basin area to some 90 meters above the Grosmont platform. This suggests that the contact between the Woodbend and Winterburn Groups may be diachronous in this area (see also Cutler, 1983) and that the lower portion of the Nisku Formation in north-central Alberta is time equivalent to the uppermost Ireton basin-fill strata in central Alberta.

CONTROLS ON SHELF DEVELOPMENT

The deposition of the Woodbend Group occurred along a tectonically quiet portion of the passive continental margin of western North America. This tectonic quiescence makes it likely that Woodbend depositional history was governed largely by eustatic fluctuations. Indeed, Woodbend Group sedimentation appears to coincide well with the published eustatic sea level curve (Johnson et al., 1985). There may, however, be some circular reasoning in this interpretation because Alberta was one of the reference areas during the study of Devonian eustasy. Alternatively, a change in subsidence rates from fast to slow, overprinted by eustatic sea level fluctuations, could have produced a similar sedimentation pattern.

The history of sea level fluctuations during Woodbend Group deposition (T-R cycle IIc of Johnson et al., 1985) (Fig. 2.20) can be divided into four phases that correlate to one or several stages in Woodbend shelf development. The first phase is characterized by a sea level fall, which is believed to have initiated the Cooking Lake platform (Wendte, 1974; 1992), followed by a rapid sea level rise (Fig. 2.20). This sea level rise resulted in the backstepping and drowning of carbonate platforms (see stage 1 of Woodbend shelf development), the break-up of the Cooking Lake platform and the formation of the Rimbey-Meadowbrook reef trend and its northern extension, which can be interpreted as a raised platform rim (cf. Schlager, 1992).

The following, second phase is characterized by an overall sea level stillstand and (possible) sea level fall (Fig. 2.20) and is interpreted to be equivalent to stage 2 (clastic sedimentation) and possibly stage 3 (initiation and catch-up of carbonate platform sedimentation) of Woodbend shelf development. Significant clastic input started during this phase and it is possible that this sea level stillstand, and perhaps the subsequent lowering of sea level, were responsible for the initiation of clastic sedimentation. This interpretation implies that the LI 4 unit (lower Ireton Formation) represents a low-stand clastic wedge (cf. Switzer et al., 1994; Wendte et al., 1995). That a possible sea level drop was not recorded as an unconformity may be due to the basinal position of the study area or the fact that subsidence counterbalances sea level falls, thereby masking their effects (Playford et al., 1989). However, other factors, such as climate changes,

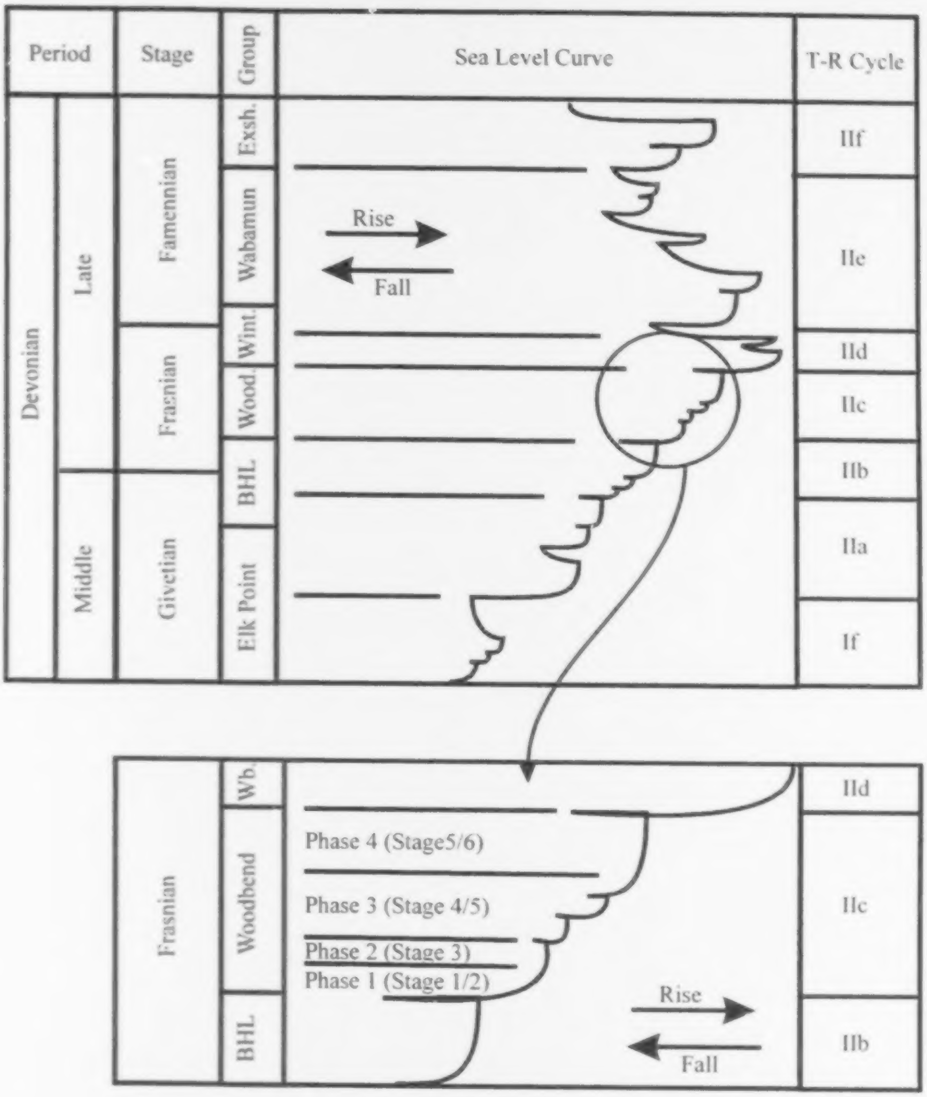
Period
Stage
Group
Sea Level Curve
T-R Cycle
Devonian
Late
Middle
Famennian
Frasnian
Givetian
Exsh.
Wabamun
Wint.
Wood.
BHL
Elk Point
Rise
Fall
IIf
IIe
IId
IIc
IIb
IIa
If
Frasnian
Wb.
Woodbend
BHL
Phase 4 (Stage5/6)
Phase 3 (Stage 4/5)
Phase 2 (Stage 3)
Phase 1 (Stage 1/2)
Rise
Fall
IId
IIc
IIb

Fig. 2.20: Eustatic sea level curve for the Givetian to Famennian of Euramerica (modified after Johnson et al., 1985). The bottom graph shows an enlargement of the Woodbend part of the sea level curve (T-R cycle IIc) and its relationship to the interpreted phases in shelf development (see text).

availability of new transport paths and mechanisms, as well as hinterland tectonics (e.g. the Ellesmerian orogeny; Stoakes, 1992) may also have influenced clastic input.

Step-wise, gradual rises in sea level characterize the third phase of middle Frasnian eustatic history (Fig. 2.20), which is interpreted to be equivalent to stages 3 and 4 (carbonate platform progradation) of Woodbend shelf development. The step-wise rises in sea level are represented in the rock record by the Grosmont shallowing upward cycles (Cutler, 1983). Carbonate production of the Grosmont platform, however, appears to have easily outpaced each rise in sea level. This resulted in the southward progradation of the carbonate platform as well as in basinward transport of carbonate material as indicated by the calcareous character of age equivalent basin-fill strata (Figs. 2.12, 2.13).

A second prolonged sea level stillstand and subsequent sea level fall followed by a sea level rise characterizes the fourth phase of middle Frasnian eustasy (Fig. 2.20). This phase is interpreted to be equivalent to stages 5 (mixed carbonate-siliciclastic sedimentation) and 6 (clastic basin-fill) of Woodbend shelf development. The postulated sea level stillstand is consistent with the fact that Grosmont carbonate production rapidly approached sea level. This resulted in the prograding of extended tidal flats and the subaerial exposure of parts of this tidal flat as indicated by the development of extensive brecciated layers at the top of the UG 9 (UGM 3b) unit. The abrupt change from peritidal to deep subtidal deposition is interpreted to reflect the following sea level rise.

Woodbend shelf development in the study area is unique in that the shallowing of the shelf and the progradation of shallow water sediments appear to have started earlier than in other areas. This suggests that sea level was not the only factor controlling shelf development. In other parts of the basin (e.g. Southern Alberta Shelf) Woodbend carbonate complexes did only keep up with sea level and did not prograde significantly into basinal areas (Switzer et al., 1994). It appears that the basinal relief was too great to allow initiation of new carbonate production areas. Significant input of siliciclastics in the study area created a shallow shelf environment while other areas still experienced deep water conditions. The origin of the siliciclastic material and the mode of transport from its source to the Woodbend shelf are debatable. Stoakes (1980; 1992) favored a submarine transport by currents from the area of the Ellesmerian orogeny. Alternatively, clastic material may have been sourced from the Canadian Shield and/or wind and river transport may have contributed to basin-fill and shelf clastics. An aeolian origin appears to be likely for silts and sands present in the UG 9 (UGM 3b) unit.

The result of the deposition of the lower Ireton clastic wedge was the creation of a large shallow shelf area (Figs. 2.12, 2.13, 2.15b) in the northern part of the study area. Apparently, this area was shallow enough to allow carbonate production resulting in the nucleation of the (lower) Grosmont platform (LG 4 unit; Fig. 2.16a). The presence of a widespread hardground surface between the lower Ireton Formation and the LGM indicates that input of clastic material decreased or even stopped for an extended period of time, allowing for ideal conditions for carbonate production. Similar to the situation described above, the initiation of the small Grosmont embayment reef (Figs. 2.17b, 2.19) and the progradation of larger Leduc buildups, such as Redwater and Morinville (Fig. 2.13), was probably helped by the infilling and shallowing of the Eastern Shale Basin and Grosmont embayment.

Fluctuations in carbonate production appear to have been an additional factor in Woodbend shelf development. Once carbonate production was initiated, the Grosmont carbonate platform prograded rapidly as long as much of the platform remained under shallow water, yet open marine conditions. Gradual, step-wise sea level rises, as evident in the LG 5 (LGM), UG 6 (UGM 1), UG 7 (UGM 2) and UG 8 (UGM 3a) units, ensured a large subtidal carbonate factory (James, 1984b; Read, 1989) with sufficient accommodation space to supply abundant amounts of carbonates for platform progradation and winnowing of carbonate sediment into basinal areas. Progradation of tidal flats, however, most evident during in the UG 8 (UGM 3a) and UG 9 (UGM 3b) units, caused the subtidal carbonate factory to shrink (cf. Ginsburg, 1971) and, therefore, inhibited and slowed further progradation of the Grosmont platform (Figs. 2.12, 2.13).

It appears that fluctuations in carbonate production also partially controlled the amount of siliciclastic in Grosmont platform lithofacies. The presence of fine siliciclastics in peritidal and deeper subtidal facies indicates a relatively continuous influx of terrigeneous clastics (cf. Osleger and Montanez, 1996). Carbonate production stalled, either because of the effects of a rise in sea level or because of tidal flat progradation and subsequent exposure of platform sediments. Examples of siliciclastic deposits caused by a sea level rise related interruption in carbonate production are the Grosmont shale-breaks.

Silty and sandy carbonates at the top of the UGM 3b are an example for siliciclastic deposits while carbonate production was low due to tidal flat progradation.

CONCLUSIONS

Log marker stratigraphy, facies analysis and mapping of lithofacies distribution suggest that Woodbend shelf development proceeded in six phases. During the first phase a rapid sea level rise caused termination of carbonate and clastic deposition resulting in backstepping of carbonate platforms and buildups and an increase in the topographical relief of the basin. Strong clastic input during the second phase infilled the northern part of the basin and produced a shallow shelf platform which acted as a nucleus for renewed carbonate platform development during the third phase. Carbonate platform progradation progressed rapidly during the fourth phase which was characterized by periodic sea level rises and a large, subtidal carbonate factory. The prolonged sea level stillstand of phases 5 and 6 caused progradation of the tidal flats and widespread exposure of the platform slowing down carbonate production and allowing clastic sedimentation to dominate and eventually terminate platform and reef growth.

This study shows that Woodbend shelf development was controlled by a combination of eustasy (or alternatively, subsidence overprinted by eustasy), and changes in sediment input and production. Clastic sedimentation was important in establishing suitable conditions for carbonate production as well as for the final termination of Woodbend reef and platform growth in the study area. Especially during a sea level stillstand carbonate production was also governed by autocyclic processes which lead to an areal increase in tidal flats and a decrease in subtidal, carbonate producing areas.

REFERENCES

Andrichuk, J.M., 1958, Stratigraphy and facies analysis of Upper Devonian reefs in Leduc, Stettler, and Redwater areas, Alberta. American Association of Petroleum Geologists Bulletin, v. 42, p. 1-93.

Assereto, R.L., and Kendall, C.G.St.C., 1977, Nature, origin and classification of peritidal tepee structures and related breccias. Sedimentology, v. 24, p. 153-210.

Belyea, H.R., 1952, Notes on the Devonian system of the north-central plains of Alberta. Geological Survey of Canada, Paper 52-27.

Cutler, W.G., 1983, Stratigraphy and sedimentology of The Upper Devonian Grosmont Formation, Alberta, Canada. Canadian Bulletin of Petroleum Geology, v. 31, p. 282-325.

Dembicki, E.A., 1994, The Upper Devonian Grosmont Formation: well log evaluation and regional mapping of a heavy oil carbonate reservoir in northeastern Alberta. Unpubl. M.Sc. thesis, University of Alberta, Edmonton, 221 p.

Embry, A.F., and Klovan, J.E., 1971, A Late Devonian reef tract on northeastern Banks Island, Northwest Territories. Bulletin of Canadian Petroleum Geology, v. 19, p. 730-781.

Embry, A.F., and Klovan, J.E., 1972, Absolute water depth limits of the Late Devonian paleoecological zones. Geologische Rundschau, v. 61, p. 672-686.

Ginsburg, R.N., 1971, Landward movement of carbonate mud: new model for regressive cycles in carbonates. American Association of Petroleum Geologists Bulletin, v. 55, p. 340, abstract.

Hardie, L.A., and Ginsburg, R.N., 1977, Layering: the origin and environmental significance of lamination and thin bedding. In: Hardie, L.A., ed., Sedimentation on the modern tidal flats of northwest Andros Island, Bahamas, Johns Hopkins University Press, Baltimore, p. 50-123.

Harrison, R.S., 1982, Geology and production history of the Grosmont carbonate pilot project, Alberta, Canada. In: Meyer, R.F., Wynn, J.C., and Olson, J.C., eds., The future of heavy crude and tar sands. Second International Conference on heavy crude and tar sands, Caracas, Venezuela, February 7-17, 1982, v.1, p. 199-204.

Harrison, R.S., 1984, The bitumen bearing Paleozoic carbonate trends of northern Alberta. In: Meyer, R.F., Early, J.W., Barnea, J., and Johnston, R.L., convs., Exploration for heavy crude oil and bitumen. American Association of Petroleum Geologists Research Conference, Santa Maria, CA, October 28 - November 2, 1984.

Harrison, R.S., and McIntyre, B.G., 1981, The geologic setting of the Grosmont thermal recovery project, northeastern Alberta. Seminar on Advances in Petroleum Recovery and Upgrading Technology, Calgary, Alberta, May 26-28, 1981, 11p.

Illing, L.V., 1959, Deposition and diagenesis of Upper Paleozoic carbonate sediments in Western Canada. 5th World Petroleum Congress, New York, Proceedings Section 1, p. 23-52.

James, N.P., 1984a, Reefs. In: Walker, R.G., ed., Facies models, second edition, Geoscience Canada Reprint Series No. 1, p. 121-133.

James, N.P., 1984b, Shallowing upward sequences in carbonates. In: Walker, R.G., ed., Facies models, second edition, Geoscience Canada Reprint Series No. 1, p. 213-228.

Johnson, J.G., Klapper, G., and Sandberg, C.A., 1985, Devonian eustatic fluctuations in Euramerica. Geological Society of America Bulletin, v. 96, p. 567-587.

Kendall, C.G.St.C, and Warren, J., 1987, A review of the origin and setting of tepees and their associated fabrics. Sedimentology, v. 34, p. 1007-1027.

Klovan, J.E., 1964, Facies analysis of the Redwater reef complex, Alberta, Canada. Bulletin of Canadian Petroleum Geology, v. 12, p. 1-100.

Krebs, W., 1974, Devonian carbonate complexes of central Europe. In: Laporte, L.F., ed., Reefs in time and space. Society of Economic Paleontologists and Mineralogists Special Publication No. 18, p. 155-208.

Logan, B.W., Hoffmann, P., and Gebelein, C.D., 1974, Algal mats, cryptalgal fabrics, and structures Hamelin Pool, Western Australia. In: Logan, B.W., ed., Evolution and diagenesis of quarternary carbonate sequences, Shark Bay, Western Australia. American Association of Petroleum Geologists, Memoir 22, p. 140-194.

Luo, P., Dembicki, E.A., Machel, H.G., and Huebscher, H., 1993, Diagenesis and reservoir characteristics of the heavy-oil carbonate trend in western Canada - refined evaluation of reservoir characteristics of the Grosmont Formation. AOSTRA report 7 of 7, January 31, 1993, 170 p.

Luo, P., Huebscher, H., Dembicki, E.A., and Machel, H.G., 1992, Diagenesis and reservoir characteristics of the heavy-oil carbonate trend in western Canada - continued investigation of reservoir characteristics of the Grosmont Formation. AOSTRA report 6 of 7, July 31, 1992, 141 p.

Machel, H.G., and Hawlader, H.M., 1990, Diagenesis and reservoir characteristics of the heavy-oil carbonate trend in western Canada - preliminary investigation of facies, diagenesis, porosity, and bitumen saturation of the Grosmont Formation. AOSTRA report 2 of 7, July 31, 1990, 169 p.

Machel H.G., and Hunter, I.G., 1994, Facies models for Middle and Late Devonian shallow-marine carbonates, with comparisons to modern reefs: a guide for facies analysis. Facies, v. 30, p. 155-176.

Mazzullo, J., Alexander, A., Tieh, T., and Menglin, D., 1992, The effects of wind transport on the shapes of quartz sand grains. Journal of Sedimentary Petrology, v. 62, p. 961-971.

McCrossan, R.G., 1961, Resistivity mapping and petrophysical study of Upper Devonian inter-reef calcareous shales of central Alberta, Canada. American Association of Petroleum Geologists Bulletin, v. 45, p. 441-470.

McGillivray J.G., and Mountjoy, E.W., 1975, Facies and related reservoir characteristics, Golden Spike reef complex, Alberta. Bulletin of Canadian Petroleum Geology, v. 23, p. 753-809.

Moore, P.F., 1989, The Kaskaskia sequence: reefs, platforms and foredeeps, the lower Kaskaskia sequence - Devonian. In: Ricketts, B.D., ed., Western Canada Sedimentary Basin: a case history. Canadian Society of Petroleum Geologists, p. 139-164.

Oliver T.A., and Cowper, N.W., 1963, Depositional environments of the Ireton Formation, central Alberta. Bulletin of Canadian Petroleum Geology, v. 11, p. 183-202.

Osleger, D.A., and Montanez, I.P., 1996, Cross-platform architecture of a sequence boundary in mixed siliciclastic-carbonate lithofacies, Middle Cambrian, southern Great Basin, USA. Sedimentology, v. 43, p. 197-217.

Playford, P.E., Hurley, N.F., Kerans, C., and Middleton, M.F., 1989, Reefal platform development, Devonian of the Canning Basin, Western Australia. In: Crevello, P.D., Wilson, J.L., Sarg, J.F., and Read, J.F., eds., Controls on carbonate platform and basin deveopment, Society of Economic Paleontologists and Mineralogists, Special Publication No. 44, p. 187-202.

Read, J.F., 1989, Controls on evolution of Cambrian-Ordovician passive margin, U.S. Appalachians. In: Crevello, P.D., Wilson, J.L., Sarg, J.F., and Read, J.F., eds., Controls on carbonate platform and basin deveopment, Society of Economic Paleontologists and Mineralogists, Special Publication No. 44, p. 147-165.

Schlager, W., 1992, Sedimentology and sequence stratigraphy of reefs and carbonate platforms. American Association of American Petroleum Geologists Continuing Education Short Course Note Series No. 34, 71 p.

Scholle, P.A., Arthur, M.A., and Ekdale, A.A., 1983, Pelagic Environment. In: Scholle, P.A., Bebout, D.G., and Moore, C.H., eds., Carbonate depositional environments. American Association of American Petroleum Geologists, Memoir 33, p. 619-691.

Shinn, E.A., 1983, Tidal flat environment. In: Scholle, P.A., Bebout, D.G., and Moore, C.H., eds., Carbonate depositional environments. American Association of American Petroleum Geologists, Memoir 33, p. 171-210.

Shinn, E.A., 1986, Modern carbonate tidal flats: their diagnostic features. Colorado School of Mines Quarterly, v. 81, p. 7-35.

Stoakes, F.A., 1980, Nature and control of shale basin fill and its effect on reef growth and termination: Upper Devonian Duvernay and Ireton Formations of Alberta, Canada. Bulletin of Canadian Petroleum Geology, v. 28, p. 345-410.

Stoakes, F.A., 1992a, Woodbend megasequence. In: Wendte, J.C., Stoakes, F.A., and Clarence, C.V., Devonian-Early Mississippian carbonates of the Western Canada Sedimentary Basin: a sequence stratigraphic framework. Society for Sedimentary Geology (SEPM) Short Course No. 28, p. 183-206.

Stoakes, F.A., 1992b, Nature and succession of basin fill strata. In: Wendte, J.C., Stoakes, F.A., and Clarence, C.V., Devonian-Early Mississippian carbonates of the Western Canada Sedimentary Basin: a sequence stratigraphic framework. Society for Sedimentary Geology (SEPM) Short Course No. 28, p. 127-144.

Switzer, S.B., Holland, W.G., Christie, D.S., Graf, G.C., Hedinger, A.S., McAuley, R.J., Wierzbicki, R.A., and Packard, J.J., 1994, Devonian Woodbend - Winterburn strata of the Western Canada Sedimentary Basin. In: Mossop, G.D., and Shetsen, I., comps., Geological Atlas of the Western Canada Sedimentary Basin. Canadian Society of Petroleum Geologists and Alberta Research Counsil, p. 165-202.

Theriault, F., 1988, Lithofacies, diagenesis, and related reservoir properties of the Upper Devonian Grosmont Formation, northern Alberta. Bulletin of Canadian Petroleum Geology, v. 36, p. 52-69.

Van Wagoner, J.C., Mitchum, R.M., Jr., Posamentier, H.W., and Vail, P.R., 1987, Key definitions of sequence stratigraphy. In: Bally, A.W., ed., Atlas of seismic stratigraphy, v. 1, American Association of Petroleum Geologists Studies in Geology No. 27, p. 11-14.

Walls, R.A., 1983, Golden Spike reef complex. In: Scholle, P.A., Bebout, D.G., and Moore, C.H., eds., Carbonate depositional environments. American Association of American Petroleum Geologists, Memoir 33, p. 445-453.

Wendte, J.C., 1974, Sedimentation and diagenesis of the Cooking Lake platform and Lower Leduc reef facies, Upper Devonian, Redwater, Alberta. Unpubl. Ph.D. thesis, University of California, Santa Cruz, 222 p.

Wendte, J.C., 1992, Platform evolution and its control on reef inception and localization. In: Wendte, J.C., Stoakes, F.A., and Clarence, C.V., Devonian-Early Mississippian carbonates of the Western Canada Sedimentary Basin: a sequence stratigraphic framework. Society for Sedimentary Geology (SEPM) Short Course No. 28, p. 41-87.

Wendte, J., Bosman, M., Stoakes, F., and Bernstein, L., 1995, Genetic and stratigraphic significance of the Upper Devonian Frasnian Z Marker, west-central Alberta. Bulletin of Canadian Petroleum Geology, v. 43, p. 393-406.

Wilson, J.L., 1975, Carbonate facies in geologic history. Springer Verlag, New York, 472 p.

CHAPTER 3

PETROGRAPHY, DIAGENESIS AND POROSITY EVOLUTION OF UPPER DEVONIAN WOODBEND GROUP CARBONATES, NORTH-CENTRAL ALBERTA

INTRODUCTION

Hydrocarbon reservoirs are generally described in terms of their reservoir characteristics, the most important of them being porosity and permeability. Compared to siliciclastic reservoirs, the description of carbonate reservoirs is a complicated undertaking. Carbonate reservoirs are characterized by primary, facies dependent porosity and/or by a wide variety of texturally and genetically different secondary, diagenetic pore types (Choquette and Pray, 1970; Roehl and Choquette, 1985). The importance of diagenesis in carbonate reservoir development is due to the susceptibility of carbonate minerals to mineral conversion reactions, cementation and dissolution processes.

In view of these points it is surprising that the diagenetic history and porosity evolution of the Upper Devonian Woodbend Group of north-central Alberta (Fig. 3.1) have not been studied in detail, although Woodbend Group carbonates contain several hydrocarbon reservoirs, (1) the giant Grosmont heavy oil trend, and (2) associated gas pools (House, Granor, Liege, McLean, Saleski; see Fig. 3.2). It has also been postulated that the Cooking Lake platform margin and the overlying northern extension of the Rimbey-Meadowbrook reef trend acted as a conduit for long range migration of formation waters as well as hydrocarbons (e.g. Gussow, 1954; Machel and Mountjoy, 1987). An understanding of the distribution of diagenetic phases, especially of major pore creating and occluding phases, would, therefore, help delineate reservoir heterogeneity and possible pathways and barriers for fluid flow in the Woodbend Group.

Earlier diagenetic studies were restricted to the pilot project area of the Grosmont heavy oil reservoir (Fig. 3.2) (Theriault, 1988; Machel and Hawlader, 1990; Luo et al., 1993; Luo and Machel, 1995) or dealt with only a few aspects of diagenesis (Theriault

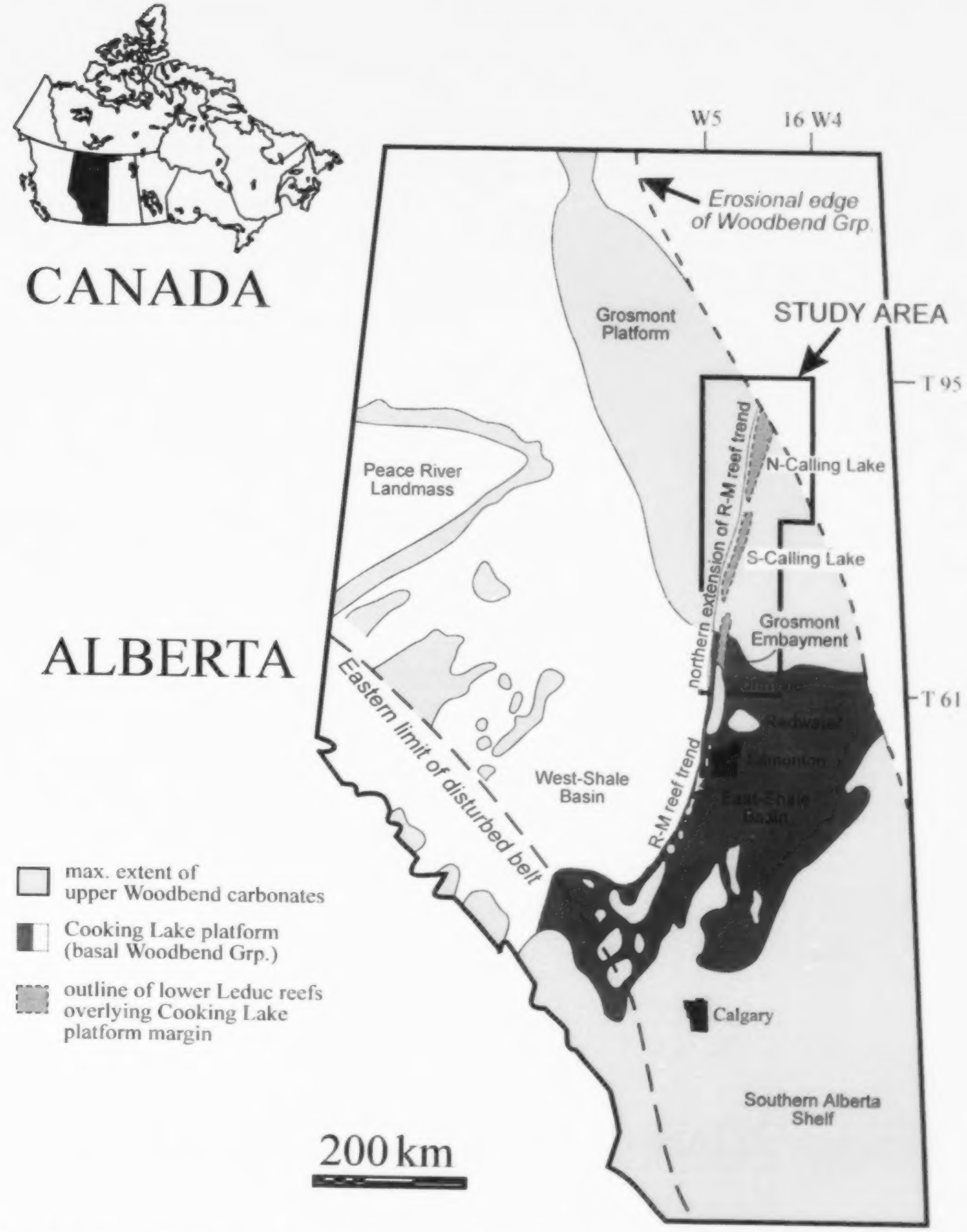
CANADA
ALBERTA
W5
16 W4
Erosional edge of Woodbend Grp.
STUDY AREA
T 95
T 61
Grosmont Platform
Peace River Landmass
N-Calling Lake
S-Calling Lake
Grosmont Embayment
northern extension of R-M reef trend
Eastern limit of disturbed belt
West-Shale Basin
R-M reef trend
Redwater
Edmonton
East-Shale Basin
Calgary
Southern Alberta Shelf
max. extent of upper Woodbend carbonates
Cooking Lake platform (basal Woodbend Grp.)
outline of lower Leduc reefs overlying Cooking Lake platform margin
200 km

Fig. 3.1: Simplified distribution of platform and reef carbonates of the Late Devonian Woodbend Group (modified after Switzer et al., 1994) and location of the study area in Alberta. Shown are the aerial extent of the Cooking Lake platform (basal Woodbend Grp.), of overlying lower Leduc reefs (northern extension of R-M reef trend), and of platform and reef carbonates of the upper Woodbend Group. R-M reef trend = Rimbey-Meadowbrook reef trend.

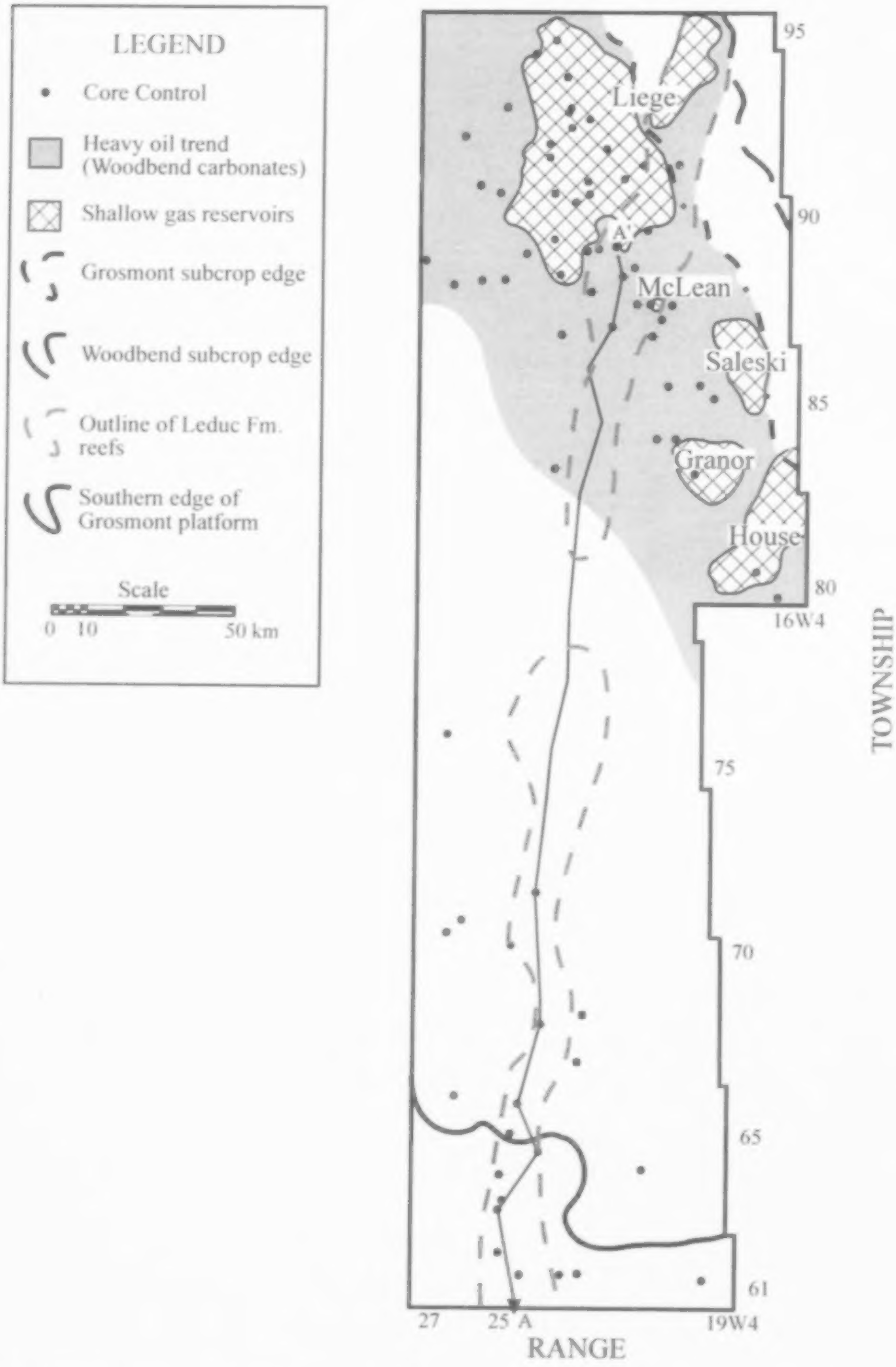
LEGEND
Core Control
Heavy oil trend (Woodbend carbonates)
Shallow gas reservoirs
Grosmont subcrop edge
Woodbend subcrop edge
Outline of Leduc Fm. reefs
Southern edge of Grosmont platform
Scale
0 10 50 km
Liege
A'
McLean
Saleski
Granor
House
95
90
85
80
16W4
75
70
65
61
27
25 A
19W4
RANGE
TOWNSHIP

Fig. 3.2: Distribution of Woodbend Group carbonate complexes and location of hydrocarbon reservoirs in the study area. Also shown are the locations of studied cores and cross-section A-A'.

and Hutcheon, 1987; Larson, 1988). The objective of the present chapter is to provide an overview of the diagenesis of Woodbend carbonates in the study area, to place the observed diagenetic phases in a paragenetic sequence, and to discuss their distribution and their effects on porosity evolution and reservoir quality. This discussion serves as an introductory chapter to Woodbend diagenesis and is generally limited to petrographic analysis, either because of lack of other data or, as in the case of dolomitization and karstification, because a detailed discussion follows in later chapters (Chapter 4 and 5, respectively).

GEOLOGIC SETTING

The Upper Devonian (Frasnian) Woodbend Group of north-central Alberta is part of a thick succession of carbonate dominated shelf sediments that were deposited during the passive margin stage of the Western Canada Sedimentary Basin. Woodbend Group sediments are underlain by argillaceous carbonates of the Waterways Formation (Beaverhill Lake Group) and are generally overlain by carbonates of the Nisku Formation (Winterburn Group).

Ten units comprise the Woodbend Group in north-central Alberta (Fig. 3.3). The lowest units are carbonate platform deposits of the Cooking Lake Formation and equivalent basin-fill sediments (bituminous limestones) of the Majeaux Lake Member. These strata are overlain by Leduc Formation buildups or Duvernay Formation and lower Ireton Formation basin-fill sediments. The following units of the Woodbend Group are carbonate platform deposits of the Grosmont Formation. Based on the position of thin shale markers (Harrison, 1982) the Grosmont Formation can be divided into the lower Grosmont (LGM) and the upper Grosmont 1, 2, 3a and 3b (UGM 1, UGM 2, UGM 3a and UGM 3b, respectively). Due to the overall shallowing and progradation of the Grosmont platform the LGM unit is dominated by open marine platform facies whereas UGM 1 through UGM 3b were deposited in progressively more restricted environments. To the south and west Grosmont deposits grade into Ireton Formation basin-fill sediments, to the south also into age equivalent strata of the Rimbey-Meadowbrook (Leduc

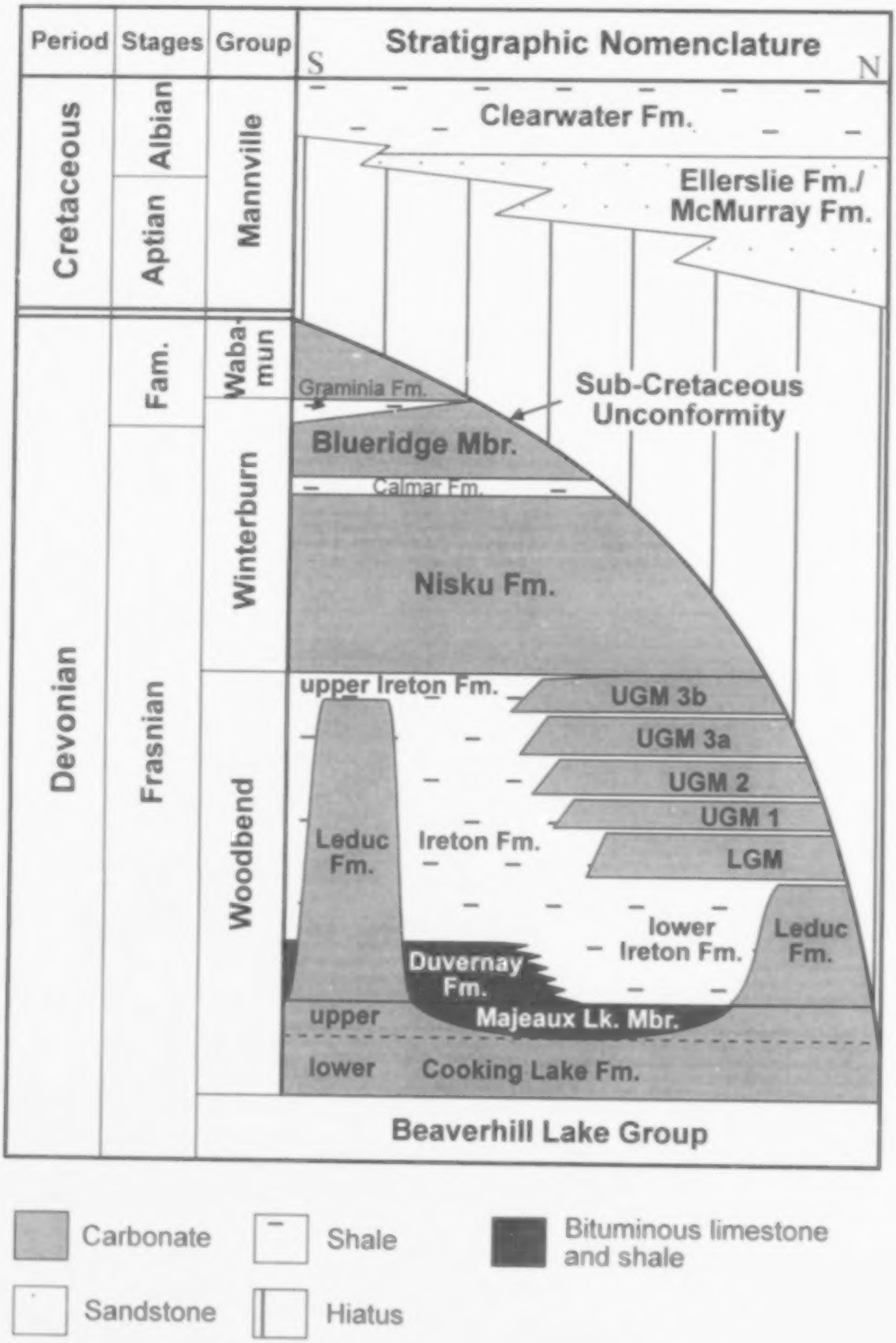
Period
Stages
Group
Stratigraphic Nomenclature
S
N
Cretaceous
Albian
Aptian
Mannville
Clearwater Fm.
Ellerslie Fm./
McMurray Fm.
Devonian
Fam.
Frasnian
Waba-
mun
Winterburn
Woodbend
Graminia Fm.
Sub-Cretaceous
Unconformity
Blueridge Mbr.
Calmar Fm.
Nisku Fm.
upper Ireton Fm.
UGM 3b
UGM 3a
UGM 2
UGM 1
LGM
Leduc
Fm.
Ireton Fm.
lower
Ireton Fm.
Leduc
Fm.
Duvernay
Fm.
upper
Majeaux Lk. Mbr.
lower
Cooking Lake Fm.
Beaverhill Lake Group
Carbonate
Shale
Bituminous limestone
and shale
Sandstone
Hiatus

Fig. 3.3: Stratigraphic nomenclature of the principal Upper Devonian and Lower Cretaceous units encountered in the study area.

Formation) reef trend (Figs. 3.1, 3.3). The youngest Woodbend unit, the upper Ireton Formation, consists of patchy, argillaceous to silty carbonates in the northern part of the study area which grade into thick shales (up to 50 m) in the southern part.

The present burial depth of the Woodbend Group varies from 1,500 m in the southwest to only 250 m in the northeast, due to a slight structural dip towards the southwest of approximately 5.5 m per km (Theriault, 1988). In the northernmost part of the study area the Woodbend Group is truncated by the sub-Cretaceous unconformity, partially to completely eroded, and overlain by Lower Cretaceous clastics of the Mannville Group.

METHODS

Diagenetic phases and textures were investigated by means of thin section petrography. Over 400 samples from 34 different wells were examined by normal light microscopy and cathodoluminescence microscopy. All thin sections were stained with alizarin red S and potassium ferricyanide (Dickson, 1966) to determine carbonate mineral composition and to estimate the Fe-content of calcites and dolomites. About 50 samples were impregnated with blue resin to better describe and estimate porosity.

To better distinguish between different calcites and to interpret their origin 53 calcite samples were analyzed for their stable isotope composition (Table 3.1). Twenty mg of calcite powder was obtained for each analysis with a dental drill. Sample powders were reacted with 100% phosphoric acid at 25°C for 24 hours following the procedure described by McCrea (1950). The isolated CO_2 was analyzed with a VG 602 mass spectrometer. Both oxygen and carbon isotope data are reported relative to Pee Dee Belemnite (PDB) in the standard δ-notation (Craig, 1957).

Table 3.1: Calcite stable isotope data

Well ID	Unit	Depth [m]	Depth [ft]	Sample type	$\delta^{18}O$ [PDB]	$\delta^{13}C$ [PDB]
01-32-61-23W4	Leduc	1160.4	3807	Stromatoporoid	-9.09	2.30
	Leduc	1150.9	3776	Coral	-7.79	2.90
	Leduc	1146.7	3762	BCC II	-10.63	1.56
	Leduc	1143.6	3752	Coral	-9.12	2.17
13-35-61-23W4	Leduc	1041.2	3416	BCC II	-8.64	1.66
	Leduc	1041.2	3416	Whole rock	-10.70	1.68
	Leduc	1032.7	3388	BCC II	-12.55	0.58
	Leduc	1029.3	3377	Radial-fibrous cement	-7.14	2.00
07-31-61-24W4	Leduc	1065.6	3496	BCC III	-12.66	-3.29
	Leduc	1064.7	3493	BCC III	-12.46	-2.93
05-24-63-25W4	Leduc	1333.5	4375	BCC III	-13.35	-5.64
	Leduc	1333.5	4375	BCC III	-11.32	-5.66
09-39-65-24W4	Leduc	1053.4	3456	BCC II	-12.47	4.04
14-26-64-21W4	u. Ireton	816.0	2677	Whole rock	-6.87	-0.27
	u. Ireton	802.2	2632	Whole rock	-7.04	-0.51
05-19-65-24-W4	UGM 3a	1141.5	3745	Whole rock	-6.13	-0.23
	UGM 3a	1132.6	3716	Whole rock	-7.10	0.08
	UGM 3b	1113.7	3654	Whole rock	-5.35	-0.70
	UGM 3b	1113.7	3654	Brachiopod	-6.20	-0.54
	UGM 3b	1093.6	3588	Whole rock	-6.86	-0.11
	u. Ireton	1045.5	3430	Whole rock	-5.90	0.52
06-16-66-24W4	LGM	1105.5	3627	BCC III	-12.43	-11.20
	UGM 2	1042.7	3421	BCC III	-12.20	-7.50
	UGM 3a	1005.2	3298	BCC III	-11.27	-9.28
	UGM 3a	1005.2	3298	BCC III	-11.64	-9.45
04-33-68-22W4	Majeaux Lk.	1049.1	3442	Whole rock	-5.70	1.06
	Majeaux Lk.	1033.6	3391	Whole rock	-6.96	1.00
06-20-68-23W4	UGM 3b	898.3	2947	BCC III	-11.98	-11.33
03-28-70-24W4	UGM 3b	855.3	2806	BCC III	-13.24	-6.60
10-17-83-18W4	LGM	445.8	1463	Crinoid	-5.82	1.85
	LGM	445.8	1463	Brachiopod	-5.33	2.69
	LGM	443.0	1453	Stromatoporoid	-8.97	3.27
	LGM	421.5	1383	Stromatoporoid	-9.54	3.29
	UGM 1	393.0	1289	Whole rock	-9.79	-0.20
	UGM 2	388.5	1275	Brachiopod	-5.65	0.38
	UGM 3b	321.8	1056	Dedolomite	-14.12	-4.85

Table 3.1 (contd.): Calcite stable isotope data

Well ID	Unit	Depth [m]	Depth [ft]	Sample type	$\delta^{18}O$ [PDB]	$\delta^{13}C$ [PDB]
10-14-84-19W4	LGM	477.0	1565	Whole rock	-7.42	3.24
	LGM	463.0	1519	Whole rock	-8.29	2.64
	LGM	441.0	1447	Whole rock	-7.27	1.82
	UGM 1	422.8	1387	Whole rock	-8.16	0.25
	UGM 3a	386.5	1268	Dedolomite	-13.34	-4.39
06-34-85-19W4	LGM	449.0	1473	Whole rock	-7.10	2.78
	LGM	441.8	1449	Stromatoporoid	-10.40	3.04
	LGM	441.8	1449	BCC II	-13.18	4.13
	LGM	429.0	1407	Stromatoporoid	-10.52	3.26
06-09-87-19W4	LGM	333.5	1094	Whole rock	-5.13	3.26
	UGM 1	322.0	1056	Stromatoporoid	-9.49	1.28
	UGM 1	314.8	1033	Whole rock	-5.62	1.83
14-17-87-20W4	UGM 3a	317.6	1042	Microstalactitic cement	-11.72	-5.41
03-34-88-20W4	Leduc	457.2	1500	BCC IV	-14.42	11.28
	Leduc	425.5	1396	BCC IV	-14.39	12.01
06-11-89-25W4	LGM	627.5	2059	Whole rock	-9.18	-1.47

DIAGENETIC PROCESSES AND PRODUCTS

Woodbend Group carbonates were subject of an intense diagenetic evolution that encompassed diagenesis in the marine, burial and meteoric environments (Fig. 3.4). Early, marine and shallow burial diagenesis is evident in undolomitized platform and reefal limestones (Fig. 3.5) from the presence of early internal sediments and extensive calcite cementation. Dolomitization during subsequent burial was likely the single most important event for reservoir development because it preserved and/or increased reservoir porosity (Fig. 3.4). Sulfate emplacement and removal (Fig. 3.4) also had a large impact on reservoir quality since it plugged or reactivated porosity. Early dissolution of carbonate bioclasts occurred throughout the Woodbend Group and is evident from abundant moldic porosity, especially in platform dolostones. However, its importance is dwarfed in comparison by carbonate dissolution and intense fracturing during karstification (Fig. 3.4) of Woodbend carbonates in the northern part of the study area (Fig. 3.5). An overview of the diagenetic phases encountered in the study area, their inferred position in the paragenetic sequence, and a generalized porosity history of important reservoir lithologies is presented in Fig. 3.4.

Internal Sedimentation

Early internal sediments.- Early internal sediments occur in primary pores such as interparticle, moldic and fenestral pores in limestone of the Woodbend Group (e.g. in the LGM). Early internal sediments consist mostly of carbonate material, such as micrite to microsparite with minor peloids and bioclasts, and of minor quartz silt, and dolomite crystal fragments. The presence of sediment particles and the fact that this type of internal sediment generally fills pore spaces before the onset of cementation indicates its syndepositional origin. Some internal sediments consisting entirely of micrite and microsparite, however, were deposited on early fibrous and bladed calcite cements (Fig. 3.6a) and may be sedimentary or diagenetic in origin (e.g. vadose silt; Dunham, 1969). Early internal sediments are a volumetrically minor feature and are of negligible importance for reservoir characterization.

Fig. 3.4: Paragenetic sequence, estimated burial history and porosity development of Woodbend Group carbonates in north-central Alberta. Subsurface temperature is derived assuming a geothermal gradient of 30°C km^{-1} and a surface temperature of 25°C. The two burial curves represent the northern and southern burial history end members. In the paragenetic sequence, solid lines represent periods during which diagenetic processes were most intense. Dashed lines indicate periods of lesser intensity.

Maximum burial depth of the first (Paleozoic) burial episode was derived by comparison with the thicknesses of preserved Paleozoic strata near the study area (see Richards et al., 1994). Timing and maximum depth of the second (Mesozoic/Cenozoic) burial episode were extrapolated from published data from the southern end and central portions of the Rimbey-Meadowbrook reef trend (Laflamme, 1990; Amthor et al., 1993). A linear gradient in dip and amount of Cretaceous/Tertiary overburden was assumed between the southern and central regions of the reef trend and the study area to estimate the maximum burial depth of the Woodbend Group in north-central Alberta.

The end of marine (M) and shallow burial (SB) diagenesis and the beginning of burial-uplift period 1 (B-U 1) has been set at a burial depth of around 500m. This depth is approximately coinciding with the onset of chemical compaction (cf. Lind, 1993). The beginning of the second episode of burial-uplift (B-U 2) is determined by renewed subsidence in response to the Laramide orogeny. Subaerial exposure (SE) and its effects only occurred in the northern part of the study area. Porosity development curves show representative scenarios for limestones, dolostones and karstified intervals.

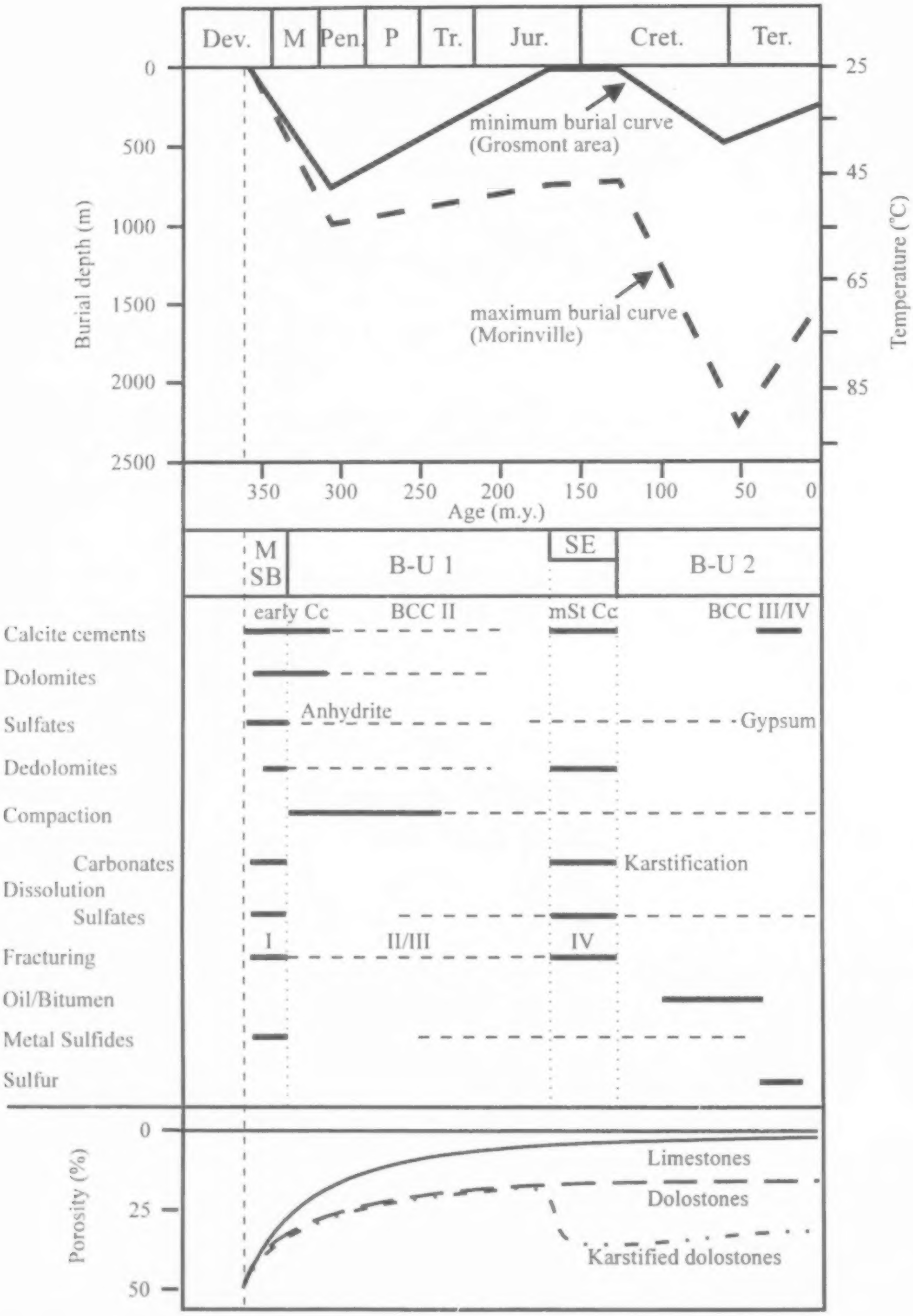

Dev.
M
Pen.
P
Tr.
Jur.
Cret.
Ter.
Burial depth (m)
0
500
1000
1500
2000
2500
Temperature (°C)
25
45
65
85
minimum burial curve
(Grosmont area)
maximum burial curve
(Morinville)
350
300
250
200
150
100
50
0
Age (m.y.)
M
SB
B-U 1
SE
B-U 2
early Cc
BCC II
mSt Cc
BCC III/IV
Calcite cements
Dolomites
Sulfates
Anhydrite
Gypsum
Dedolomites
Compaction
Carbonates
Dissolution
Sulfates
Karstification
I
II/III
IV
Fracturing
Oil/Bitumen
Metal Sulfides
Sulfur
Porosity (%)
0
25
50
Limestones
Dolostones
Karstified dolostones

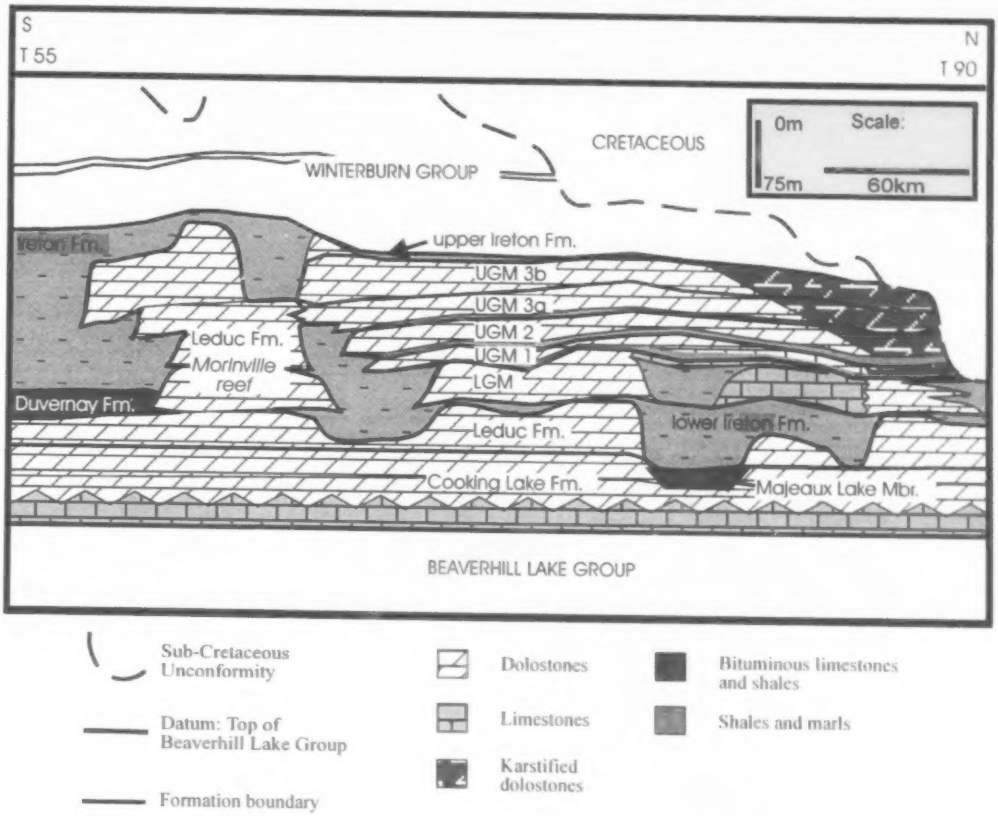
S
T 55
N
T 90
CRETACEOUS
0m
Scale:
75m
60km
WINTERBURN GROUP
Ireton Fm.
upper Ireton Fm.
UGM 3b
UGM 3a
UGM 2
UGM 1
LGM
Leduc Fm.
Morinville reef
Duvernay Fm.
Leduc Fm.
lower Ireton Fm.
Cooking Lake Fm.
Majeaux Lake Mbr.
BEAVERHILL LAKE GROUP
Sub-Cretaceous Unconformity
Datum: Top of Beaverhill Lake Group
Formation boundary
Dolostones
Limestones
Karstified dolostones
Bituminous limestones and shales
Shales and marls

Fig. 3.5: North-south cross section through the Woodbend Group in north-central Alberta. Shown is the distribution of the three main lithologies and diagenetic reservoir classes in the potential reservoir intervals as discussed in the text (limestones, dolostones, karstified intervals). This section follows the northern extension of the Rimbey-Meadowbrook reef trend from township 90 to the Morinville reef in the south. For location of cross-section (A-A') see Fig. 3.2.

Fig. 3.6a: Marine, bladed cements (BC) and several layers of radial-fibrous (FC) cements lining micritic components and early cavity. Early cements were followed by internal sediment and dolomite cement 1 (DC 1), which grew on the internal sediment (arrow). Rest pore spaces and fracture II (F) are filled by clear blocky calcite cement I. Stained thin section, well location 1-32-61-23W4, 3762' (UGM 3b).

Fig. 3.6b: Fenestral pore lined by radial-fibrous calcite cement (FCC). The centre of the pore was subsequently filled by clear blocky calcite cement II. Stained thin section, well location 13-35-61-23W4, 3377' (UGM 3b).

Fig. 3.6c: Neomorphosed limestone and calcitized dolomite rhombs (DD). Porosity contains blue epoxy. Stained thin section, well location 3-34-88-20W4, 941' (UGM 3a).

Fig. 3.6d: Partially dolomitized sample showing a sharp contact between rock matrix, dolomitized by replacement dolomite I (RD 1), and undolomitized component (black, at bottom of photograph). Not early compaction fracture II and pseudomorph after anhydrite laths. Both are filled by Fe-dolomite cement (FDC). Well location 6-35-85-19W4, 453.0 m (LGM).

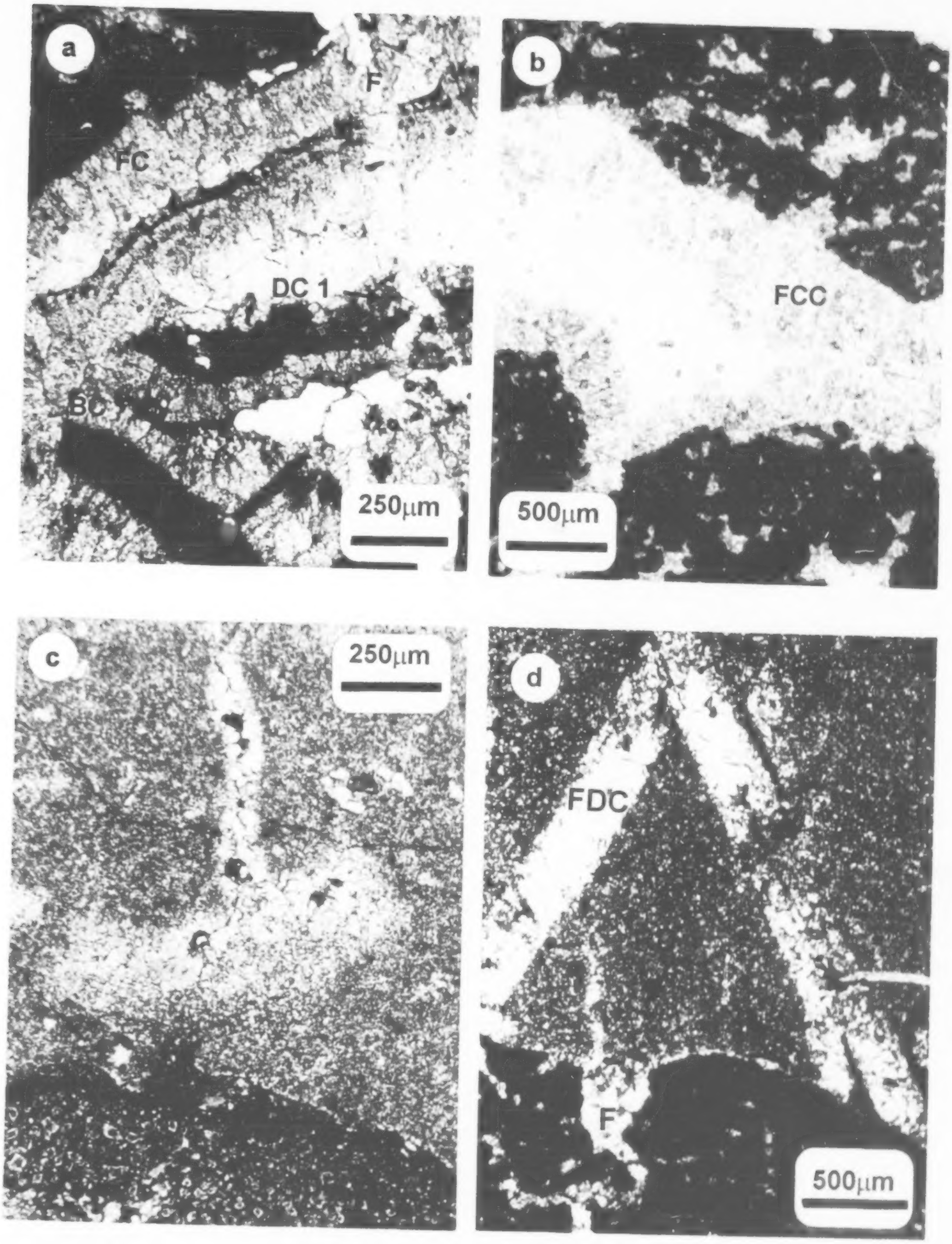
a
F
FC
DC 1
BC
250μm
b
FCC
500μm
c
250μm
d
FDC
F
500μm

Cave filling sediments.- The occurrence of cave filling sediments is restricted to large-scale secondary porosity, i.e to karst related caves and fracture systems (fracture IV). Cave filling sediments are of great, though localized importance in dolostones of the Upper Grosmont Formation along the Woodbend subcrop beneath the sub-Cretaceous unconformity (see Chapter 5), because cave-fills partially to completely occlude cavernous and fracture porosity. Cave filling sediments are characterized by allochthonous deposits consisting of shales and sands that have a mineralogical composition close to those of the Lower Cretaceous Mannville Group (Luo et al., 1992). These sediments also contain varying amounts of dolomite rhombs (sucrosic dolomite) and rock fragments from the surrounding carbonate host rock.

Calcite Cementation and Neomorphism

Early calcite cements.- A variety of early, marine or shallow burial calcite cements have been preserved in non-dolomitized intervals of the Woodbend Group. Four main types have been distinguished in thin sections. These are fibrous cement, bladed cement, syntaxial cement and blocky calcite cement I. Radiaxial calcite cements which are so commonly described from Frasnian reefs of Alberta (McGillivray and Mountjoy, 1975; Walls et al., 1979; Walls and Burrowes, 1985) and Australia (Kerans et al., 1986) were not observed in the study area. Early calcite cements occlude an estimated 70 to 100 % of primary pores in predominantly limestone intervals (Fig. 3.5). Hence, most limestone intervals have porosities of less than 5 % and are of minor importance as hydrocarbon reservoirs.

Bladed cements (Figs. 3.6a, 3.7a) occur in the back reef and platform environments and their occurrence does not appear to be substrate dependent. Bladed cements are 50 to 200 μm long and 10 to 30 μm wide and non-luminescent. They are particularly common in interparticle and intraparticle pores of semi-restricted facies and can completely occlude all pores. They also occur as cement crusts lining systems of larger pore spaces such as moldic and fenestral pores and early fractures. Bladed cements were subject to recrystallization and only their ghost structures are preserved in recrystallized calcite mosaics.

Radial-fibrous cements (Fig. 3.7b) occur primarily in reefal or lagoonal facies

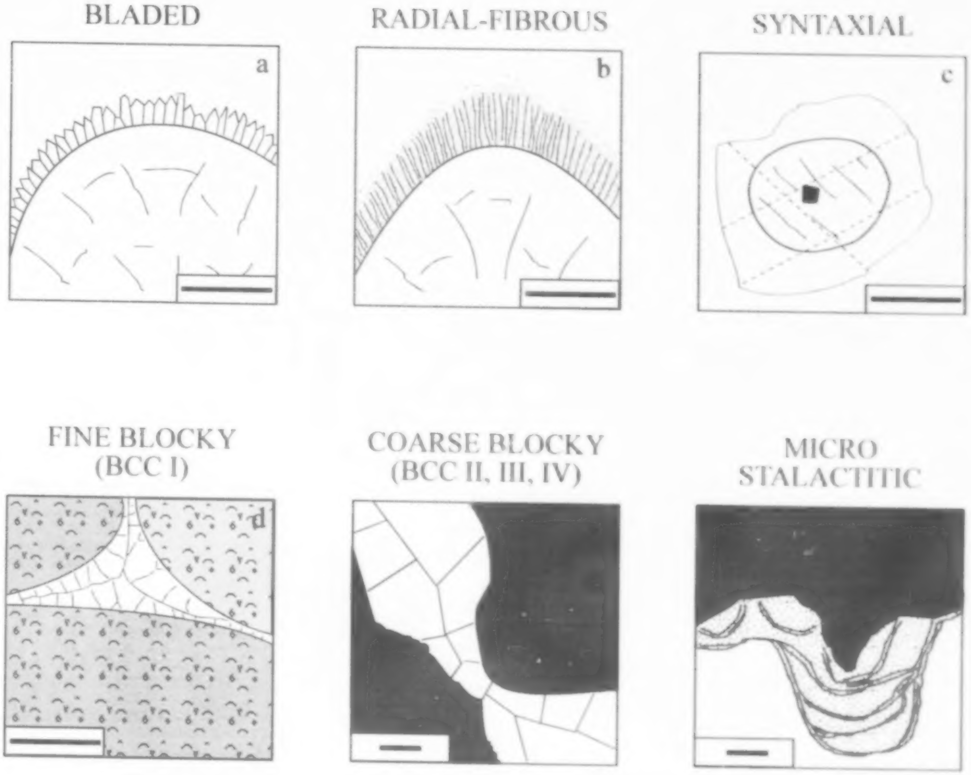
BLADED
a
RADIAL-FIBROUS
b
SYNTAXIAL
c
FINE BLOCKY
(BCC I)
d
COARSE BLOCKY
(BCC II, III, IV)
MICRO
STALACTITIC

Fig. 3.7: Types of calcite cement recognized in the Woodbend Group of north-central Alberta. Scale bars = 500μm.

which were deposited under open marine conditions. These cements are developed directly on carbonate components and pore walls (Figs. 3.6a, 3.6b). If developed as crusts on individual components, they are most commonly observed on bioclasts, such as brachiopods, corals, stromatoporoids, calcispheres and gastropods, that themselves had a fibrous microstructure. Radial-fibrous cements are 50 to 500 μm long, but only a few to 10 μm wide. They are non-luminescent, but may show orange specks indicating some diagenetic alteration. The only analyzed radial-fibrous cement sample has a δ^{18}O composition of -7.1 ‰ PDB, and a δ^{13}C composition of 2.0 ‰ PDB.

Syntaxial cements (Fig. 3.7c) occur in open marine facies and have predominantly developed on CRINOID fragments. This cement type is mostly non-luminescent, but contains red/orange specks indicating some diagenetic alteration.

Blocky cement I (BCC I) (Figs. 3.6a, 3.7a) occurs in primary pore spaces and early fractures. BCC I is developed directly on sediment components and pore walls or on radial-fibrous and bladed cements. Individual crystals are equidimensional and between 10 μm to 100 μm in diameter. This cement type is non-luminescent to dull orange luminescent and may show fine zonation. Pure blocky calcite cement I samples have not been analyzed for their stable isotope composition. However, bioclasts and whole rock limestone samples that are cemented by BCC I have a depleted δ^{18}O composition ranging from -10.7 to -5.1 ‰ PDB and a δ^{13}C composition ranging from -1.5 to 3.3 ‰ PDB.

Neomorphism.- Neomorphic fabrics (Bathurst, 1975) are present in fine grained limestones and in limestones near sulfate beds. Characteristic are microsparitic fabrics consisting of irregularly interlocking crystals mosaics (Fig. 3.6c). Neomorphic fabrics in limestones may be the result of the conversion of aragonite to high Mg-calcite or of high Mg-calcite to low Mg-calcite. Neomorphic fabrics may be also caused by aggrading neomorphism or crystal enlargement, whereby larger crystals cannibalize smaller crystals of the same mineral type. Neomorphic fabrics are more common in "clean" limestones as compared to argillaceous limestones. Since these lithologies do not comprise major reservoir units in the study area, the importance of limestone neomorphism for reservoir characterization is very limited.

Late calcite and Fe-calcite cements.- Four generations of late calcite cements can be distinguished on the basis of crystal habit, crystal size, cathodoluminescence and stable isotope composition (Table 3.1, Fig. 3.8). The term late cement refers to all types that formed after compaction. Late calcite cements fill in primary as well as secondary pores and are present in limestones, dolostones, and karstified dolostones. The overall importance of late cements is limited since they occlude at the most 5 to 10 % of the reservoir. Complete occlusion of carbonate porosity by late calcite cements is very localized (i.e. m-scale in vertical direction).

Blocky (Fe-) calcite cement II (BCC II) consists of equidimensional crystals with crystal diameters between 50μm and 200μm (Fig. 3.7e). BCC II occurs primarily in interparticle, fenestral and moldic porosity of undolomitized limestones (Fig. 3.6b), but is also present in fractures. In stained thin sections this cement type reveals prominent, alternating zones of pink (Fe-poor) calcite and dark purple to blue Fe-calcite, which corresponds to alternating yellow and dark purple luminescent (CL) zones. Yellow luminescent calcite is dominant in early zones, whereas purple luminescent Fe-calcite is characteristic in later growth stages. BCC II cements have oxygen isotope compositions ranging from -12.6 to -10.7 ‰ PDB. Their carbon isotope composition ranges between 0.6 to 1.7 ‰ PDB.

Microstalactitic calcite cement (Fig. 3.7f) occurs underneath the roof of karst related secondary pores (vugs, fractures and caves). This cement type consists of alternate bands of coarse (200μm to 1,000μm crystal size), clear, prismatic to blocky crystals and fine to medium crystalline (crystal size between 50μm and 100μm), dark, blocky to rhombic crystals. Microstalactitic cements are dark purple luminescent and display no or weak zonation. The only analyzed sample of microstalactitic calcite cement has a $\delta^{18}O$ composition of -11.7 ‰ PDB and a $\delta^{13}C$ composition of -5.4 ‰ PDB.

Blocky (Fe-)calcite cement III (BCC III) occurs in secondary pores (vugs and fractures) and post-dates dolomite cement II, BCC I and II. It consists of equidimensional crystals with a crystal diameter between 100μm and 5mm (Figs. 3.7e; 3.10a; 3.13a-c). In stained thin sections this cement type shows zones of pink (Fe-poor) calcite and light purple calcite that is slightly enriched in Fe. The cathodoluminescence reveals equivalent yellow to dull orange-red zones (Fig. 3.13b). BCC III cements show distinctly depleted

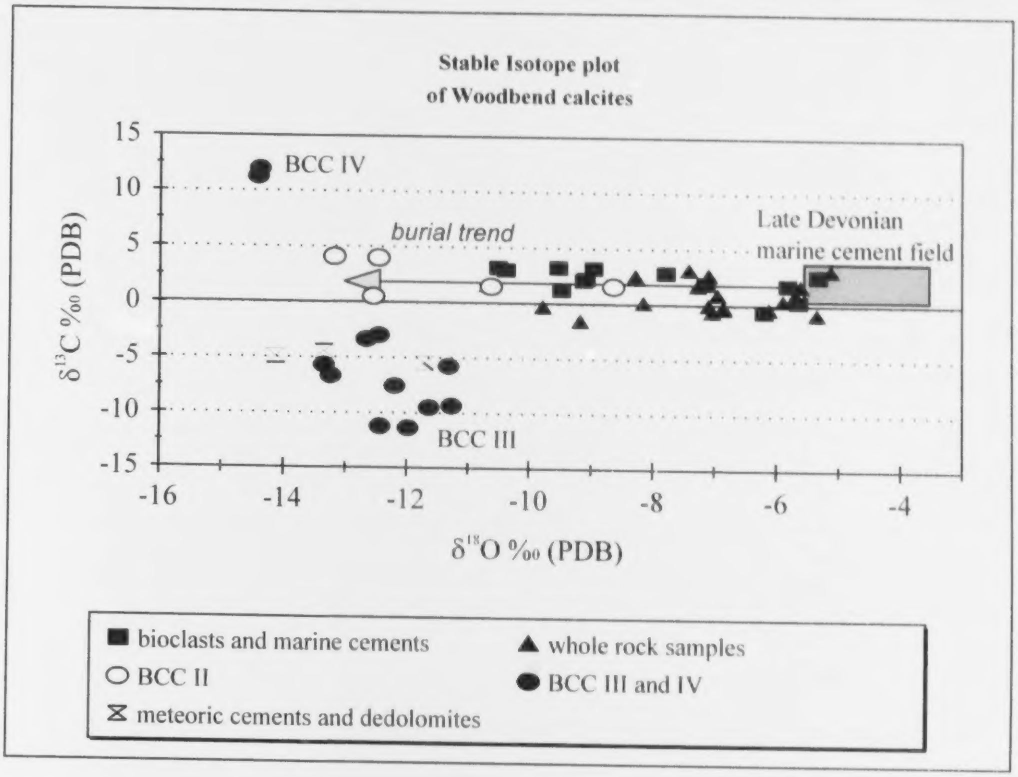

Fig. 3.8: Carbon-oxygen isotope plot of calcite samples from the Woodbend Group in north-central Alberta. Shown are isotope analysis results from bioclasts, early and late calcite cements, dedolomites and whole rock samples. The Late Devonian marine cement field was derived from data published by Carpenter and Lohmann (1989). The burial trends (arrow) was inferred from bioclast, whole rock and earlier cement (incl. BCC II) data. The $\delta^{18}O$ data in the burial trend reflect increasing temperature during burial, $\delta^{13}C$ values remained in the marine range. Later cement generations and dedolomites plot in distinct fields reflecting influx of meteoric water along the sub-Cretaceous unconformity and different carbon sources (soils, hydrocarbons) compared to earlier calcites. See text and Table 3.1 for more details.

stable isotope compositions ($\delta^{18}O$ ranges from -13.4 to -11.3 ‰ PDB, $\delta^{13}C$ ranges from -11.3 to -3.0 ‰ PDB). BCC III occurs most commonly in Leduc Formation buildups, but is also present in directly overlying portions of the Grosmont Formation.

Blocky calcite cement IV (BCC IV) also occurs in secondary pores. The relationship of this cement type to BCC III, however, is unclear because they do not occur together. Whereas BCC III is widely distributed throughout the study area, especially in reefal buildups of the Leduc Formation, BCC IV only occurs in the Leduc Formation beneath the Grosmont heavy oil reservoir. BCC IV consists of equidimensional crystals with a crystal diameter between 100μm and 10mm (Fig. 3.7e). They exhibit no apparent zonation and display a uniform dull yellow cathodoluminescence colour. Their oxygen isotope composition is characteristically depleted ($\delta^{18}O$ ranges from -14.4 to -13.3 ‰ PDB), but their carbon isotope composition is enriched ($\delta^{13}C$ ranges from 4.1 to 12.0 ‰ PDB).

Stable isotope systematics and origin of calcite cements.- As the previous description of the different cement types illustrated, calcite cements have widely varying petrographic and geochemical characteristics. Stable isotopes (Table 3.1, Fig. 3.8) help to interpret the origin of these cements as well as to decipher the diagenetic history of Woodbend limestones.

Early, non-blocky calcite cements, i.e. bladed, radial-fibrous and syntaxial calcite cements are interpreted as early, submarine cements, because of their occurrence in reefal and deep subtidal limestones of the Leduc and lower Grosmont Formations, and because of a lack of discontinuity surfaces and early dissolution fabrics in these limestones, which would be indicative of meteoric diagenesis. All three cement types have been observed in reefal facies in other Devonian successions (Mountjoy and Krebs, 1983; Walls and Burrowes, 1985; Kerans et al., 1986), and have been interpreted to be of marine origin. Unfortunately, bladed and syntaxial cements are also precipitated in the meteoric phreatic zone (James and Choquette, 1990) and their interpretation can, therefore, only be tentative.

Stable isotope compositions of bioclasts and whole rock samples show a wide compositional range in $\delta^{18}O$ values but their range of $\delta^{13}C$ values is relatively narrow

(Fig. 3.8). Most bioclast samples have $\delta^{13}C$ values which are very close to published values for Upper Devonian marine calcites of +2.0 ‰ PDB (Carpenter and Lohmann, 1989; see Fig. 3.8). Whole rock samples have a wider range of $\delta^{13}C$ values ranging from -1.47 to 3.24 ‰ PDB. Depleted carbon isotope compositions of whole rock samples are common in units that are dominated by peritidal facies, i.e. UGM 1 through UGM 3b. This depletion in the $\delta^{13}C$ of composition in peritidal samples may reflect differences in the $\delta^{13}C$ composition of the Devonian restricted marine water masses relative to open-ocean waters (cf. Patterson and Walter, 1994). The distribution of the oxygen isotope composition most likely represents various mixtures between original sedimentary components and later cements, especially blocky calcite cement I (BCC I). Lighter oxygen isotope composition correlates well with increasing alteration of shells (estimated from the amount of yellow luminescent specks in originally non-luminescent shells) and sediments and/or with an increasing amount of primary pores in shells (e.g. in stromatoporoids and corals) which were subsequently cemented. The observed tendency of decreasing oxygen isotope composition can be explained by two possible processes, (1) cementation of limestone by cements precipitated from meteoric water or (2) increasing temperature of precipitating waters during burial cementation. The most common early cement is blocky, clear, iron-poor calcite cement, a cement type that has been reported from the meteoric phreatic (James and Choquette, 1990) as well as from the burial environment (Prezbindowski, 1985; Choquette and James, 1990). Both scenarios may have played a role during precipitation of BBC I cements and early stabilization of limestones.

Late calcite cements (BCC II, III, IV and microstalactitic cement) have widely differing isotope compositions that are characteristic for different diagenetic environments (Fig. 3.8). The BCC II samples with the lowest $\delta^{18}O$ may represent the end member of the previously discussed burial trend (Fig. 3.8). These BCC II samples have oxygen isotope compositions ($\delta^{18}O \approx -12.5$ ‰ PDB) that are even more depleted than previously discussed whole rock samples, probably reflecting higher temperatures of pore waters under deeper burial conditions. Alternatively, the depleted oxygen isotope compositions could be the result of the input of meteoric water into the carbonate aquifer. The carbon isotope compositions of BCC II fall in the range of the surrounding limestones, which probably reflects the incorporation of local carbon derived from pressure solution

(Dickson and Coleman, 1980; Moore, 1985).

Microstalactitic cements are characteristic for the meteoric environment (Kendall and Broughton, 1978; Jones et al., 1984) and their isotopic composition reflects input of meteoric water as well as input of soil derived ^{13}C depleted CO_2. Possible paleosols, i.e. unconsolidated weathering horizons, and thin coal beds are present at some locations along the sub-Cretaceous unconformity or in overlying sediments of the Lower Mannville Group (e.g. 11-24-88-25W4, 10-17-83-19W4; see Chapter 5). Precipitation of this cement is, therefore, likely related to subaerial exposure and subsequent karstification of Woodbend Group carbonates along the sub-Cretaceous unconformity.

Blocky calcite cements III and IV (BCC III and IV) have the most unusual isotope compositions (Fig. 3.8). Their oxygen isotope composition is characteristically depleted, but their carbon isotope composition may be depleted (BCC III) or enriched (BCC IV). BCC III is the more common both in occurrence and area of distribution, whereas BCC IV is restricted to areas that were affected by the biodegradation and waterwashing of hydrocarbons. It is suggested that hydrocarbons were the source for both the low and high-^{13}C CO_2 incorporated in these cements. Low-^{13}C CO_2 results from the oxidative degradation of organic matter and hydrocarbons, and was incorporated into BCC III. These cements are, therefore, comparable to similar cements related to conventional oil pools and oil field waters (Carothers and Kharaka, 1980; Suchecki and Land, 1983). The formation of BCC III may be related to the migration of hydrocarbons through the Cooking Lake platform margin and the northern extension of the Rimbey-Meadowbrook reef trend. Formation of high-^{13}C CO_2 requires a different mechanism. In natural, thermogenic gas CO_2 enriched in ^{13}C can be found in equilibrium with methane above a temperature of 100°C (Hudson, 1977). This explanation is unlikely because Woodbend strata in the study area were not buried deep enough to reach organic maturity (Stoakes and Creaney, 1985), and the burial temperature, therefore, did probably not exceed 80°C. ^{13}C enriched CO_2 is also the byproduct of bacterial reduction of CO_2 to CH_4 (Claypool and Kaplan, 1974). For example, Whiticar et al. (1986) observed CO_2 with a $\delta^{13}C$ composition of up to +15 ‰ PDB to be in equilibrium with biogenic methane at temperatures between -1.3 and +58°C. Given a reservoir temperature of around 35°C (as recorded on well log headers) and the presence of large amounts of CH_4 associated with the Grosmont heavy-oil deposits, this process could be responsible for the origin of ^{13}C enriched CO_2. The mechanism favored here is high-^{13}C CO_2 generation by fermentation of hydrocarbons and/or products of oxidative degradation of hydrocarbons by anaerobic bacteria (Dimitrakopoulos and Muehlenbachs, 1987). Degradation of hydrocarbons by fermentation commences when (1) oxidative degradation is complete and/or (2) when oxidizing conditions are no longer present in the reservoir. Two petrographical observations support this interpretation. BCC IV is found as the last stage after formation of BCC III. Furthermore, BCC IV is only present in the lower portion of the Grosmont heavy oil reservoir which is furthest from the unconformity and karstified zones, where Woodbend formation waters mix with locally recharged Cretaceous formation waters (Bachu and Underschultz, 1993). Input of meteoric formation waters would also explain the depleted oxygen isotope composition of BCC III and IV as has been suggested for similar cements in the Lower Cretaceous Clearwater Formation (Hutcheon et al., 1989).

Effects on porosity development.- Although calcite cementation was detrimental to porosity in all lithologies it was most effective in limestone intervals. Primary porosity in the Woodbend limestones of the Majeaux Lake Member and LGM was almost completely occluded by early marine calcite cements. Secondary molds, vugs and fractures were filled by later cements, especially by BCC I and II. This nearly complete cementation results in the overall low porosity values of Woodbend limestones, which generally ranges between 2 and 5 %. In dolostone, however, calcite cements have little or no effect on porosity. Early calcite cements were obliterated by dolomitization or were dissolved at some point. Minor, very localized pore occlusion has to be attributed to microstalactitic cements and BCC III and IV.

Dolomite replacement and cementation

Dolomite petrography.- Five types of dolomite can be distinguished petrographically in Woodbend Group carbonates. Two types are replacement dolomites, the other three types are dolomite cements or overgrowths (Fig. 3.9). Dolomite geochemistry and origin are examined in detail in Chapter 4 and are not included in this discussion.

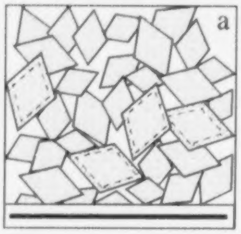

Replacement dolomite 1:
fine to medium crystalline,
planar-e to planar-s mosaic dolomite
orange-red, zoned luminescence

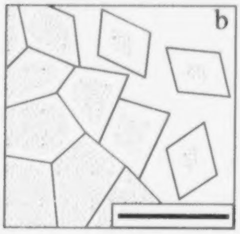

Replacement dolomite 2:
medium to coarse crystalline,
planar-e to non-planar mosaic dolomite
dull red, homogeneous luminescence

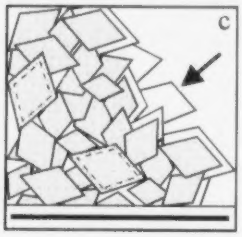

Dolomite cement 1:
fine to medium crystalline,
clear overgrowth on replacement dolomite or
clear euhedral to subhedral cement
orange-red, weakly zoned luminescence

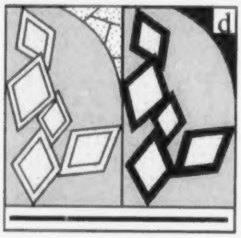

Fe-Dolomite cement:
fine to medium crystalline,
overgrowth on replacement dolomite or
euhedral to subhedral cement
no luminescence (left part of diagram)

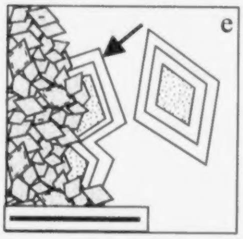

Dolomite cement 2:
coarse crystalline, zoned, euhedral cement
orange-red, zoned luminescence

Fig. 3.9: Dolomite types observed in the Woodbend Group of north-central Alberta. Scale bars = 500μm.

Replacement dolomite I.- This type of replacement dolomite is light grey, dark grey, light brown, dark brown or light green in hand specimen, depending on the amount and colour of impurities and reflecting the colour of the precursor limestone. It appears to be the earliest preserved dolomite phase and preferentially replaced matrix of precursor limestones. Replacement dolomite I (Figs. 3.9a; 3.10a-d) crystals are euhedral to subhedral and their crystal size ranges between 20μm and 100μm. Most crystals are cloudy and show no zoning under plane light, but display weak, dull red and orange luminescent zones (Fig. 3.10b,d). Replacement dolomite I is predominantly present in the northern part of the Grosmont platform (Fig. 3.11).

Replacement dolomite II.- The second type of replacement dolomite is uniformly grey or light brown in hand specimen. This type of dolomite can be restricted to replacement of calcitic bioclasts, appear in clusters in replacement dolomite I matrix, or be pervasive. Compared to replacement dolomite I the average crystal size is larger, ranging from 70μm to 200μm, and crystal texture is dominantly subhedral to anhedral (Figs. 3.9b; 3.12a-d; 3.13a-c; 3.15c-d). Intervals that are pervasively dolomitized by replacement dolomite II have a relatively tight crystal mosaic and intercrystalline porosity is generally low. Although many crystals display a cloudy core and a clearer rim under normal light there is no apparent CL zonation, but the crystals are uniformly dull red (Fig. 3.12b). Replacement dolomite type II is the main type in the Cooking Lake and Leduc Formations, in pervasively dolomitized parts of the LGM, which directly overly Leduc buildups and in the southern part of the Grosmont platform (Fig. 3.11). This distribution suggests formation from burial fluids that migrated through the Leduc buildups into the Grosmont Formation.

Dolomite cement I.- This type of dolomite cement formed a clear, limpid overgrowth around replacement dolomite I in especially porous intervals (Figs. 3.9c; 3.12a). It also formed narrow cement fringes around fossil molds. Where developed as cement crystal size ranges from 50μm to 150μm. Dolomite cement I is generally uniformly red to orange luminescent.

Fe-dolomite cement.- Similar to dolomite cement I this type of cement formed clear overgrowths around replacement dolomite I crystals (Fig. 3.10c). It also grew in fractures and cleavage planes of the earlier replacement dolomite and formed cements in

Fig. 3.10a: Cloudy, replacement dolomite I is followed by single overgrowth zones and complete rhombs (DC) of clear dolomite cement I (arrow). The large pink crystals are pore filling blocky calcite III cements. Stained thin section, well location 5-24-63-24W4, 4375' (Leduc Fm.).

Fig. 3.10b: Zoned, orange luminescent type I replacement dolomites in dull red luminescent limestone matrix. Thin section, cathodoluminescence light, well location 10-17-83-18W4, 455.0 m (LGM).

Fig. 3.10c: Replacement dolomite type I in dark brown, micritic limestone matrix. Thin section, well location 10-17-83-18W4, 455.0 m (LGM).

Fig. 3.10d: Same view as in (c) but under cathodoluminescence light. Clearly visible are the non-luminescent Fe-dolomite overgrowth zones which are not apparent under are plain light.

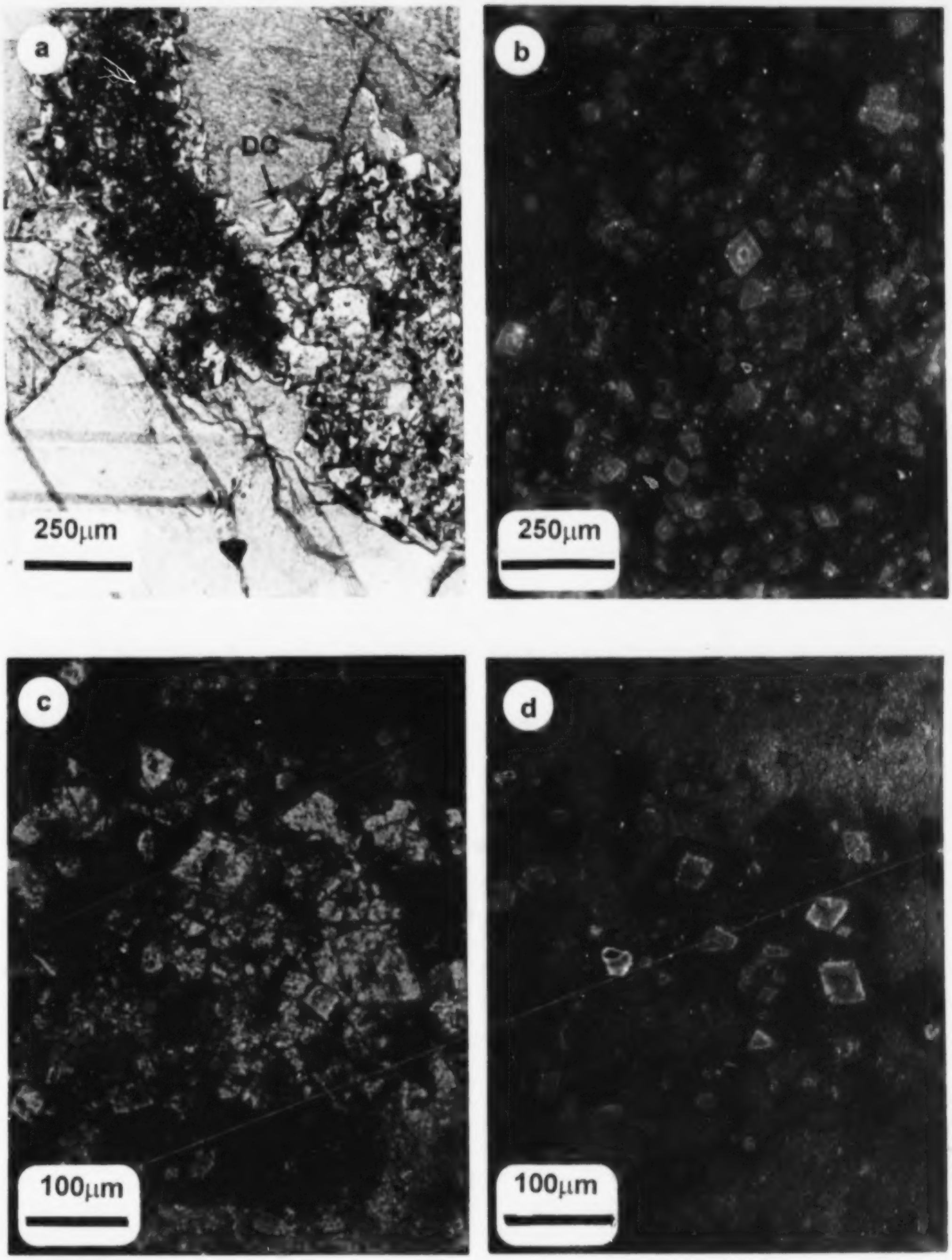
a
DC
250µm
b
250µm
c
100µm
d
100µm

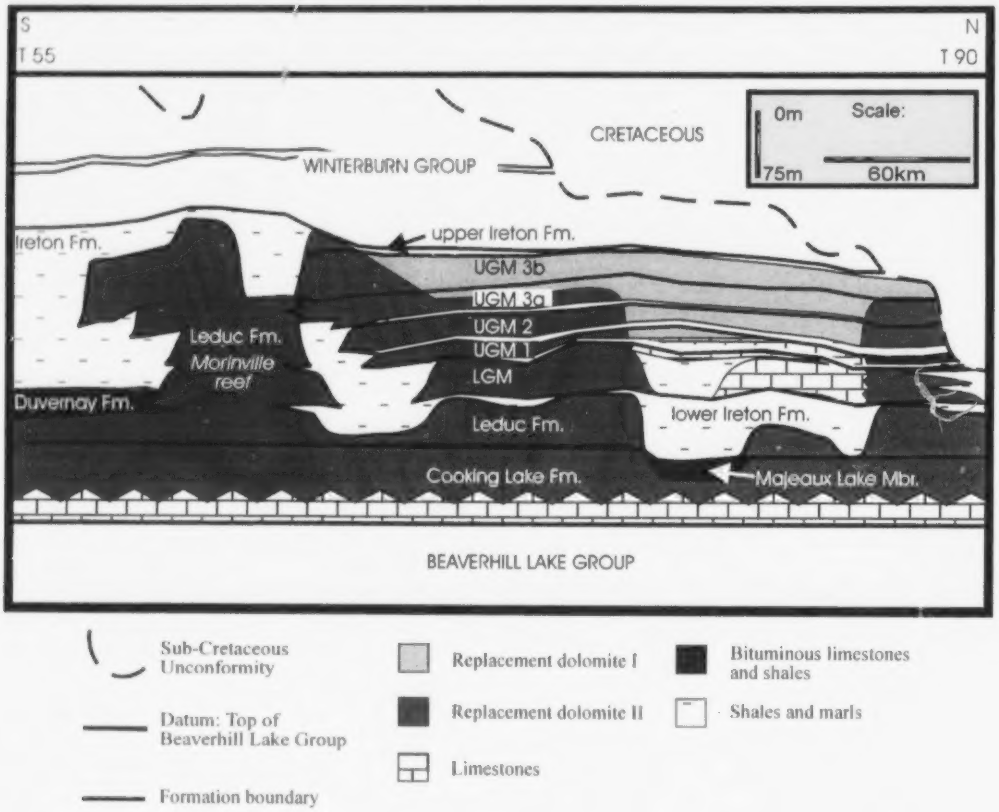
S
T 55
N
T 90
0m
Scale:
75m
60km
CRETACEOUS
WINTERBURN GROUP
Ireton Fm.
upper Ireton Fm.
UGM 3b
UGM 3a
UGM 2
UGM 1
LGM
Leduc Fm.
Morinville reef
Duvernay Fm.
Leduc Fm.
lower Ireton Fm.
Cooking Lake Fm.
Majeaux Lake Mbr.
BEAVERHILL LAKE GROUP
Sub-Cretaceous Unconformity
Datum: Top of Beaverhill Lake Group
Formation boundary
Replacement dolomite I
Replacement dolomite II
Limestones
Bituminous limestones and shales
Shales and marls

Fig. 3.11: North-south cross section through the Woodbend Group in north-central Alberta showing the distribution of replacement dolomites. Replacement dolomite I predominate dolostones in the northern part of the Grosmont platform. Replacement dolomite II occurs in the Cooking Lake and Leduc Formations as well as in directly overlying portions of the Grosmont Formation. This section follows the northern extension of the Rimbey-Meadowbrook reef trend from township 90 to the Morinville reef in the south. For location of the cross-section (A-A') see Fig. 3.2.

Fig. 3.12a: Dense mosaic of type II replacement dolomites. Thin section, well location 6-16-66-24W4, 3677' (Leduc Fm.).

Fig. 3.12b: Same view as in (a) but under cathodoluminescence light, showing the for type II replacement dolomites characteristic red to dull red, mottled luminescence.

Fig. 3.12c: Dense mosaic of type II replacement dolomites crosscut by stylolite (St). Thin section, well location 7-31-61-24W4, 3996' (Leduc Fm.).

Fig. 3.12d: Type II replacement dolomite crosscut by solution seams. Laminae consisting of coarse dolomites with clear rims are separated from laminae consisting of smaller, cloudy dolomite crystals. In some instances (arrow) individual dolomite crystals appear to crosscut solution seams. However, oil stain (O) in solution seams always crosscuts dolomite crystals implying that these crystals do not crosscut the seam and that apparent continuity of dolomite crystals is probably related to only minor displacement. Thin section, well location 4-33-68-22W4, 3470' (lower Cooking Lake Fm.).

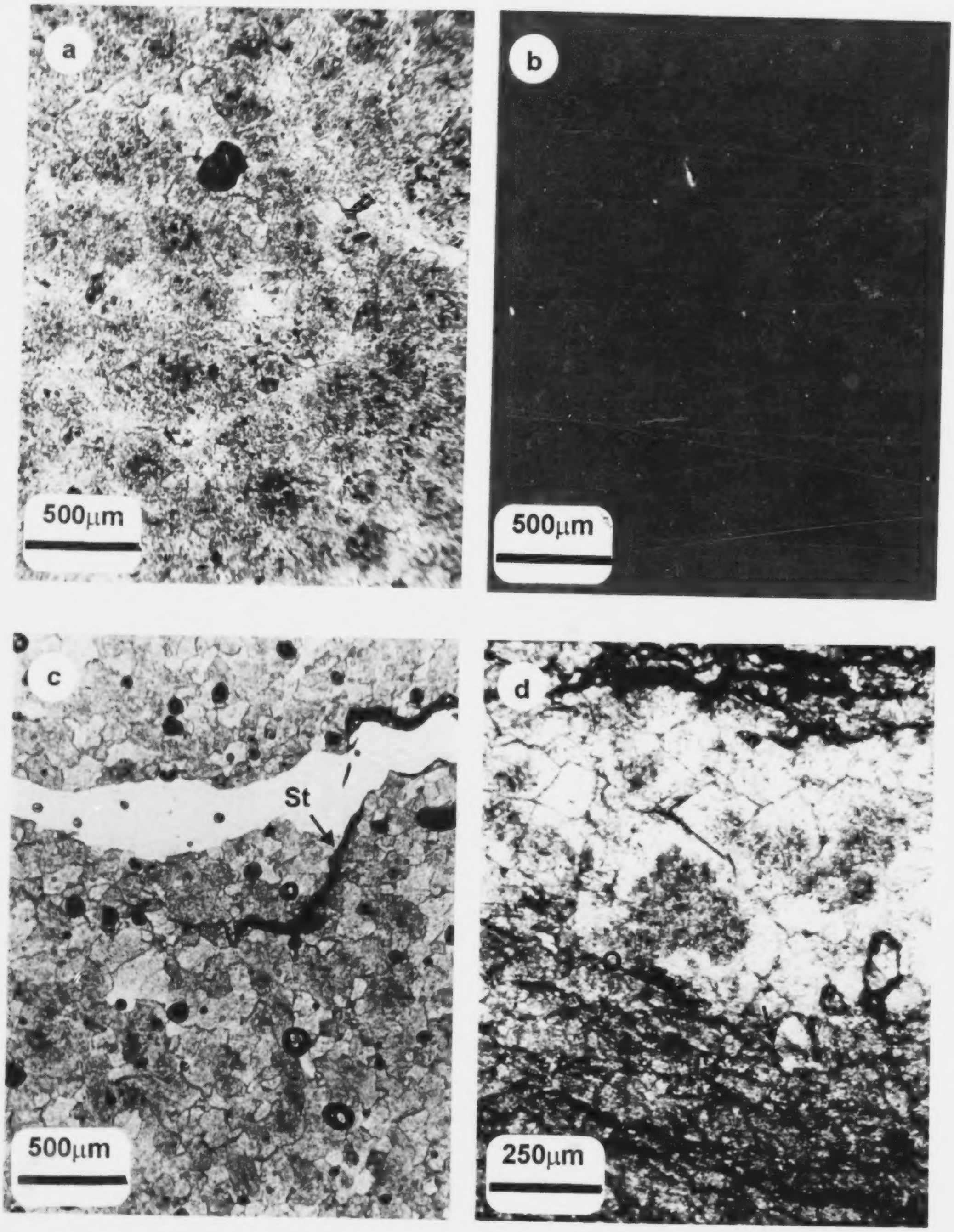
a
500μm
b
500μm
c
St
500μm
d
250μm

Fig. 3.13a: Zoned dolomite cement II (DC) developed on cloudy, brown-grey replacement dolomite II. Rest of pore space was filled by blocky calcite cement III. Thin section, well location 6-16-66-24W4, 3298' (UGM 3a).

Fig. 3.13b: Same view as in (a) but under cathodoluminescence light.

Fig. 3.13c: Dolomite cement II (DC) in pore space later filled by blocky calcite cement III (BCC III). Pyrite replaces dolomite at the interface between replacement dolomite II (upper edge of photomicrograph) and dolomite cement II. Stained thin section, well location 6-16-66-24W4, 3421' (UGM 2).

Fig. 3.13d: Pore space filled by pink, blocky calcite cement, anhydrite laths (A) and sulphur cement (S). Rest pore space is lined by brown oil stain. Stained thin section, well location 10-17-84-19W4, 499.5 m (LGM).

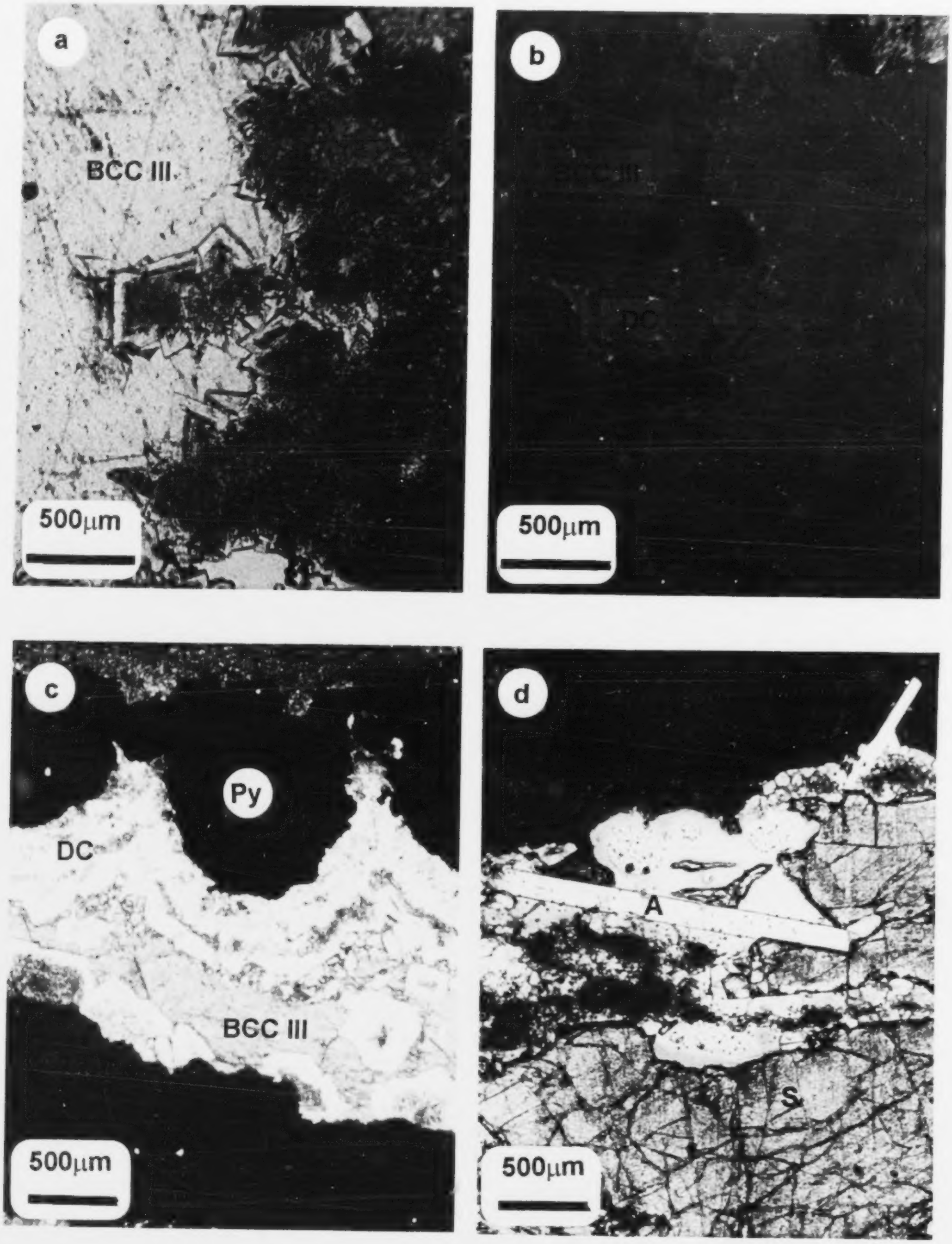
a
BCC III
500µm
b
BCC III
DC
500µm
c
Py
DC
BCC III
500µm
d
A
S
500µm

molds of previously dissolved anhydrite and/or gypsum laths (Fig. 3.6d). Because of their high iron content these cements are turquoise to light blue in stained thin section and are non-luminescent (Figs. 3.9d; 3.10d). This dolomite cement type is restricted to partially dolomitized intervals of the LGM and UGM 1.

Dolomite cement II.- Minor dolomite cement II lines secondary pore spaces such as anhydrite dissolution vugs and third generation fractures in dolomitized rocks (Figs. 3.9e; 3.13a-c). Dolomite cement II is coarse crystalline, ranging from 200μm to 400μm in diameter, displays sweeping extinction between crossed polars and often shows two or more growth zones under plane light. This zoning of dolomite cement II corresponds to CL zonation, with individual zones ranging from bright red and orange to dull red (Fig. 3.13b). Dolomite cement II occurs dominantly in the Cooking Lake and Leduc Formations as well as in the southern portions of the Grosmont Formation.

Effects on porosity development.- Intercrystalline porosity occurs in dolostones that consist of euhedral to subhedral crystals and comprises most of the matrix porosity in dolomitized intervals. Uniform size and euhedral shape of replacement dolomite crystals may also be responsible for improved permeabilities of completely dolomitized rocks (Wardlaw, 1979). In the upper Grosmont Formation matrix porosity is commonly in the range of 5 to 15% (Luo et al., 1994; Luo and Machel, 1995). Intercrystalline pores are mostly open and provide significant matrix permeability, but are occluded locally by dolomite cement I and Fe-dolomite cement, by late calcite cements I and II, and by poikilotopic gypsum cement.

The origin of intercrystalline pores is subject to debate. Intercrystalline porosity may be created by dolomitization itself if it follows the commonly expressed dolomitization reaction (Bathurst, 1975).

(1) $$2CaCO_3+Mg^{2+}\rightleftharpoons CaMg(CO_3)_2+Ca^{2+}$$

This reaction would result in a volume loss leading to porosity creation of about 13 % (Morrow, 1990). However, most dolomitized rocks appear not to have undergone volume changes. Instead, dolomitization is thought to have proceeded via volume for volume replacement (Friedman and Sanders, 1967) preserving the sediments original volume and porosity. Following this line of thought, dolomitization did not create porosity, but rather altered already present porosity and provided the rigid, compaction-resistant framework to preserve it (Purser et al., 1994). Petrographical observations suggest that much of the intercrystalline porosity may have been caused by later removal of remnant calcite matrix.

Dedolomitization

Calcitized dolomite (Fig. 3.6c) is present in minor amounts throughout the Grosmont Formation. Most commonly, dedolomite is observed in partially dolomitized intervals of the LGM and UGM 1, and in the UGM 2, UGM 3a and UGM 3b units where these are in proximity (less than 10 m) to the sub-Cretaceous unconformity.

In partially dolomitized intervals of the LGM and UGM 1 calcitization affected small dolomite crystals (< 20 μm). The calcitization process is usually complete, so that it is difficult to ascertain whether it was an actual replacement process or whether calcitization proceeded via complete dissolution and later cementation of the crystal mold by BCC I. Reservoir characteristics were not affected by this type of calcitization. Theriault and Hutcheon (1987) interpreted calcitization in limestone intervals to have occurred early in diagenetic history concomitant with dolomitization. During the dolomitization process dolomitizing solutions, initially supersaturated with respect to dolomite, may have become saturated with respect to both dolomite and calcite. Early calcian dolomites and zones containing calcian dolomites would be dissolved and replaced by calcite. Alternatively, dolomites may have been dissolved by fluids undersaturated with respect to dolomite and the resulting dolomite crystal molds were later filled by calcite cement.

Unconformity related calcitization affected fine grained dolomites (less than 50 μm in diameter) and is associated with strongly karstified or weathered horizons. The extent of the calcitization process varies from selective, affecting only cloudy cores or particular zones of dolomite crystals, to complete. Calcitized dolostones of this type are red-orange luminescent and have a stable isotope composition (δ^{18}O of -13.3 to -14.1 ‰ PDB, δ^{13}C of -4.4 to -4.9 ‰ PDB) close to that of microstalactitic cement (Fig. 3.8). They often retain the fabrics as well as the porosity and permeability characteristics of their precursors (Fig. 3.6c). However, in some cases intercrystalline porosity is destroyed by calcite cement overgrowth on the calcitized crystals. The proximity of this type of dedolomite to the unconformity and its isotopic composition suggest that the calcitization process is related to long-term subaerial exposure and influx of meteoric water. Requirements for calcitization under these conditions, such as (1) low Mg/Ca ratio of the calcitizing solution, (2) high rate of water flow due to increased permeability, (3) high CO_2 partial pressure, (4) pH below 7.8 at a temperature below 50°C (De Groot, 1967), were probably met during Mesozoic karstification. A remaining problem, however, is the availability of calcium. Calcium may be derived from adjacent limestones and dolostones (Fig. 3.6c) and from the dissolution of sulfates (Back et al., 1983). Sulfate dissolution may have contributed major amounts of Ca, driving further dissolution of dolomite and concomitant precipitation of calcite (Back et al., 1983).

Sulfate emplacement and cementation

Syndepositional and diagenetic anhydrites.- Evidence and indications for syndepositional and diagenetic growth of anhydrite exist in many peritidal carbonate intervals and underlying subtidal Woodbend carbonates in the study area. Synsedimentary anhydrite occurs in the upper units of the Grosmont Formation and thin intervals of the LGM commonly in association with peritidal deposits (Fig. 3.14) (see also Chapter 2). The distribution of synsedimentary anhydrites is restricted to strata that are located about 100 to 150 m below the sub-Cretaceous unconformity suggesting that anhydrites were removed from strata that are in proximity to the Woodbend subcrop limit. Synsedimentary anhydrites are grayish translucent in hand specimens. They show planar bedding and are interlayered with dolostones or recrystallized limestones, or fill fenestral pores and early fractures. Synsedimentary anhydrites consist of masses of fibrous, microcrystalline or felted crystals.

Diagenetic anhydrites occur as displacive nodules, as cements in fossil molds, and as isolated, lath shaped crystals. Most occurrences of diagenetic anhydrites are closely associated with syndepositional anhydrites. Displacive anhydrite nodules and anhydrite cement in fossil molds occur in peritidal and underlying subtidal facies of the Grosmont Formation (Fig. 3.14). Minor amounts of diagenetic, nodular anhydrite are also present in the Leduc Formation. Similar to syndepositional anhydrites nodular anhydrites and anhydrite cements are grayish translucent in hand specimens (Fig. 3.15a) and consist of

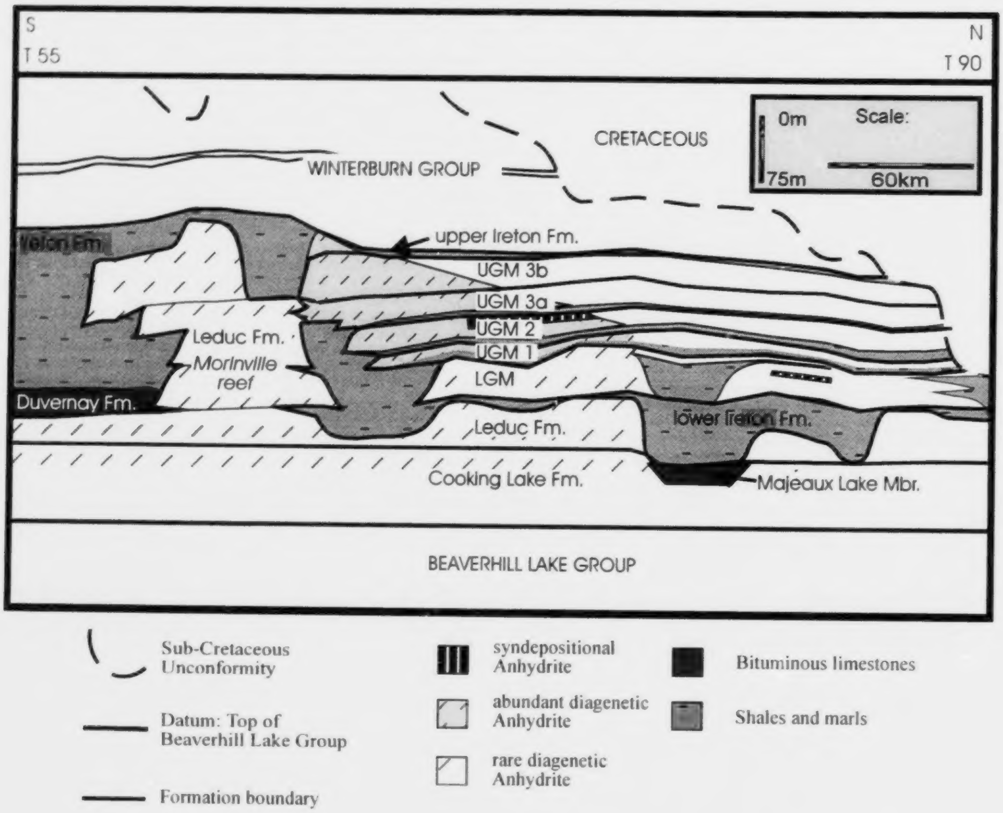
S
T 55
N
T 90
CRETACEOUS
Scale:
0m
75m
60km
WINTERBURN GROUP
Ireton Fm.
upper Ireton Fm.
UGM 3b
UGM 3a
UGM 2
UGM 1
LGM
Leduc Fm.
Morinville reef
Duvernay Fm.
Leduc Fm.
lower Ireton Fm.
Cooking Lake Fm.
Majeaux Lake Mbr.
BEAVERHILL LAKE GROUP
Sub-Cretaceous Unconformity
Datum: Top of Beaverhill Lake Group
Formation boundary
syndepositional Anhydrite
abundant diagenetic Anhydrite
rare diagenetic Anhydrite
Bituminous limestones
Shales and marls

Fig. 3.14: North-south cross section through the Woodbend Group in north-central Alberta. Shown is the distribution of syndepositional and diagenetic anhydrites in Woodbend Group carbonates. This section follows the northern extension of the Rimbey-Meadowbrook reef trend from township 90 to the Morinville reef in the south. For location of the cross-section (A-A') see Fig. 3.2.

Fig. 3.15a: Sulfates infilling vugs, moulds and fractures in dolostone interval. Most of the infilling material is light grey anhydrite, the outer rims consist of white appearing gypsum indicating beginning sulfate dissolution. Coin is 17.5 mm in diameter. Core photograph, well location 10-18-76-25W4, 3484' (UGM 1).

Fig. 3.15b: Located a few feet above (a). Only one pore is filled by white gypsum, all other pores are devoid of sulfates. This situation is interpreted to have been caused by sulfate dissolution creating vuggy and moldic porosity in this dolostone interval. Coin is 17.5 mm in diameter. Core photograph, well location 10-18-76-25W4, 3479' (UGM 1).

Fig. 3.15c: Black, cryptocrystalline gypsum (G) replacing corroded lath shaped anhydrite (A) along the outer rim of an anhydrite nodule. Coarse crystals in the upper, right hand corner are type II replacement dolomite. Thin section, X Nicols, well location 11-4-72-23W4, 3114' (LGM).

Fig. 3.15d: Similar situation as in (c). Poikilotopic gypsum (G) has almost completely replaced lath shaped (?) anhydrite (arrow). The outer edge of the nodule is indicated by replacement dolomite II (D). Thin section, X Nicols, well location 11-4-72-23W4, 3063' (UGM 1).

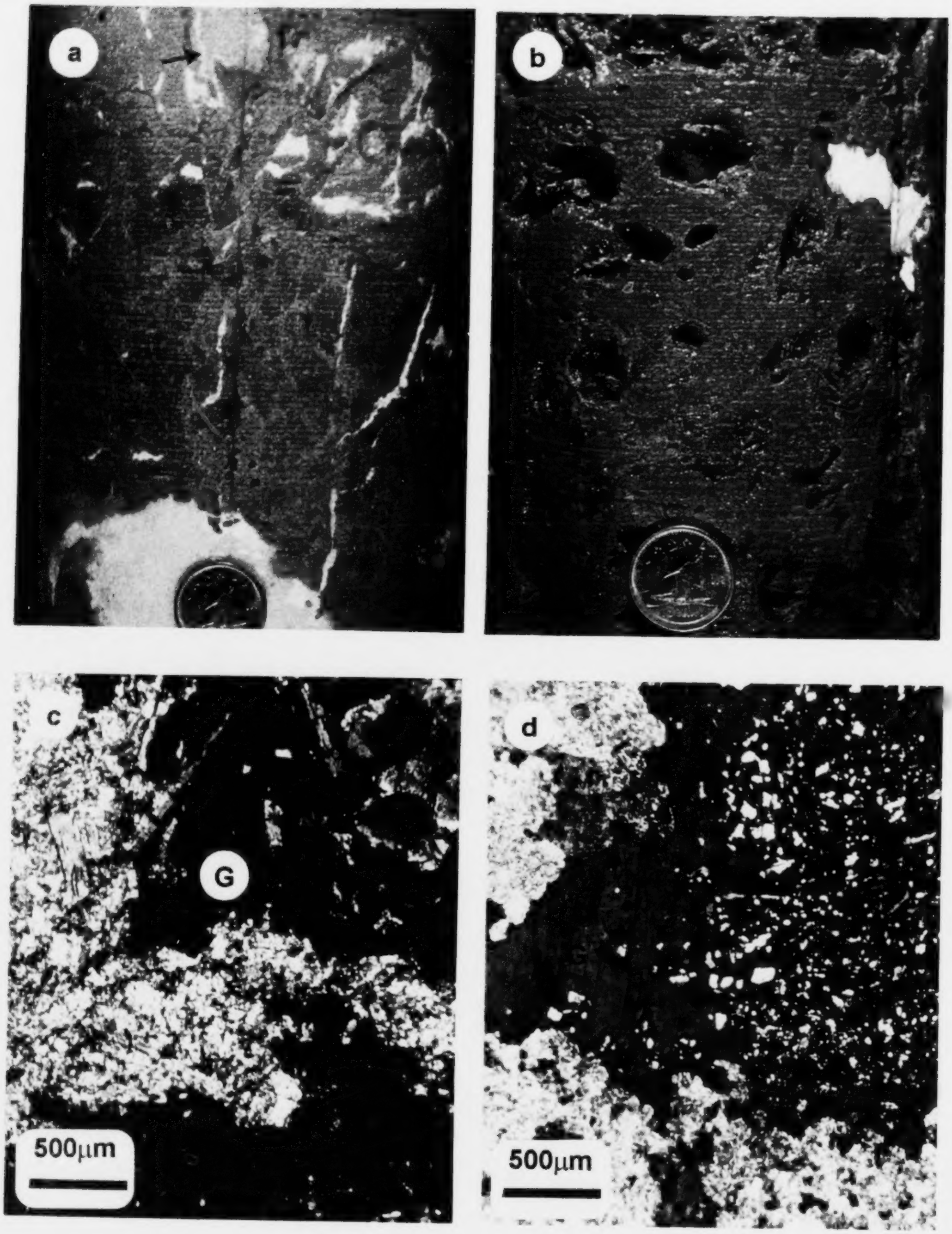
a
b
c
G
500µm
d
500µm

masses of fibrous, microcrystalline, felted, lath shaped (Figs. 3.15c-d) crystals. Close to the Woodbend subcrop dissolution of anhydrite created irregular vugs that resemble anhydrite nodules in shape and size as well as reopened fossil molds (Fig. 3.15b). Lath shaped anhydrite occurs as displacive phase dispersed in peritidal dolostones, as replacement of fibrous calcite in stromatoporoids, and as cement in secondary pores (Fig. 3.13d). Lath shaped crystal molds are common in intervals where anhydrites were removed.

Replacive gypsum and gypsum cement.- Gypsum is developed as cryptocrystalline replacement of anhydrite (Fig. 3.15c) and as poikilotopic replacement of anhydrite (Fig. 3.15d) and/or cement. Both types of gypsum are present in Grosmont Formation intervals where anhydrite is dissolved. Gypsum may completely replace anhydrite in vugs and molds (Fig. 3.15b), but generally occurs only on the outside rim of an anhydrite filled vug or mold (Figs. 3.15a-d).

Poikilotopic gypsum cement is often developed in the dolomite rock matrix near anhydrite and/or gypsum filled vugs and molds. Gypsum crystals are often several cm in diameter and effectively occlude intercrystalline porosity.

Effects on porosity development.- Sulfates are an important pore occluding phase in the study area, especially in the UGM 3a and 3b units south of township 80 and west of range 25W4 (Fig. 3.14). Layers of sedimentary anhydrite have practically no porosity and may act as local permeability barriers. Nodular anhydrite and anhydrite cement, although they have little effect on dolomite matrix porosities (intercrystalline porosity), occlude much of the larger pore spaces such as vugs, fossil molds and fractures, resulting in the estimated reduction of overall reservoir porosities by about 5 to 10 %. Gypsum cement, which is probably the result of anhydrite conversion during early stages of anhydrite dissolution locally occludes dolomite matrix porosity. Because of its small quantity, however, gypsum cement is overall negligible in determining reservoir characteristics.

Dissolution

Early calcite dissolution.- Dissolution of former aragonitic bioclasts (e.g. mollusc fragments) and porous calcitic fossils such as corals and stromatoporoids resulted in the formation of moldic porosity. Crinoids and brachiopods are generally the most resistant to dissolution. Occurrence of moldic porosity, furthermore, appears to be correlative to the grain and/or crystal size and, therefore, permeability of the carbonate host rock. Bioclasts tend to be preserved in fine grained, tight carbonate intervals. In porous and permeable zones dissolution was most complete. Molds occurring in limestone are completely filled by early internal sediments and early as well as late calcite cements. In dolostones molds may be partially filled by dolomite cement I and anhydrite but more often remained open (Fig. 3.16a). Overall, this pore type contributes only small amounts of porosity (< 1 %). In some facies types, however, e.g. in dolomitized *Amphipora* floatstones, fossil molds contribute significantly (as much as 10 %) to overall porosity.

The timing of early calcite dissolution relative to dolomitization remains unclear. Some fossil molds, characterized by matrix dolomites growing into the mold, appear to have formed prior to or during dolomitization. In other cases, bioclasts were removed after dolomitization and either remained open or were filled by later dolomite cements. In the later case a distinction between cemented fossil molds and dolomitized bioclasts may often not be possible or is based on ghost structures in dolomite crystals. The different pathways of bioclasts and fossil molds in dolomitized intervals are summarized in Fig. 3.17.

Sulfate dissolution.- Removal of sulfates resulted in the formation of considerable moldic and vuggy porosity (Fig. 3.15b), mostly in the Grosmont Formation. It is likely that dissolution of sulfates was an active process during much of Woodbend Group diagenesis. Concave walls of sulfate molds and the presence of pre-compactional cements in these pores indicate that sulfate removal started before compaction.

Sulfate dissolution molds are common in peritidal and underlying subtidal sediments of the Grosmont Formation. Most common are lath shaped molds after anhydrite and/or gypsum which are commonly open in dolostones. In limestones molds were filled by blocky calcite cement I and II or Fe-dolomite cement. The effect of

Fig. 3.16a: Early carbonate dissolution molds (arrow) and compaction fractures (F) in bioturbated biomudstone facies. Well location 13-22-83-22W4, 558.0 m (UGM 3a).

Fig. 3.16b: Top view of karst related fracture breccia. Fractures are filled with bitumen. Well location 14-17-87-20W4, 1039' (UGM 3a).

Fig. 3.16c: Top view of core sample displaying vertical karst fractures and carbonate dissolution vugs (arrows). Vugs and fractures are partially filled by cave-filling sediments. Coin is 17.5 mm in diameter. Well location 14-17-87-20W4, 1037' (UGM 3a).

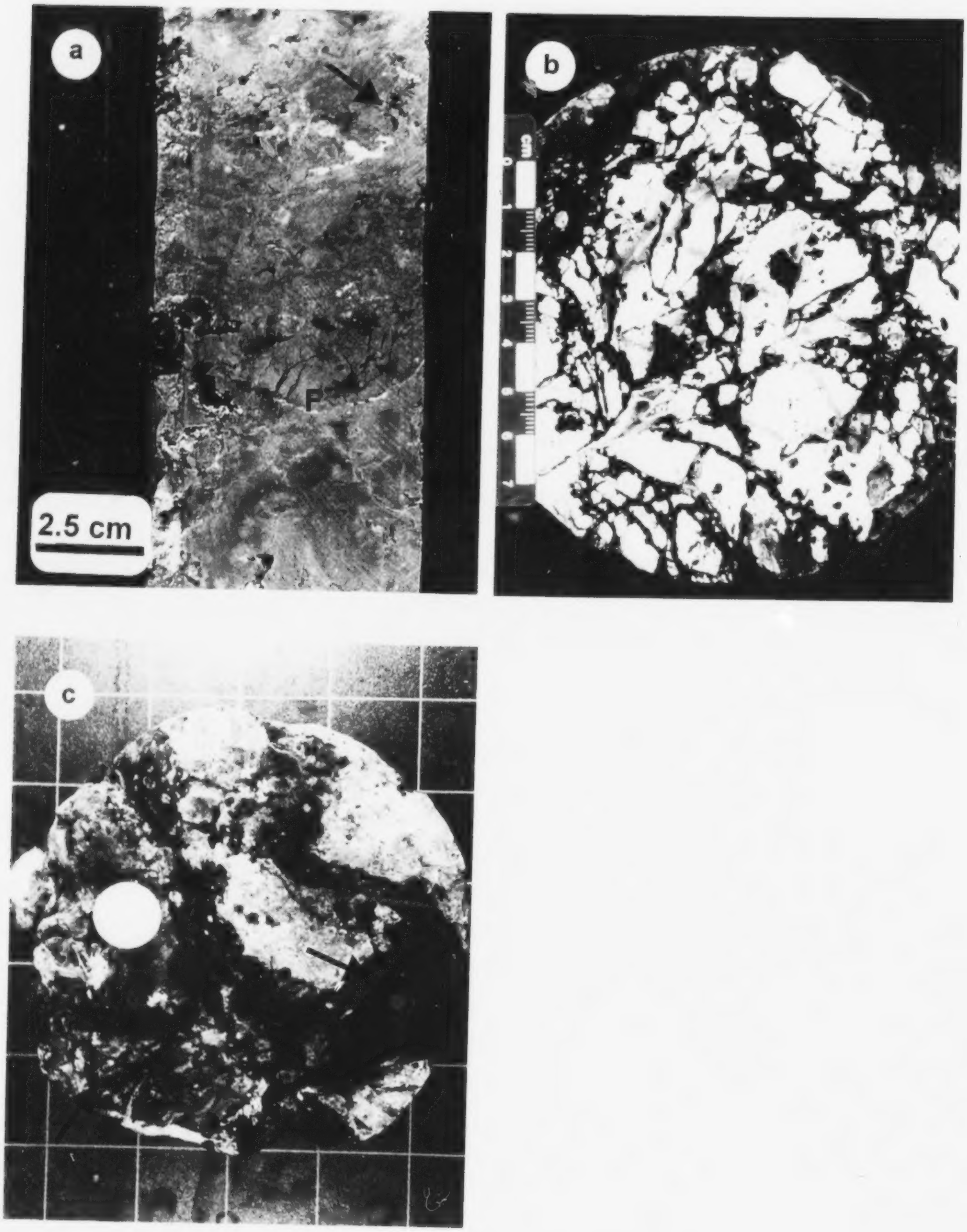
a
2.5 cm
P
b
cm
0
1
2
3
4
5
6
7
c

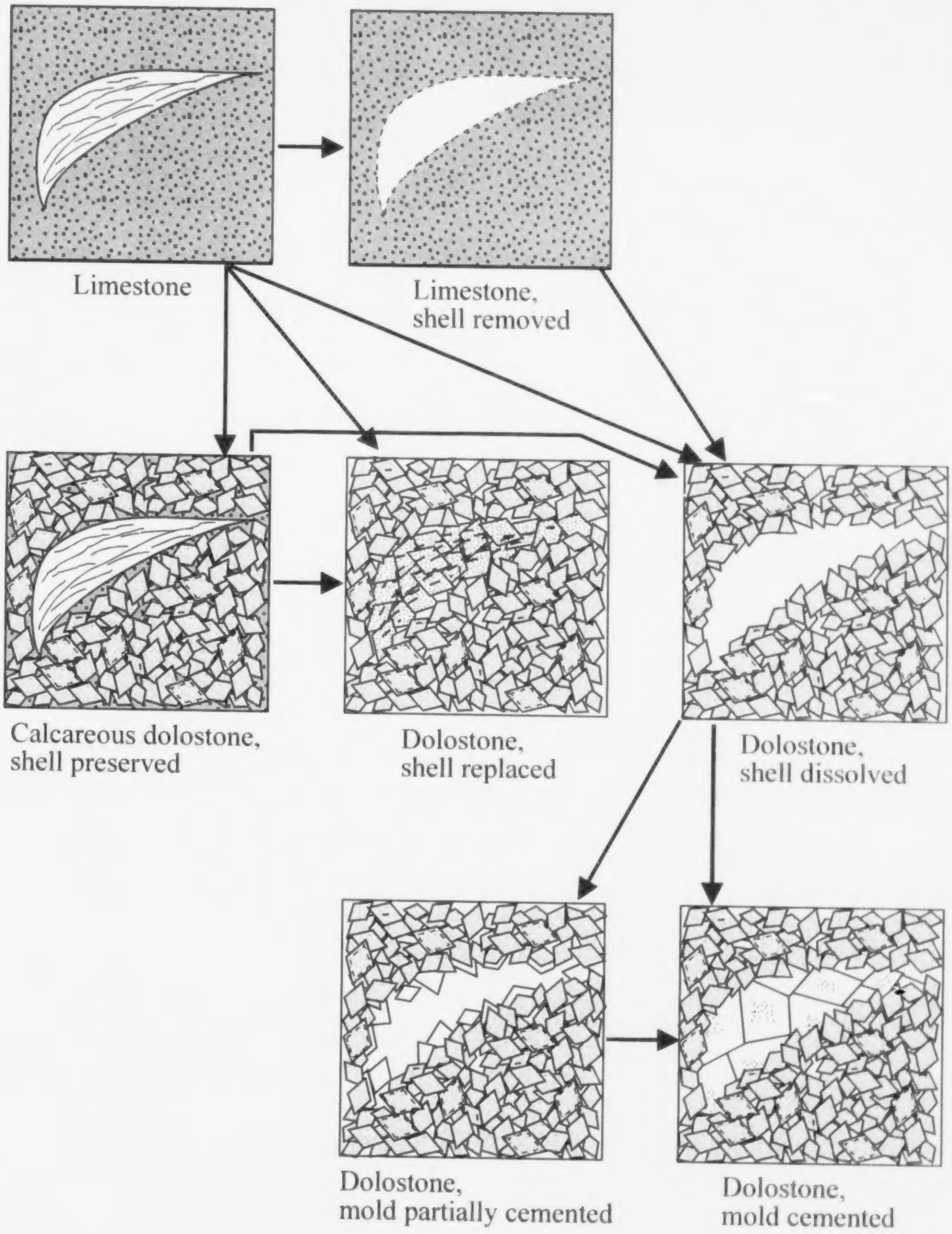
Limestone
Limestone, shell removed
Calcareous dolostone, shell preserved
Dolostone, shell replaced
Dolostone, shell dissolved
Dolostone, mold partially cemented
Dolostone, mold cemented

Fig. 3.17: Possible pathways for creation and destruction of bioclast molds in Woodbend dolostones. All situations shown are present in the study area.

evaporite molds on overall porosity characteristics is minor.

Sulfate dissolution vugs resemble sulfate nodules in shape and size (few mm to several cm in diameter), and are most common in peritidal carbonates of the upper Grosmont Formation. These vugs are generally unfilled but may be lined by pyrite, dolomite cement II, blocky calcite cement III, or sulfur. Dissolution vugs added significant amounts (5 to 10 %) of secondary porosity to the upper Grosmont Formation. Dissolution of nodular anhydrite appears to have proceeded via conversion to gypsum that advanced from the nodule rim inward (Fig. 3.15a-b). In some areas sulfate dissolution was so extensive that it caused collapse of overlying strata (Cutler, 1983; and Chapter 5, this volume). The timing of vug formation is difficult to constrain. The lack of anhydrite and gypsum directly beneath the sub-Cretaceous unconformity suggests removal of sulfates by meteoric water during Mesozoic karstification (see Chapter 5). Alternatively, sulfates may have been dissolved by ascending basinal waters. Sulfate dissolution by ascending waters is supported by high concentrations of dissolved SO_4^{2-} in Grosmont formation waters of northeastern Alberta (Bachu and Underschultz, 1993).

Karstification.- Carbonate dissolution related to subaerial exposure of Woodbend carbonates along the sub-Cretaceous unconformity created large amounts of secondary porosity. Secondary pores created by karstification include micron-sized intracrystalline pores, mm to cm-sized vugs (Fig. 3.16c) and meter-sized caverns. The contribution of karstification to overall reservoir porosities is significant. Porosity of karstified interval averages 20 to 25 %, and can locally exceed 40 % (Luo et al., 1993). Carbonate dissolution due to karstification is restricted to the Grosmont subcrop edge in the northern part of the study area (Fig. 3.5). The effects of karstification are pervasive and are not limited to particular facies types or lithologies, although dolostones of the UGM 2, UGM 3a, and UGM 3b are the most affected. Karst related carbonate dissolution is most intense in an interval between 0 to 20 m below the sub-Cretaceous unconformity. Karst related pores are an especially effective reservoir because these pores are rarely occluded (by cave-filling sediments). In addition, karstified intervals are characterized by abundant fractures (Figs. 3.17b,c) (generally more than 5 fractures per m of core), which create, together with cavern systems, permeability pathways. Hence, reservoir permeabilities in karstified intervals reach from >100 mD to several darcies (Luo et al., 1993). Karst related fabrics and their distribution are discussed in greater detail in Chapter 5.

Fracturing

Fracturing is an important process creating secondary porosity and, more importantly, permeability in Woodbend Group carbonates. Four fracture generations are distinguished by size and orientation and by the type of infilling cement and/or sediment.

The earliest fractures (fracture I) are synsedimentary and are interpreted to be related to desiccation and dewatering processes. This type of fracture is generally short (mm to a few cm), less than one mm wide and has a vertical to sub-vertical orientation. In limestone intervals type I fractures are filled by early internal sediments and early, marine, fibrous or bladed calcite cements. This fracture type is associated with peritidal facies types and is most common in the upper Grosmont Formation. The effects of this fracture type on overall reservoir characteristics are negligible.

The second fracture generation consists of irregular, vertical to sub-vertical fractures that range from a few cm to several dm in length and a few μm to one mm in width. This fracture type occurs in clean carbonates (limestones as well as dolostones) throughout the Woodbend Group. In limestones this fracture type is occluded by Fe-dolomite cement, BCC II and/or BCC III (Figs. 3.6a,d). In dolostones type II fractures remained open (Fig. 3.16a).

Type III fractures terminate at and radiate from dissolution vugs and molds. This fracture type ranges from a few cm to several dm in length and reaches a width of several mm. Type III fractures occur in (mostly dolomitized) intervals of the Grosmont Formation that contain sulfate nodules or vugs resulting from sulfate dissolution (Fig. 3.14a). Gypsum is the most common fracture fill suggesting that fracturing may have been caused by gypsum crystallization. Other fracture filling or lining phases include pyrite, and rare BCC III. Intervals affected by this fracture type can have fracture densities of several fractures per meter of core, creating effective though fairly localized permeability pathways.

The most abundant fracture generation (fracture IV) is related to karstification, i.e.

it occurs in proximity to dissolution caves and brecciated intervals indicating collapse of carbonate strata. Type IV fractures contribute greatly to the permeability of the upper Grosmont Formation in the northern part of the study area (Fig. 3.5). This fracture type (Figs. 3.16b,c) ranges from several cm to several m in length and from <1mm to several cm in width. Fracture orientation is random. Fracture density ranges from a few per meter of core to several tens per meter of core. High fracture density and resulting brecciation (Fig. 3.16b) is most abundant in the first 20 m below the sub-Cretaceous unconformity. Fracture fill by cave-filling sediments occurs locally (Fig. 3.16c).

Other diagenetic phases

Chert.- Microcrystalline, spherulitic and fibrous chert is present as minor replacement and cement (?) in limestone intervals, especially in the Majeaux Lake Member, the LGM and the UGM 1. Chert replaced micritic mud in argillaceous, deeper water limestones and replaced bioclast fragments or cemented intraparticle pores (?). Because the amount of chert present is minuscule, its effect on reservoir properties is negligible.

Compaction.- Compaction encompasses two processes, early mechanical compaction and later chemical compaction. Signs of mechanical compaction are relatively rare and include broken shell fragments, concave walls of molds and compactional fracturing (Fig. 3.16a) and draping. The sparsity of these signs suggests that mechanical compaction was often prevented by early cementation and/or its signs were obliterated by later phases such as dolomitization.

Signs of chemical compaction are common and include several types of solution seams. In argillaceous limestones low amplitude seams (amplitude <1 mm) with clay residue dominate. Large amplitude stylolites (amplitude several cm) occur in "clean" limestones. Solution seams are most abundant in argillaceous limestones (several tens to hundreds per meter of core. In "clean" limestones solution seams density is less than 10 per meter of core. Solution seams are less abundant (less than one per meter of core) in dolostones varying from low amplitude style seams to medium amplitude stylolites (amplitude few mm to 1 cm) (Figs. 3.12c,d).

Although compaction probably started early, the main phase of compaction, including the formation of most solution seams, post-dates early calcite cements and replacement dolomitization (Figs. 3.12c-d). Karstification, late evaporite dissolution and hydrocarbon emplacement post-date compaction. Compaction certainly reduced primary and secondary pores either by more effective packing of components or by dissolution of carbonate material and its reprecipitation as later cement in surrounding pore spaces (Wong and Oldershaw, 1981; Scholle and Halley, 1985). In dolomitized intervals, however, solution seams may act as horizontal permeability pathways (Fig. 3.12d).

Metal sulfides.- Pyrite is present as cement and as minor replacement of dolomite (Fig. 3.13c). Pyrite occurs as finely disseminated particles in dolostones the upper Grosmont Formation some pyrite comprising up to several percent of the rock matrix. It occurs in even greater concentration as early cement of hardground surfaces or as pore lining and replacement phase of sulfate dissolution vugs. Crystal size is generally $<100\mu m$ but reaches 2 mm when developed as replacement phase (Fig. 3.13c). The association of metal sulfides with sulfate dissolution porosity indicates the presence of sulfate in the system and its later reduction by bacteria to sulfide.

Hydrocarbons.- Bitumen and heavy oil are ubiquitous in most Woodbend units in the northern part of the study area which is part of the giant Grosmont heavy oil reservoir (Fig. 3.2). Bitumen and heavy oil are present in all Grosmont units and in the Leduc Formation. Bitumen saturation is highest in the UGM 2, UGM 3a and UGM 3b units. Grosmont bitumen has undergone extensive biodegradation and waterwashing (Hoffmann and Strausz, 1986; Brooks et al., 1989). Large amounts of methane, which was probably a byproduct of biodegradation, is also present, forming a chain of shallow gas pools along the Woodbend subcrop (Fig. 3.2). In the southern and central part of the study area only rare traces of oil stain (Fig. 3.12d) could be found, mainly in the area of the northern Rimbey-Meadowbrook reef trend. Oil emplacement post-dated all paragenetic phases, including karst, with the possible exception of BCC III and IV and sulfur cements which at least in part are related to biodegradation of hydrocarbons.

Sulfur.- Sulfur cements are very rare and are only present together with sulfates and oil or bitumen (Fig. 3.13d). Although they are developed as coarse crystals, their association with biodegraded bitumen suggests a biological origin of the sulfur, probably via biogenic sulfate reduction.

PARAGENETIC SEQUENCE

Syndepositional and early diagenetic processes, such as early, marine calcite cementation, emplacement of syndepositional anhydrite and perhaps the earliest dolomite (replacement dolomite I) occurred during the Late Devonian (Frasnian). Later dolomites and anhydrites, early metal sulfides as well as early carbonate dissolution and early dedolomitization are interpreted to have developed during shallow burial.

The first burial-uplift period, lasting from the Mississippian to the Jurassic (Fig. 3.4). The beginning of this period is defined by burial depth of at least 500 m, which approximates the onset of chemical compaction (Lind, 1993). The maximum burial depth of approximately 700 to 1,000 m (estimated from thicknesses of Paleozoic strata present near the study area) was reached during Pennsylvanian time when major epeirogenic uplift and subsequent sea level drop started a long period of subaerial exposure and erosion of Paleozoic carbonate sequences (Richards et al., 1994). Neomorphic fabrics, pressure solution seams, dolomite cement II, and (Fe-)calcite cement (BCC II) are interpreted to have formed during this period.

Following the first burial-uplift period, the northern part of the study area was subjected to a period of subaerial exposure resulting in extensive erosion and karstification during the Mesozoic era, most likely during the Jurassic and Early Cretaceous periods (Fig. 3.4 and Chapter 5). Karstification resulted in the development of carbonate and evaporite dissolution pores and karst related fractures (fracture IV) in the Grosmont heavy-oil reservoir. The subsequent infilling of these pores and fractures by cave-fill sediments and microstalactitic calcite cements as well as dedolomitization related to the sub-Cretaceous unconformity are also interpreted to have formed during this period.

The Woodbend Group was subsequently buried again under Late Cretaceous and

Tertiary sediments which have since then been partially removed (Fig. 3.4). During this second burial-uplift phase an estimated maximum burial depth of approximately 2,200 m was reached in the southern part of the study area (Morinville reef), whereas the northern part experienced only moderate burial (approximately 500 m). Hydrocarbon migration and subsequent biodegradation occurred during this period. Associated calcite (BCC III and IV) and sulfur cements also formed during this period.

Some diagenetic processes, such as the formation of fractures II and III, sulfate dissolution and the formation of gypsum and late pyrites probably occurred during several periods and/or their position in the paragenetic sequence is uncertain (Fig. 3.4).

DIAGENETIC RESERVOIR CLASSES

The diagenetic events discussed in the previous paragraphs form a composite paragenetic sequence (Fig. 3.4). In other words, the diagenetic products are never found in one hand specimen or sample. Some phases appear to be mutually exclusive, others phases (early calcite cementation) have been obliterated by some later phase (e.g. dolomitization) and are, therefore, not preserved in many locations.

Detailed paragenetic sequences can be defined on a variety of scales, ranging from individual pores and pore types (Schroeder, 1986), over individual facies types and lithologies to scales including whole stratigraphic units, reservoirs and aquifers. For the purpose of this regional study, it is important to generalize the many different diagenetic pathways to a few simplified pathways that describe the overall porosity development in regional scale diagenetic reservoir classes. Regional scale diagenetic reservoir classes invariably describe and/or are defined by the most important and widespread diagenetic phases, whereas minor phases have practically no effect on the overall lithologic and reservoir characteristics. Three diagenetic reservoir classes are defined in this study. The first two encompass the two main lithologies in Woodbend carbonates, (1) limestones and argillaceous limestones, and (2) dolostones (Fig, 3.5). The third diagenetic reservoir zone encompasses carbonates that have been affected by subaerial exposure and subsequent karstification (Fig. 3.5). Table 3.2 gives an overview of the overall, visually estimated

Table 3.2: Relative abundance of diagenetic phases

	Diag. Reservoir Class 1 Limestones	Diag. Reservoir Class 2 Dolostones Cook. Lk. & Leduc Fms.	Diag. Reservoir Class 2 Dolostones Grosmont Fm.	Diag. Reservoir Class 3 Karsted dolostones
Early internal sediment	++	+	+	?
Cave-filling sediment	-	-	-	++
Bladed calcite cement	++	-	-	-
Radial-fibrous calcite cement	++	-	-	-
Syntaxial calcite cement	+	-	-	-
BCC I	+++	-	-	-
Neomorphic calcite	++	+	+	-
BCC II	+++	+	+	-
BCC III	+	++	+	-
BCC IV	-	+	-	+
Replacement dolomite I	++	+	+++	+++
Replacement dolomite II	-	+++	++	++
Dolomite cement I	-	++	++	++
Fe-dolomite cement	++	-	+	-
Dolomite cement II	+	+	+	+
Early dedolomite	++	-	+	-
Late dedolomite	-	-	-	++
Syndep. anhydrite	+	-	++	-
Diag. anhydrite	+	+	++	-
Gypsum cement	+	-	+	-
Early carbonate dissolution	+	++	+++	?
Sulfate dissolution	+	?	++	+++
Late carbonate dissolution (Karst)	-	-	-	+++
Fracture I	+	+	+	+
Fracture II	++	++	++	++
Fracture III	+	+	++	++
Fracture IV	-	-	-	+++
Chert	+	+	+	+
Compaction seams	+++	+	+	+
Pyrite	++	+	++	++
Hydrocarbons	+	+	++	+++
Sulfur	+	+	-	-

Visual estimate and extrapolation from representative samples: +++ abundant; ++ common: + rare; - not o abundance of diagenetic phases in the three diagenetic reservoir classes.

Limestones and argillaceous limestones are dominated by calcite diagenesis. Early as well as late calcite cements almost completely occluded primary and secondary porosity. Dolomitization and anhydrite emplacement did not affect or only slightly affected these lithologies. Although some early dissolution of carbonate components and fracturing occurred, secondary porosity creation remained minor (less than 5 %) throughout diagenetic history. Compaction, however, played a considerable role and probably contributed carbonate for burial cementation. As a result, limestones and argillaceous limestones have low average porosities of 1 to 5 % (Fig. 3.4, and Luo et al., 1993, Luo et al., 1994). Dominant pore types are molds and fractures as well as minor interparticle pores. The distribution of limestones appears to be facies-dependent. Limestones are commonly associated with deeper water, mud dominated and argillaceous facies, and open marine platform facies (see Chapter 2). Consequently, limestones are stratigraphically restricted to units dominated by these facies types, such as the Cooking Lake Formation, the Majeaux Lake Member, the LGM and the UGM 1 (Fig. 3.5).

Diagenetic reservoir class 2 describes all intervals that have been mostly to completely dolomitized. Early, syndepositional diagenetic phases are generally obliterated, although they were probably present. The most dominating diagenetic phases are replacement dolomites and dolomite cements. As discussed previously, dolomitization may have created porosity or may have altered already present porosity and protected it from destruction by compaction. Dolomitization also affected permeability characteristics by creating uniform intercrystalline pores (Wardlaw, 1979). Other important phases include fracturing and anhydrite emplacement and removal, which created moldic and vuggy porosity. Cements are generally rare and consist primarily of dolomite cements infringing on intercrystalline pores, molds and vugs. Other cements such as calcite, gypsum and pyrite have had overall little effect but may be of local importance. Porosity of dolostones varies on average between 10 and 25 % (Fig. 3.13) depending on the dolomite texture and the amount of dolomite cements present. Replacement dolomite I forms euhedral to subhedral crystal mosaics that porosities of 15 to 25 %. Replacement dolomite II form subhedral to anhedral crystal mosaics and, consequently, have lower porosities of 5 to 15 %. The presence of anhydrite occludes porosity and may create a barrier to fluid flow.

The complete removal of anhydrite, on the other hand, raised porosity values to 30 %. Dolostone distribution is predominantly but not entirely facies dependent. Replacement dolomite I, which is the predominant dolomite type in the upper Grosmont Formation, is associated with restricted, shallow water facies which were at least temporarily subject to strong evaporation (Fig. 3.11). Replacement dolomite II, however, occurs throughout the Leduc Formation as well as underlying parts of the Cooking Lake platform margin and directly overlying parts of the Grosmont Formation (Fig 3.11). This distribution suggests that this replacement dolomite type was formed by fluids that migrated through the Cooking Lake platform margin and Leduc buildups into the Grosmont Formation (see Chapter 4; cf. Machel and Mountjoy, 1987).

Diagenetic reservoir class 3 encompasses intervals whose reservoir characteristics have been considerably changed by karstification. Karstification was generally restricted to the northern part of the study area (north of township 80), which was subaerially exposed during the late Mesozoic and is now subcropping beneath the sub-Cretaceous unconformity. Most affected were dolomitized intervals of the UGM 2, UGM 3a, and UGM 3b units (Fig. 3.5). Lower units were little affected. The diagenetic development of these units prior to karstification is, therefore, equivalent to the diagenetic development of diagenetic reservoir class 2. During subaerial exposure, however, sulfates and carbonates underwent major dissolution, creating abundant (5 to 20 %) secondary porosity and resulting in the complete removal of sulfate minerals. Carbonate dissolution created a variety of pore types ranging from micron-sized, intracrystalline pores to vugs, fractures and channels. Furthermore, previously present intercrystalline and fracture porosity was commonly enhanced. Karst related porosity destruction, either by cementation (microstalactitic cements), dedolomitization or cave infill, is of only local importance. Overall, karstification enhanced porosity values to an average of 25 to 40 % (Fig. 3.4, and Luo et al., 1993). Karstified intervals also have the highest bitumen saturation (Luo et al., 1993; Dembicki, 1994; Dembicki and Machel, 1996) and their enhanced porosities and permeabilities probably supported the extreme biodegradation and waterwashing of Grosmont heavy oils (Brooks et al., 1989).

SUMMARY AND CONCLUSIONS

Woodbend carbonates in north-central Alberta have a complex diagenetic history during which they passed through a sequence of diagenetic environments ranging from marine, shallow and deep burial to subaerial exposure and renewed burial. The widespread distribution of many diagenetic phases such as calcite cements, dolomites and sulfates suggest that regional factors controlled much of the Woodbend diagenesis. For example, the distribution patterns of replacement dolomite II and blocky calcite cement III suggest involvement of fluids that migrated through the Cooking Lake platform margin and Leduc reefs into the overlying Grosmont Formation. The distribution of other diagenetic phases, especially in the northern part of the study area, appears to have been controlled by more local factors. For example, karstification is restricted to the Grosmont subcrop edge beneath the sub-Cretaceous unconformity (Fig. 3.5). Karstification and hydrocarbon distribution in the Grosmont heavy-oil reservoir likely controlled the distribution of oil related phases such as blocky calcite cement IV.

The diagenetic reservoir development of limestones was dominated by pore destructing phases such as compaction and calcite cementation, resulting in low average limestone porosities of 1 to 5 %. Creation of secondary porosity was negligible to minor (less than 5 %) and was mainly related to early dissolution of bioclasts. In addition, secondary porosity was occluded by late diagenetic calcite cements.

Dolomitization appears to have redistributed original porosity and preserved porosity due to the lesser susceptibility of dolomite to compaction. Consequently, dolomitized intervals have higher average porosities of between 10 to 25 %. Secondary porosity, due to early dissolution of bioclasts, removal of sulfates and fracturing, contributed appreciable amounts of porosity (5 to 10 %). Overall reservoir characteristics of Woodbend dolostones are good since secondary pores are not or only partially occluded by cements and pores are, at least locally, connected by fractures. Reservoir heterogeneity results mainly from local porosity plugging by anhydrite and gypsum and from differences in crystal mosaics of replacement dolomites.

Karstified intervals are prime hydrocarbon reservoirs due to their greatly increased porosity (average 20 to 25 %, maximum 40 %) and permeability values (average 100 mD, maximum several Darcies). However, karstification also increased reservoir heterogeneity due to the heterogeneous distribution of fractures, breccias and caves. Due to their greatly enhanced porosity and permeability characteristics, compared to adjacent Devonian and Cretaceous units, the Grosmont Formation serves as local sink for formation fluids from these units (Bachu and Underschultz, 1993). This process was likely responsible for the extreme biodegradation and waterwashing of hydrocarbons in the Grosmont heavy-oil reservoir compared to heavy oils contained in the Lower Cretaceous Mannville Group (Athabasca oil sands) which directly overlies the Grosmont Formation.

REFERENCES

Amthor, J.E., Mountjoy, E.W., and Machel, H.G., 1993, Subsurface dolomites in Upper Devonian Leduc buildups, central part of Rimbey-Meadowbrook reef trend, Alberta, Canada. Bulletin of Canadian Petroleum Geology, v. 41, p. 164-185.

Bachu, S., and Underschultz, J.R., 1993, Hydrogeology of formation waters, northeastern Alberta Basin. American Association of Petroleum Geologists Bulletin, v. 77, p. 1745-1768.

Back, W., Hanshaw, W.W., Plummer, L.N., Rahn, P.H., Rightmire, C.T., and Rubin, M., 1983, Process and rate of dedolomitization: mass transfer and ^{14}C dating in a regional carbonate aquifer. Geological Society of America Bulletin, v. 94, p. 1415-1429.

Bathurst, R.G.C., 1975, Carbonate sediments and their diagenesis, 2nd enlarged edition, Developments in Sedimentology No. 12, Elsevier, Amsterdam, 658 p.

Brooks, P.W., Fowler, M.G., and Macqueen, R.W., 1989, Biomarker geochemistry of Cretaceous oil and tar sands and Palaeozoic carbonate trend bitumens, Western Canada Basin. In: Meyer, R.F., and Wiggins, E.J., eds., Proceedings, Fourth UNITAR/UNDP International Conference on heavy crude and tar sands, Alberta Oil Sands Technology and Research Authority, Edmonton, v. 2, Geology, Chemistry, p. 594-606, Discussion, p. 629-631.

Carothers, W.W., and Kharaka, J.K., 1980, Stable carbon isotopes of HCO_3^- in oil field waters - implications for the origin of CO_2. Geochimica et Cosmochimica Acta, v. 44, p. 323-332.

Carpenter, S.J., and Lohmann, K.C., 1989, $\delta^{18}O$ and $\delta^{13}C$ variations in Late Devonian marine cements from the Golden Spike and Nevis reefs, Alberta, Canada. Journal of Sedimentary Petrology, v. 59, p. 792-814.

Choquette, P.W., and James, N.P., 1990, Limestones - the burial diagenetic environment. In: McIlreath, I.A., and Morrow, D.W., eds., Diagenesis. Geoscience Canada Reprint Series 4, p. 75-111.

Choquette, P.W., and Pray, L.C., 1970, Geologic nomenclature and classification of porosity in sedimentary carbonates. American Association of Petroleum Geologists Bulletin, v. 54, p. 207-250.

Claypool, G.E., and Kaplan, I.R., 1974, The origin and distribution of methane in marine sediments. In: Kaplan, I.R., ed., Natural gases in marine sediments, Plenum, New York, p. 99-139.

Craig, H., 1957, Isotopic standards for carbon and oxygen and correlation factors for mass-spectrometric analysis of carbon dioxide. Geochimica et Cosmochimica Acta, v. 12, p. 133-149.

Cutler, W.G., 1983, Stratigraphy and sedimentology of the Upper Devonian Grosmont Formation, Alberta, Canada. Bulletin of Canadian Petroleum Geology, v. 31, p. 282-325.

De Groot, K., 1967, Experimental dedolomitization. Journal of Sedimentary Petrology, v. 37, p. 1216-1220.

Dembicki, E.A., 1994, The Upper Devonian Grosmont Formation: well log evaluation and regional mapping of a heavy oil carbonate reservoir in northeastern Alberta. Unpubl. M.Sc. thesis, University of Alberta, Edmonton, 221 p.

Dembicki, E.A., and Machel, H.G., 1996, Recognition and delineation of paleokarst zones by the use of wireline logs in the bitumen-saturated Upper Devonian Grosmont Formation of northeastern Alberta, Canada. American Association of Petroleum Geologists Bulletin, v. 80, p. 695-712.

Dickson, J.A., 1966, Carbonate identification and genesis as revealed by staining. Journal of Sedimentary Petrology, v. 36, p. 491-505.

Dickson, J.A.D., and Coleman, M.L., 1980, Changes in carbon and oxygen isotope composition during limestone diagenesis. Sedimentology, v. 27, p. 107-118.

Dimitrakopoulos, R., and Muehlenbachs, K., 1987, Biodegradation of petroleum as a source of ^{13}C-enriched carbon dioxide in the formation of carbonate cement. Chemical Geology, v. 65, p. 283-291.

Dunham, R.J., 1969, Early vadose silt in Townsend mound (reef), New Mexico. In:

Friedman, G.M., ed., Depositional environments in carbonate rocks, Society of Economic Paleontologists and Mineralogists Special Publication No. 14, p. 139-181.

Friedman, G.M., and Sanders, J.E., 1967, Origin and occurrence of dolostones. In: Chlingar, G.V., Bissell, H.J., and Fairbridge, R.W., eds., Carbonate rocks, Developments in Sedimentology No. 9A, Elsevier, Amsterdam, p. 267-348.

Gussow, W.C., 1954, Differential entrapment of oil and gas: a fundamental principle. American Association of Petroleum Geologists Bulletin, v. 38, p. 816-853.

Harrison, R.S., 1982, Geology and production history of the Grosmont carbonate pilot project, Alberta, Canada. In: Meyer, R.F., Wynn, J.C., and Olson, J.C., eds., The future of heavy crude and tar sands. Second International Conference on heavy crude and tar sands, Caracas, Venezuela, February 7-17, 1982, v. 1, p. 199-204.

Hoffmann, C.F., and Strausz, O.P., 1986, Bitumen accumulation in Grosmont platform complex, Upper Devonian, Alberta, Canada. American Association of Petroleum Geologists Bulletin, v. 70, p. 1113-1128.

Hudson, J.D., 1977, Stable isotopes and limestone lithification. Journal of the Geological Society of London, v. 133, p. 637-660.

Hutcheon, I., Abercombie, H.J., Putnam, P., Gardner, R., and Krouse, H.R., 1989, Diagenesis and sedimentology of the Clearwater Formation at Tucker Lake. Bulletin of Canadian Petroleum Geology, v. 37, p. 83-97.

James, N.P., and Choquette, P.W., 1990, Limestones - the meteoric diagenetic environment. In: McIlreath, I.A., and Morrow, D.W., eds., Diagenesis. Geoscience Canada Reprint Series 4, p. 35-73.

Jones, B., Lockhart, E.B., and Squair, C., 1984, Phreatic and vadose cements in the Tertiary Bluff Formation of Grand Cayman Island, British West Indies. Bulletin of Canadian Petroleum Geology, v. 32, p. 382-397.

Kendall, A.C., and Broughton, P.L., 1978, Origin of fabrics in speleothems composed of columnar calcite crystals. Journal of Sedimentary Petrology, v. 48, p. 519-538.

Kerans, C., Hurley, N.F., and Playford, P.E., 1986, Marine diagenesis in Devonian reef complexes of the Canning Basin, Western Australia. In: Schroeder, J.H., and Purser, B.H., eds., Reef diagenesis, Springer Verlag, Berlin, p. 357-380.

Laflamme, A.K., 1990, Replacement dolomitization in the Upper Devonian Leduc and Swan Hills Formations, Caroline area, Alberta, Canada. Unpubl. M.Sc. thesis, McGill University, Montreal, 138p.

Larson, P.A., 1988, Origins of Grosmont Formation dolomite (northeast Alberta): Modelling the results of geochemical analysis. In: McMillan, N.J., Embry, A.F., and Glass, D.J., eds., Devonian of the world, Volume II. Canadian Society of Petroleum Geologists Memoir 14, p. 525-530.

Lind, I.L., 1993, Stylolites in chalk from Leg 130, Ontong Java Plateau. In: Berger, W.H., Kroenke, J.W., Mayer, L.A., eds., Proceedings of the Ocean Drilling Program, Scientific Results, v. 130, p. 445-451.

Luo, P., Dembicki, E.A., Machel, H.G., and Huebscher, H., 1993, Diagenesis and reservoir characteristics of the heavy-oil carbonate trend in Western Canada - refined evaluation of reservoir characteristics of the Grosmont Formation. AOSTRA report 7 of 7, January 31, 1993, 170 p.

Luo, P., Huebscher, H., Dembicki, E.A., and Machel, H.G., 1992, Diagenesis and reservoir characteristics of the carbonate heavy-oil trend in Western Canada - continued investigation of reservoir characteristics of the Grosmont Formation. AOSTRA report 6 of 7, July 31, 1992, 141 p.

Luo, P., and Machel, H.G., 1995, Pore size and pore throat types in a heterogeneous dolostone reservoir, Devonian Grosmont Formation, Western Canada Sedimentary Basin. American Association of Petroleum Geologists Bulletin, v. 79, p. 1698-1720.

Luo, P., Machel, H.G., and Shaw, J., 1994, Petrophysical properties of matrix blocks of a heterogeneous dolostone reservoir - the Upper Devonian Grosmont Formation, Alberta, Canada. Bulletin of Canadian Petroleum Geology, v. 42, p. 465-481.

Machel H.G., and Hawlader, H.M., 1990, Diagenesis and reservoir characteristics of the heavy-oil carbonate trend in Western Canada - preliminary investigation of facies, diagenesis, and bitumen saturation of the Grosmont Formation. AOSTRA report 2 of 7, July 30, 1990, 168 p.

Machel, H.G., and Mountjoy, E.W., 1987, General constraints on extensive pervasive dolomitization - and their application to the Devonian carbonates of western Canada. Bulletin of Canadian Petroleum Geology, v. 35, p. 143-158.

McCrea, J.M., 1950, On the isotopic chemistry of carbonates and a paleotemperature scale. Journal of Chemical Physics, v. 18, p. 849-857.

McGillivray, J.G., and Mountjoy, E.W., 1975, Facies and related reservoir characteristics, Golden Spike reef complex, Alberta. Bulletin of Canadian Petroleum Geology, v. 23, p. 753-809.

Moore, C.H., 1985, Upper Jurassic subsurface cements: a case history. In: Schneidermann, N., and Harris, P.M., eds., Carbonate cements. Society of Economic

Paleontologists and Mineralogists Special Publication No. 36, p. 291-308.

Morrow, D.W., 1990, Dolomite - part 1: the chemistry of dolomitization and dolomite precipitation. In: McIlreath, I.A., and Morrow, D.W., eds., Diagenesis. Geoscience Canada Reprint Series 4, p. 113-123.

Mountjoy, E.W., and Krebs, W., 1983, Diagenesis of Devonian reefs and buildups, western Canada and Europe - a comparison. Zeitschrift der deutschen Geologischen Gesellschaft, v. 134, p. 5-60.

Patterson, W.P., and Walter, L.M., 1994, Depletion of ^{13}C in seawater $\sum CO_2$ on modern carbonate platforms: significance for the carbon isotopic record of carbonates. Geology, v. 22, p. 885-888.

Prezbindowski, D.R., 1985, Burial cementation - is it important ? A case study, Stuart City Trend, south central Texas. In: Schneidermann, N., and Harris, P.M., eds., Carbonate cements. Society of Economic Paleontologists and Mineralogists Special Publication No. 36, p. 241-264.

Purser, B.H., Brown, A., and Aissaoui, D.M., 1994, Nature, origins and evolution of porosity in dolomites. In: Purser, B.H., Tucker, M.E., and Zenger, D.H., Dolomites, A volume in honour of Dolomieu, Special Publication No. 21 of the International Association of Sedimentologists, Blackwell, Oxford, p. 283-308.

Richards, B.C., Barclay, J.E., Bryan, D., Hartling, A., Henderson, C.M., and Hinds, R.C., 1994, Carboniferous strata of the Western Canada Sedimentary Basin. In: Mossop, G.D., and Shetsen, I., comps., Geological Atlas of the Western Canada Sedimentary Basin. Canadian Society of Petroleum Geologists and Alberta Research Counsil, p. 221-250.

Roehl, P.O., and Choquette, P.W., eds., 1985, Carbonate petroleum reservoirs. Springer Verlag, New York, 622p.

Scholle, P.A., and Halley, R.B., 1985, Burial diagenesis: out of sight, out of mind. In: Schneidermann, N., and Harris, P.M., eds., Carbonate cements. Society of Economic Paleontologists and Mineralogists Special Publication No. 36, p. 309-334.

Schroeder, J.H., 1986, Diagenetic diversity in Paleocene coral knobs from the Bir Abu-Husein area, S Egypt. In: Schroeder, J.H., and Purser, B.H., eds., Reef diagenesis, Springer Verlag, Berlin, p. 132-158.

Stoakes, F.A., and Creaney, S., 1985, Sedimentology of a carbonate source rock: the Duvernay Formation of central Alberta. In: Eliuk, L., ed., Carbonates in subsurface and outcrop. Society of Economic Paleontologists and Mineralogists Core Workshop No. 7, p. 343-375.

Suchecki, R.K., and Land, L.S., 1983, Isotopic geochemistry of burial-metamorphosed volcanogenic sediments, Great Valley sequence, northern California. Geochimica et Cosmochimica Acta, v. 47, p. 1487-1499.

Theriault, F., 1988, Lithofacies, diagenesis and related reservoir properties of the Upper Devonian Grosmont Formation, northern Alberta. Bulletin of Canadian Petroleum Geology, v. 36, p. 52-69.

Theriault, F., and Hutcheon, I., 1987, Dolomitization and calcitization of the Devonian Grosmont Formation, northern Alberta. Journal of Sedimentary Petrology, v. 57, p. 955-966.

Walls, R.A., and Burrowes, G., 1985, The role of cementation in the diagenetic history of Devonian reefs, Western Canada. In: Schneidermann, N., and Harris, P.M., eds., Carbonate cements. Society of Economic Paleontologists and Mineralogists Special Publication No. 36, p. 185-220.

Walls, R.A., Mountjoy, E.W., and Fritz, P., 1979, Isotopic composition and diagenetic history of carbonate cements in Devonian Golden Spike reef, Alberta, Canada. Geological Society of America Bulletin, v. 90, p. 963-982.

Wardlaw, N.C., 1979, Pore systems in carbonate rocks and their influence on hydrocarbon reservoir efficiency. In: Geology of carbonate porosity, American Association of Petroleum Geologists Continuing Education Course Notes Series 11, p. E1-E24.

Whiticar, M.J., Faber, E., and Schoell, M., 1986, Biogenic methane formation in marine and freshwater environments: CO_2 reduction vs. acetate fermentation - Isotopic evidence. Geochimica et Cosmochimica Acta, v. 50, p. 693-709.

Wong, P.K., and Oldershaw, A., 1981, Burial cementation in the Kaybob reef complex, Alberta, Canada. Journal of Sedimentary Petrology, v. 51, p. 507-520.

CHAPTER 4

DOLOMITIZATION AND DOLOMITE MODIFICATION IN THE WOODBEND GROUP OF NORTH-CENTRAL ALBERTA, CANADA

INTRODUCTION

The Upper Devonian (Frasnian) Woodbend Group of north-central Alberta constitutes a major depositional cycle consisting of a lower transgressive phase and an upper regressive phase. The transgressive phase, consisting of the basal Cooking Lake carbonate platform and overlying Leduc buildups, and the regressive phase, represented by the Grosmont carbonate platform, are separated by regionally extensive Ireton Formation shales or marls that act as an aquitard between the two carbonate complexes. Both carbonate complexes are extensively dolomitized. The textural composition, geochemistry and distribution patterns of the Cooking Lake/Leduc and Grosmont dolomites are in general sufficiently different to invoke separate dolomitization models.

Cooking Lake replacement dolomites are restricted to a relatively narrow zone (8-25 km) along the western margin of the Cooking Lake platform (Andrichuk, 1958a; b). Leduc buildups are dolomitized only where they overlie the Cooking Lake platform margin, whereas reefs situated off the margin remained limestones. Based on this spatial distribution, Illing (1956; 1959) was the first to propose a burial origin of these dolomites via the shale compaction model. Based on mass balance calculations, stable isotope data and the idea that the Cooking Lake platform margin acted as a fluid conduit ("leaky pipeline") during oil migration (Stoakes and Creaney, 1984) more recent papers conclude that these strata were dolomitized during burial (50° - 60°C) by as yet unspecified fluids that migrated along this fluid conduit (Machel and Mountjoy, 1987; Amthor et al., 1993).

Due to the wide spectrum of stable isotope compositions of replacement dolomites found in Grosmont platform carbonates, the origin of these dolomites has been attributed to several dolomitization events. Most of the Grosmont dolomites are interpreted to be of early, hypersaline origin (Theriault and Hutcheon, 1987), mainly because of the evaporitic character of the Grosmont platform, although a mixed meteoric-marine mechanism has also been suggested (Larson, 1988). The burial, shale compaction model has been invoked for (lower) Grosmont dolomites that are enriched in ^{13}C relative to most Grosmont dolomites and occur in proximity to Grosmont shale deposits (Theriault and Hutcheon, 1987).

Shields and Brady (1995) recently suggested that reflux of evaporated seawater was responsible for most "early" replacement dolomites in the Devonian of the Western Canada Sedimentary Basin. These authors argued, on the basis of regional and stratigraphic distribution of replacement dolomites in Devonian carbonates of the Western Canada Sedimentary Basin (see also Potma and Wong, 1995), that dolomitizing brines originated on widespread, Late Devonian evaporitic tidal flats, and migrated into adjacent and/or underlying carbonate complexes. However, Shields and Brady (1995) did not substantiate their model with petrographical and geochemical data, nor did they conclusively demonstrate that reflux brines migrated into underlying successions (Machel et al., 1996). In addition, hydraulic continuity between Devonian carbonate complexes is generally interrupted by regional shale aquitards (Bachu and Underschultz, 1993).

The uncertainties involved in proposing models for the origin of "early" replacement dolomites reflect the fact that the geochemical composition of these dolomites is different from their respective modern analogues. This common discrepancy between ancient dolomites and their modern counterparts has led several workers to suggest that the geochemistry of ancient dolomites records a long history of dolomitization episodes, recrystallization and stabilization rather than reflecting their original geochemistry (Land, 1985; Hardie, 1987; Banner et. al, 1988; Cander et al., 1988; Gregg and Shelton, 1990; Gregg et al., 1992; Mazzullo, 1992; Montanez and Read, 1992; Kupecz et al., 1993 Kupecz and Land, 1994).

In the light of these recent developments in dolomite research, the Woodbend Group appears to be an excellent setting to investigate the stabilization of dolomites. The Woodbend Group contains several types of dolomite and the available database is regionally extensive. This study documents the petrography and geochemistry of Woodbend Group dolomites and their spatial distribution. Standard and cathodoluminescence petrography, stable isotope and trace element data were used to distinguish different dolomite types and to gain insight about their diagenetic path. Furthermore, the location of the study area was chosen to cover an area that included both groups of dolomites described in the literature. The study area also includes several sites where hydraulic communication between the northern extension of the Rimbey-Meadowbrook reef trend and the Grosmont platform is possible and, therefore, provides an opportunity to test 1) the influence of hydraulic communication in general, and 2) the influence of the Cooking Lake platform margin and overlying Leduc reefs as fluid conduit in particular on dolomitization and/or dolomite stabilization.

GEOLOGIC SETTING

The Upper Devonian (Frasnian) Woodbend Group comprises a 300 to 340 m thick sequence of shallow-water platform carbonates (Cooking Lake and Grosmont Formations), reefal buildups (Leduc Formation) and basin-filling shales, marls and limestones (Majeaux Lake Member, Duvernay and Ireton Formations). The Woodbend Group is underlain by argillaceous carbonates of the Waterways Formation (Beaverhill Lake Group) and is generally overlain by carbonates of the Nisku Formation (Winterburn Group). In the northernmost part of the study area, however, the Woodbend Group is truncated by the sub-Cretaceous unconformity and subcrops underneath Lower Cretaceous sandstones and shales of the Mannville Group (Figs. 4.1 and 4.2).

In the study area, which is situated in north-central Alberta between townships 61 and 90 and between range 19 west of the fourth meridian and the fifth meridian (Fig. 4.1), the Woodbend Group can be divided into 10 units (Fig. 4.2). The lowest units are carbonate platform deposits of the Cooking Lake Formation and bituminous, basinal limestones of the Majeaux Lake Member. The western margin of the Cooking Lake platform is overlain by Leduc Formation buildups. Stratigraphically equivalent areas off the platform margin are overlain by lower Ireton Formation shales and/or by bituminous limestones and shales of the Duvernay Formation. In much of the study area these units are overlain by carbonate platform deposits of the Grosmont Formation (Figs. 4.1, 4.2) which represent the second, regressive part of the Woodbend Group. Based on

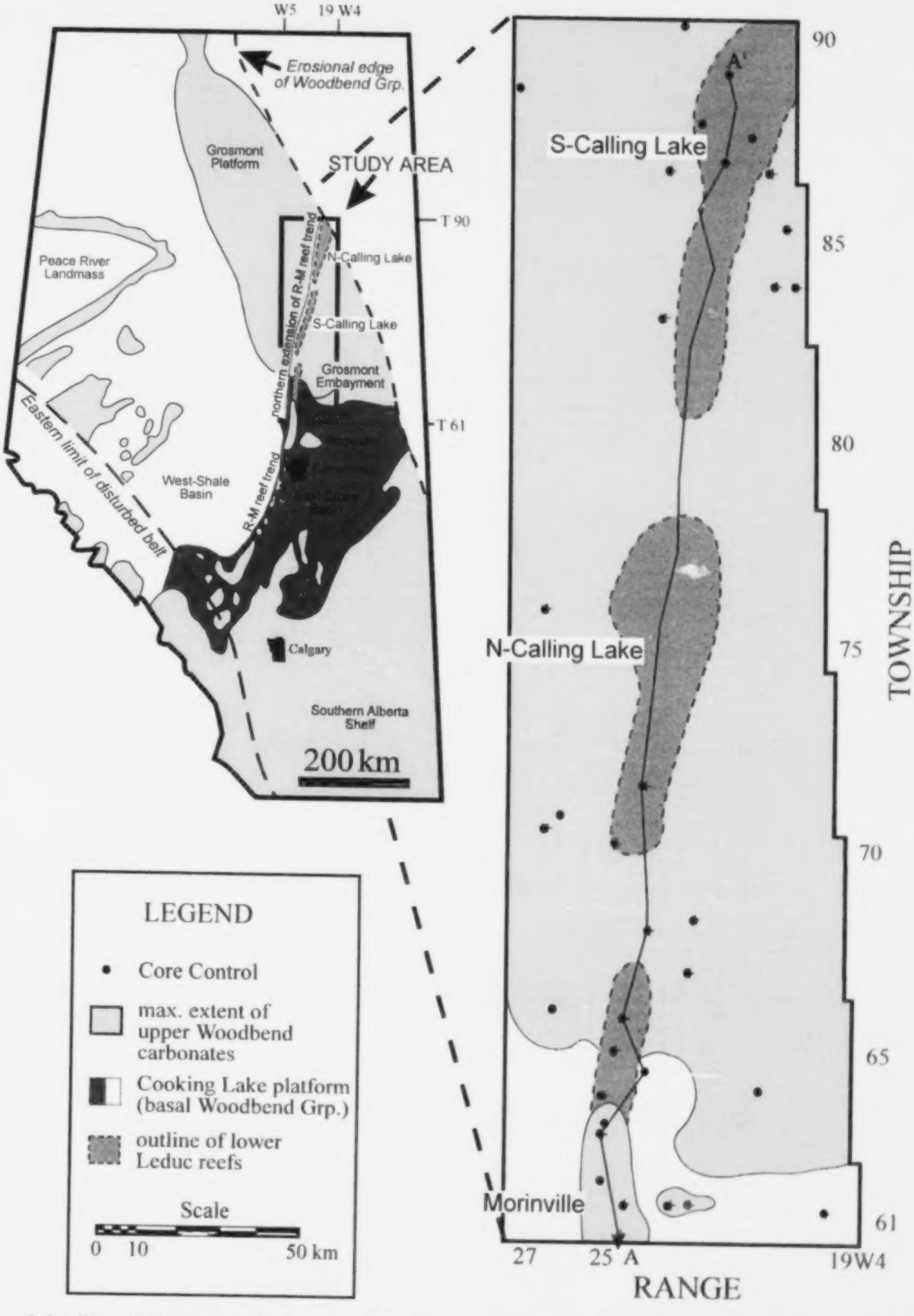
W5
19 W4
Erosional edge of Woodbend Grp.
Grosmont Platform
STUDY AREA
T 90
Peace River Landmass
N-Calling Lake
northern extension of R-M reef trend
S-Calling Lake
Grosmont Embayment
T 61
Eastern limit of disturbed belt
West-Shale Basin
R-M reef trend
East-Shale Basin
Calgary
Southern Alberta Shelf
200 km
LEGEND
Core Control
max. extent of upper Woodbend carbonates
Cooking Lake platform (basal Woodbend Grp.)
outline of lower Leduc reefs
Scale
0
10
50 km
A'
S-Calling Lake
N-Calling Lake
Morinville
90
85
80
75
70
65
61
TOWNSHIP
27
25
A
19W4
RANGE

Fig. 4.1: Simplified distribution of platform and reef carbonates of the Late Devonian Woodbend Group and location of the study area in Alberta. Detailed map of the study area shows core control, location of cross-section A-A', and the location of Leduc reefs (Morinville, N and S Calling Lake). R-M reef trend = Rimbey-Meadowbrook reef trend.

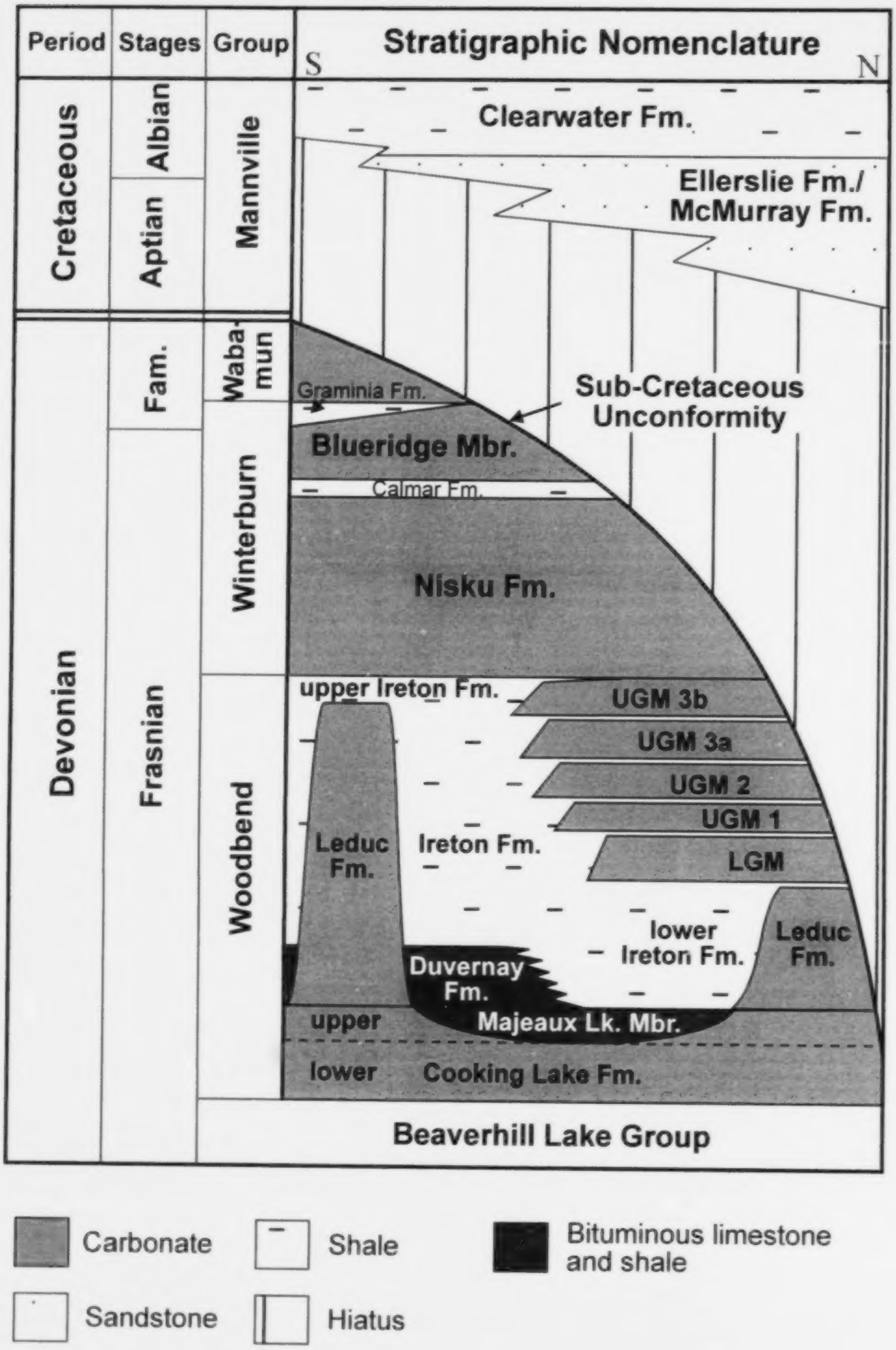
Period
Stages
Group
Stratigraphic Nomenclature
S
N
Cretaceous
Albian
Aptian
Mannville
Clearwater Fm.
Ellerslie Fm./
McMurray Fm.
Devonian
Fam.
Frasnian
Wabamun
Winterburn
Woodbend
Graminia Fm.
Sub-Cretaceous
Unconformity
Blueridge Mbr.
Calmar Fm.
Nisku Fm.
upper Ireton Fm.
UGM 3b
UGM 3a
UGM 2
UGM 1
LGM
Leduc
Fm.
Ireton Fm.
lower
Ireton Fm.
Leduc
Fm.
Duvernay
Fm.
upper
Majeaux Lk. Mbr.
lower
Cooking Lake Fm.
Beaverhill Lake Group
Carbonate
Shale
Bituminous limestone
and shale
Sandstone
Hiatus

Fig. 4.2: Stratigraphic nomenclature of the principal Upper Devonian and Lower Cretaceous units encountered in the study area.

interlayered, thin, regionally extensive shale markers (Harrison, 1982), the Grosmont Formation can be divided into the lower Grosmont (LGM) and the upper Grosmont 1, 2, 3a and 3b (UGM 1, UGM 2, UGM 3a and UGM 3b, respectively). Due to an overall shallowing and progradation of the Grosmont platform the LGM unit is dominated by open marine platform limestones, whereas UGM 1 through UGM 3b were deposited in progressively more restricted environments, which coincides with increasing amount of dolostones. Grosmont carbonate platform deposits grade laterally into Ireton Formation basin fill sediments (Fig. 4.2). The youngest part of the Woodbend Group, the upper Ireton Formation, consists of patchy, argillaceous to silty dolostones in the northern part of the study area which grade into thick shales (up to 50 m) in the southern part.

In terms of hydrostratigraphy, the arrangement of Woodbend Group deposits into a lower carbonate complex (Cooking Lake and Leduc Fms.), an upper carbonate complex (Grosmont Fm.), and an intervening, regionally extensive shale unit (Ireton Fm.) divides the Woodbend Group into two aquifers in most parts of the study area. Only in the southernmost portion of the study area, where the Grosmont platform is not present and Leduc reef growth continued until the end of the Woodbend deposition (Fig. 4.2), Woodbend Group carbonates act as a single aquifer. Hydraulic continuity between the upper and lower Woodbend aquifers is possible along the Leduc reef trend in areas that were not or only thinly covered by the Ireton shales (Fig. 4.3).

Upper Devonian strata in north-central Alberta dip slightly to the southwest at a rate of approximately 5.5 m per km (Theriault, 1988). Over the total north-south extent (290 km) of the study area, this dip results in widely varying present day burial depths that range from only 250 m in the northeast and 1,500 m in the southwest. In the northernmost part of the study area the Woodbend Group is truncated by the sub-Cretaceous unconformity, partially to completely eroded, and overlain by Lower Cretaceous clastics of the Mannville Group.

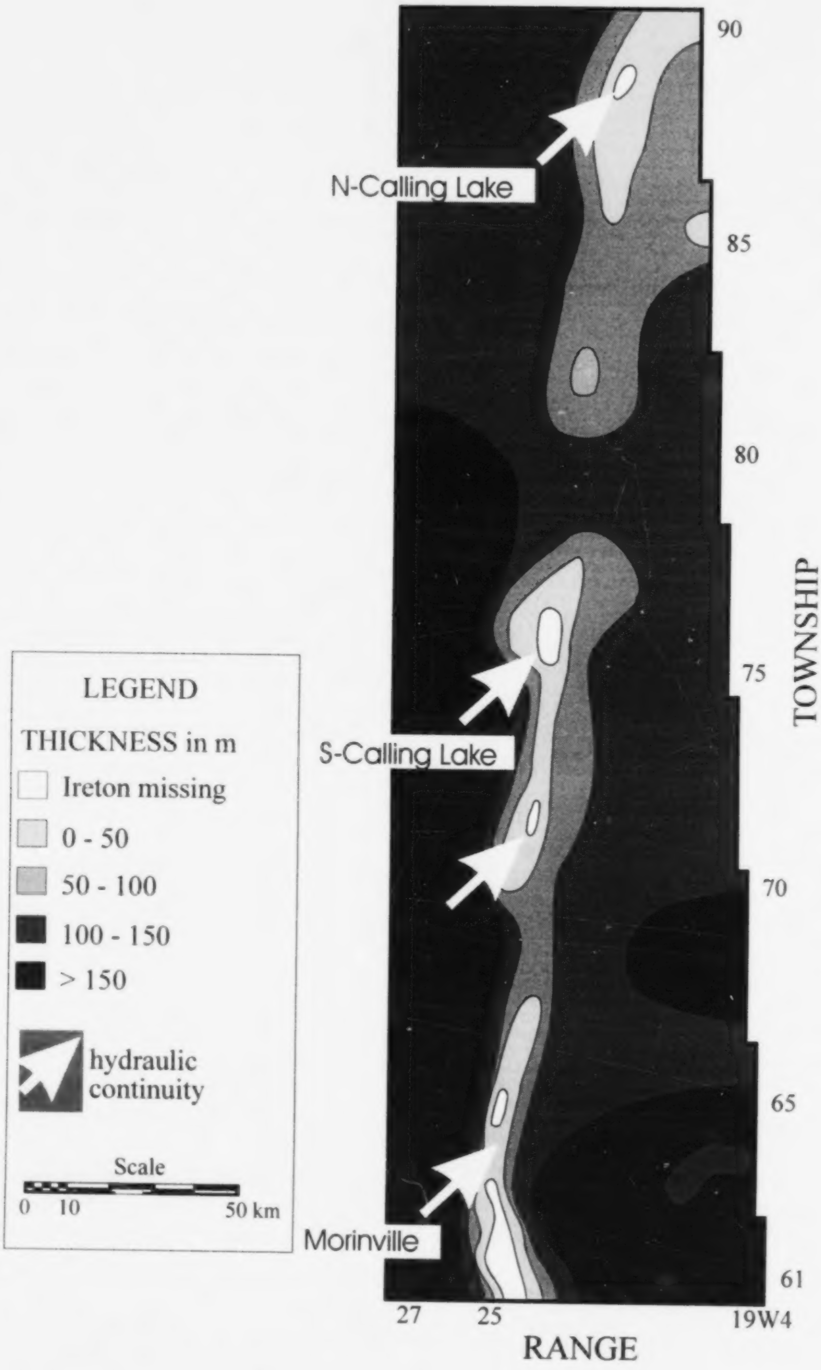
N-Calling Lake
S-Calling Lake
Morinville
LEGEND
THICKNESS in m
Ireton missing
0 - 50
50 - 100
100 - 150
> 150
hydraulic continuity
Scale
0 10 50 km
90
85
80
75
70
65
61
TOWNSHIP
27
25
19W4
RANGE

Fig. 4.3: Isopach map of the Ireton Fm. aquitard as measured from well logs. Arrows point to the location of isopach thins above Leduc reef crests indicating likely sites of hydraulic communication between the Cooking Lake/Leduc and Grosmont aquifer.

DATABASE AND METHODS

Cored intervals from 36 different wells were described and sampled for thin section petrography and geochemical analysis. Most wells penetrate the Grosmont Formation and/or the uppermost parts of the Leduc Formation. Intervals that penetrate the lower Leduc and Cooking Lake Formations are scarce and are generally located along the Leduc reef trend.

Over 400 samples were examined with a petrographic microscope. Thin sections were routinely stained with Alizarin S and potassium ferricyanide (Dickson, 1966) to determine carbonate mineral composition and to estimate the Fe-content of calcites and dolomites. Selected thin sections were impregnated with blue epoxy to better describe and estimate porosity. All thin sections were examined by cathodoluminescence using a cold cathode Premier American Technologies ELM-3R Luminoscope. Operating conditions for petrography were a beam voltage of 15 to 20 kV (photography 16 to 18 kV) and a beam current of 0.5 mA in a 35 to 50 mTorr vacuum under an air atmosphere. The crystal sizes reported below are average values of 50 measurements per sample obtained in thin section by measuring the longest dimension of dolomite crystals along linear traverses.

Ninety one dolomite samples were analyzed for their stable isotope composition. Approximately 20 to 30 mg of dolomite powder (bulk sample of replacement dolomites) were collected for each analysis from thin section cut offs using a dental drill. Sample powders were reacted with 100% phosphoric acid at 25°C for 1 week following the procedure described by McCrea (1950). The isolated CO_2 was analyzed either with a VG 602 or with a Finnigan-MT 252 mass spectrometer. Results were generally reproducible to within ±0.03 and ±0.02 ‰ for $\delta^{18}O$ and $\delta^{13}C$, respectively. Analytical values were corrected for the dolomite - phosphoric acid fractionation by subtracting 0.82 ‰ from the uncorrected $\delta^{18}O$ values (Sharma and Clayton, 1964). Both oxygen and carbon isotope data are reported relative to Pee Dee Belemnite (PDB) in the standard δ-notation (Craig, 1957).

Dolomites from 26 polished thin sections were analyzed on a JEOL JXA-8900R electron microprobe. Operating conditions for the microprobe were 15kV accelerating voltage, 15nA beam current at Faraday cup, 5 μm beam diameter, and peak sample times of 20 seconds. Individual spots were analyzed for Ca, Mg, Fe, Mn, Sr and Na. Lower detection limits for these elements are 110 ppm for Ca, 100 ppm for Mg, 140 ppm for Fe, 130 ppm for Mn, 160 ppm for Sr, and 110 ppm for Na at a 95 % confidence level for all elements.

The Ca content of dolomite samples was also determined by powder X-ray diffraction using a Rigaku Geigerflex fitted with a Co tube (wavelength = 1.79026 Å). Ten mg of dolomite powder was mixed with an internal quartz standard (30 % of dolomite sample weight) and mounted as an ethanol slurry. Samples were analyzed in a single scan ranging from 10° to 90° 2theta at 1°/min. Mole % $CaCO_3$ was determined by measuring the position of the d_{104} peak following the procedure outlined by Goldsmith et al. (1961). The variation in $CaCO_3$ content of dolomite samples as determined by X-ray diffraction and electron microprobe analysis are generally less than ±2%.

PETROGRAPHY

Replacement dolomites comprise at least 95 % of all dolomites in the Woodbend Group. Two different types of replacement dolomites have been recognized and classified according to average crystal size and crystal boundary shape. Both crystal size and crystal boundary shape were determined based on petrographic analysis and cathodoluminescence microscopy of thin sections.

Less than 5 % of Woodbend dolomites are dolomite cements. Dolomite cements are only considered here if they formed overgrowth zones on replacement dolomites, which can be considered part of the host dolomite crystal and are in optical continuity with the actual replacement dolomite. A more comprehensive description of the different types of dolomite cements found in the Woodbend Group of north-central Alberta has been given in Chapter 3.

Replacement dolomite type 1

This type of replacement dolomite is light grey, grey, light brown or light green in hand specimen, depending on the amount and colour of impurities and retaining the colour of the precursor limestone. Replacement dolomite 1 appears to be the earliest preserved dolomite phase and preferentially replaced the matrix of limestones. This dolomite type represents the typical Grosmont dolomite and is present in all platform facies, but is most common in peritidal and shallow subtidal facies. Replacement dolomite 1 crystals are euhedral to subhedral and form loosely interlocking, planar-e to planar-s crystal mosaics. These mosaics are typically fabric-retentive and have porosities of between 10 to 25 %. Crystal sizes range from 20μm to 100μm. Individual crystals are cloudy, they show straight extinction patterns and no zoning under plane light. However, zoning patterns, as revealed by cathodoluminescence, varies widely from well developed multiple zonations to absent zonation. The different luminescence patterns are used to subdivide replacement dolomite 1 further into three subtype categories.

Subtype 1a shows very fine and well preserved, alternating yellow, orange and red zones if viewed with cathodoluminescence (Fig 4.4a). This dolomite type is most common as isolated rhombs in only partially dolomitized intervals, notably in the LGM and UGM 1 units, yet it is rare in completely dolomitized intervals. This subtype is often overgrown by non-luminescent ferrous dolomite cement.

Subtype 1b has a dominantly orange-red luminescence colour. Zoning is weak, but still recognizable and individual zones appear faded (Fig. 4.4b). Furthermore, individual zones or larger areas of the crystal appear corroded, dissolved and refilled or replaced by red to dull red dolomite, resulting in an irregular luminescence pattern (Fig. 4.4 c and d). This subtype is common in largely to completely dolomitized intervals of the UGM 1 and UGM 2 units.

Subtype 1c is the most common variety of type 1 replacement dolomite. It has a homogeneous or mottled red to dull red luminescence (Fig. 4.5 a and b). Zoning, if present, is restricted to dull orange to dull red zones along the outer edges of the crystals. In porous intervals this subtype is often overgrown by clear, red luminescent dolomite cement, in which case the crystal also appears to have zoning.

Replacement dolomite 1 is cross-cut by "syndepositional" diagenetic features such

Fig. 4.4a: Zoned, orange luminescent type 1 replacement dolomites (subtype 1a) in dull red luminescent limestone matrix. Thin section, well location 10-17-83-18W4, 455.0 m (LGM).

Fig. 4.4b: Red luminescent type 1 replacement dolomite (subtype 1b) in orange luminescent limestone matrix. Cores of individual dolomite rhombs display only weak zoning or are entirely homogenized and often have an irregular outline. Thin section, well location 10-17-83-18W4, 388.5 m (UGM 2).

Fig. 4.4c: Overview cathodoluminescence photomicrograph of porous planar-e dolomite (replacement dolomite subtype 1b). Thin section, well location 10-17-83-18W4, 387.5 m (UGM 2).

Fig. 4.4d: Detailed view of (c). Extensively corroded, red to dull red luminescent type 1 replacement dolomite (subtype 1b). Dull red areas of dolomite crystals appear corroded (arrow) and have a mottled luminescence.

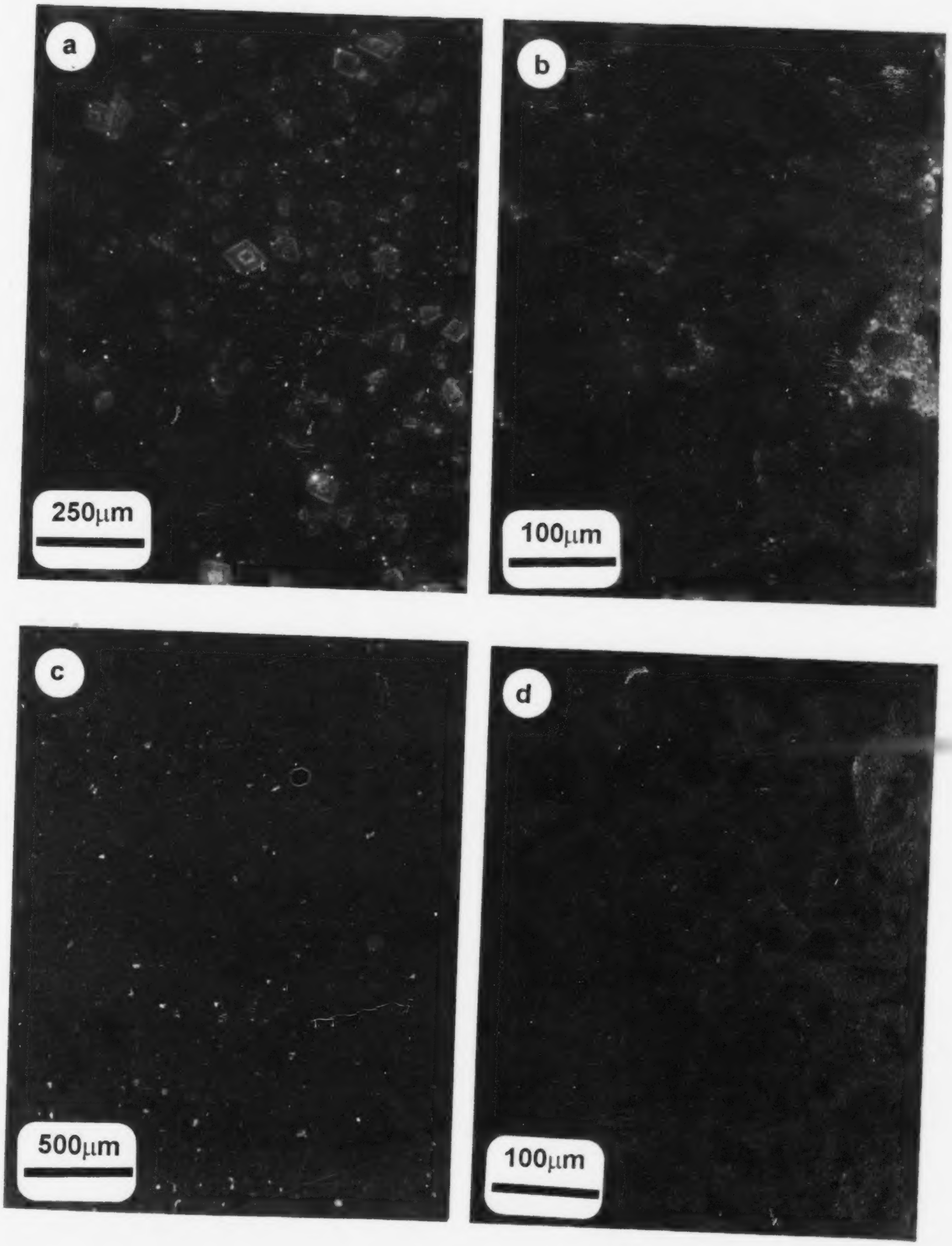
a
250μm
b
100μm
c
500μm
d
100μm

Fig 4.5a: Overview cathodoluminescence photomicrograph of planar-s subtype 1c replacement dolomite with mostly homogeneous cathodoluminescence. Thin section, well location 10-17-83-18W4, 343.0 m (UGM 3a).

Fig. 4.5b: Detailed view of (a). Subtype 1c replacement dolomite with mostly homogeneous cathodoluminescence. Darker areas contain specks of lighter luminescent dolomite. Only few crystals show zonation (arrow).

Fig. 4.5c: Dense, planar-s mosaic of type 2 replacement dolomites. Thin section, well location 3-34-88-20W4, 1530' (Leduc Fm.).

Fig. 4.5d: Cathodoluminescence photomicrograph of (c), showing the for type 2 replacement dolomites characteristic red to dull red, mottled to homogeneous luminescence.

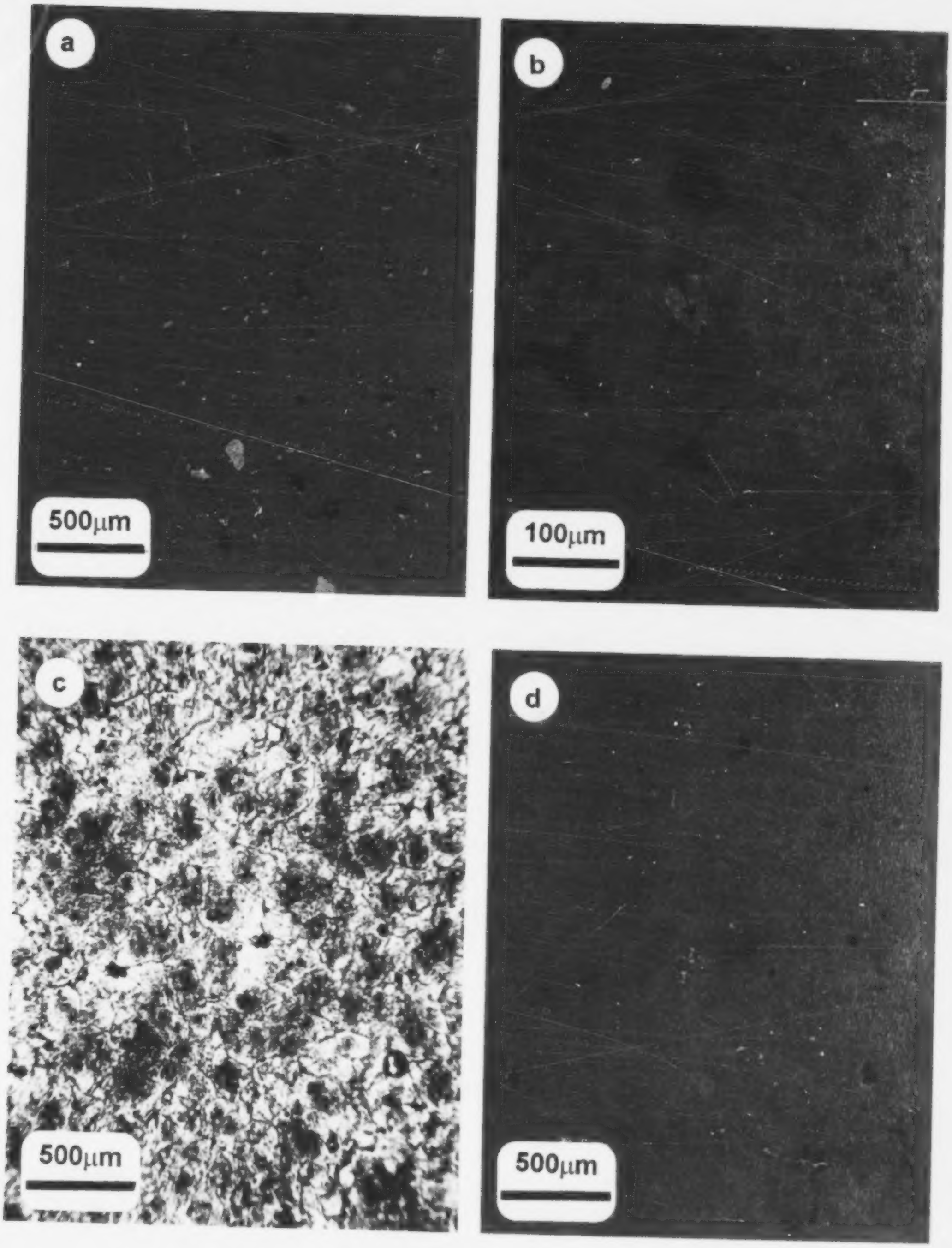
a
500μm
b
100μm
c
500μm
d
500μm

as desiccation fractures as well as by "late" diagenetic low and high amplitude stylolites. Furthermore, replacement dolomite 1 occurs as dolomite intraclasts in Grosmont shale breaks. Individual intraclasts are well rounded and crystal boundaries are abraded (Fig. 4.6a).

Replacement dolomite type 2

The second type of replacement dolomite is uniformly grey or light brown in hand specimen. This type of dolomite occurs mostly as a pervasive replacement phase, but can also be restricted to replacement of bioclasts. Replacement dolomite 2 represents the typical Leduc dolomite and is present throughout the northern extension of the Rimbey-Meadowbrook reef trend as well as in adjacent portions of the Grosmont platform. Compared to replacement dolomite 1 the average crystal size is larger, ranging from $70\mu m$ to $350\mu m$. Replacement dolomite 2 has a cloudy, irregular shaped core and a clear, outer rim. The boundary between rim and core is characteristically diffuse (Fig. 4.5c). Cathodoluminescence colour of replacement dolomite 2 ranges from uniform to mottled dull red, showing no apparent zoning (Fig. 4.5d). Based on its carbon isotope composition, replacement dolomite 2 is further subdivided into subtype 2a ($\delta^{13}C \simeq +2$ ‰ PDB) and subtype 2b ($\delta^{13}C \geq +3$ ‰ PDB). Dolomite crystal texture of replacement dolomite 2 is dominantly subhedral. Subsequently, intervals that are pervasively dolomitized by replacement dolomite 2 have a relatively tight planar-s crystal mosaic (Fig. 4.5 c and d) that is typically fabric obliterative. Intercrystalline porosities are generally lower than in replacement dolomite 1 mosaics ranging between 5 and 15 %. Replacement dolomite 2 is also cross-cut by solution seams (Fig. 4.6b).

REGIONAL DISTRIBUTION

Type 1 replacement dolomites are generally restricted to the upper members of the Grosmont Formation (Fig. 4.7). They are most common in the northern part of the study area and decrease in abundance southward. Occurrences of replacement dolomite 1 in the Leduc and Cooking Lake Formations are rare and commonly restricted to lenses

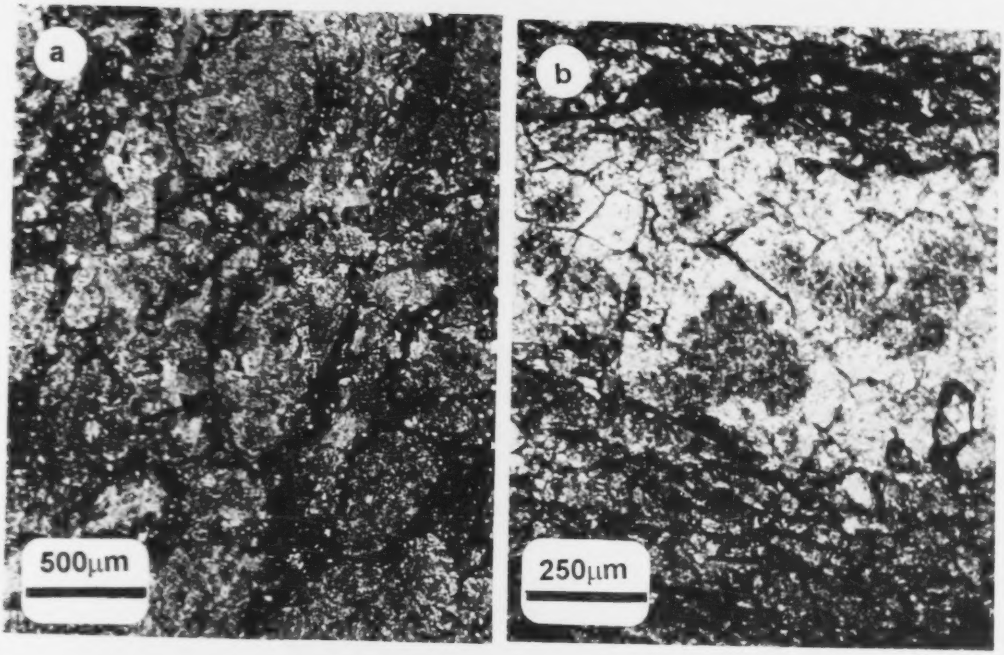

Fig. 4.6a: Well rounded, reworked dolomite intraclasts in silty, marl matrix. Individual dolomite crystals are generally abraded. Thin section, well location 6-2-92-21W4, 248.5 m (UGM 3a; 3rd shale break).

Fig. 4.6b: Type 2 replacement dolomites crosscut by solution seams. Thin section, well location 4-33-68-22W4, 3470' (Lower Cooking Lake Formation).

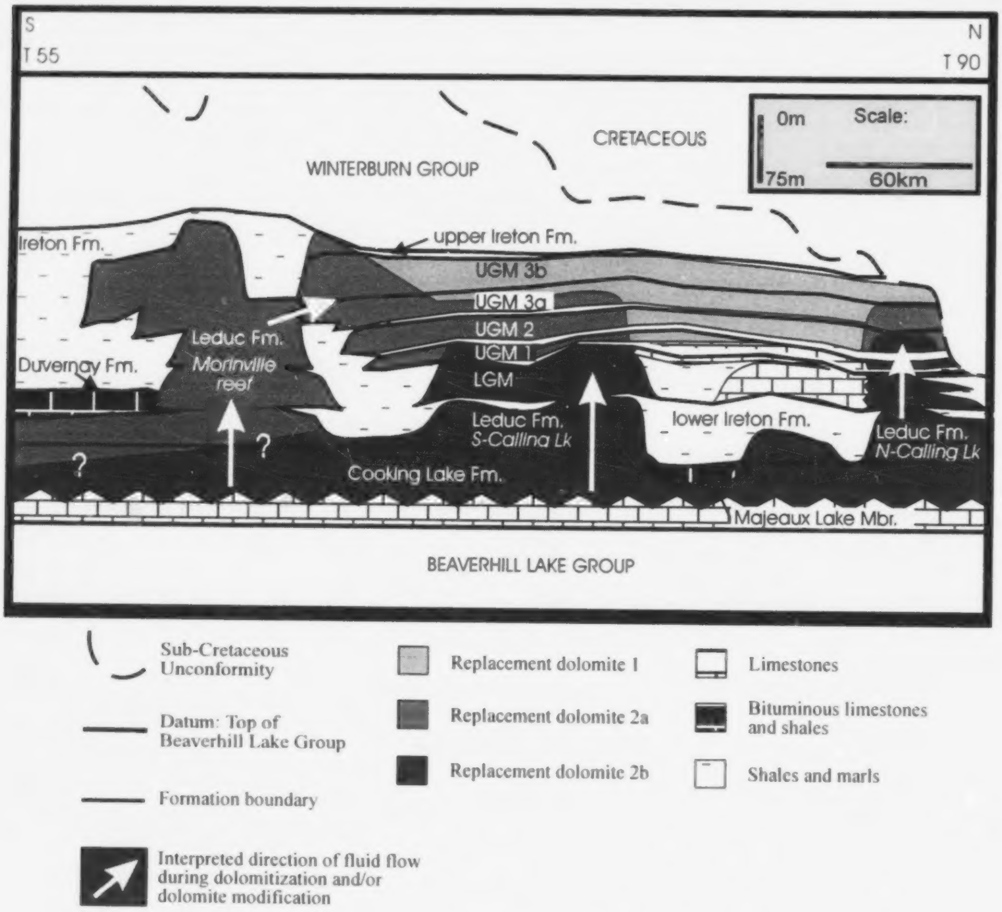
S
T 55
N
T 90
CRETACEOUS
WINTERBURN GROUP
0m
Scale:
75m
60km
Ireton Fm.
upper Ireton Fm.
UGM 3b
UGM 3a
UGM 2
UGM 1
LGM
Leduc Fm.
Morinville reef
Duvernay Fm.
Leduc Fm.
S-Calling Lk
lower Ireton Fm.
Leduc Fm.
N-Calling Lk
?
?
?
Cooking Lake Fm.
Majeaux Lake Mbr.
BEAVERHILL LAKE GROUP
Sub-Cretaceous Unconformity
Datum: Top of Beaverhill Lake Group
Formation boundary
Interpreted direction of fluid flow during dolomitization and/or dolomite modification
Replacement dolomite 1
Replacement dolomite 2a
Replacement dolomite 2b
Limestones
Bituminous limestones and shales
Shales and marls

Fig. 4.7: North-south cross section through the Woodbend Group in north-central Alberta. Cross section follows the northern extension of the Leduc (Rimbey-Meadowbrook) reef trend from the Morinville reef in the south to the subcrop edge of the Grosmont Formation in the northern part of the study area (Fig 4.1). Shown is the distribution of replacement dolomite types 1, 2a, and 2b as well as the extent of the principal lithologies of the Woodbend Group. Arrows indicate possible sites of hydraulic communication between the Cooking Lake/Leduc and the Grosmont aquifers, as well as the presumed direction of fluid flow during dolomitization.

surrounded by matrix that consists of replacement dolomite 2. Subtype 1c is by far the most common. Replacement dolomite subtypes 1a and 1b are restricted to the UGM 1 and UGM 2 members of the Grosmont Formation. Furthermore, dolomite patches in partially dolomitized intervals of the LGM member of the Grosmont Formation, which commonly remained undolomitized, dominantly consist of replacement dolomite subtype 1a. Regionally, replacement dolomite subtypes 1a and 1b occur only in the northern part of the study area and are absent in the southern part.

Replacement dolomite 2 is the dominant dolomite type in the Leduc and Cooking Lake Formations throughout the study area (Fig. 4.7). Dolomite occurrences in Leduc Formation reefs and in the underlying Cooking Lake platform margin north of the Morinville reef (Fig.4.1) are generally present in the form of the ^{13}C-enriched subtype 2b (Fig. 4.7). Replacement dolomite 2 in the Morinville reef as well as isolated occurrences of replacement dolomite in the Cooking Lake Formation off the reef trend are commonly present as subtype 2a (δ^{13}C composition ~ +2 ‰ PDB) (Fig 4.7). Replacement dolomite 2 is also predominant in the southern part of the upper members of the Grosmont Formation (Fig. 4.7).

Almost all type 2 replacement dolomite in the Grosmont Formation is present in the form of subtype 2a. Replacement dolomite subtype 2b is only rarely present in the Grosmont Formation, and it occurs only in areas of the Grosmont platform that directly overly reefs of the northern Leduc reef trend (Figs. 4.1, 4.3, 4.7). At these locations, replacement dolomite subtype 2b pervasively dolomitized the LGM, which is developed as limestone in most parts of the Grosmont platform (Fig. 4.7, 4.8). Replacement dolomite subtype 2b grades upwards into subtype 2a (Fig. 4.7).

GEOCHEMISTRY

Replacement dolomites were first classified according to the petrographical characteristics outlined above. While choosing areas for microsampling (stable isotope analysis and XRD) and microprobe analysis, special care was taken to avoid areas with several types of replacement dolomites and/or dolomite cement overgrowth. In some

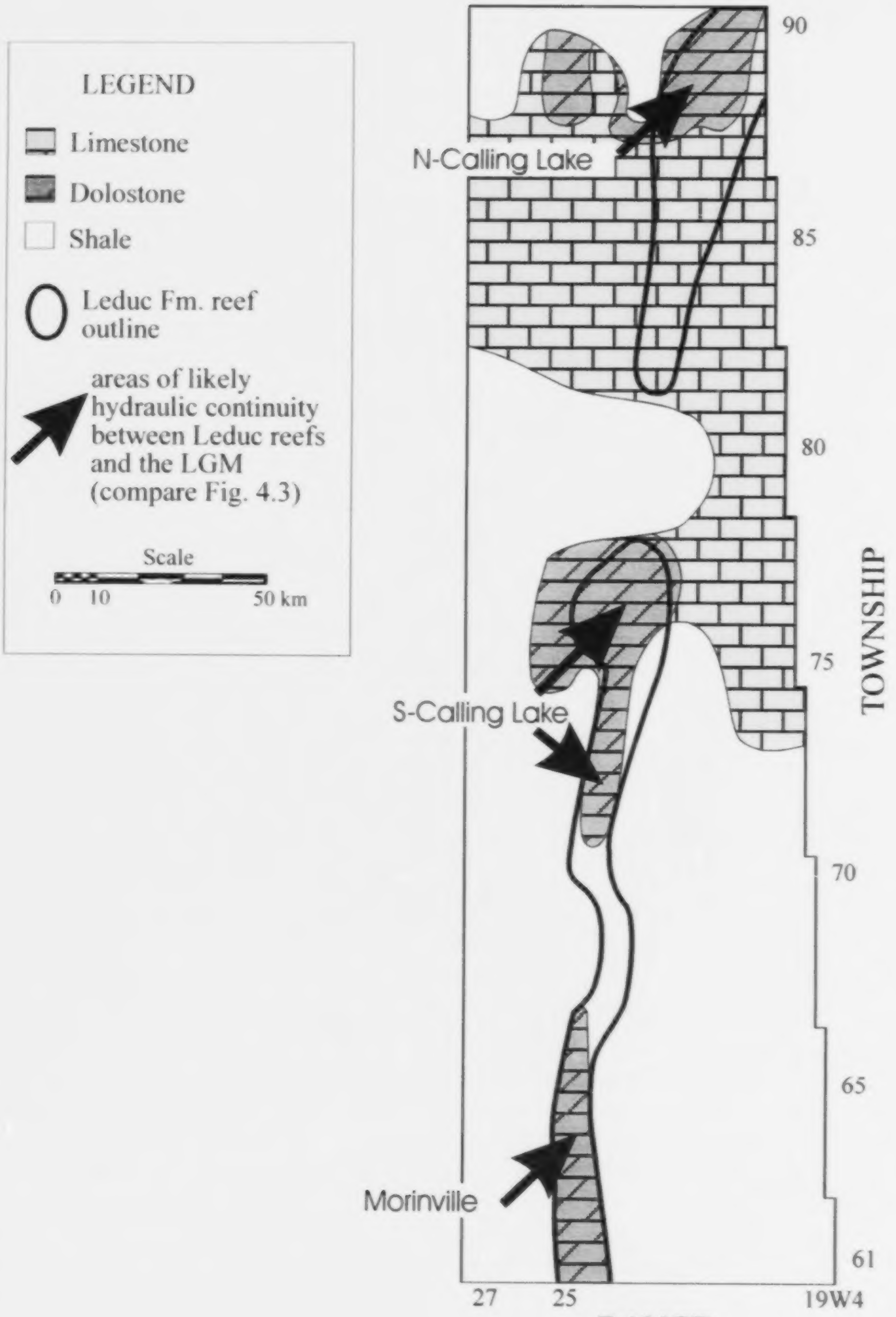
LEGEND
Limestone
Dolostone
Shale
Leduc Fm. reef outline
areas of likely hydraulic continuity between Leduc reefs and the LGM (compare Fig. 4.3)
Scale
0
10
50 km
N-Calling Lake
S-Calling Lake
Morinville
90
85
80
75
70
65
61
TOWNSHIP
27
25
19W4
RANGE

Fig. 4.8: Distribution of lithologies in the LGM. Note that dolostones are generally restricted to areas that are situated above Leduc Fm. reefs, where the intervening Ireton aquitard is thin or absent (Fig. 4.3).

cases, however, sampling of dolomite overgrowth was unavoidable. The same aliquots of sample powders were used for stable isotope and XRD analyses. Results of microprobe and XRD analyses are listed in Table 4.1, results of stable isotope analyses are listed in Table 4.2. Overall results of the geochemical analyses of Woodbend dolomites are summarized in Table 4.3.

Major and trace elements

Replacement dolomite 1 samples are non-stoichiometric to stoichiometric (49.2 to 56.9 mole % $CaCO_3$). Replacement dolomite 1 samples with luminescent zones (subtype 1a and 1b) tend to be non-stoichiometric (54.3 to 56.9 mole % $CaCO_3$), and cores of these subtypes can be even more enriched in $CaCO_3$ (up to 64.7 mole %) as determined by microprobe analysis. Replacement dolomite 1 samples that show uniform luminescence (subtype 1c) are near-stoichiometric to stoichiometric (49.3 to 50.8 mole % $CaCO_3$), as are replacement dolomite 2 samples (48.0 to 50.3 mole % $CaCO_3$). There is an overall trend of increasing stoichiometry with increasing crystal size of Woodbend replacement dolomites (Fig. 4.9a), but $CaCO_3$ content of individual dolomite types does not covary with crystal size (Fig. 4.9a).

Replacement dolomite 1 samples are enriched in Sr relative to replacement dolomite 2 (Table 4.1 and 4.3). Strontium concentrations in type 1 replacement dolomites vary between 0 (below detection limit of microprobe) and 443 ppm (avg. 203 ppm). In type 2 replacement dolomites Sr content varies from 2 to 187 ppm (avg. 89 ppm). Sr concentration in Leduc replacement dolomite 2 is generally lower than in Grosmont replacement dolomite 2 (Fig. 4.9b). Strontium concentration in type 1 replacement dolomite does not appear to be related to crystal size (Fig. 4.9b), but samples with greater Sr content generally are of subtype 1a and 1b (with clear or diffuse zoning). Strontium content in replacement dolomite 2 samples shows a weak trend of decreasing concentration with increasing crystal size (Fig. 4.9b).

Sodium content in type 1 replacement dolomites varies from 0 to 336 ppm (avg. 180 ppm). Type 2 replacement dolomites have slightly lower Na contents ranging from 2 to 183 ppm (avg. 82 ppm). Sodium concentration in replacement dolomite 2 slightly increases with crystal size (Fig. 4.9c). Leduc replacement dolomite 2 contains less Na than

Table 4.1: Geochemistry of Woodbend dolomites

Well ID	Unit	Depth [m]	Depth [ft]	Dol. Type	Xl Size [μm]	$\delta^{18}O$ ‰ PDB	$\delta^{13}C$ ‰ PDB	$CaCO_3$ mole % XRD	$CaCO_3$ mole % Probe	$MgCO_3$ mole % Probe	Fe ppm	Mn ppm	Sr ppm	Na ppm
06-16-66-24W4	u. Cook. Lk.	1186.6	3893	2	172	-5.86	5.28	50.0	49.5	50.3	981	148	91	23
	Leduc	1120.8	3677	2	222	-5.37	1.70	49.2	49.8	50.1	533	23	74	48
	Leduc	1103.4	3620	2	91	-5.73	2.85	50.7	49.3	50.3	2410	250	100	28
	UGM 2	1045.5	3430	2	120	-5.56	2.65	50.4	49.7	50.0	1272	101	178	173
	UGM 2	1042.7	3421	2	115	-6.92	0.88	51.2	49.8	49.9	1560	68	78	138
	UGM 3a	1005.2	3298	2	176	-5.34	2.12	50.9	49.3	50.5	917	109	84	88
03-28-70-24W4	u. Cook. Lk.	1087.5	3568	2	200	-5.95	4.50	50.2	49.7	50.2	360	150	77	67
	u. Cook. Lk.	1075.5	3528	2	237	-5.83	3.50	50.7	49.8	50.2	36	188	74	98
	Leduc	1068.6	3506	2	166	-5.92	7.81	50.5	50.0	49.9	656	14	2	2
	Leduc	1051.0	3448	2	186	-5.97	3.93	50.0	50.1	49.8	230	135	12	39
	UGM 3b	865.3	2839	1	65	-4.46	-0.33	50.2	49.9	50.1	273	10	37	166
	UGM 3b	857.1	2812	1	92	-4.45	1.47	50.0	49.8	50.1	192	68	104	242
	UGm 3b	855.3	2806	1	59	-4.43	0.00	50.7	49.7	50.2	80	73	85	135
10-17-83-18W4	LGM	455.0	1493	1	51				55.8	41.5	19625	1185	0	225
	UGM 1	396.8	1302	1	73	-5.70	0.35		56.9	42.4	5210	210	443	230
	UGM 2	388.5	1275	1	79				54.3	44.8	1690	212	296	146
	UGM 2	387.5	1271	1	65	-5.39	0.23		50.8	48.2	7601	186	196	0
	UGM 2	367.5	1206	1	24	-3.98	-3.78		49.6	40.2	338	111	296	336
	UGM 3a	342.0	1122	1	72	-3.88	0.22		49.3	50.6	652	0	396	144
03-34-88-20W4	Leduc	466.3	1530	2	211	-6.14	5.70	51.2	48.0	50.8	2302			
	Leduc	464.2	1523	2	150	-6.27	5.46	50.5	48.3	50.4	2543			
	Leduc	457.2	1500	2	212	-6.67	5.81	50.5	48.9	50.2	6862	314	102	105
	Leduc	403.9	1325	2	218	-7.57	2.96	51.2	48.6	50.1	2470			
	LGM	352.4	1156	2	230	-7.01	4.71	50.0	47.7	50.6	5660			
	LGM	349.9	1148	2	187	-7.04	4.88	50.1	49.8	50.0	968	103	103	77
	UGM 2	326.1	1070	2	77	-6.68	5.42	50.5	50.3	49.2	2962	253	187	183

Table 4.2: Dolomite stable isotope data

Well ID	Unit	Depth [m]	Depth [ft]	Dol. type	XL size [μm]	$\delta^{18}O$ [PDB]	$\delta^{13}C$ [PDB]
04-29-61-19W4	u. Ireton	825.1	2707	2	153	-5.96	-0.36
07-31-61-24W4	u. Ireton	1065.6	3496	2	190	-4.79	0.99
	u. Ireton	1064.1	3491	2	348	-5.76	0.45
	u. Ireton	1050.0	3445	1	56	-4.96	-0.21
10-33-62-21W4	u. Ireton	884.2	2901	1	95	-4.86	0.76
16-22-62-25W4	Leduc	1133.9	3720	2	302	-5.52	1.85
	Leduc	1128.1	3701	2	151	-5.24	1.77
	Leduc	1126.2	3695	2	298	-5.26	1.68
05-24-63-25W4	Leduc	1333.5	4375	2	177	-4.93	2.75
	Leduc	1330.8	4366	2	348	-6.16	2.85
	Leduc	1134.5	3722	2	188	-6.15	1.40
	Leduc	1119.8	3674	2	173	-5.86	1.62
09-36-63-25W4	Leduc	1054.9	3461	2	174	-6.04	1.17
	Leduc	1051.3	3449	2	154	-6.80	0.75
03-24-64-25W4	Leduc	1105.2	3626	2	201	-5.54	1.79
12-06-65-24W4	UGM 3a	1175.0	3855	2	143	-6.29	1.97
	u. Ireton	1083.5	3555	1	89	-5.65	-0.28
05-19-65-24W4	UGM 2	1229.3	4033	2	124	-6.13	0.86
	UGM 2	1223.2	4013	1	72	-3.54	1.09
	UGM 2	1223.2	4013	2	153	-5.31	1.18
	u. Ireton	1061.0	3418	1	42	-5.35	1.29
06-16-66-24W4	u. Cook. Lk.	1186.6	3893	2	172	-5.86	5.28
	Leduc	1120.7	3677	2	222	-5.37	1.70
	Leduc	1105.5	3627	1	76	-5.20	2.99
	Leduc	1103.4	3620	2	91	-5.73	2.85
	UGM 2	1045.5	3430	2	120	-5.56	2.65
	UGM 2	1042.7	3421	2	115	-6.92	0.88
	UGM 3a	1005.2	3298	2	176	-5.34	2.12
06-20-67-25W4	Majeaux Lk.	1012.9	3323	2	184	-6.86	2.11
05-14-67-25W4	u. Ireton	1051.0	3448	2	103	-5.27	0.39
	u. Ireton	1043.9	3425	1	44	-4.92	-0.17
04-33-68-22-22W4	l. Cook. Lk.	1059.5	3476	2	236	-7.39	1.83
	l. Cook. Lk.	1057.7	3470	2	112	-6.43	1.97
	UGM 3b	801.0	2628	1	43	-4.24	-0.78

Table 4.2 (contd.): Dolomite stable isotope data

Well ID	**Unit**	**Depth [m]**	**Depth [ft]**	**Dol. type**	**XL size [μm]**	**δ^{18}O [PDB]**	**δ^{13}C [PDB]**
06-20-68-23W4	UGM 3b	909.5	2984	1	56	-5.45	0.97
	UGM 3b	901.9	2959	2	172	-5.39	0.29
	UGM 3b	892.1	2927	2	194		
03-28-70-24W4	u. Cook. Lk.	1087.5	3568	2	200	-5.95	4.50
	u. Cook. Lk.	1075.3	3528	2	237	-5.83	3.50
	Leduc	1068.6	3506	2	166	-5.92	4.81
	Leduc	1051.0	3448	2	186	-5.97	3.93
	UGM 3b	865.3	2839	1	65	-4.46	-0.33
	UGM 3b	857.1	2812	1	92	-4.45	1.47
	UGM 3b	855.3	2806	1	59	-4.43	0.40
15-17-71-25W4	Leduc	1016.8	3336	1	94	-5.57	1.35
	UGM 1	918.4	3013	2	85	-6.26	0.16
	UGM 1	903.7	2965	1	34	-4.27	-1.08
10-01-71-26W4	UGM 3a	976.6	3204	1	10	-3.95	0.02
11-04-72-23W4	Leduc	949.1	3114	2	223	-5.75	3.74
	UGM 1	936.0	3071	2	241	-5.79	2.88
	UGM 1	929.9	3051	2	286	-5.83	2.72
10-18-76-25W4	UGM 1	1076.2	3531	1	32	-4.29	0.42
	UGM 1	1068.9	3507	1	73	-4.61	1.46
	UGM 1	1062.2	3485	1	48	-5.42	0.54
	UGM 1	1054.9	3461	1	79	-4.77	-0.53
	UGM 2	1043.9	3425	1	92	-4.43	-1.48
10-17-83-18W4	UGM 1	396.8	1302	1	73	-5.70	0.35
	UGM 2	387.5	1271	1	65	-5.39	0.23
	UGM 3a	367.0	1204	1	24	-3.98	-3.78
	UGM 3a	342.0	1122	1	72	-3.88	0.22
10-14-84-19W4	UGM 2	413.0	1355	1	54	-3.93	0.36
	UGM 2	402.5	1321	1	79	-3.19	-0.09
	UGM 2	392.0	1283	1	28	-2.58	-0.15
	UGM 3a	389.8	1279	1	15	-2.59	0.11
	UGM 3a	378.3	1241	1	78	-3.55	0.64
06-34-85-19W4	UGM 2	395.0	1296	1	18	-4.82	1.05
	UGM 2	392.0	1286	1	53	-6.53	0.49
	UGM 2	367.0	1204	2	128	-4.78	-0.35
	UGM 3a	340.0	1115	1	66	-5.04	0.27
06-09-87-19W4	UGM 1	320.3	1051	1	72	-3.05	1.18
	UGM 3a	274.5	901	1	10	-3.94	3.49
	UGM 3a	260.8	855	1	52	-4.61	-1.03
	UGM 3a	248.0	814	1	48	-5.28	-3.02

Table 4.2 (contd.): Dolomite stable isotope data

Well ID	Unit	Depth [m]	Depth [ft]	Dol. type	XL size [μm]	$\delta^{18}O$ [PDB]	$\delta^{13}C$ [PDB]
14-17-87-20W4	UGM 3b	313.0	1027	1	14	-4.11	-1.38
03-34-88-20W4	Leduc	466.3	1530	2	211	-6.14	5.70
	Leduc	434.2	1523	2	150	-6.27	5.46
	Leduc	457.2	1500	2	212	-6.67	5.81
	Leduc	403.9	1325	2	218	-7.57	2.96
	LGM	352.3	1156	2	230	-7.01	4.71
	LGM	349.9	1148	2	187	-7.04	4.88
	UGM 2	326.1	1070	2	77	-6.68	5.42
	UGM 3a	277.4	910	2	89	-5.06	0.02
06-11-89-25W4	LGM	629.5	2065	2	144	-6.15	2.14
	LGM	627.5	2059	2	126	-5.35	0.86
	UGM 2	583.5	1914	1	94	-3.26	2.17
	UGM 2	571.8	1876	1	44	-4.72	0.03
	UGM 3b	542.0	1778	1	76	-3.81	2.27
	UGM 3b	533.5	1750	1	30	-3.78	-0.40

Table 4.3: Estimated geochemical composition of Frasnian dolomites and observed values of Woodbend Group replacement dolomites. Estimated Devonian values (trace element composition assumed similar or equal to modern conditions). **a)** Seawater $\delta^{18}O$ as calculated in the text. Seawater $\delta^{13}C$ calculated using values of Frasnian marine calcite cements ($\delta^{13}C$ = +1.5 to +3.5‰) and assuming $\delta^{13}C$ LMC-HCO_3^- = 2.2‰ at 25°C (Turner, 1982). Sr, Fe and Mn from Veizer (1983). **b)** $\delta^{18}O$ as calculated in the text. $\delta^{13}C$ assumed equal to marine calcite, and after Saller (1984) and Aissaoui et al. (1986). Sr from Vahrenkamp and Swart (1990), Na from Sass and Bein (1988), Fe and Mn from Montanez and Read (1992). **c)** $\delta^{18}O$ as calculated in text. $\delta^{13}C$ assumed equal to Holocene evaporitive dolomites (McKenzie, 1981; Pierre et al., 1984; Gregg et al., 1992). Sr from Behrens and Land (1972) and Fritz and Katz (1972). Na from Fritz and Katz (1972) and Sass and Bein (1988). Fe and Mn after Montanez and Read (1992).

	Estimated Late Devonian (Frasnian) Values			Measured Values	
	Seawater[a]	Marine Dol.[b]	Evap. Dol.[c]	Repl.Dol. 1	Repl. Dol. 2
$\delta^{18}O$ ‰ PDB (SMOW)	(-3.6 to -1.0)	-3.0 to +0.3	-2.9 to +2.4	-6.53 to -2.58	-7.57 to -4.78
$\delta^{13}C$ ‰ PDB	-0.7 to +1.3	+1.5 to +3.5	-5.5 to +3.5	-3.78 to +3.49	-0.36 to +5.81
Sr [ppm]	8	50 to 300	600 to 1000	0 to 443	2 to 187
Na [ppm]	35000	0 to 250	200 to 900	0 to 336	2 to 183
Fe [ppm]	0.002	10 to 2000	10 to >2000	80 to 7601	36 to 5660
Mn [ppm]	0.0002	2 to 275	2 to >275	0 to 212	14 to 314

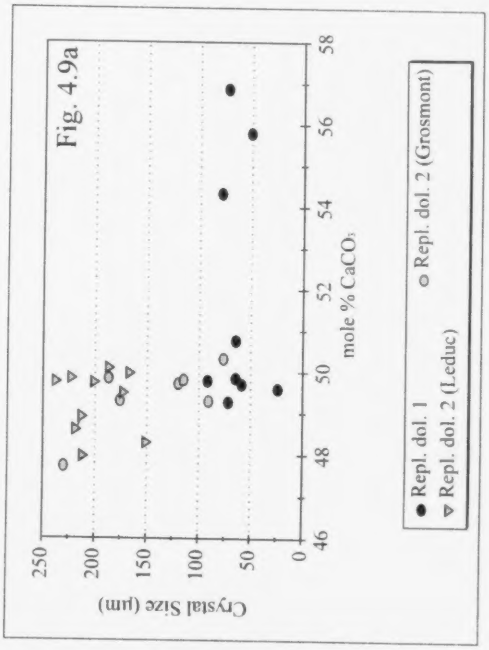

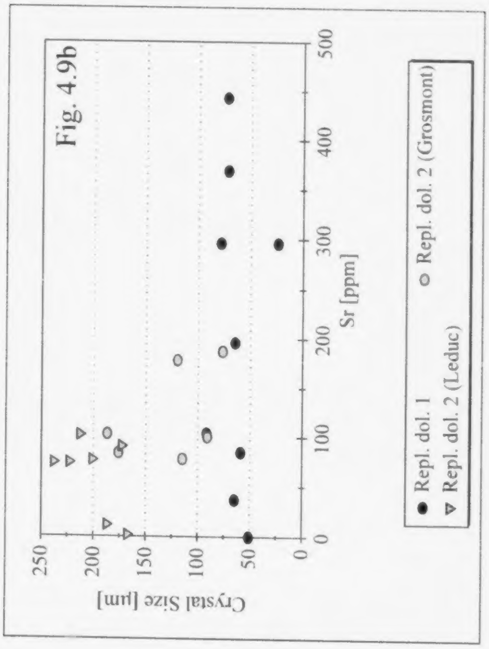

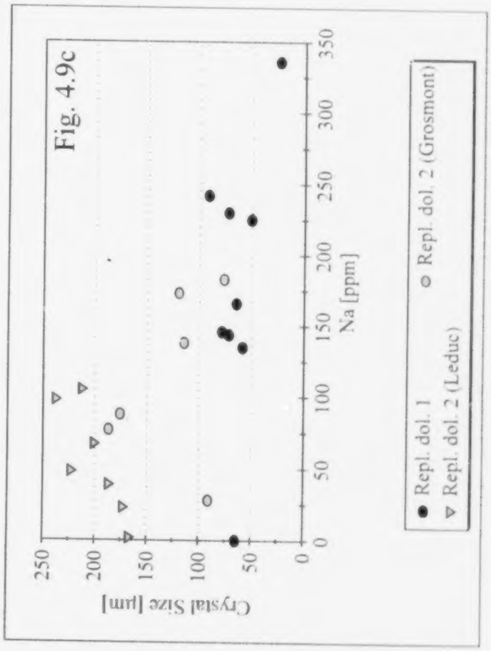

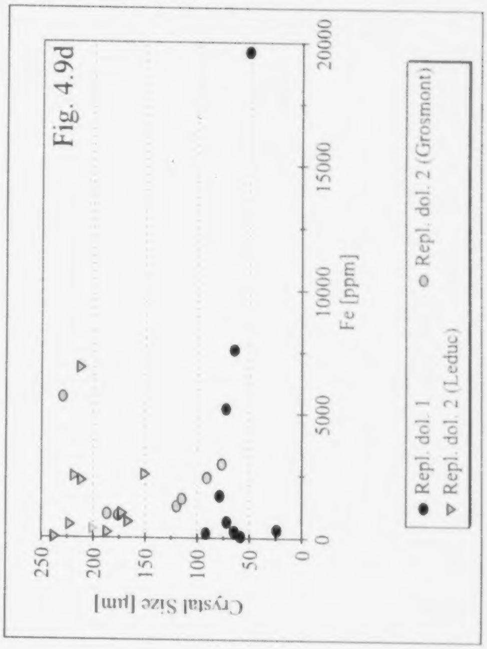

Fig. 4.9: Crystal size versus element concentration in replacement dolomites. **(a)** Crystal size (µm) versus mole % $CaCO_3$. **(b)** Crystal size (µm) versus Sr (ppm). **(c)** Crystal size (µm) versus Na (ppm). **(d)** Crystal size (µm) versus Fe (ppm).

Grosmont replacement dolomite 2. Sodium in replacement dolomite 1 does not covary with crystal size (Fig. 4.9c).

Concentrations of Fe and Mn vary widely in both dolomite types (Table 4.1 and 4.3). Iron contents range from 80 to 7601 ppm in replacement dolomite 1 (avg. 2005 ppm). One sample of replacement dolomite 1 has even higher concentrations of Fe (19625 ppm) due to an Fe-dolomite overgrowth. Iron contents in replacement dolomite 2 range between 36 and 5660 ppm (avg. 1925 ppm). Manganese contents in replacement dolomite 1 range between 0 and 212 ppm (avg. 109 ppm). The replacement dolomite 1 sample with Fe dolomite overgrowth contains considerably more Mn (1185 ppm). Replacement dolomite 2 samples contain between 14 to 314 ppm Mn (avg. 143 ppm). Iron and Mn show no covariant trends with respect to dolomite type, crystal size, or $CaCO_3$ content. As an example, a plot of Fe concentration vs. crystal size is shown in Fig. 4.9d.

Stable Isotopes

Oxygen isotope compositions ($\delta^{18}O$) of replacement dolomite 1 range from -6.53 to -2.58 ‰ PDB (Table 4.2; Fig. 4.10; avg. -4.45 ‰ PDB). These values are similar to the reported oxygen isotope composition of Late Devonian marine calcites, which range between -5.5 and -3.5 ‰ PDB (Carpenter and Lohmann, 1989; Hurley and Lohmann, 1989). However, they are enriched with respect to $\delta^{18}O$ values found in the early calcites present in the Woodbend Group of north-central Alberta ($\delta^{18}O$ from -10.7 to -5.1 ‰ PDB, see Chapter 3). Compared to replacement dolomite type 2, type 1 dolomites are relatively enriched in $\delta^{18}O$ as well as in Ca, Sr and Na. The $\delta^{18}O$ composition of replacement dolomite 1 shows no covariant trends with crystal size (Fig. 4.11), $CaCO_3$ content (Fig. 4.12a) or Sr and Na concentration (Fig. 4.12b,c). However, $\delta^{18}O$ values in replacement dolomite 1 decrease with increasing concentrations in Mn (Fig 4.12d).

Type 2 replacement dolomite has $\delta^{18}O$ values between -7.57 and -4.78 ‰ PDB (Table 4.2; Fig. 4.10; avg. -5.99 ‰ PDB). They slightly overlap with the oxygen isotope composition of type 1 replacement dolomites but are generally depleted compared to these. Oxygen isotope composition of type 2 replacement dolomites does not covary with crystal size (Fig. 4.11), $CaCO_3$ content (Fig. 4.12a), or trace element concentration (Fig. 4.12b to d).

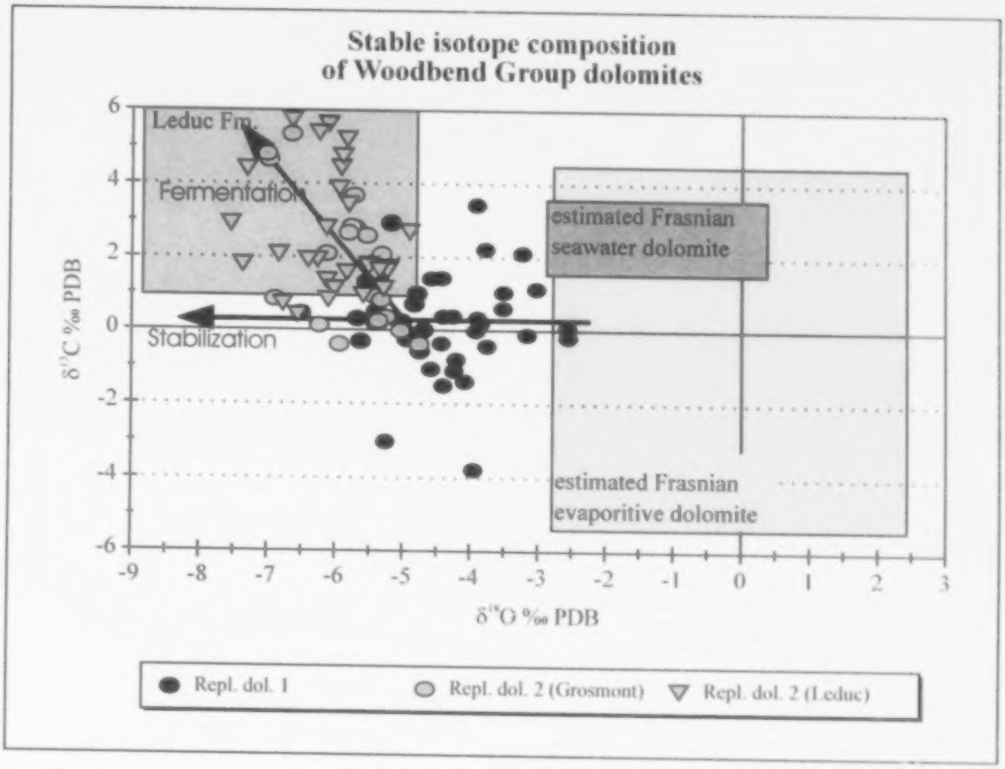

Fig 4.10: Oxygen versus carbon stable isotope composition of Woodbend Group replacement dolomites. Estimated compositions of Frasnian marine and evaporitive dolomites were calculated as described in the text (see also Table 4.2). Field of Leduc Formation replacement dolomites from the central part of the Rimbey-Meadowbrook reef trend from Amthor et al. (1993). Note that type 2 replacement dolomite in the study area has isotopic compositions close to or within the range of Leduc Fm. dolomites described by Amthor et al. (1993). Arrows indicate interpreted trends during dolomite diagenesis.

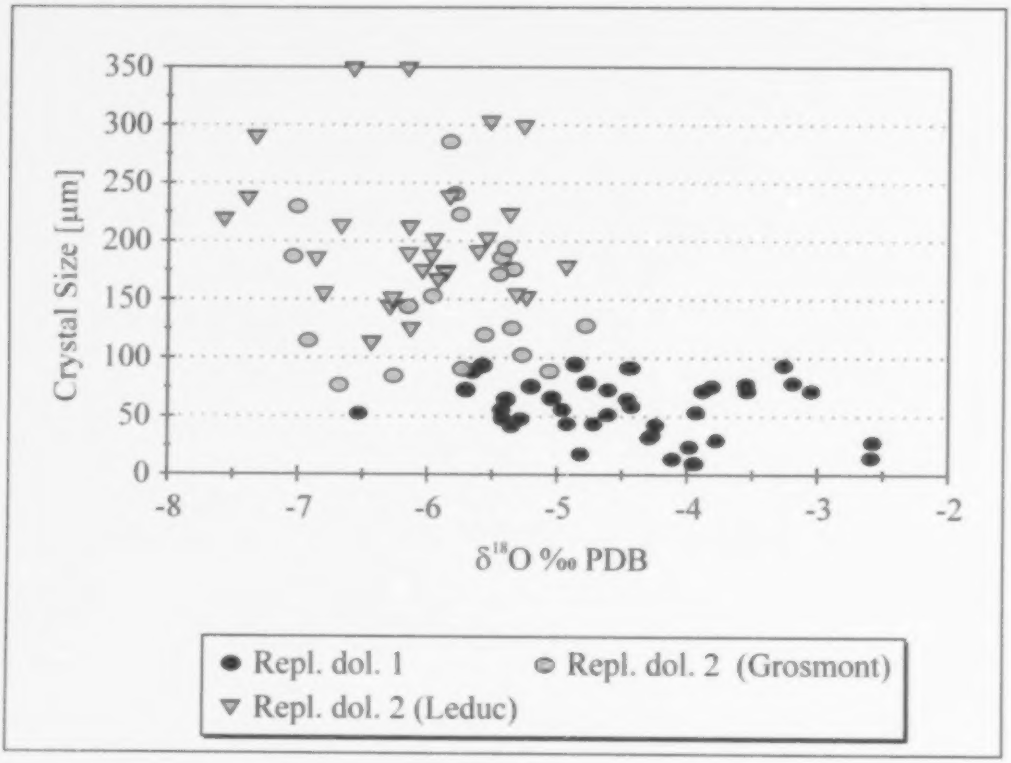

Fig. 4.11: Oxygen isotope ($\delta^{18}O$) composition of replacement dolomites versus crystal size (µm).

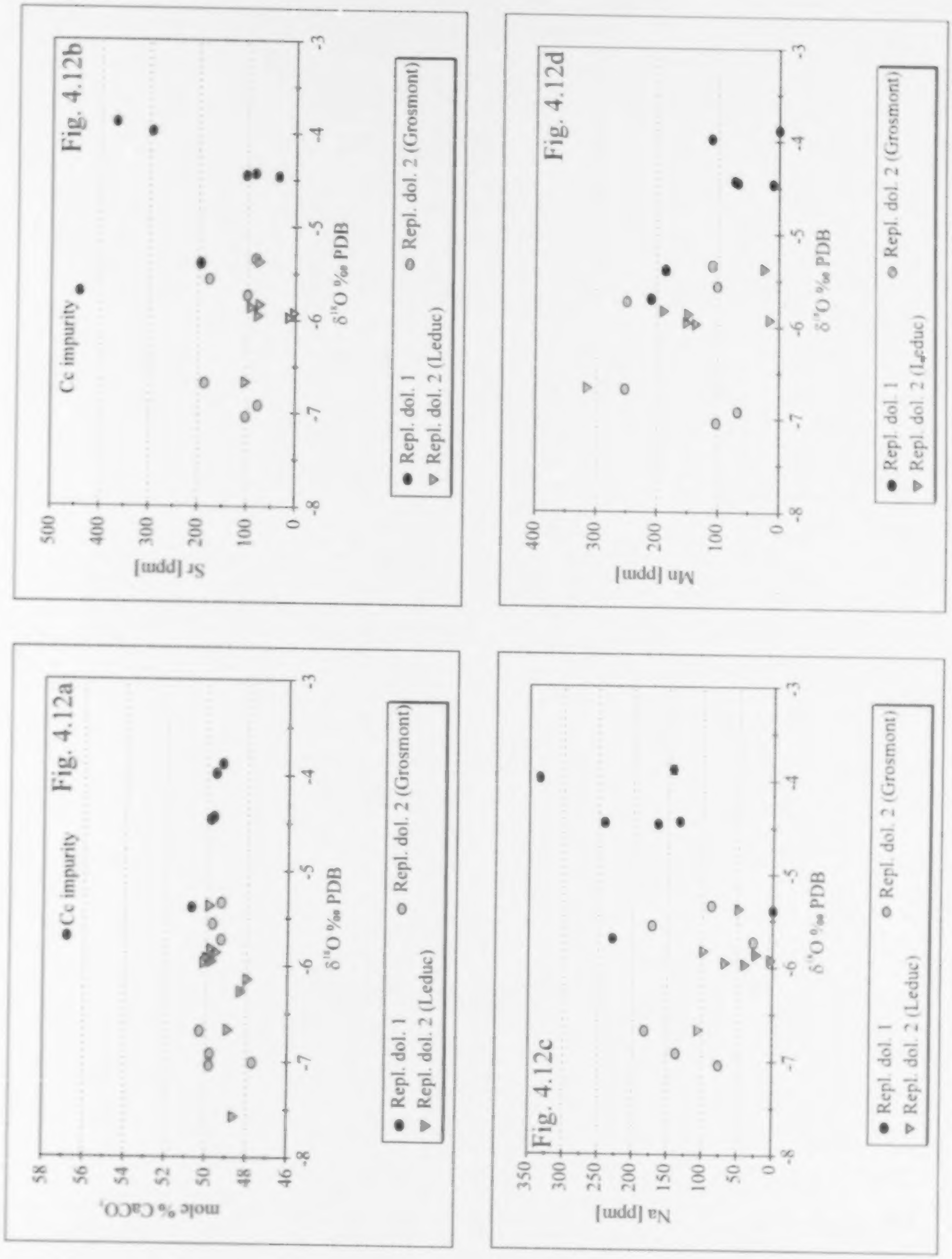

Fig. 4.12: Oxygen isotope composition ($\delta^{18}O$) versus element concentrations in replacement dolomites. **(a)** $\delta^{18}O$ composition versus mole % $CaCO_3$. **(b)** $\delta^{18}O$ composition versus Sr (ppm). **(c)** $\delta^{18}O$ composition versus Na (ppm). **(d)** $\delta^{18}O$ composition versus Mn (ppm).

Type 1 replacement dolomite has widely varying $\delta^{13}C$ compositions that range from -3.78 and +3.49 ‰ PDB (Table 4.2 and 4.3; Fig. 4.10; avg. 0.25 ‰ PDB). These values are mostly depleted and only in a few cases enriched with respect to the reported $\delta^{13}C$ values of Late Devonian marine calcites, which range from +1.5 to +3.5 ‰ PDB (Carpenter and Lohmann, 1989, Hurley and Lohmann, 1989). Carbon isotope compositions of replacement dolomite 1 are, however, within the range of $\delta^{13}C$ values observed in Woodbend limestones in the study area, which range from -1.5 and +3.3 (see Chapter 3). Depleted values of $\delta^{13}C$ in dolomites and calcites are observed especially in facies that are interpreted to have been deposited in restricted marine, peritidal environments. Carbon isotope compositions of type 1 replacement dolomites show no covariant trends with $\delta^{18}O$ composition, crystal size, major element or trace element content (not shown).

Type 2 replacement dolomite samples are generally enriched in $\delta^{13}C$ relative to type 1 replacement dolomites. Carbon isotope composition varies between -0.36 and +5.81 ‰ PDB (Table 4.2 and 4.3; Fig. 4.10; avg. 2.37 ‰ PDB). Type 2 replacement dolomites can be subdivided into two groups based on their $\delta^{13}C$ composition. Subtype 2a has $\delta^{13}C$ compositions near the reported Late Devonian marine calcites. The second group, subtype 2b, is characteristically enriched ($\delta^{13}C \geq +3$ ‰ PDB) in $\delta^{13}C$ relative to subtype 2a and to Late Devonian marine calcites. The $\delta^{13}C$ values of type 2 replacement dolomite do not covary with $\delta^{18}O$, crystal size, major or trace element composition. However, subtype 2b dolomites tend to be coarse crystalline (> 200 μm) and enriched in $MgCO_3$.

The oxygen isotope composition of replacement dolomite 1 and of replacement dolomite 2 does not show any systematic variations with respect to the regional or stratigraphic position of the dolomite samples in the Woodbend Group. The $\delta^{18}O$ composition of both replacement dolomite types also shows no trend with (present) burial depth (or present structural elevation; Fig. 4.13), although the difference in the present structural elevation of the Woodbend Group in the southern and northern part of the study area is 1,250 m over a regional distance of 290 km. The $\delta^{13}C$ composition of replacement dolomite 1 also does not vary regionally. Carbon isotope compositions of replacement dolomite 2, however, show a regional and stratigraphic trend. In the northern part of the study area replacement dolomite 2 is characteristically enriched in ^{13}C (subtype 2b) in the

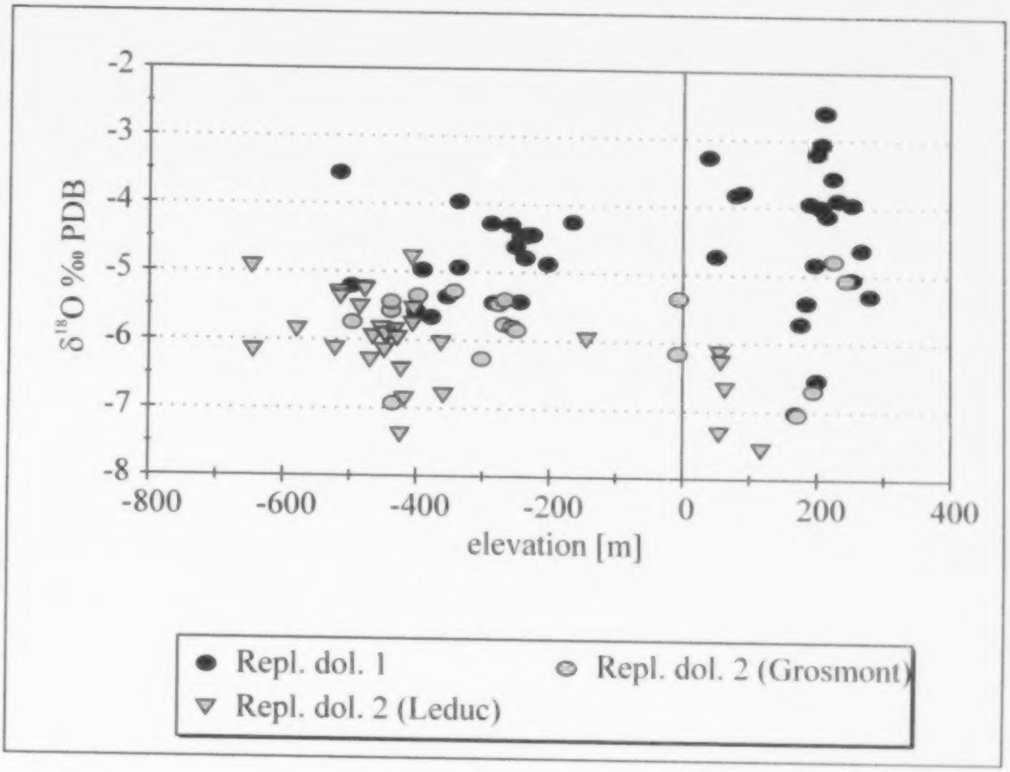

Fig 4.13: Oxygen isotope composition ($\delta^{18}O$) composition of replacement dolomites versus present structural elevation. Neither type 1 nor type 2 replacement dolomites show strong depth trends.

Calling Lake Leduc reefs (Figs. 4.1, 4.3). Dolomites enriched in ^{13}C occur also in portions of the Grosmont platform that directly overlie these Leduc reefs (Fig. 4.7; Fig. 4.14) resulting in the formation of halos of ^{13}C-enriched dolomites (subtype 2b) in the Grosmont platform (Fig. 4.7; 4.14) (Huebscher and Machel, 1995). Type 2 replacement dolomite that has a $\delta^{13}C$ composition of around +2 ‰ PDB (subtype 2a) occurs predominantly in the southern part of the Grosmont platform and in the Morinville reef (Fig. 4.7). The distribution of ^{13}C-enriched dolomite (subtype 2b) in the Morinville reef is uncertain (Fig. 4.7).

DISCUSSION

Origin and modification of replacement dolomite 1

Several lines of evidence suggest that type 1 replacement dolomites formed syndepositionally or during shallow burial (cf. Theriault and Hutcheon, 1987). Replacement dolomite 1 is dominantly present in the upper members of the Grosmont Formation (UGM 2, UGM 3a and UGM 3b) which are characterized by prograding carbonate platform deposits, extended restricted marine tidal flat deposits and the common presence of evaporite beds and evaporite pseudomorphs (Cutler, 1983; see also Chapter 2). Dolomite abundance decreases in the more open marine Grosmont members (LGM and UGM 1). A syndepositional or early diagenetic origin for replacement dolomite 1 is also indicated by the presence of well rounded intraclasts of replacement dolomite 1 (Fig. 4.6a) reworked into shaly beds (i.e. the Grosmont shale breaks) which mark flooding of the Grosmont platform at the beginning of a shallowing upward cycle (Cutler, 1983). An early origin of replacement dolomite 1 is further supported by the presence of fine crystalline, planar-e crystal mosaics and relics of non-stoichiometric, Ca-rich dolomites (in the form of subtypes 1a and 1b). All this evidence suggests that replacement dolomite 1 formed syndepositionally most likely from seawater that was evaporated to gypsum saturation.

Although sedimentological and petrographical evidence indicate the syndepositional origin of replacement dolomite 1, some present day geochemical characteristics are

Fig 4.14: Stable isotope composition of Woodbend Group replacement dolomites versus depth in two representative wells. **(a)** Well 3-34-88-20W4 is representative of the situation where Grosmont Fm. carbonates directly overly Leduc reefs. The entire Woodbend section (Cooking Lake, Leduc and Grosmont formations) is pervasively dolomitized by type 2 replacement dolomite. The intervening Ireton Formation aquitard is thin (Fig. 4.3). All replacement dolomites, except for the uppermost Grosmont Formation dolomites (subtype 2a), are enriched in ^{13}C ($\delta^{13}C$ around +5 ‰ PDB; subtype 2b). **(b)** Well 10-14-84-19W4 is representative of the general dolomite distribution in the Grosmont Formation. The two Woodbend aquifers are separated by a thick Ireton Formation aquitard. The Cooking Lake Formation as well as the LGM and UGM 1 members of the Grosmont Formation are limestones. The upper members of the Grosmont Formation are pervasively dolomitized by type 1 replacement dolomite with a $\delta^{13}C$ composition of around 0‰ PDB.

Fig. 4.14a: (3-34-88 20W4)

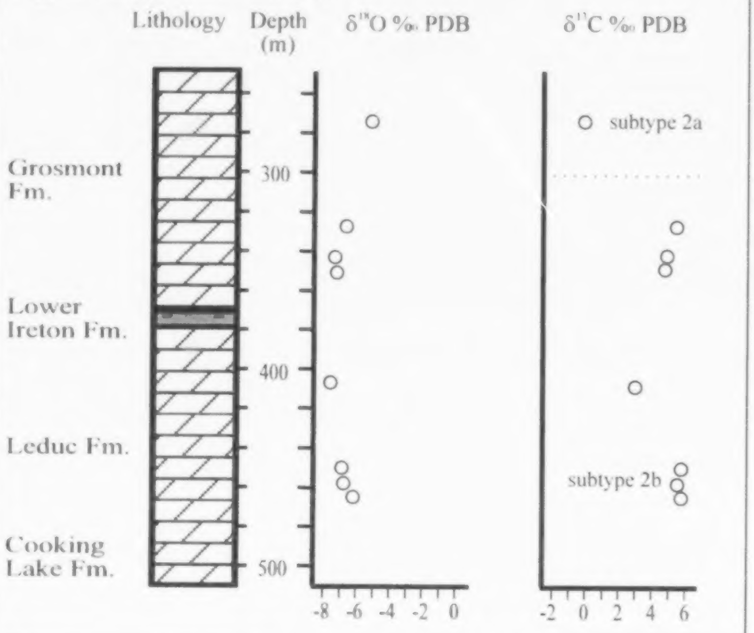

Fig. 4.14b: (10-14-84-19W4)

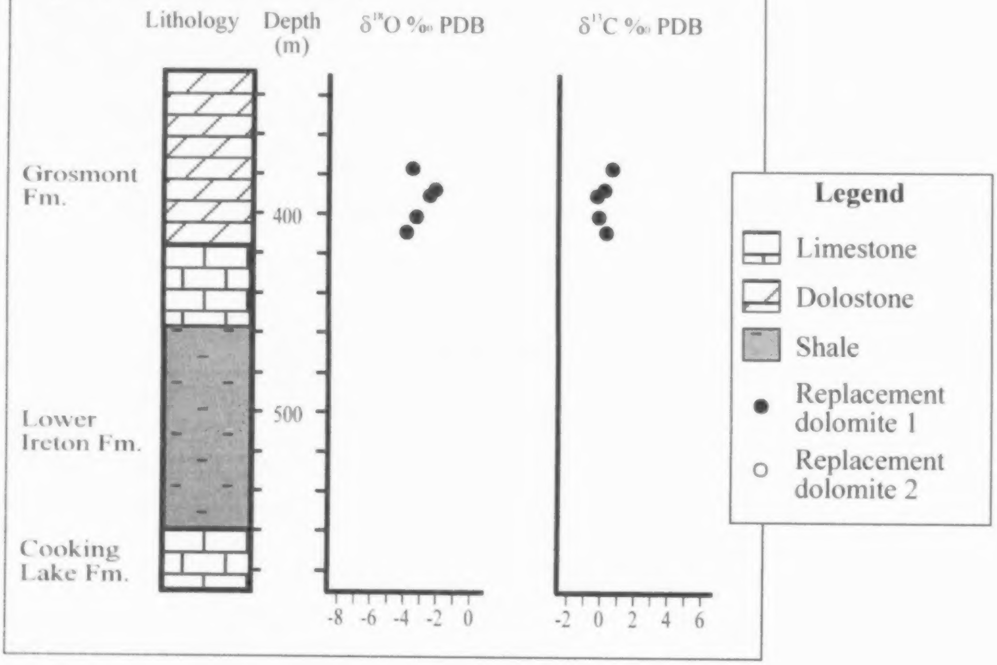

generally inconsistent with expected characteristics of dolomites that have formed syndepositionally from seawater evaporated to gypsum saturation. For example, most replacement dolomite 1 is non-stoichiometric, contains lower concentrations of Na and Sr than Cenozoic hypersaline dolomite (see Table 4.2; cf. Behrens and Land, 1972; Fritz and Katz, 1972), and is depleted in ^{18}O, whereas modern evaporitic dolomites are enriched in ^{18}O (McKenzie, 1981; Pierre et al., 1984; Gregg et al., 1992). However, it can be expected, that similar to many modern examples, syndepositional Woodbend dolomites were unstable and were susceptible to later modification. The following discussion evaluates the textural and geochemical characteristics of replacement dolomite 1 for signs of dolomite modification and for "memory" of the postulated precursor phase.

Petrographic evidence.- Evidence for modification in type 1 replacement dolomites include, 1) increasing number of non-planar crystal boundaries with increasing crystal size; 2) increasing corrosion of non-luminescent and orange luminescent zones with increasing crystal size; and 3) increasing amount of homogeneous dull red luminescent dolomite (subtype 1c) with increasing crystal size (Figs. 4.4 a and b, 4.5b).

The observed petrographic and textural relationships are consistent with the idea that the different subtypes of replacement dolomite 1 characterize progressive stages in stabilization of these early dolomites. Some fine crystalline dolomites retained their planar texture and complex zoning patterns (subtype 1a). Texturally more mature dolomites (coarser crystalline and higher number of non-planar crystal boundaries) commonly show corroded internal growth zones (subtype 1b) and subsequent replacement of these "early" zones by dull red dolomite. The end-product is a texturally mature, medium to coarse crystalline dolomite with dominantly non-planar crystal boundaries (subtype 1c). Such texturally mature dolomites appear to have lost all zonation that may have been present in precursor dolomites resulting in a homogenized luminescence pattern (cf. Cander et al., 1988; Holail et al., 1988). These observations further suggest that dolomite modification proceeded via partial dissolution of the unstable precursor phase accompanied by precipitation of a more stable dolomite (Land, 1985; Sibley, 1990; Nordeng and Sibley, 1994).

Major element evidence.- Diagenetic stabilization of type 1 replacement dolomites is also supported by their major element composition. The major element composition of replacement dolomite 1 varies widely from stoichiometric or near-stoichiometric (49.3 to 50.8 mole % $CaCO_3$; subtype 1c) to non-stoichiometric (54.3 to 56.8 mole % $CaCO_3$; relic cores up to 64.7 mole % $CaCO_3$; subtype 1a). The presence of relics of non-stoichiometric, planar dolomite strongly suggests that type 1 replacement dolomites have undergone diagenetic modification. The presence of an originally non-stoichiometric dolomite phase is also supported by the fact that Ca content in type 1 replacement dolomites decreases with 1) increasing number of non-planar crystal boundaries (Figs. 4.4 b to d, 4.5 a and b), and 2) increasing amount of homogenization of luminescence patterns (Figs. 4.4 a to d, 4.5 a and b).

Modern examples of syndepositional dolomites typically are non-stoichiometric (up to 62 mole % $CaCO_3$) and poorly ordered (McKenzie, 1981; Carballo et al., 1987; Mazzullo et al., 1987). It has been suggested that near-stoichiometric dolomites can precipitate directly from Mg-rich, hypersaline fluids (Sass and Bein, 1988). Sibley (1990), however, has shown that the precipitation of stoichiometric dolomite is not only dependent on the Mg/Ca ratio of the dolomitizing solution but is also a function of the interaction time between the solution and the precipitating solid.

Trace element evidence.- Modification of type 1 replacement dolomites is at best suggested by the measured concentrations of Sr (0 to 443 ppm) and Na (0 to 336 ppm) which are lower than in Cenozoic evaporitic dolomites. Strontium and Na concentration of modern dolomites that precipitated from evaporated seawater range between 600 and 1000 ppm for Sr (Behrens and Land, 1972; Banner, 1995) and between 200 to 900 ppm for Na (Fritz and Katz, 1972). Unfortunately clear evidence for dolomite modification in the form of covariant trends of Sr and Na concentrations with crystal size (Figs. 4.9b, c) or $\delta^{18}O$ composition (Figs. 4.12b, c) is lacking.

Alternatively to dolomite modification, low concentrations of strontium in early dolomite results from seawater dolomitization. For example, early dolomites from the Little Bahama Bank, interpreted to be of seawater origin, have Sr concentrations of 50 to 300 ppm varying linearly as a function of dolomite $MgCO_3$ content (Vahrenkamp and

Swart, 1990). It is, however, unlikely that type 1 replacement dolomites formed from normal seawater since Sr concentrations in non-stoichiometric replacement dolomite 1 are generally higher than in non-stoichiometric modern seawater dolomites (Fig. 4.15). This implies that type 1 replacement dolomites formed from and/or have been modified by fluid with a higher Sr/Ca ratio than modern seawater. Elevated fluid Sr/Ca ratios result, for example, from gypsum precipitation and replacement of aragonite and high-Mg calcite during dolomitization (Land, 1980).

Concentrations of Fe (0 to 7601 ppm; Fe dolomite overgrowth: 19625 ppm) and Mn (0 to 314 ppm; Fe dolomite overgrowth: 1185 ppm) in replacement dolomite 1 are similar to or higher than Fe (10 to 2000 ppm) and Mn (5 to 273 ppm) in Cenozoic marine and evaporitic dolomites (Montanez and Read, 1992, and references therein). High concentrations of Fe and Mn in type 1 replacement dolomites could have resulted from 1) precipitation in a relatively reducing environment, 2) increased concentrations of Mn and Fe due to release of these elements from oxides, clays and organic detritus, or 3) dolomite modification in Fe-rich, generally basin derived waters (Montanez and Read, 1992).

Stable isotope evidence.- The significant depletion in ^{18}O of replacement dolomites 1 relative to Cenozoic marine and evaporitic dolomites is an obvious difference in the geochemistry of these dolomites. The $\delta^{18}O$ composition of Woodbend Group replacement dolomites ranges from -6.53 to -2.58 ‰ PDB (Table 4.2 and 4.3; Fig. 4.10), compared to $\delta^{18}O$ values for Cenozoic marine and evaporitive dolomites which range between around +1.0 to +6.0 ‰ PDB (Behrens and Land, 1972; McKenzie, 1981; Aissaoui et al., 1986; Gregg et al., 1992; Vahrenkamp and Swart, 1994). Relative to Cenozoic dolomite the depleted $\delta^{18}O$ signature of Woodbend Group replacement dolomites could indicate 1) dolomite precipitation from Late Devonian seawater or modified seawater depleted in ^{18}O relative to present day seawater (Veizer et al., 1986; Hudson and Anderson, 1989), 2) precipitation from unaltered seawater at elevated temperatures, or 3) dolomite modification and stabilization by ^{18}O depleted fluids and/or fluids at elevated temperatures.

In order to determine the degree and environment of diagenesis of Woodbend

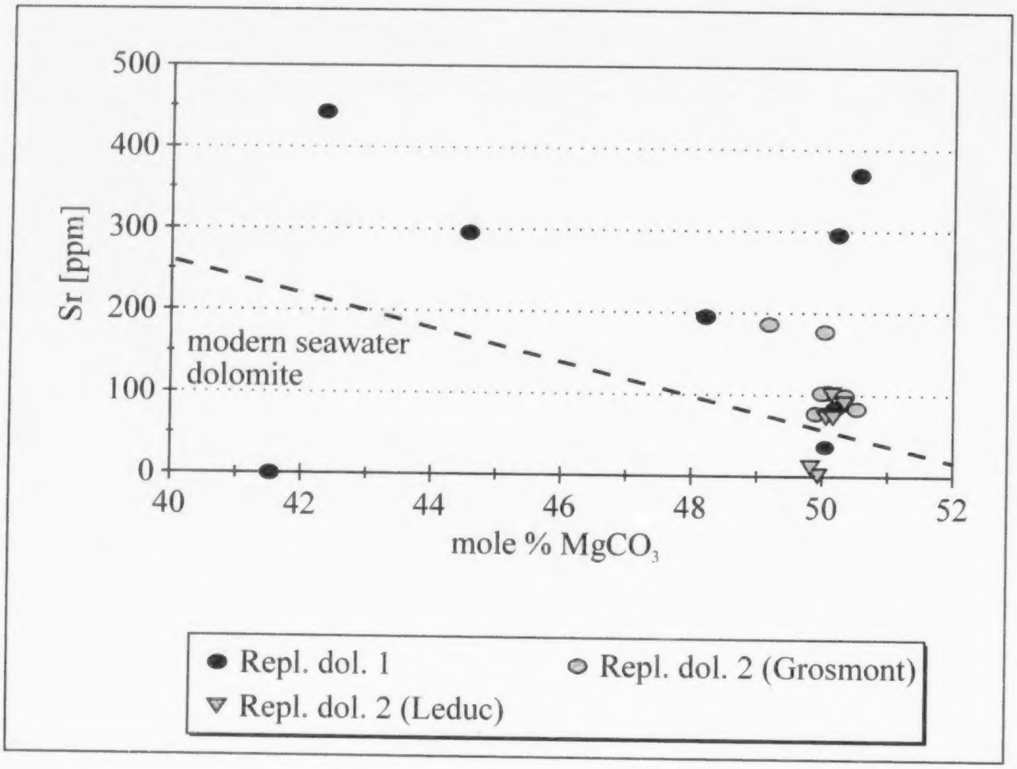

Fig. 4.15: Mole % $MgCO_3$ versus Sr content (ppm) in Woodbend Group replacement dolomites. The line designated as "modern seawater dolomite" represents $MgCO_3$ versus Sr content in Cenozoic marine dolomites from the Bahamas (Vahrenkamp and Swart, 1990). These dolomites are assumed to have formed from seawater (Sr/Ca ratio = 0.0195).

Group replacement dolomites, it is necessary to estimate the maximum range of $\delta^{18}O$ composition of Late Devonian seawater and to calculate from these values the theoretical maximum range of Late Devonian seawater and evaporitive dolomites. The procedure used in this study follows the methodology used and described by Montanez and Read (1992). The oxygen isotope composition of Late Devonian (Frasnian) seawater was calculated using published $\delta^{18}O$ values of Late Devonian (Frasnian) marine cements. These Frasnian marine cements have worldwide $\delta^{18}O$ values of between -5.5 and -3.5 ‰ PDB (Carpenter and Lohmann, 1989; Hurley and Lohmann, 1989). The original mineralogy of these cements is uncertain as all cements are now present as low-Mg calcites. If marine cements, which presumably consisted of either aragonite or high-Mg calcite, recrystallized under low water-rock ratios, a "memory" of their original $\delta^{18}O$ composition may have been preserved (Given and Lohmann, 1985). The following discussion assumes that the reported $\delta^{18}O$ values of Late Devonian (Frasnian) marine calcite cements have, indeed, retained a "memory" of their original $\delta^{18}O$ composition. Correcting $\delta^{18}O$ composition of Frasnian calcite cements for possible enrichment in ^{18}O of the precursor carbonate (high-Mg calcite with 10 to 15 mole % $MgCO3$, and aragonite) (Tarutani et al., 1969), using $10^3 \ln \alpha_{\text{calcite-water}} = 2.78 * 10^6 T^{-2}$ (°K) - 2.89 (Friedman and O'Neil, 1977), and assuming a precipitation temperature of 25°C (average temperature of tropical seawater after Hudson and Anderson, 1989), the range of $\delta^{18}O$ values of Late Devonian (Frasnian) seawater is estimated to have been -3.6 to -1.0 ‰ SMOW (Table 4.2). Seawater evaporated to or near gypsum saturation should be about 3 to 4 ‰ enriched in ^{18}O (Sofer and Gat, 1975). The oxygen isotope composition of evaporated Frasnian seawater would, consequently, range between -0.6 and +3.0 ‰ SMOW (Table 4.2).

The theoretical maximum range of $\delta^{18}O$ compositions of Frasnian seawater and evaporitic dolomites were calculated assuming $10^3 \ln \alpha_{\text{dolomite-water}} = 2.78 * 10^6 T^{-2}$ (°K) + 0.91 (Land, 1985) for stoichiometric dolomite, and $10^3 \ln \alpha_{\text{dolomite-water}} = 2.78 * 10^6 T^{-2}$ (°K) + 0.11 (Fritz and Smith, 1970) for Ca-rich protodolomites. Frasnian seawater dolomites were calculated to have a $\delta^{18}O$ composition of between -3.0 and +0.3 ‰ PDB (Table 4.2; Fig. 4.10), using the calculated $\delta^{18}O$ range for Frasnian seawater and a precipitation temperature of 25°C. Frasnian evaporitive dolomites were estimated to have a $\delta^{18}O$ composition of between -2.9 and +2.4 ‰ PDB (Table 4.2; Fig. 4.10), using the estimated maximum $\delta^{18}O$ range for Frasnian evaporated seawater and a precipitation temperature of 30 to 40°C, which reflects the commonly elevated temperatures of sabkha pore waters (McKenzie, 1981).

Actually measured $\delta^{18}O$ values of Woodbend replacement dolomite 1, which is assumed to have formed in a gypsum saturated, hypersaline environment, are depleted relative to the calculated values for Frasnian evaporitive dolomites (Fig. 4.10). Even assuming Late Devonian seawater was depleted in ^{18}O, either globally or locally, by about 2.5 ‰ SMOW, only replacement dolomites with the most enriched $\delta^{18}O$ values would fall into the calculated Frasnian evaporitive dolomite field (Fig. 4.9). The depletion of even the presumably least altered type 1 replacement dolomites relative to the calculated Frasnian evaporitive dolomites shows that Woodbend Group replacement dolomites interpreted to be of evaporitive origin did in fact not retain their original $\delta^{18}O$ composition. This is indicative of diagenetic modification of these dolomites by either ^{18}O depleted fluids, e.g. meteoric or mixed-meteoric marine fluids, and/or fluids at elevated temperatures. However, input of meteoric water does not seem a likely alternative given the evaporitic setting of the Grosmont platform and the lack of evidence for early meteoric diagenesis.

The $\delta^{13}C$ compositions of type 1 replacement dolomites fall for the most part within the range predicted for Frasnian evaporitive dolomites. Estimates for the carbon isotope composition of Frasnian marine and evaporitive dolomites (Table 4.3; Fig 4.10) were derived by comparison with Cenozoic marine and evaporitive dolomites. Direct comparisons of Cenozoic and Frasnian $\delta^{13}C$ values are possible because both Cenozoic (Saller, 1984; Aissaoui et al., 1986) and Frasnian (Carpenter and Lohmann, 1989; Hurley and Lohmann, 1989) marine calcites have $\delta^{13}C$ signatures of around +1.5 to +3.5 ‰ PDB, which indicates a similar carbon isotope composition of the ocean reservoir during these times. The similarity in carbon isotope composition can be applied to dolomites assuming that similar processes influenced the $\delta^{13}C$ composition of dolomites in Cenozoic and Frasnian marine environments. Cenozoic evaporitive dolomites show a wide range in $\delta^{13}C$ composition between around -5.5 and +3.5 ‰ PDB (McKenzie, 1981; Pierre et al., 1984; Gregg et al., 1992). Woodbend Group type 1 replacement dolomites have a very similar range of $\delta^{13}C$ values between -3.78 and +3.49 ‰ PDB (Table 4.3; Fig. 4.10). Cenozoic and, therefore, Frasnian evaporitive dolomites are commonly depleted in $\delta^{13}C$ relative to observed and/or expected marine dolomites, which generally have the same $\delta^{13}C$ range (+1.5 to +3.5 ‰ PDB) as marine calcites (Saller, 1984; Aissaoui et al., 1986). The following processes could be responsible for the depletion in ^{13}C in evaporitive dolomites, 1) precipitation from concentrated, evaporated, ^{13}C-depleted fluids of marine origin (Lazar and Erez, 1990; Patterson and Walter, 1994), 2) precipitation from ^{12}C-enriched fluids due to introduction of organic carbon via sulfate reduction (Howarth and Marino, 1984; Pierre et al., 1984), and 3) inheritance of the isotopic signature from the precursor carbonate. The influence of bacterial sulfate reduction is strongly suggested by the common association of replacement dolomite 1 with early diagenetic anhydrites and pyrite.

Evidence from regional distribution.- The fact that type 1 replacement dolomite is present predominantly in the upper members of the Grosmont Formation and that its frequency of occurrence increases with increasing amount of restricted marine and tidal flat facies with an increased potential for evaporitic conditions supports the interpretation of its evaporitive origin. The increase in the amount of the presumably least altered replacement dolomite subtypes 1a and 1b away and downwards from evaporitic facies is consistent with dolomitization and/or dolomite modification by downward percolating fluids. Little altered dolomites are mostly preserved in open marine, subtidal facies farthest away from the likely site of origin of the syndepositional dolomitizing fluids. In contrast, evaporitic, intertidal facies are dominated by the texturally and geochemically more mature subtype 1c. This distribution would be expected if the dolomite modifying fluids were of syndepositional origin and/or entered the Grosmont Formation from above. Upper members of the Grosmont Formation appear to have been exposed longer to the dolomitizing fluids than lower members of the Grosmont Formation resulting in the development of more tightly interlocking, planar-s mosaics of stoichiometric dolomites. Dolomite modification may have set in because of the possible long interaction time between fluids and rocks (Sibley, 1990) in these intervals as well as because of the relatively high Mg/Ca ratio in seawater evaporated to gypsum precipitation.

The previous discussion of dolomite texture, geochemistry and distribution lead to the conclusion that occurrences of type 1 replacement dolomite in the Grosmont Formation have a syndepositional or early diagenetic origin and were most likely formed by seawater evaporated to gypsum saturation. Dolomite modification may have started very early, while the dolomites were still in contact with the dolomitizing fluids. Early diagenetic modification of unstable, syndepositional dolomites has been reported to occur in Holocene dolomites immediately below the depositional surface (McKenzie, 1981, Gregg et al., 1992).

Using the paleotemperature equation of Land (1985), the average $\delta^{18}O$ composition of replacement dolomite 1, and the calculated $\delta^{18}O$ values of Frasnian evaporated seawater (-0.6 to +3.0 ‰ SMOW) the temperature of formation/modification was estimated to have been in the range of 40 to 55°C. The lower temperature limit, considering sabkha pore water temperatures range between 30 and 40°C, could have been reached at the depositional surface. The higher temperature limit was probably reached within the first several hundred meters of burial (Fig. 4.16).

Origin of replacement dolomite 2

Type 2 replacement dolomite is texturally and geochemically distinct from type 1 replacement dolomite in that it is texturally and geochemically more homogeneous. Replacement dolomite 2 forms unimodal, medium to coarse crystalline, mostly planar-s crystal mosaics. Individual crystals are very uniform petrographically, and show a homogeneous dull-red luminescence. Major and trace element concentrations are also very uniform. All type 2 replacement dolomites are stoichiometric to near-stoichiometric and are depleted in Sr (2 to 187 ppm) and Na (2 to 183 ppm) relative to replacement dolomite 1. No covariant trends are present between trace element concentrations, major element composition and $\delta^{18}O$ composition of type 2 replacement dolomites. The development of such a uniform dolomite mosaic can be explained by the slow growth of few crystals from a solution that is not highly saturated with respect to dolomite (Sibley and Gregg, 1987).

Oxygen isotope evidence.- Leduc Formation dolomites, which are equivalent to replacement dolomite 2 in this study, are interpreted to have formed in the burial environment under elevated temperature conditions based on their oxygen isotope

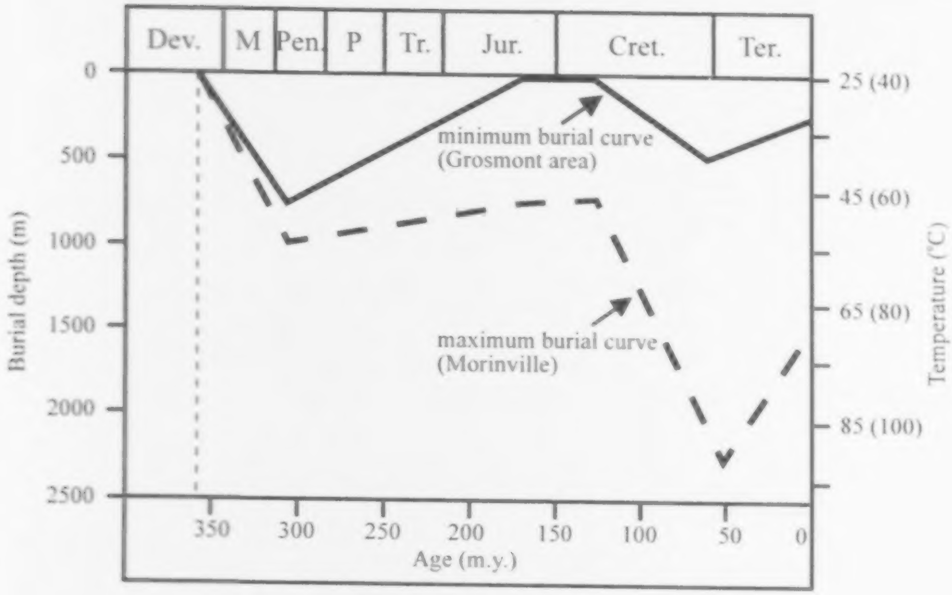

Fig. 4.16: Burial history plot of the Woodbend Group in north-central Alberta. Subsurface temperatures are derived assuming a geothermal gradient of 30°Ckm^{-1} and surface temperatures of 25°C (normal marine environment) and 40°C (sabkha environment), respectively. The two burial curves represent the northern and southern burial history end members.

Maximum burial depth of the first (Paleozoic) burial episode was derived by comparison with the thicknesses of preserved Paleozoic strata near the study area (see Richards et al., 1994). Timing and maximum depth of the second (Mesozoic/Cenozoic) burial episode were extrapolated from published data from the southern end and central portions of the Rimbey-Meadowbrook reef trend (Laflamme, 1990; Amthor et al., 1993). A linear gradient in dip and amount of Cretaceous/Tertiary overburden was assumed between the southern and central regions of the reef trend and the study area to estimate the maximum burial depth of the Woodbend Group in north-central Alberta.

composition (Amthor et al., 1993; Mountjoy and Amthor, 1994). However, the paleotemperature estimates on which these interpretations are based have inherent uncertainties, because of the unknown origin and isotopic composition of the dolomitizing fluid. The following paleotemperature estimates are based on the assumption that the dolomitizing fluids in the Cooking Lake platform margin and overlying Leduc reefs were isotopically little altered fluids of marine parentage (Amthor et al., 1993; Mountjoy and Amthor, 1994). Fluids of marine parentage are the most commonly invoked dolomitizing fluids, because seawater and its derivatives are the only common source for Mg in sedimentary sequences and, therefore, the most viable dolomitizing agent (Land, 1985). Using these assumptions and the paleotemperature equation of Land (1985), the average $\delta^{18}O$ composition of replacement dolomite 2, and the estimated maximum $\delta^{18}O$ values of Frasnian seawater (-3.6 to -1.0 ‰ SMOW) the temperature of formation was estimated to have been in the range of 49 to 65°C. Using a geothermal gradient of 30°C km^{-1} and a surface temperature of 25°C, these temperatures could have been reached at a burial depth of 700 to 1300 m (Fig. 4.16). In the southern part of the study area (Morinville reef) this burial depth was reached at the end of the Devonian or the beginning of the Mississippian (Fig. 4.16; cf Amthor et al., 1993; Mountjoy and Amthor, 1994), and little change in burial temperature occurred until maximum burial during the Late Cretaceous. In the northern part of the study area (Northern Calling Lake reef), the calculated burial depths and temperatures necessary for replacement dolomite 2 formation were attained for a much shorter time period, i.e approximately between the Late Devonian and the end of the Paleozoic. During the Mesozoic the Woodbend Group carbonates of the northern part of the study area were subaerially exposed (see Chapter 5). This puts constraints on the timing of dolomitization for the entire Rimbey-Meadowbrook reef trend and its northern extension, because replacement dolomite 2 are of nearly identical composition throughout the reef trend. Dolomitization did likely not occur during the Cretaceous/Tertiary burial phase (Fig. 4.16) because, 1) burial temperatures greater 60°C were only reached in the southern part of the study area (Fig. 4.16), and 2) there is no variation in the $\delta^{18}O$ composition of type 2 replacement dolomites with present structural elevation (Fig. 4.13), which is expected if the $\delta^{18}O$ values reflected Cretaceous/Tertiary depth and temperature differences along the reef trend (Fig. 4.16).

Carbon isotope evidence.- The carbon isotope composition of Woodbend Group type 2 replacement dolomites ranges between -0.36 and +5.81 ‰ PDB. These values are for the most part within the range of Frasnian marine and evaporitive dolomites (subtype 2a) or are slightly enriched in ^{13}C (subtype 2b) with respect to these dolomites. At the calculated temperature of replacement dolomite 2 formation, CO_2 enriched in ^{13}C forms as a the byproduct of bacterial reduction of CO_2 to CH_4 (Claypool and Kaplan, 1974) and as product bacterial fermentation of organic matter (Claypool and Kaplan, 1974; Irwin et al., 1977; Carothers and Kharaka, 1980). Whiticar et al. (1986) observed CO_2 with a $\delta^{13}C$ composition of up to +15 ‰ PDB to be in equilibrium with biogenic methane at temperatures between -1.3 and +58°C. Bacterial fermentation of organic matter operates at burial depths between 100 and >1,000 m and has been inferred as a source for ^{13}C-enriched dolomites associated with concretions (Hennessy and Knauth, 1985; Curtis et al., 1986).

The spatial variation in carbon isotope composition of type 2 replacement dolomites (Fig. 4.14a) probably reflects local variations in the diagenetic environment. In the Morinville reef and the southern Grosmont platform, areas where large rock volumes were replaced by type 2 replacement dolomites, carbon isotopes appear to have been essentially rock buffered and type 2 replacement dolomites (subtype 2a) retained similar values to observed or suggested precursor phases. In contrast, in the relatively small reefs of the northern extension of the Rimbey-Meadowbrook reef trend as well as in overlying strata of the Grosmont Formation, type 2 replacement dolomites are enriched in ^{13}C (subtype 2b). Figure 4.17 demonstrates that ^{13}C-enriched dolomites formed from fluids that were slightly enriched in ^{13}C relative to rock buffered to rock buffered fluids at the suggested temperature of replacement dolomite 2 formation of 49 to 65°C. Assuming that the ^{13}C-enriched CO_2 was derived from bacterial fermentation of organic matter ($\delta^{13}C$ of dissolved HCO_3^- = +15 ‰ PDB; Irwin et al., 1977) a contribution of 5 to 10 % organically derived carbon was required form replacement dolomite subtype 2b.

The most likely source for organically derived CO_2 are organic rich limestones of the Majeaux Lake Member (Figs. 4.2 and 4.7). It is suggested that compaction driven flow was the probable mode of transportation. Bacterial fermentation of organic matter can be active at a depth range of 10 and >1000 m (Irwin et al., 1977), and much of the

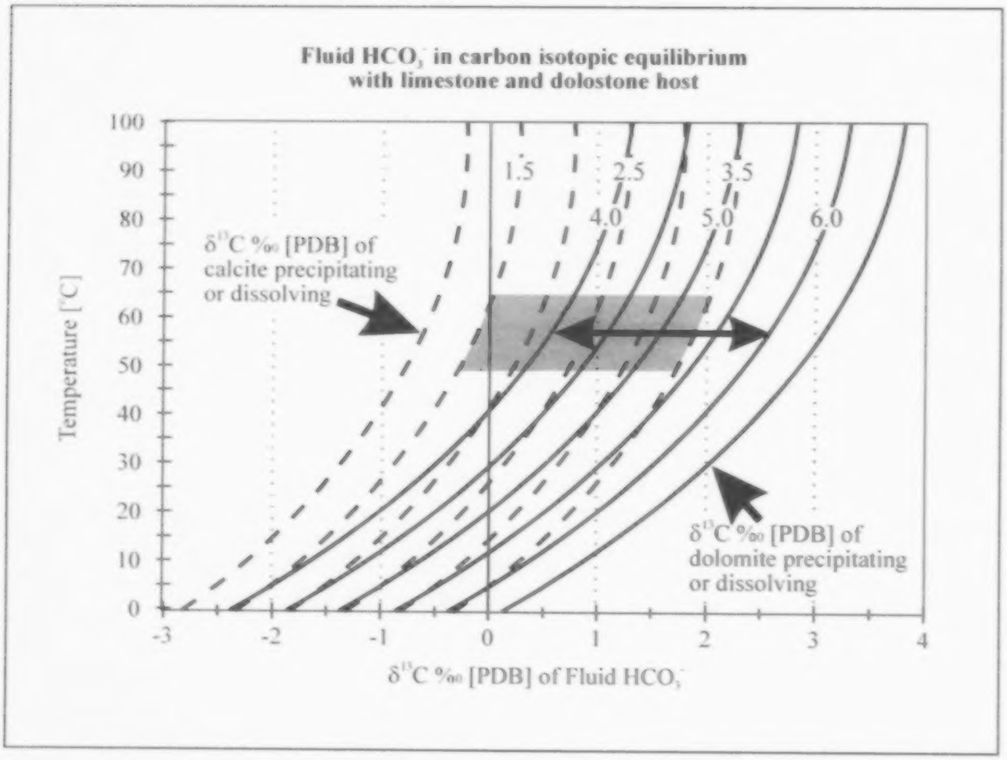

Fig. 4.17: Temperature versus $\delta^{13}C$ composition of dissolved HCO_3^- in water. Lines for equilibrium precipitation plotted using the carbon isotope fractionation relationships published by Ohmoto and Rye (1979). Calcite equilibrium lines = dashed lines, dolomite equilibrium lines = solid lines; numbers indicate $\delta^{13}C$ values of the minerals. The diagram shows the $\delta^{13}C$ composition of dolomite (or calcite) and fluid HCO_3^- that would be in carbon isotope equilibrium at a given temperature. The graph can be used to determine the $\delta^{13}C$ composition of a diagenetic fluid that would be in carbon isotopic equilibrium with dissolving dolomite or calcite. The graph can also be used to calculate the $\delta^{13}C$ value of dolomite precipitating from a given fluid at a given temperature. The grey shaded area marks the carbon isotope composition of Frasnian marine calcite cements (Carpenter and Lohmann, 1989; Hurley and Lohmann, 1989) at the presumed formation temperature of type 2 replacement dolomites (49 to 65°C; see text). Note that most Woodbend limestones are depleted in ^{13}C with respect to this value. The double sided arrow marks the composition of ^{13}C-enriched type 2 replacement dolomites (subtype 2b). The graph shows that these dolomites could not have entirely formed from rock-buffered fluids at the presumed temperature range, indicating a fraction of organic carbon, derived from organic matter fermentation, in the fluid HCO_3^-.

physical compaction and porosity loss in limestones also occurs in this depth range (Feazel and Schatzinger, 1985). The organic rich limestones of the Majeaux Lake Member are 1) overlain by relatively impermeable Ireton shales, 2) underlain by porous and permeable carbonates of the Cooking Lake Formation, and 3) adjacent to porous and permeable Leduc Formation reefs. Hydrogeological models for similar situations (Hugo, 1990; Kaufman, 1994) suggest that compaction driven flow should result in downward drainage of Majeaux Lake pore fluids and lateral flow towards the Leduc reef trend. Inside the reef trend compaction should drive formation waters vertically up into the overlying Grosmont aquifer.

Regional distribution.- The influence of burial fluids during dolomitization and/or dolomite modification is indicated particularly by the regional distribution of replacement dolomite 2. As noted previously, replacement dolomite 2 is the dominant dolomite type in the Cooking Lake and Leduc Formations. In the Grosmont Formation it only occurs in the southern part of the Grosmont platform as well as in intervals that are immediately adjacent to reefs of the Leduc reef trend (Fig. 4.7). From a hydrostratigraphic point of view, replacement dolomite 2 is predominant in the Cooking Lake/Leduc aquifer and is present in the Grosmont aquifer only where it is in hydraulic communication with the underlying Cooking Lake/Leduc aquifer. Figures 4.3 and 4.7 identify types and location of possible hydraulic communication and ascending cross-formational fluid flow between the two Woodbend aquifers. Cross-formational fluid flow could also occur between the Leduc Formation - Morinville reef and the southern Grosmont platform where these are laterally continuous (Fig. 4.7). This connection between the two carbonate complexes appears to be present in strata of UGM 3a equivalent age (see Chapter 2), forming a fluid flow conduit between two aquifers generally separated by shales and marls of the Grosmont embayment. Cross-formational fluid flow between the two Woodbend aquifers is also possible in areas along the Leduc reef trend where the intervening Ireton Formation aquitard is very thin or missing (Fig. 4.3).

Ascending cross-formational fluid flow during dolomitization and/or dolomite modification is indicated by three sets of observations. Firstly, the LGM is dolomitized preferentially in areas above Leduc reefs where the intervening Ireton Formation aquitard is thin or absent (Figs. 4.3, 4.8). Secondly, the LGM is pervasively dolomitized by type 2 replacement dolomites (subtype 2b) in these areas, which stands in contrast to the general occurrence of Ca-rich subtype 1a and 1b replacement dolomites in partially dolomitized intervals of the LGM. Lastly, ^{13}C-enriched subtype 2b replacement dolomites occur in the UGM 1 to UGM 3a above pervasively dolomitized intervals of the LGM, forming mappable halos of ^{13}C-enriched dolomite (Huebscher and Machel, 1995). This occurrence of type 2 replacement dolomites in the upper members of the Grosmont Formation is the most convincing argument for ascending cross-formational fluid flow. Figures 4.14 a and b show the contrast in dolomite occurrence and dolomite stable isotope composition in areas above and off the Leduc reef trend. Areas above the reef trend are dominated by replacement dolomite subtype 2b, whereas replacement dolomite 1 occurs elsewhere throughout most of the Grosmont platform. This distribution suggests that replacement dolomite 1 was converted to replacement dolomite 2 in the upper members of the Grosmont Formation by ascending fluids that migrated from the Cooking Lake/Leduc aquifer into the Grosmont aquifer. This implies that ascending fluids were also responsible for the formation of replacement dolomite 2 in the LGM.

The observations and interpretations discussed above are consistent with the hypothesis that the Cooking Lake platform margin and overlying Leduc reefs acted as fluid conduit for dolomitizing and/or dolomite modifying fluids (Illing, 1956 and 1959; Machel and Mountjoy, 1987; Amthor et al., 1993; Mountjoy and Amthor, 1994). Amthor et al. (1993) suggested that dolomitizing fluids originated in part from the surrounding shales as well as from an unspecified source area in southern Alberta. Based on mass balance calculations these authors conclude that regional scale fluid flow, such as topography driven flow or tectonic loading, is the most likely explanation for the regional scale dolomitization of the Rimbey-Meadowbrook reef trend.

CONCLUSIONS

Carbonate platform deposits of the Upper Devonian Grosmont Formation were extensively dolomitized at the depositional surface or during shallow burial by seawater evaporated to gypsum saturation. Early dolomites likely consisted of metastable, Ca-rich protodolomites that were later modified to (near-) stoichiometric dolomites. The stratigraphic distribution of modified dolomites vs. Ca-dolomites in the Grosmont Formation suggest that these Grosmont dolomites were modified by downward percolating evaporated seawater. Dolomite modification probably began shortly after dolomite formation in the shallow burial environment when early replacement dolomites were still in contact with dolomitizing brines.

Based on regional distribution and stable isotope composition, type 2 replacement dolomites are interpreted to have formed by warm, burial fluids that migrated through the Cooking Lake/Leduc aquifer into the Grosmont aquifer. In the upper members of the Grosmont Formation these burial fluids likely caused further modification of type 1 replacement dolomites. In the LGM, the upward migration of fluids from the underlying Leduc reefs caused pervasive dolomitization. Replacement dolomitization of the Cooking Lake and Leduc Formations was likely caused by long range migration of basinal fluids along the Rimbey-Meadowbrook reef trend. Burial compaction, however, is interpreted to have acted locally as mechanism to introduce organically derived ^{13}C-enriched carbon, which was incorporated into type 2 replacement dolomites of the northern Leduc reef trend and overlying parts of the Grosmont Formation.

In conclusion, the results of this study suggest that Woodbend Group replacement dolomites were formed by two genetically and compositionally different fluid types and hydrologic processes. Moreover, the possibility that textural and compositional similarities in replacement dolomites record the effects of extensive dolomite diagenesis rather than the original conditions during dolomite formation has to be seriously considered. It is likely that precursor phases are present in other Devonian dolostones of the Western Canada Sedimentary Basin that have been interpreted on the basis of their present day textures and geochemical composition. Careful analysis of these precursor phases as well as analysis of the later dolomite generations will be required to develop a coherent model of replacement dolomitization in this basin.

REFERENCES

Aissaoui, D.M., Buigues, D., and Purser, B.H., 1986, Model of reef diagenesis: Muroroa Atoll, French Polynesia. In: Schroeder, J.H., and Purser, B.H., eds., Reef diagenesis, Springer, Berlin, p. 27-52.

Amthor, J.E., Mountjoy, E.W., and Machel, H.G., 1993, Subsurface dolomites in Upper Devonian Leduc buildups, central part of Rimbey-Meadowbrook reef trend, Alberta, Canada. Bulletin of Canadian Petroleum Geology, v. 41, p. 164-185.

Andrichuk, J.M., 1958a, Stratigraphy and facies analysis of Upper Devonian reefs in Leduc, Stettler, and Redwater areas, Alberta. American Association of Petroleum Geologists Bulletin, v. 42, p. 1-93.

Andrichuk, J.M., 1958b, Cooking Lake and Duvernay (Late Devonian) sedimentation in Edmonton area of central Alberta, Canada. American Association of Petroleum Geologists Bulletin, v. 42, p. 2189-2222.

Bachu, S., and Underschultz, J.R., 1993, Hydrogeology of formation waters, northeastern Alberta Basin. American Association of Petroleum Geologists Bulletin, v. 77, p. 1745-1768.

Banner, J.L., 1995, Application if the Trace element and isotope geochemistry of strontium to studies of carbonate diagenesis. Sedimentology, v. 42, p. 805-824.

Banner, J.L., Hanson, G.N., and Meyers, W.J., 1988, Water-rock interaction history of regionally extensive dolomites of the Burlington-Keokuk Formation (Mississippian): isotopic evidence. In: Shukla, V., and Baker, P.A., eds., Sedimentology and geochemistry of dolostones, Society of Economic Sedimentologists and Mineralogists Special Publication No. 43, p. 97-113.

Behrens, E.W., and Land, L.S., 1972, Subtidal Holocene dolomite, Baffin Bay, Texas. Journal of Sedimentary Petrology, v. 42, p. 155-161.

Cander, H.S., Kaufman, J., Daniels, L.D., and Meyers, W.J., 1988, Regional dolomitization of shelf carbonates in the Burlington-Keokuk Formation (Mississippian), Illinois and Missouri: constraints from cathodoluminescent zonal stratigraphy. In: Shukla, V., and Baker, P.A., eds., Sedimentology and geochemistry of dolostones, Society of Economic Paleontologists and Mineralogists Special Publication No. 43, p. 129-144.

Carballo, J.D., Land, L.S., and Miser, D.L., 1987, Holocene dolomitization of supratidal sediments by active tidal pumping, Sugarloaf Key, Florida. Journal of Sedimentary Petrology, v. 57, p. 153-165.

Carothers, W.W., and Kharaka, J.K., 1980, Stable carbon isotopes of HCO_3^- in oil field waters - implications for the origin of CO_2. Geochimica et Cosmochimica Acta, v. 44, p. 323-332.

Carpenter, S.J., and Lohmann, K.C., 1989, $\delta^{18}O$ and $\delta^{13}C$ variations in Late Devonian marine cements from the Golden Spike and Nevis reefs, Alberta, Canada. Journal of Sedimentary Petrology, v. 59, p. 792-814.

Claypool, G.E., and Kaplan, I.R., 1974, The origin and distribution of methane in marine sediments. In: Kaplan, I.R., ed., Natural gases in marine sediments, Plenum, New York, p. 99-139.

Craig, H., 1957, Isotopic standards for carbon and oxygen and correlation factors for mass-spectrometric analysis of carbon dioxide. Geochimica et Cosmochimica Acta, v. 12, p. 133-149.

Cutler, W.G., 1983, Stratigraphy and sedimentology of the Upper Devonian Grosmont Formation, Alberta, Canada. Bulletin of Canadian Petroleum Geology, v. 31, p. 282-325.

Curtis, C.D., Coleman, M.L., and Love, L.G., 1986, Pore water evolution during sediment burial from isotopic and mineral chemistry of calcite, dolomite and siderite concretions. Geochimica et Cosmochimica Acta, v. 50, p. 3221-2334.

Dickson, J.A., 1966, Carbonate identification and genesis as revealed by staining. Journal of Sedimentary Petrology, v. 36, p. 491-505.

Feazel, C.T., and Schatzinger, R.A., 1985, Prevention of carbonate cementation in petroleum reservoirs. In: Schneidermann, N., and Harris, P.M., eds., Carbonate cements, Society of Economic Sedimentologists and Mineralogists Special Publication No. 36, p. 97-106.

Friedman, I., and O'Neil, J.R., 1977, Data of geochemistry, 6th edition, Chapter KK. Compilation of stable isotope fractionation factors of geochemical interest. United States Geological Survey Professional Paper 440-KK, p. 1-12.

Fritz, P., and Katz, A., 1972, The sodium distribution of dolomite crystals. Chemical Geology, v. 10, p. 237-244.

Fritz, P., and Smith, D.C.W., 1970, The isotopic composition of secondary dolomites. Geochimica et Cosmochimica Acta, v. 34, p. 1161-1173.

Given, R.K., and Lohmann, K.C., 1985, Derivation of the original isotopic composition of Permian marine cements. Journal of Sedimentary Petrology, v. 55, p. 430-439.

Goldsmith, J.R., Graf, D.L., and Heard, H.C., 1961, Lattice constants of the calcium-magnesium carbonates. American Mineralogist, v. 46, p. 453-457.

Gregg, J.M., Howard, S.A., and Mazzullo, S.J., 1992, Early diagenetic recrystallization of Holocene (<3000 years old) peritidal dolomites, Ambergris Cay, Belize. Sedimentology, v. 39, p. 143-160.

Gregg, J.M., and Shelton, K.L., 1990, Dolomitization and dolomite neomorphism in the back reef facies of the Bonneterre and Davies Formations (Cambrian), southeastern Missouri. Journal of Sedimentary Petrology, v. 60, p. 549-562.

Hardie, L.A., 1987, Dolomitization: a critical view of some current views. Journal of Sedimentary Petrology, v. 57, p. 166-183.

Harrison, R.S., 1982, Geology and production history of the Grosmont carbonate pilot project, Alberta, Canada. In: Meyer, R.F., Wynn, J.C., and Olson, J.C., eds., The future of heavy crude and tar sands. Second International Conference on heavy crude and tar sands, Caracas, Venezuela, February 7-17, 1982, v. 1, p. 199-204.

Hennessy, J., and Knauth, L.P., 1985, Isotopic variations in dolomite concretions from the Monterey Formation, California. Journal of Sedimentary Petrology, v. 55, p. 120-130.

Holail, H., Lohmann, K.C., and Sanderson, I., 1988, Dolomitization and dedolomitization of Upper Cretaceous carbonates: Bahariya oasis, Egypt. In: Shukla, V., and Baker, P.A., eds., Sedimentology and geochemistry of dolostones, Society of Economic Sedimentologists and Mineralogists Special Publication No. 43, p. 191-207.

Howarth, R.W., and Marino, R., 1984, Sulfate reduction in salt marshes, with some comparisons to sulfate reduction in microbial mats. In: Cohen, Y., Castenholz, R.W., and Halvorson, H.O., eds., Microbial mats, A.R. Liss, New York, p. 245-264.

Hudson, J.D., and Anderson, T.F., 1989, Ocean temperatures and isotopic compositions through time. Transactions Royal Society of Edinburgh, Earth Sciences, v. 80, p. 183-192.

Huebscher, H., and Machel, H.G., 1995, Cross-formational fluid flow in Devonian dolostones. The 1st SEPM Congress on Sedimentary Geology, St. Pete Beach, Florida, August 13-16, 1995, Abstract.

Hugo, K.J., 1990, Mechanisms of groundwater flow and oil migration associated with Leduc reefs. Bulletin of Canadian Petroleum Geology, v. 38, p. 307-319.

Hurley, N.F., and Lohmann, K.C., 1989, Diagenesis of Devonian reefal carbonate in the Oscar Range, Canning Basin, Western Australia. Journal of Sedimentary Petrology, v. 59, p. 127-146.

Illing, L.V., 1956, Dolomitization in relation to porosity in carbonate rocks. American Association of Petroleum Geologists, Program, 41st Annual Meeting, Chicago, p. 13-14.

Illing, L.V., 1959, Deposition and diagenesis of Upper Paleozoic carbonate sediments in Western Canada. 5th World Petroleum Congress, New York, Proceedings Section 1, p. 23-52.

Irwin, H., Curtis, C., and Coleman, M., 1977, Isotopic evidence for source of diagenetic carbonates formed during burial of organic-rich sediments. Nature, v. 269, p. 209-213.

Kaufman, J., 1994, Numerical models of fluid flow in carbonate platforms: implications for dolomitization. Journal of Sedimentary Research, v. A64, p.128-139.

Kupecz, J.A., Montanez, I.P., and Gao, G., 1993, Recrystallization of dolomite with time. In: Rezak, R., and Lavoie, D., eds, Carbonate microfabrics, Frontiers in sedimentology, Springer, New York, p. 187-194.

Kupecz, J.A., and Land, L.S., 1994, Progressive recrystallization and stabilization of early-stage dolomite: Lower Ordovician Ellenburger Group, west Texas. In: Purser, B.H., Tucker, M.E., and Zenger, D.H., eds., Dolomites, A volume in honour of Dolomieu, Special Publication No. 21 of the International Association of Sedimentologists, Blackwell, Oxford, p. 255-279.

Laflamme, A.K., 1990, Replacement dolomitization in the Upper Devonian Leduc and Swan Hills Formations, Caroline area, Alberta, Canada. Unpubl. M.Sc. thesis, McGill University, Montreal, 138 p.

Land, L.S., 1980, The isotopic and trace element chemistry of dolomites: the state of the art. In: Zenger, D.H., Dunham, J.B., and Ethington, R.L., eds., Concepts and models of dolomitization, Society of Economic Paleontologists and Mineralogists Special Publication No. 28, p. 87-110.

Land, L.S., 1985, The origin of massive dolomite. Journal of Geological Education, v. 33, p. 112-125.

Larson, P.A., 1988, Origins of Grosmont Formation dolomite (northeast Alberta): Modelling the results of geochemical analysis. In: McMillan, N.J., Embry, A.F., and Glass, D.J., eds., Devonian of the world, Volume II. Canadian Society of Petroleum Geologists Memoir 14, p. 525-530.

Lazar, B., and Erez, J., 1990, Extreme ^{13}C depletions in seawater-derived brines and their implications for the past geochemical cycle. Geology, v. 18, p. 1191-1194.

Machel, H.G., and Mountjoy, E.W., 1987, General constraints on extensive pervasive dolomitization - and their application to the Devonian carbonates of western Canada. Bulletin of Canadian Petroleum Geology, v. 35, p. 143-158.

Machel, H.G., Mountjoy, E.W., and Amthor, J.E., in press, Mass balance and fluid flow constraints on regional-scale dolomitization, Late Devonian, Western Canada Sedimentary Basin - Discussion, Bulletin of Canadian Petroleum Geology.

Mazzullo, S.J., 1992, Geochemical and neomorphic alteration of dolomite: a review. Carbonates and Evaporites, v. 7, p. 21-37.

Mazzullo, S.J., Reid, A.M., and Gregg, J.M., 1987, Dolomitization of Holocene Mg-calcite supratidal deposits, Ambergris Cay, Belize. Geological Society of America Bulletin, v. 98, p. 224-231.

McCrea, J.M., 1950, On the isotopic chemistry of carbonates and a paleotemperature scale. Journal of Chemical Physics, v. 18, p. 849-857.

McKenzie, J.A., 1981, Holocene dolomitization of calcium carbonate sediments from the coastal sabkhas of Abu Dhabi, U.A.E.: a stable isotope study. Journal of Geology, v. 89, p. 185-198.

Montanez, I.P., and Read, J.F., 1992, Fluid-rock interaction history during stabilization of early dolomites, Upper Knox Group (Lower Ordovician), U.S. Appalachians. Journal of Sedimentary Petrology, v. 62, p. 753-778.

Mountjoy, E.W., and Amthor, J.E., 1994, Has burial dolomitization come of age? Some answers from the Western Canada Sedimentary Basin. In: Purser, B.H., Tucker, M.E., and Zenger, D.H., eds., Dolomites, A volume in honour of Dolomieu, Special Publication No. 21 of the International Association of Sedimentologists, Blackwell, Oxford, p. 203-229.

Nordeng, S.H., and Sibley, D.F., 1994, Dolomite stoichiometry and Ostwald's step rule. Geochimica et Cosmochimica Acta, v. 58, p. 191-196.

Ohmoto, H., and Rye, R.O., 1979, Isotopes of sulfur and carbon. In: Barnes, H.L., ed., Geochemistry of hydrothermal ore deposits, Wiley, New York, p. 509-565.

Patterson, W.P., and Walter, L.M., 1994, Depletion of ^{13}C in seawater $\sum CO_2$ on modern carbonate platforms: significance for the carbon isotopic record of carbonates. Geology, v. 22, p. 885-888.

Pierre, C., Ortlieb, L., and Person, A., 1984, Supratidal evaporitic dolomite at Ojo de

Liebre lagoon: mineralogical and isotopic arguments for primary crystallization. Journal of Sedimentary Petrology, v. 54, p. 1049-1061.

Potma, K., and Wong, P., 1995, A proposed dolomitizing model for the Upper Devonian carbonate complexes of the Western Canada Basin. The First Joint Symposium of the Canadian Society of Petroleum Geologists and the Canadian Well Logging Society, Calgary, Alberta, May 28-31, 1995, Abstract.

Richards, B.C., Barclay, J.E., Bryan, D., Hartling, A., Henderson, C.M., and Hinds, R.C., 1994, Carboniferous strata of the Western Canada Sedimentary Basin. In: Mossop, G.D., and Shetsen, I., comps., Geological Atlas of the Western Canada Sedimentary Basin. Canadian Society of Petroleum Geologists and Alberta Research Counsil, p. 221-250.

Saller, A.H., 1984, Petrologic and geochemical constraints on the origin of subsurface dolomite, Enewetak Atoll: an example of dolomitization by normal seawater. Geology, v. 12, p. 217-220.

Sass, E., and Bein, A., 1988, Dolomites and salinity: a comparative geochemical study. In: Shukla, V., and Baker, P.A., eds., Sedimentology and geochemistry of dolostones, Society of Economic Sedimentologists and Mineralogists Special Publication No. 43, p. 223-233.

Sharma, T., and Clayton, R.N., 1964, Measurement of O^{18}/O^{16} ratios of total oxygen of carbonates. Geochimica et Cosmochimica Acta, v. 29, p. 1347-1353.

Shields, M.J., and Brady, P.V., 1995, Mass balance and fluid flow constraints on regional-scale dolomitization, Late Devonian, Western Canada Sedimentary Basin. Bulletin of Canadian Petroleum Geology, v. 43, p. 371-392.

Sibley, D.F., 1990, Unstable to stable transformations during dolomitization. Journal of Geology, v. 98, p. 739-748.

Sibley D.F., and Gregg, J.M., 1987, Classification of dolomite rock textures. Journal of Sedimentary Petrology, v. 57, p. 967-975.

Sofer, Z., and Gat, J.R., 1975, The isotopic composition of evaporating brines: effect of the isotopic activity ratio in saline solutions. Earth and Planetary Sciences Letters, v. 26, p. 179-186.

Stoakes, F.A., and Creaney, S., 1985, Sedimentology of a carbonate source rock: the Duvernay Formation of central Alberta. In: Eliuk, L., ed., Carbonates in subsurface and outcrop. Society of Economic Paleontologists and Mineralogists Core Workshop No. 7, p. 343-375.

Tarutani, T., Clayton, R.N., and Mayeda, T.K., 1969, The effect of polymorphism and magnesium substitution on oxygen isotope fractionation between calcium carbonate and water. Geochimica et Cosmochimica Acta, v. 33, p. 987-996.

Theriault, F., 1988, Lithofacies, diagenesis and related reservoir properties of the Upper Devonian Grosmont Formation, northern Alberta. Bulletin of Canadian Petroleum Geology, v. 36, p. 52-69.

Theriault, F., and Hutcheon, I., 1987, Dolomitization and calcitization of the Devonian Grosmont Formation, northern Alberta. Journal of Sedimentary Petrology, v. 57, p. 955-966.

Turner, J.V., 1982, Kinetic fractionation of carbon-13 during calcium carbonate precipitation. Geochimica et Cosmochimica Acta, v. 46. p. 1183-1191.

Vahrenkamp, V.C., and Swart, P.K., 1990, New distribution coefficient for the incorporation of strontium into dolomite and its implications for the formation of ancient dolomites. Geology, v. 18, p. 387-391.

Vahrenkamp, V.C., and Swart, P.K., 1994, Late Cenozoic dolomites of the Bahamas: metastable analogues for the genesis of ancient platform dolomites. In: Purser, B.H., Tucker, M.E., and Zenger, D.H., eds., Dolomites, A volume in honour of Dolomieu, Special Publication No. 21 of the International Association of Sedimentologists, Blackwell, Oxford, p. 133-153.

Veizer, J., 1983, Chemical diagenesis of carbonates: theory and application of trace element technique. In: Arthur, M.A., et al., eds., Stable isotopes in sedimentary geology, Society of Economic Paleontologists and Mineralogists Short Course No. 10, p. 1-100.

Veizer, J., Fritz, P., and Jones, B., 1986, Geochemistry of brachiopods: oxygen and carbon isotopic records of Paleozoic oceans. Geochimica et Cosmochimica Acta, v. 50, p. 1679-1696.

Whiticar, M.J., Faber, E., and Schoell, M., 1986, Biogenic methane formation in marine and freshwater environments: CO_2 reduction vs. acetate fermentation - Isotopic evidence. Geochimica et Cosmochimica Acta, v. 50, p. 693-709.

CHAPTER 5

DEVELOPMENT AND DISTRIBUTION OF PALEOKARST IN THE GROSMONT HEAVY-OIL RESERVOIR, NORTHEASTERN ALBERTA

INTRODUCTION

The Upper Devonian Grosmont Formation in north-central Alberta, Canada, which subcrops beneath the Lower Cretaceous Mannville Group, hosts a giant heavy-oil reservoir with estimated reserves of about 50 billion m^3 (315 billion bbl) of bitumen in place (ERCB, 1993). Preliminary production tests between 1975 and 1986, using steam stimulation techniques, were of variable success. Among the problems were, (1) bit drops and lost mud circulation during drilling, (2) cement loss during well completion, (3) loss of injected steam, and (4) greatly varying production rates between different recovery wells (Vandermeer and Presber, 1980; Harrison, 1982). These reported problems were recognized as being related to subsurface expressions of a paleokarst system, i.e. to systems of vugs, breccias and caverns which are interconnected by fractures. The surface components of karst, such as distinctive karst landforms (see karst definition by Jennings, 1971), are problematic to identify in subsurface paleokarst studies, because of the limitations of scale and spacing of wells used as a database in such studies (White and White, 1995).

The development of vugs, breccias and caverns in the Grosmont Formation has been attributed to karstification, mainly because of their close spatial association to the Devonian subcrop beneath the sub-Cretaceous unconformity. However, although karstification is of great importance to the production geology of the Grosmont Formation, previously published studies dealt only superficially with karst, such as dolomite dissolution and calcitization (Theriault and Hutcheon, 1987), effects on matrix porosity (Luo et al. 1994), and the statistical analysis of the stratigraphic distribution and height of caves and cave like structures from well logs (Dembicki, 1994; Dembicki and Machel, 1996). It is the purpose of this paper to examine the microscopic and macroscopic evidence for karst. Microscopic karst fabrics are particularly pervasive in the Grosmont Formation, in addition to the commonly recognized megascopic features. The second objective of this paper is to document the regional and stratigraphic distribution of the Grosmont karst, and to determine its relationship to the topography of the sub-Cretaceous unconformity. A better understanding of the patterns of karst distribution will aid in resolving questions about the timing as well as the environment of Grosmont karstification, questions that have been answered only tentatively in previous studies (cf. Dembicki, 1994; Dembicki and Machel, 1996). In addition, knowledge of the Grosmont karst distribution has important implications for the petroleum industry. To improve production tests steam was injected to stimulate the reservoir (Harrison and McIntyre, 1981), because the Grosmont heavy-oils and bitumens are extensively biodegraded and waterwashed (Hoffmann and Strausz, 1986; Brooks et al., 1989). One of the main problems during these tests was that steam could often not be contained within the reservoir. This loss of injected steam can be attributed to two problems, (1) the existence of thief zones, i.e. zones of extremely high porosity and permeability in the carbonate reservoir, and (2) breaches in shaly intervals of the Grosmont Formation, the so-called shale breaks, which were used as seals during steam injection. Both problems are likely related to karstification (cf. Dembicki, 1994) and should be predictable if the distribution of karst is known. Hence, it is hoped that the results of this study will aid in both, prediction of reservoir quality and identification of better sites for future recovery projects.

GEOLOGIC SETTING

The study area is located in the central part of the Upper Devonian (Frasnian) Grosmont carbonate complex in north-central Alberta between townships 80 to 95, and ranges 16 to 25 west of the fourth meridian (Fig. 5.1). The Grosmont complex was deposited during the Woodbend megacycle (Stoakes, 1992) and comprises the upper, regressive part of this cycle, when Grosmont/Leduc carbonate complexes prograded westward over underlying (lower) Ireton shales. Following the stratigraphic nomenclature

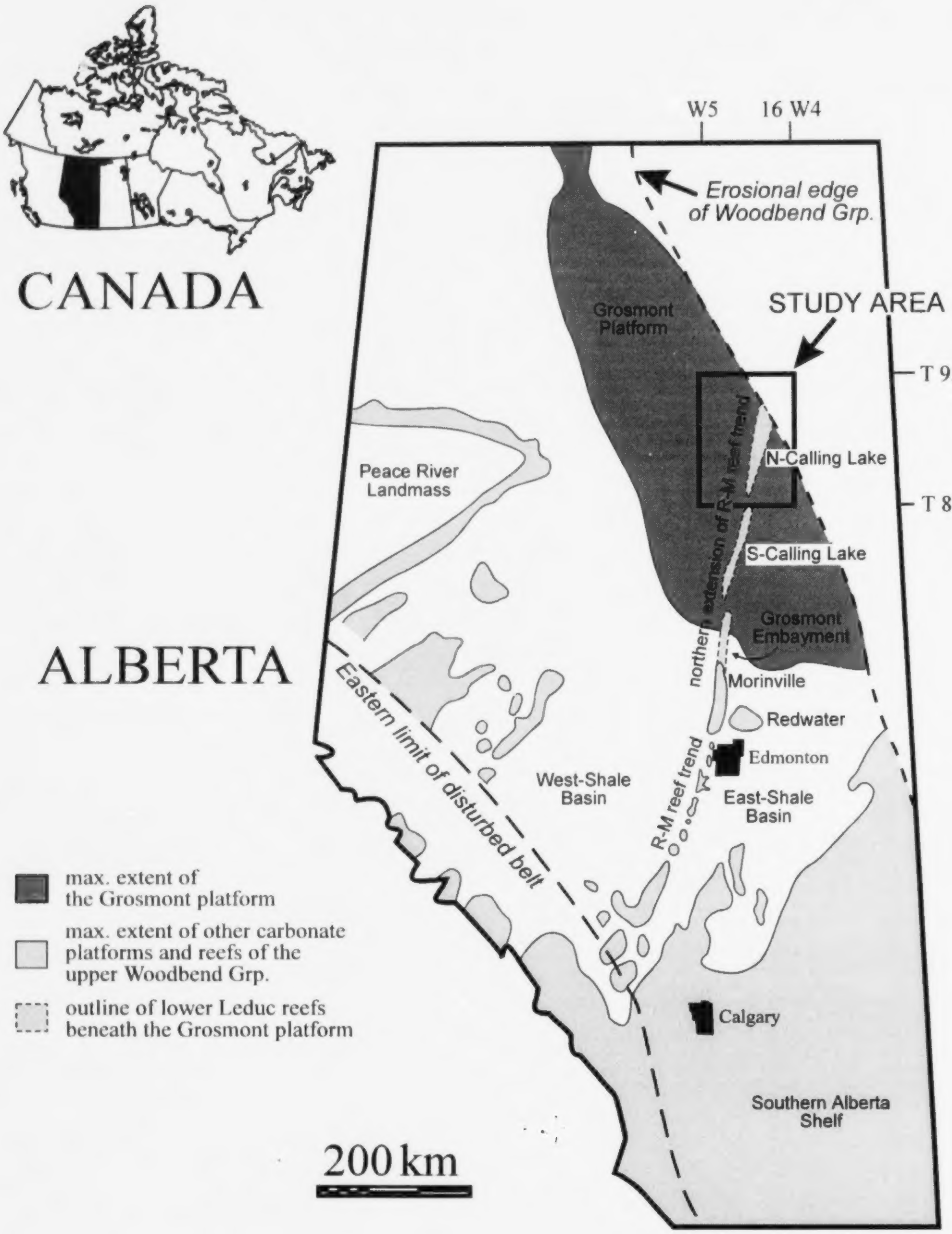
CANADA
ALBERTA
W5
16 W4
T 95
T 80
Erosional edge of Woodbend Grp.
STUDY AREA
Grosmont Platform
Peace River Landmass
N-Calling Lake
S-Calling Lake
northern extension of R-M reef trend
Grosmont Embayment
Morinville
Redwater
Edmonton
West-Shale Basin
East-Shale Basin
R-M reef trend
Eastern limit of disturbed belt
Calgary
Southern Alberta Shelf
200 km
max. extent of the Grosmont platform
max. extent of other carbonate platforms and reefs of the upper Woodbend Grp.
outline of lower Leduc reefs beneath the Grosmont platform

Fig. 5.1: Location map of study area and subsurface distribution of the Upper Devonian (Frasnian) Grosmont platform and other carbonate platforms and reefs of the upper Woodbend Group in Alberta.

established by Union Oil Canada and published by Harrison and McIntyre (1981) and Harrison (1982), the Grosmont Formation is informally subdivided into five units, the lower Grosmont (LGM) and the upper Grosmont 1, 2, 3a and 3b (UGM 1, UGM 2, UGM 3a and UGM 3b, respectively; Fig. 5.2). Regionally extensive shales and marls, the so-called Grosmont shale breaks, mark the boundaries of these units. The LGM and UGM 1 are dominantly limestone, whereas the UGM 2, UGM 3a and UGM 3b are pervasively dolomitized. The Grosmont Formation is overlain by a thin patchy shaly unit, which represents the uppermost Woodbend Group and is, in this study, informally referred to as upper Ireton Formation (Fig. 5.2).

In the southwestern part of the study area the Woodbend Group is overlain by carbonates of the Upper Devonian (Frasnian and Famennian) Winterburn and Wabamun Groups (Fig. 5.2). However, the entire Upper Devonian succession was subject to erosion that effected, due to a slight dip towards the southwest, subsequently older strata towards the northeast. In the northeastern part of the study area, the Grosmont Formation is, therefore, partially to completely removed. The resulting erosional surface, which is referred to as the sub-Cretaceous (or pre-Cretaceous) unconformity, is covered by early Cretaceous clastics of the Mannville Group (Fig. 5.2). Because of the angular character of the unconformity and the presence of Mississippian strata just southwest of the study area, which show no sign of depositional thinning or facies changes in contact with the unconformity, it is estimated that Paleozoic overburden in excess of 700 m was removed by erosion. The onset of significant subaerial exposure was related to a phase of major epeirogenic uplift and subsequent sea level drop during the Pennsylvanian period, in response to the collision of the Euramerican continent with Gondwana (Ross, 1991; Richards et al., 1994). The sub-Cretaceous unconformity represents, therefore, one or several extended periods of weathering and erosion between the Pennsylvanian and the Early Cretaceous.

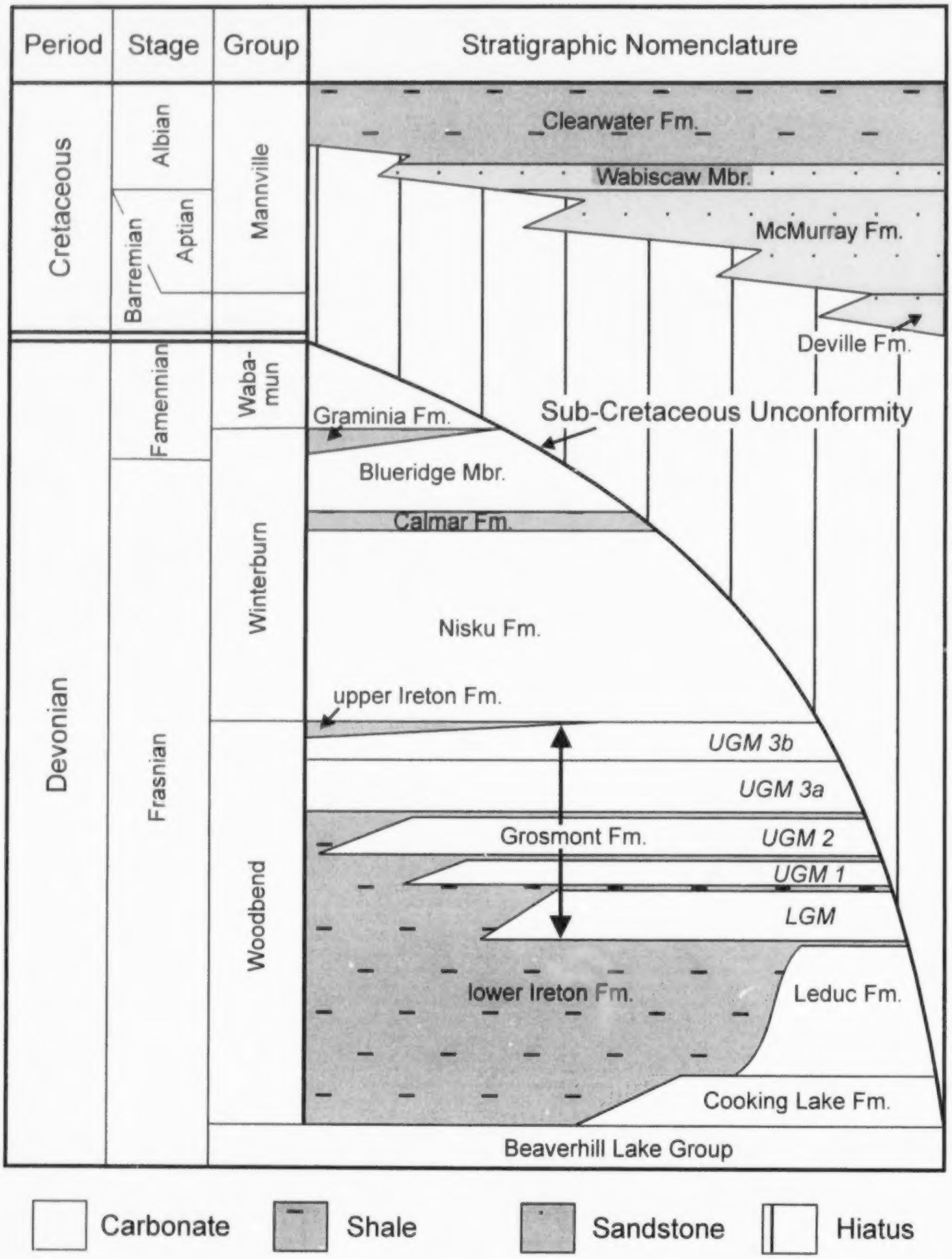
Period
Stage
Group
Stratigraphic Nomenclature
Cretaceous
Albian
Aptian
Barremian
Mannville
Clearwater Fm.
Wabiscaw Mbr.
McMurray Fm.
Deville Fm.
Devonian
Famennian
Frasnian
Waba-mun
Winterburn
Woodbend
Graminia Fm.
Sub-Cretaceous Unconformity
Blueridge Mbr.
Calmar Fm.
Nisku Fm.
upper Ireton Fm.
UGM 3b
UGM 3a
Grosmont Fm.
UGM 2
UGM 1
LGM
lower Ireton Fm.
Leduc Fm.
Cooking Lake Fm.
Beaverhill Lake Group
Carbonate
Shale
Sandstone
Hiatus

Fig. 5.2: Stratigraphic nomenclature of the principal Upper Devonian and Lower Cretaceous units encountered in the study area.

PETROGRAPHY

For the purpose of this paper, karst and related fabrics are divided into microscopic and macroscopic fabrics. Microscopic fabrics include small scale features, such as various styles of dissolution, that are only visible under the microscope, but are widespread in the matrix of karstified rock intervals. Also documented in this section are cements that occur in close proximity to karst fabrics and are interpreted to be of meteoric origin. Microscopic fabrics were investigated in thin sections impregnated with blue epoxy and stained with Alizarin red S and potassium ferricyanide. Macroscopic karst fabrics can be observed in cores, and include fractures, breccias, caves, cave filling sediments, and paleosols.

Microscopic fabrics

Dolomite dissolution.- Dolomite dissolution and resulting pore types are very common in the Grosmont Formation, especially in close proximity (less than 25 m) to the sub-Cretaceous unconformity (Theriault and Hutcheon, 1987; Luo et al., 1994). Luo et al. (1994) recognized three styles of dolomite dissolution in the Grosmont Formation, (1) intracrystalline (internal corrosion of dolomite rhombs), (2) intercrystalline (external corrosion of dolomite rhombs; Figs. 5.3a and 5.3b), and (3) pervasive dissolution. Intracrystalline porosity is commonly present in the central, cloudy parts of the dolomite rhombs, which are completely removed in some cases. External corrosion of dolomite rhombs results in the development of etched crystal surfaces and jagged or rounded edges. If dolomite dissolution, either external corrosion, internal corrosion or a combination of both, reaches a pervasive stage, dolomite crystals are largely or entirely removed, creating or greatly enhancing intercrystalline, fracture and vuggy porosity. Consequently, karstified intervals reach extremely high porosity (up to 40%) and matrix permeability values greater than 100 md (Luo et al., 1993; Luo et al., 1994).

Pervasive dolomite dissolution also resulted in the formation of poorly consolidated sucrosic dolomite. In the Grosmont heavy oil reservoir sucrosic dolomite is cemented by heavy oil or bitumen. Consequently, when bitumen is removed from a sucrosic dolomite sample by organic solvents, the sample disintegrates to a dolomite powder (Fig. 5.3c).

Fig. 5.3a: Corroded and fractured coarse grained dolomite (arrow). Pore spaces were subsequently filled by clear, blocky calcite cement (C). Well location: 14-17-87-20W4, 1064' (UGM 3a).

Fig. 5.3b: Intensely fractured and corroded matrix dolomite. Pores were subsequently cemented by clear, blocky calcite cement (C). Well location: 14-17-87-20W4, 1042' (UGM 3a).

Fig. 5.3c: Sucrosic dolomite powder. Dolomite crystals are corroded and were only cemented by bitumen that was removed from the sample by organic solvents. Coin is 17.5 mm in diameter. Well location 07-29-84-18W4, 355.0 m (UGM 2).

Fig. 5.3b: Zoned microstalactitic cement comprising alternating microsparitic, blocky calcite and coarse, clear, prismatic to blocky calcite layers. Well location 14-17-87-20W4, 1042' (UGM 3a).

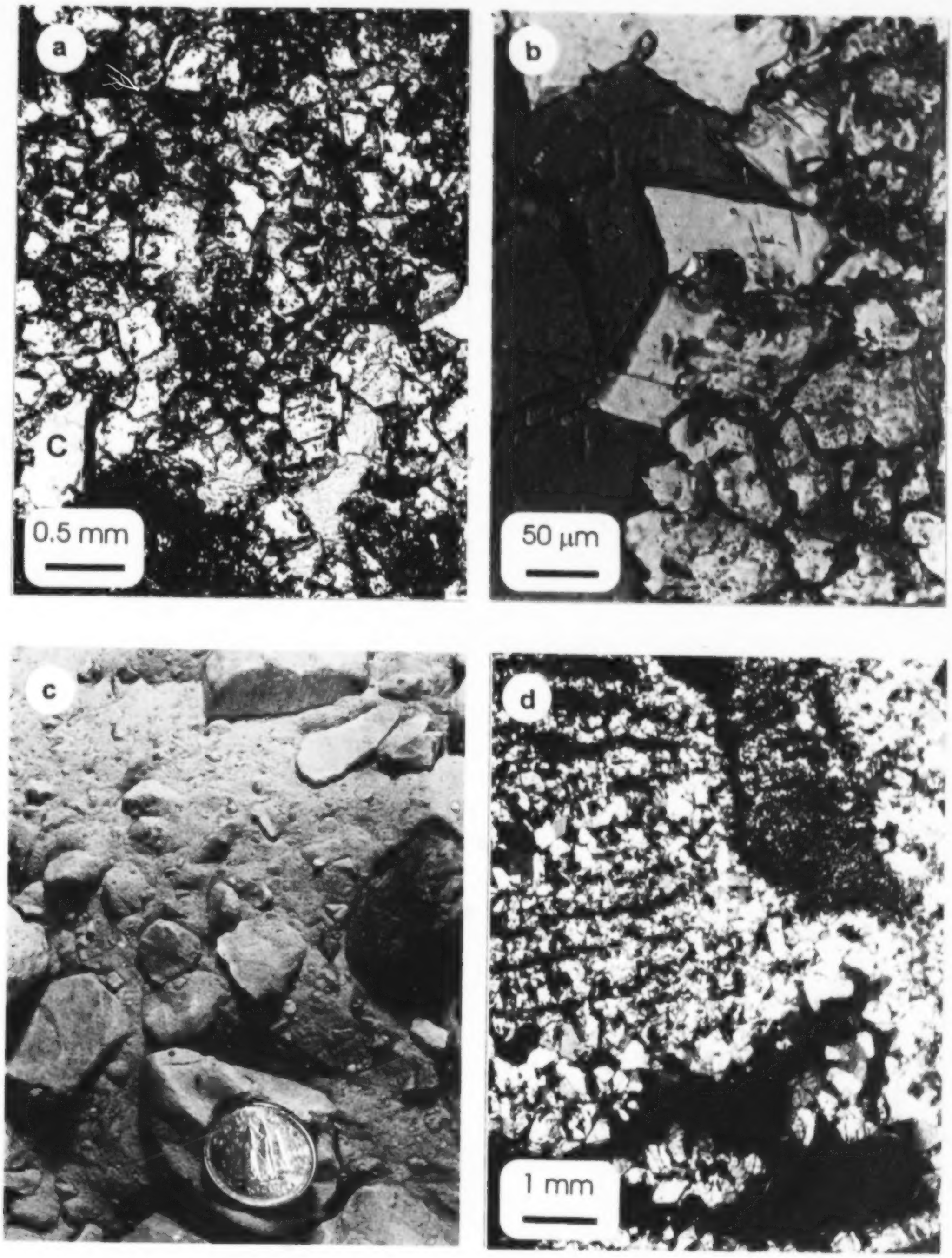
a
2
C
0.5 mm
b
50 µm
c
d
1 mm

Dolomite dissolution in the Grosmont Formation is interpreted to have been the result of the interaction between the subaerially exposed dolostones and meteoric water, because of the close spatial relationship between the dissolution features and the unconformity. Dissolution of dolomite by meteoric water proceeds until the aqueous solution has reached saturation equilibrium with respect to dolomite. In monomineralic systems, changes in saturation are primarily controlled by temperature and PCO_2 (Busenberg and Plummer, 1982). In addition to carbonic acid dissolution, dolomite dissolution in the Grosmont Formation likely continued, because of concomitant dissolution of gypsum (or anhydrite) (see Chapter 3). Gypsum (or anhydrite) dissolution would have decreased the Mg/Ca ratio resulting in undersaturation of the solution with respect to dolomite and, hence, caused continued dolomite dissolution (Back et al., 1983; Bischoff et al., 1994).

Calcitization of dolomites.- Calcitized dolomite rhombs occur commonly adjacent to, i.e. less than 10 m below, the surface of the sub-Cretaceous unconformity. Here, calcitization is associated either with paleosols and collapse breccias or with very fine grained dolomites (less than 20 μm in diameter). The extent of the calcitization process varies from selective, affecting only the cloudy cores or particular zones, to complete. Calcitized dolostones often retain the fabrics as well as the porosity and permeability characteristics of their precursors. However, in some cases intercrystalline porosity is destroyed by calcite cement overgrowth on the calcitized crystals.

Calcitization of dolomites was likely a byproduct of concomitant dolomite and gypsum (or anhydrite) dissolution as discussed above (see dolomite dissolution). Back et al. (1983) showed that sulfate dissolution and the resulting contribution of dissolved Ca causes supersaturation of the solution with respect to calcite leading to calcite precipitation. The precipitation of calcite has the effect of 1) lowering the pH and 2) removing carbonate from solution, thereby causing continued dissolution of dolomite (Back et al., 1983; Bischoff et al., 1994).

Calcite cements.- Calcite cements occlude intercrystalline, vuggy and fracture porosity, including caves. Two types of cements have been recognized. The first type is coarse crystalline (generally >0.5 mm in diameter), clear, blocky calcite (Fig. 5.3b). It grew directly on matrix dolomites or calcitized dolomite and occurs most commonly in or near calcitized intervals or fine crystalline dolostones, filling intercrystalline and fracture pores. The second type of calcite cement consists of alternate bands of coarse (0.2 to 1 mm crystal size), clear, prismatic to blocky crystals and fine to medium crystalline (crystal size between 50 μm and 0.1 mm), dark, cloudy, blocky to rhombic crystals (Fig. 5.3d). This cement type occurs beneath the roof of vugs and small caves. Similar cements, termed microstalactitic or dripstone cement, are commonly associated with caves (e.g. Kendall and Broughton, 1978; Jones et al., 1984) and form in the vadose environment.

Macroscopic fabrics

Fractures.- Intense fracturing of the Grosmont Formation is commonly observed adjacent to the sub-Cretaceous unconformity. The fracture density, which was measured by counting the natural fractures per one meter of core, varies, on average, in clean carbonates between 0 and 5 fractures per meter of logged core in intervals that are 50 m and deeper below the sub-Cretaceous unconformity, and between 5 and 10 fractures per one meter of core in intervals between 0 to 50 m below the unconformity. In proximity to caves and breccia horizons the fracture density increases to 20 fractures per meter of core. The intense fracturing produced breccias. In mixed carbonate-siliciclastics intervals, like the Grosmont shale breaks, the lower Ireton Formation marls and shales, upper Ireton Formation marls, and argillaceous and silty limestones of the lower Grosmont, the fracture density drops to less than 2 fractures per meter of core.

Most fractures are vertical to subvertical and are either filled by bitumen or are open. Many fractures show corroded, erratic, non-corresponding fracture walls with varying fracture width, indicative of solution enhancement. Cementation of fracture walls by late, blocky, sometimes ferroan calcite cements occurs but is rare.

Breccias.- The abundance of brecciated intervals and the varieties of breccias present in the Grosmont Formation make it necessary to classify them into different types. This was done on the basis of breccia fabrics, clast composition, and matrix or cement type according to the classification scheme put forward by Kerans (1990; 1993). The classification of Grosmont breccia is shown schematically in Fig. 5.4.

Fracture breccias are the result solely of fracturing of the host rock. The fracturing pattern defines the breccia clasts and there is no significant rotation of clasts. Fractures display at most a few millimeters of extensional displacement. The clasts are tightly packed, angular, with greatly varying clast sizes, and still in concordance with the host rock (Figs. 5.4a, 5.5a, 5.5b) grading into mosaic breccias. The breccia pores are generally open with some minor calcite cement lining the fracture walls. Overall porosity in fracture breccias is low to moderate (5 to 15 %).

Similar to fracture breccias, mosaic breccias consist entirely of angular clasts of the adjacent host rock interval. Clast size varies between 1 and 10 cm. Mosaic breccias differ, however, from fracture breccias in that there is some rotation and displacement of the clasts (Fig. 5.4b, 5.5c). Consequently, mosaic breccias display open, irregular fractures between neighboring clasts, and have moderate to high porosities between 10 and 20 %. Calcite cements lining the fracture walls are rare.

Chaotic breccias consist of highly rotated and displaced, large clasts from a single or a variety of host rock intervals. In the Grosmont Formation three different varieties of chaotic breccias can be distinguished on the basis of texture (matrix supported or clast supported), clast type, clast angularity, and fracture fill (matrix and/or cement)(Figs. 5.4c, 5.4d, 5.4e).

The first variety of chaotic breccia is clast supported (Fig. 5.4c) and is related to collapse of strata caused by carbonate and evaporite dissolution. Breccia components are angular, randomly rotated and derived from a variety of dolomite host rock intervals. Components range in size from 1 to 20 cm. Some of the larger clasts have a corroded rim and in some cases this rim is calcitized. Smaller clasts are completely calcitized in some cases. Component supported breccias lack a matrix in some locations, but if present the matrix consists of loose dolomite rhombs. Late, blocky calcite cements are rare, infill of breccia pores by heavy oil or bitumen, however, is common. Porosity values vary widely between 5 and 40 %. Chaotic breccias of this type are often associated with caves and occur in beds that range from a few cm to several meters in thickness.

The second type of chaotic breccia found in the Grosmont Formation is matrix supported (Figs. 5.4d, 5.5d). Breccia clasts are generally angular to subrounded and are

5.4a

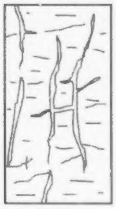

FRACTURE BRECCIA

Fabric - intense fracturing of host rock defines clasts, no significant rotation of clasts

Clasts - highly angular, in concordance with dolomite host rock

Cements - minor calcite cement

Porosity - 5 - 15 %

5.4b

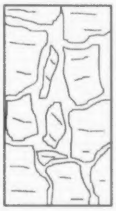

MOSAIC BRECCIA

Fabric - fitted clasts, displaying minor rotation

Clasts - highly angular, derived from single dolomite host rock type, clast size 1 - 10 cm

Cements - minor calcite cement

Porosity - 10 - 20 %

5.4c

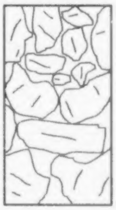

CHAOTIC BRECCIA, CLAST SUPPORTED

Fabric - randomly oriented clasts, in units ranging from a few cm to several meters in thickness

Clasts - highly angular, derived from single or a variety of dolomite host rock types, rim of clasts may be corroded and calcitized, clast size 1 - 20 cm

Matrix - loose dolomite rhombs

Cements - minor calcite cement

Porosity - 5 - 40 %

5.4d

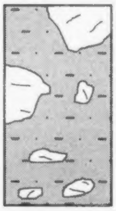

CHAOTIC BRECCIA, MATRIX SUPPORTED

Fabric - randomly oriented clasts, in units ranging from several cm to a few meters in thickness

Clasts - highly angular to subrounded, derived from a variety of dolomite host rock types, clast size 1 - 10 cm

Matrix - loose dolomite rhombs, quartz sand or silt, shale

Porosity - 2 - 15 %

5.4e

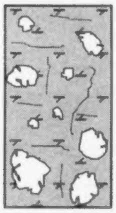

CHAOTIC BRECCIA, MATRIX SUPPORTED, PALEOSOL

Fabric - randomly oriented clasts, in units several meters in thickness

Clasts - angular to rounded, varying degree of fracturing, corrosion and calcitization

Matrix - mixture of quartz silt, shale and dolomite rhombs

Porosity - 5 - 15 %

Fig. 5.4: Schematic representation of breccia types encountered in Grosmont paleokarst. Breccias were described according to the classification scheme of Kerans (1990; 1993).

Fig. 5.5 a to d: Core slabs of karst breccias from the Grosmont Formation.

Fig. 5.5a: Fractured and corroded dolomite host rock. Intercrystalline pores in corroded areas are stained by bitumen. Coin is 17.5 mm in diameter. Well location 11-26-86-19W4, 284.25 m (UGM 2).

Fig. 5.5b: Top view of a fracture breccia. Fractures are filled with bitumen. Well location 14-17-87-20W4, 1039' (UGM 3a).

Fig. 5.5c: Mosaic breccia with slightly rotated clasts derived from one single host rock interval. Coin is 17.5 mm in diameter. Well location 10-17-84-19W4, 372.0 m (UGM 3b).

Fig. 5.5d: Vertical karst fracture infilled with chaotic breccia consisting of randomly oriented clasts and silty dolomite matrix. Well location 14-17-87-20W4, 1037' (UGM 3a).

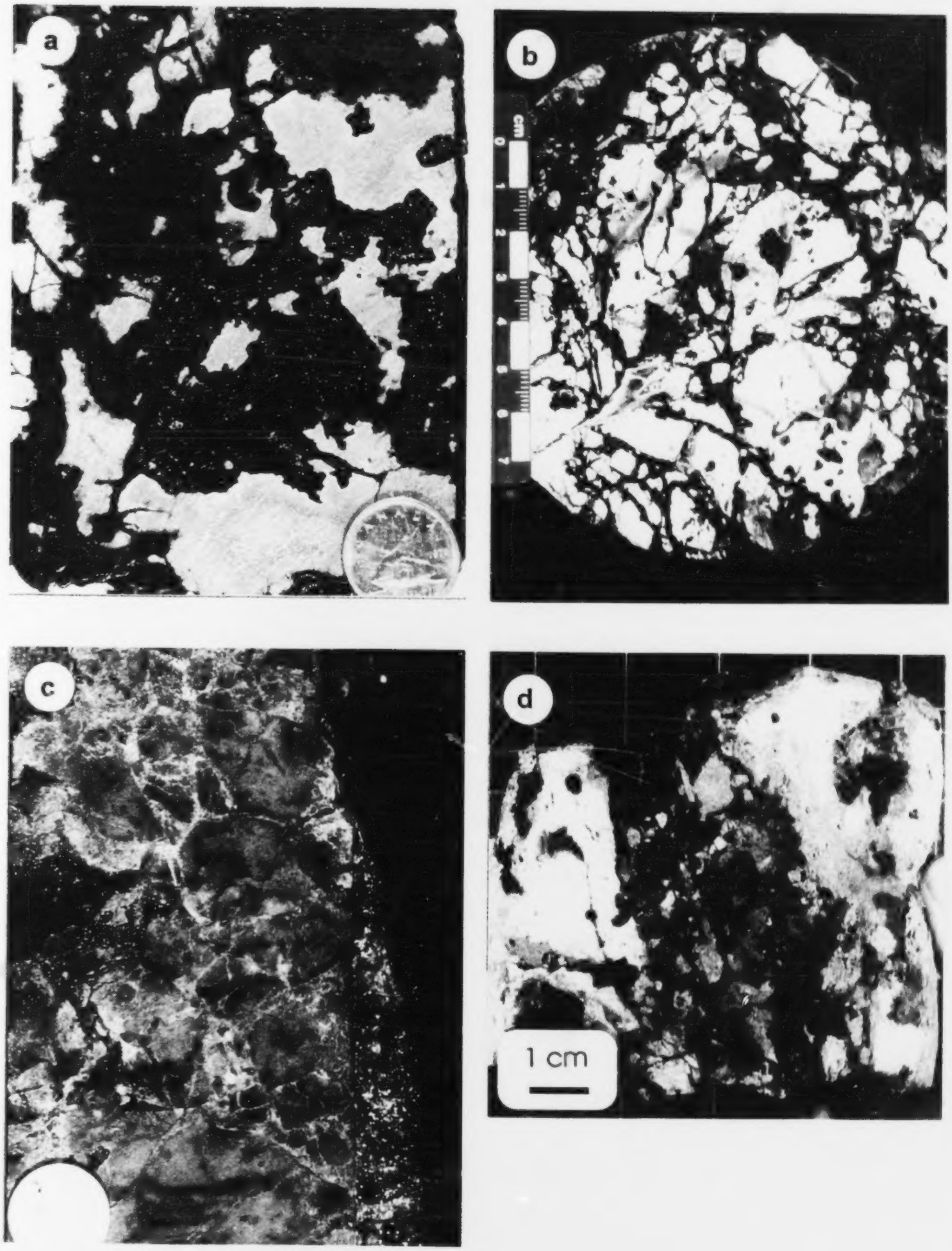
a
b
cm
0
1
2
3
4
5
6
7
c
d
1 cm

derived from variety of dolomite host rock intervals. Clast sizes range between 1 and 10 cm. The rock matrix consists either of loose dolomite rhombs or of quartz sand, silt or shale with intermixed dolomite rhombs. Colour and mineral content of the siliciclastic matrix (mainly quartz with minor K-feldspar, kaolinite, illite and chlorite) resemble those of the Lower Cretaceous Mannville Group (Luo et al., 1992). Porosity values are generally low (2 to 5 %) but reach 15 % in some places. This breccia type is infilling caves and varies in thickness from a few cm to several meters.

Another type of matrix supported, chaotic breccia is only developed at the surface of the sub-Cretaceous unconformity and is interpreted to be part of paleosol deposits (Fig. 5.4e). The components are rounded, usually irregularly shaped and corroded, and their original sedimentary structures are commonly destroyed. The component rim and, sometimes, the whole clast, is fractured, discolored and calcitized. The matrix consists of a mixture of dolomite, quartz silt and light brown clay, and contains pockets of green clay in some places. Porosity values vary between 5 and 15 %.

Caves.- Following the definition of dissolutional caves by Ford (1988), caves are hydraulic conduits that have reached a continuous minimum diameter of approximately 5 to 15 mm. This definition differs from the one introduced by Choquette and Pray (1970) who define a cave as a cavity large enough to allow passage by a human. Ford's (1988) classification is used because it includes smaller cavities, which can be measured in core, and its minimum diameter approximates the thresholds for turbulent flow, optimum rates of dissolution and transport of clastic load in porous media.

Dissolutional caves in the Grosmont Formation range from 5 to 15 mm (lower limit of dissolutional caves, sensu Ford, 1988) to several meters in vertical diameter (cf. Dembicki and Machel, 1996). The lower limit of vertical cave diameters is observed in core. Vertical diameters of caves greater 30 cm were determined by well log measurements. In most cases, caves are characterized by extensive intervals of rubbly and poorly recovered core. A second important indicator is the presence of allochthonous cave fills. Common cave fills are claystones and sandstones which have a mineralogical composition close to those of the Lower Cretaceous Mannville Group (Luo et al., 1992). Furthermore, cave fills contain varying amounts of dolomite rhombs (sucrosic dolomite) and fragments/breccia from the surrounding host rocks. Remaining open spaces are filled with water, heavy oil or with a heavy oil/dolomite slush.

Paleosols.- At some well locations the contact between the Upper Devonian carbonate rocks and the Lower Cretaceous clastics is not sharp. Instead, a clay and silt rich, unconsolidated horizon is present in some locations, reaching a maximum thickness of about 4 m. These horizons are termed paleosols in this study. However, they may not represent a fossil soil in the strictest sense because indicators for biologic activity (e.g. root traces) are commonly missing. In fact, evidence of plant growth, in the form of a thin coal bed, was found only at one well location (11-24-88-25W4). Unconsolidated intervals developed at the sub-Cretaceous unconformity may solely consist of weathering residue that was either produced on site or transported and deposited in topographic depression and fissures (cf. Ford, 1995). Paleosols are best developed in the argillaceous and silty carbonates of the UGM 3b at well location 10-17-83-18W4. Fig. 5.6 shows a generalized section through the paleosol deposit at this well location.

In the study area paleosols are commonly divided into three horizons. The lowest horizon consists of fractured, brown to grey, or black if bitumen stained, dolomite rock. In other cases, where several paleosol deposits are stacked on top of each other, the lowest horizon is a breccia, that consists of angular to subrounded host rock clasts floating in a light grey to brown, often mottled, dolomitic to calcareous silt matrix. Towards the top of the layer, the number, size and angularity of the clasts decreases. Clast edges are commonly fractured and corroded, and the corroded rim is often calcitized with the extent of clast calcitization increasing to the top of the horizon. The second horizon is a light grey to brown, mottled, dolomitic to calcareous siltstone which varies from highly fractured to unconsolidated. It is often interlayered with thin, broken laminae of green-grey, calcareous, silty shales. The third interval is commonly a poorly consolidated to rubbly, dark brown siltstone to sandstone with minor grey mottles. At the top of this horizon the sediment is disintegrated to cm-sized, angular, blocky soil peds. Soil peds are cubic to irregularly shaped weathering structures commonly developed in soils. The interior of a soil ped resembles the general composition of the soil, commonly silt or sand, which is coated on all sides with a dark (organic), clayey material. Soil peds are

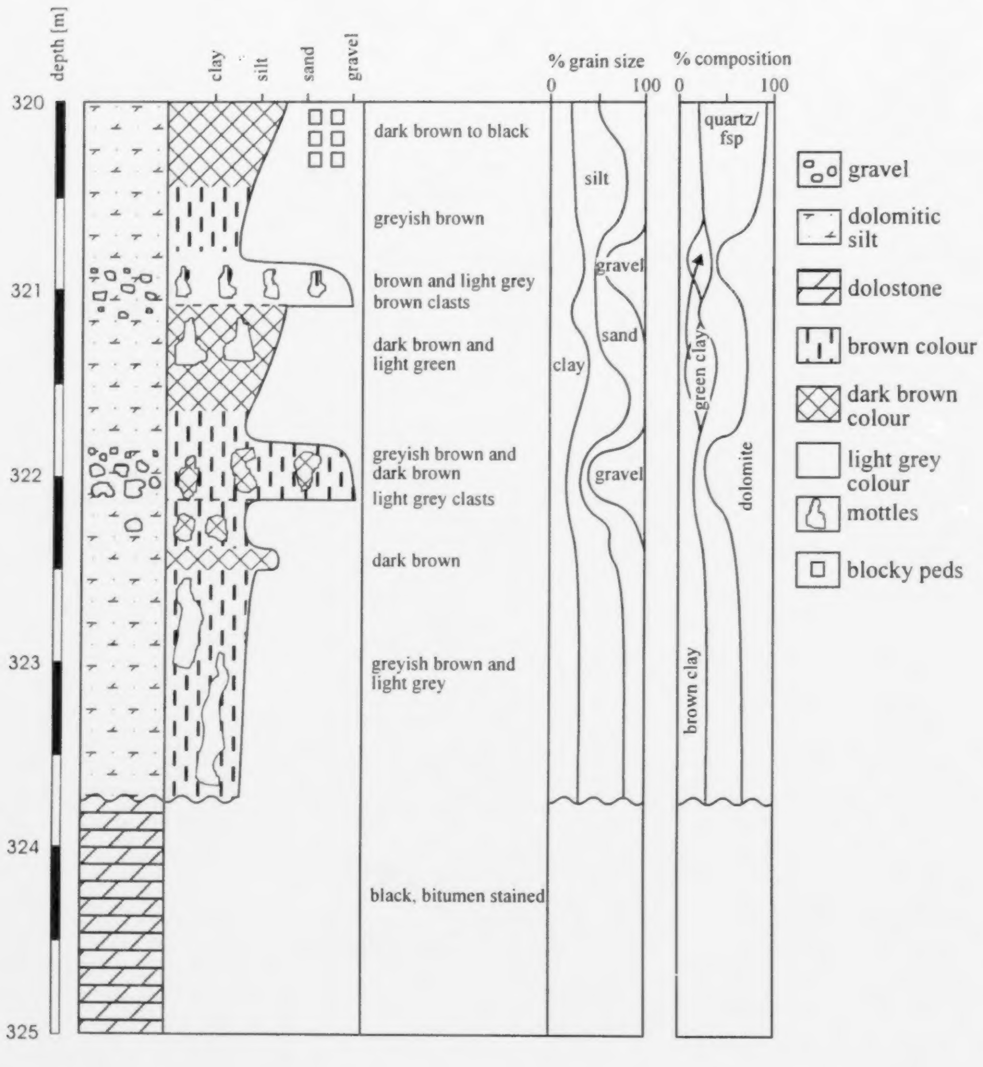
depth [m]
320
321
322
323
324
325
clay
silt
sand
gravel
dark brown to black
greyish brown
brown and light grey
brown clasts
dark brown and
light green
greyish brown and
dark brown
light grey clasts
dark brown
greyish brown and
light grey
black, bitumen stained
% grain size
0
100
silt
gravel
sand
clay
gravel
% composition
0
100
quartz/
fsp
green clay
dolomite
brown clay
gravel
dolomitic
silt
dolostone
brown colour
dark brown
colour
light grey
colour
mottles
blocky peds

Fig. 5.6: Simplified core log of paleosol deposits at well location 10-17-83-18W4.

commonly explained as the result of cracking around roots and burrows, or by swelling and shrinking due to wetting and drying (Retallack, 1990).

TOPOGRAPHY OF THE GROSMONT PALEOKARST

Assuming that the Grosmont paleokarst developed largely during the final stages of erosion of Devonian strata, the distribution of paleokarst features can best be analyzed by reconstructing the original topography of the sub-Cretaceous unconformity. Although not representing an instant in time, this unconformity can be interpreted as the final erosional surface. This surface can be reconstructed by mapping the sediment thickness between the unconformity and a regionally extensive datum above the unconformity, assuming that this datum is an approximately 'flat' surface with respect to the Cretaceous paleo-sea level. The reconstruction shown in this study is a slightly updated version of the work put forward by Ranger (1994). This particular reconstruction was chosen because it is the most recent and most detailed reconstruction (using one well per section; Ranger, 1994). Since the reconstruction of the unconformity surface is based on the thickness of overlying sediments, in this case the thickness of the Lower Mannville Group (McMurray Formation), isopach highs or areas of greater thickness represent topographic lows, whereas isopach lows represent topographic highs. However, the absolute height of "hills" protruding above the datum is not known.

On a regional scale, the study area is situated at the northern extension of the Wainwright Ridge (Ranger, 1994; Smith, 1994), informally known as the Grosmont High (Fig. 5.7). This north-south trending ridge, on top of which the McMurray Formation is missing or less than 10 to 20 m thick, is flanked in the west by the Wabasca Sub-basin and in the east by the McMurray Sub-basin. The Wabasca Sub-basin is a shallow basin with a maximum Lower Mannville thickness of about 60 m. Considering the presently available data it appears to be closed off from the general Lower Mannville drainage system. The McMurray Sub-basin accumulated a considerably greater amount of McMurray Formation sediments (>110 m in channels). Several northeast trending tributary valleys have been mapped out, originating at the Grosmont High and joining the main

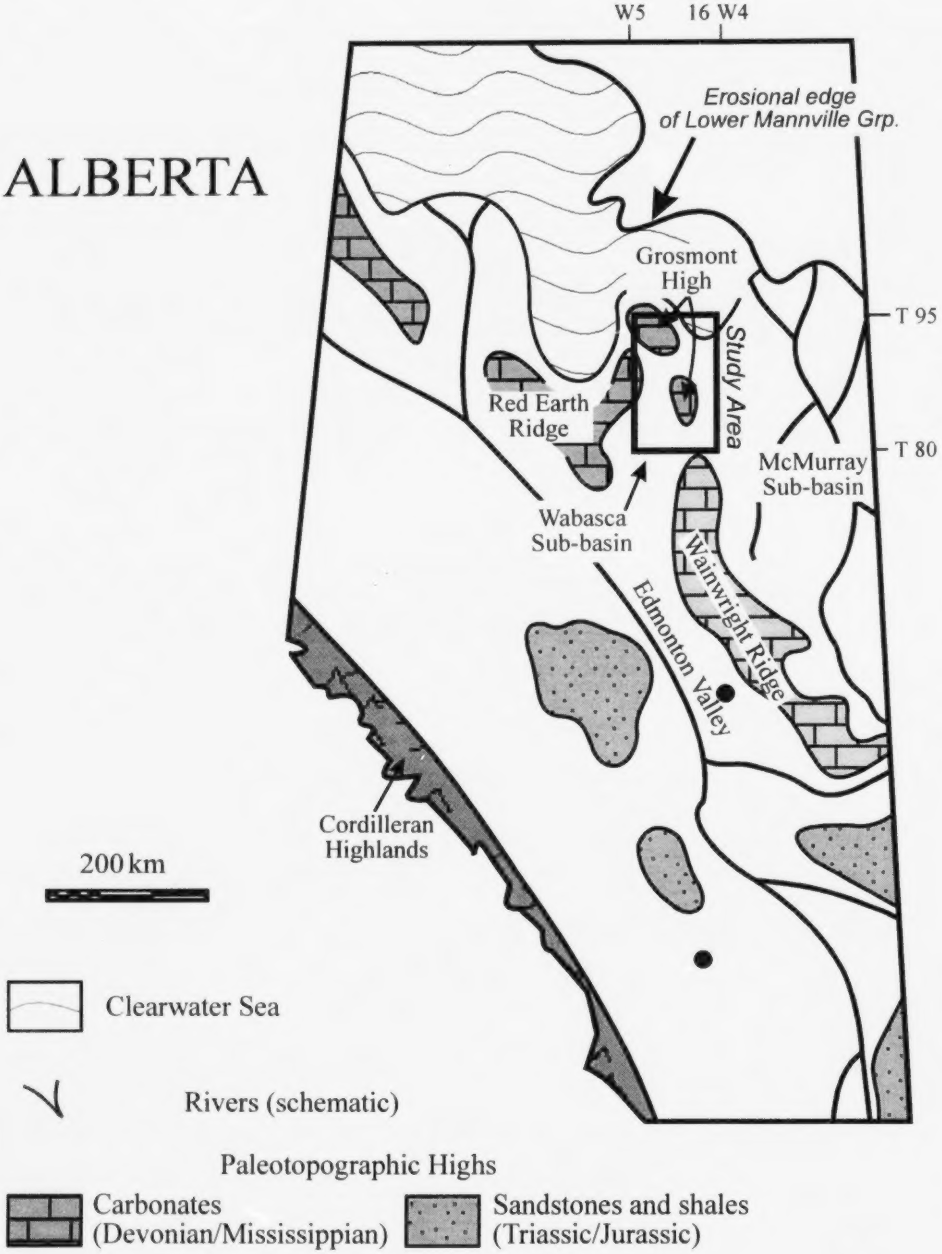
W5
16 W4
ALBERTA
Erosional edge of Lower Mannville Grp.
Grosmont High
T 95
Study Area
Red Earth Ridge
T 80
McMurray Sub-basin
Wabasca Sub-basin
Wainwright Ridge
Edmonton Valley
Cordilleran Highlands
200 km
Clearwater Sea
Rivers (schematic)
Paleotopographic Highs
Carbonates (Devonian/Mississippian)
Sandstones and shales (Triassic/Jurassic)

Fig. 5.7: Simplified Lower Cretaceous paleogeography of Alberta. Shown are the principal highlands and valleys as well as the approximate location of the Cordilleran mountain range and the Clearwater Sea (modified after Smith, 1994).

McMurray/Assiniboia valley system to the east (Ranger, 1994; Smith, 1994).

In the study area the maximum relief difference between ridges and valleys (Fig. 5.8) is 50 to 60 m. The Grosmont High, located in the central part of the study area, can be subdivided into two main ridges, a smaller southern and a larger, northern ridge (Fig. 5.8). The northern high is not only the extension of the Wainwright Ridge, but is also linked to the Red Earth Ridge in the west, effectively closing off the Wabasca Sub-basin. The Wabasca Sub-basin in the southwest exhibits several closed lows and isolated hills, but no continuous paleo-rivers. These closed lows may represent closed karst poljes, large solution valleys in the karst terrain, where an underground karst drainage system reached the surface. Closed valleys may have been the surface expression of the Wabasca Sub-basin drainage system, which could have funnelled the surface waters underground and eventually discharged into the surrounding open sub-basins. One of these open sub-basins, the McMurray Sub-basin, is located to the east of the study area. The paleotopographic map (Fig. 5.8) shows two continuous, southwest-northeast oriented valley systems, which are part of the McMurray tributary system.

The subcrop map of the Devonian bedrock beneath the sub-Cretaceous unconformity (Fig. 5.9) shows that the Grosmont High, as suggested by its name, consists mostly of resistant dolostones of the Grosmont Formation. The Red Earth High, located just to the west of the study area, consists of carbonates of the Winterburn and Wabamun Groups as well as of Mississippian carbonates (Smith, 1994) (Fig. 5.7). Compositions of other "highs" are shown in Fig. 5.7. Argillaceous dolostones and siltstones of the Winterburn and Wabamun Groups are the bedrock of the Wabasca Sub-basin (Fig. 5.9). The McMurray Sub-basin is underlain by apparently less resistant Ireton Formation shales, as well as shales and limestones of the Beaverhill Lake Group (Fig. 5.9). The development of the McMurray sub-basin was also enhanced by the dissolution of the Prairie Evaporites just to the east of the study area (Meijer Drees, 1994).

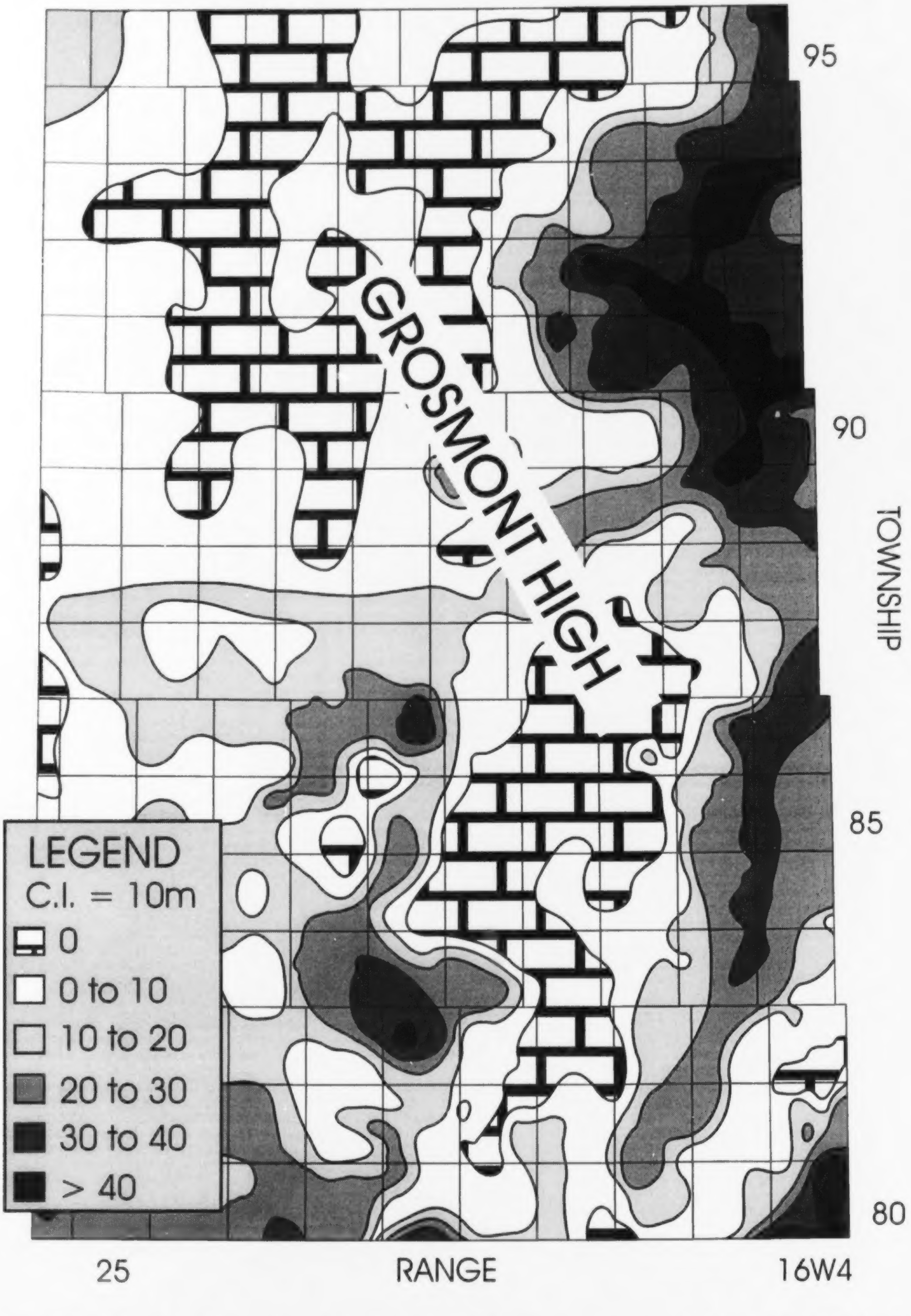
GROSMONT HIGH
LEGEND
C.I. = 10m
0
0 to 10
10 to 20
20 to 30
30 to 40
> 40
95
90
85
80
TOWNSHIP
25
RANGE
16W4

Fig. 5.8: Inferred paleotopography of the sub-Cretaceous unconformity (modified after Ranger, 1994). See text for further explanations.

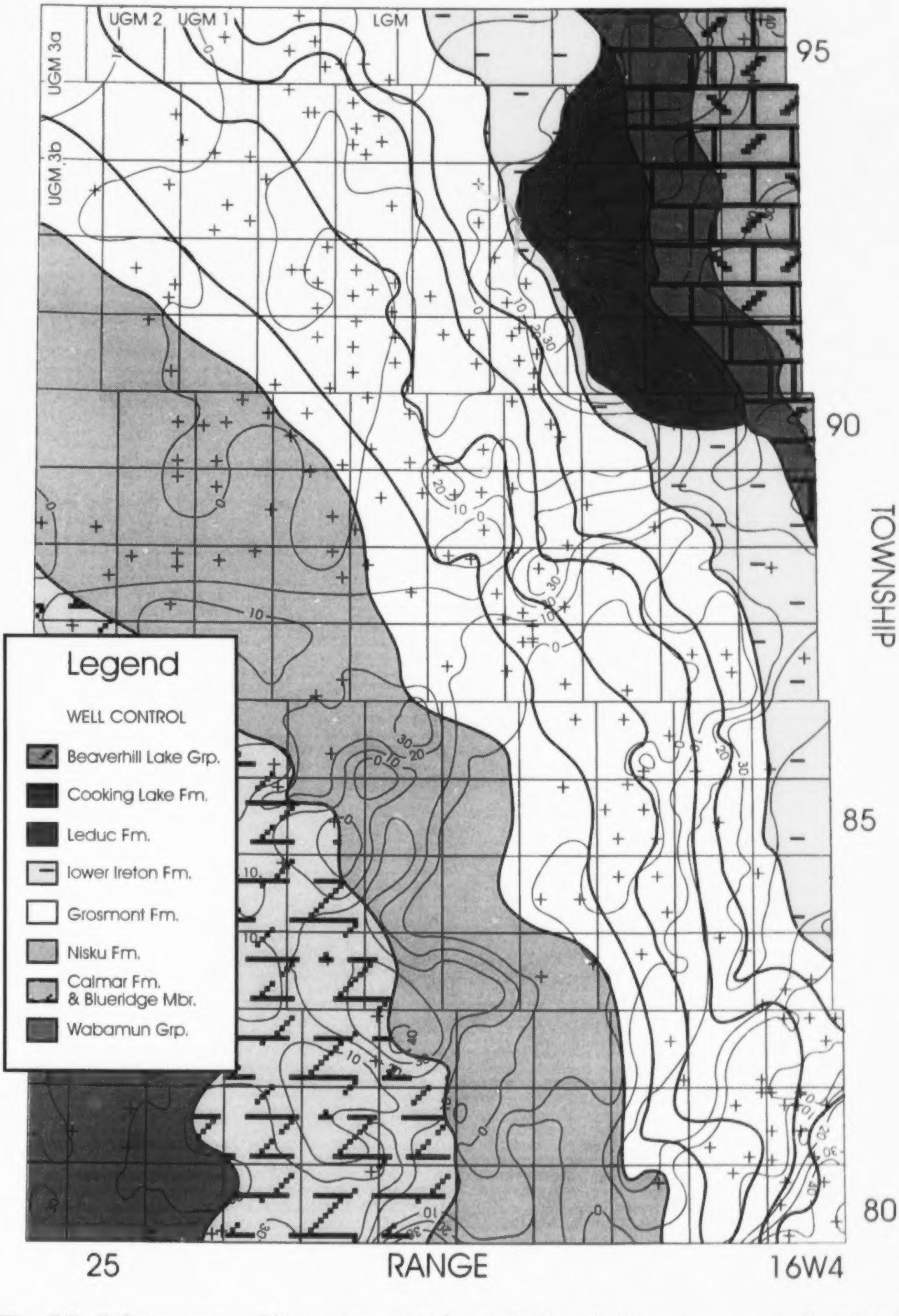
UGM 2
UGM 1
LGM
UGM 3a
UGM 3b
95
90
85
80
TOWNSHIP
25
RANGE
16W4
Legend
WELL CONTROL
Beaverhill Lake Grp.
Cooking Lake Fm.
Leduc Fm.
lower Ireton Fm.
Grosmont Fm.
Nisku Fm.
Calmar Fm.
& Blueridge Mbr.
Wabamun Grp.
0
10
20
30
40

Fig. 5.9: Subcrop map of Devonian strata beneath the sub-Cretaceous unconformity. The topography of the unconformity surface was modified after Ranger (1994).

PALEOKARST DISTRIBUTION

In addition to core observations, caliper and density logs can be used to identify intensely karstified zones such as open caves, unconsolidated and highly fractured intervals. The minimum height of a karstified interval has to exceed 0.3 meters, which is the approximate lower limit of detection by both caliper and density logs (Craig, 1988). The criteria used in this paper for identification of karst from well logs were the same as used by Dembicki (1994) and Dembicki and Machel (1996), i.e. significant caliper log excursions and density porosity readings of at least 35 %. The advantage of using well logs is that it considerably increases the available data base with respect to both the number of wells and the range and continuity of the covered intervals. Disadvantages are that it is not possible to unambiguously distinguish between different types of paleokarst phenomena, and that zones which show porosity reduction, either by infill or cementation, are not detected. This is illustrated by Figs. 5.10, 5.11 and 5.12. In Fig. 5.10 (well location 10-14-84-19W4) an example is shown where core observations correspond well with log signatures. Caliper excursions and high density porosity readings match with paleosol horizons, open caves as well as zones of connected vugs and fractures. Fig. 5.11 (well location 6-12-89-25W4) demonstrates that well logs can be used to identify paleokarst in the absence of core. The third example (Fig. 5.12, well location 10-15-93-23W4), however, shows the limitations of well log usage. Multiple layers of caves infilled by Cretaceous shale cannot be identified on either caliper and density porosity logs. The statistical analysis of the Grosmont paleokarst includes, therefore, both core and well log data.

The analysis of Grosmont karst distribution is based on a population of 227 wells in which 202 karst intervals were identified. The areal distribution of all control wells and of wells in which karst was identified is presented in Fig. 5.13. This map shows that most of the karst is located in the area of the Grosmont erosional edge. Karst distribution was further analyzed with respect to the present structural elevation, in terms of depth below the sub-Cretaceous unconformity and in terms of depth below the top of the Lower Mannville Group.

The results of the analysis of karst distribution, based on the presence of karst

WELL 10-14-84-19 W4M

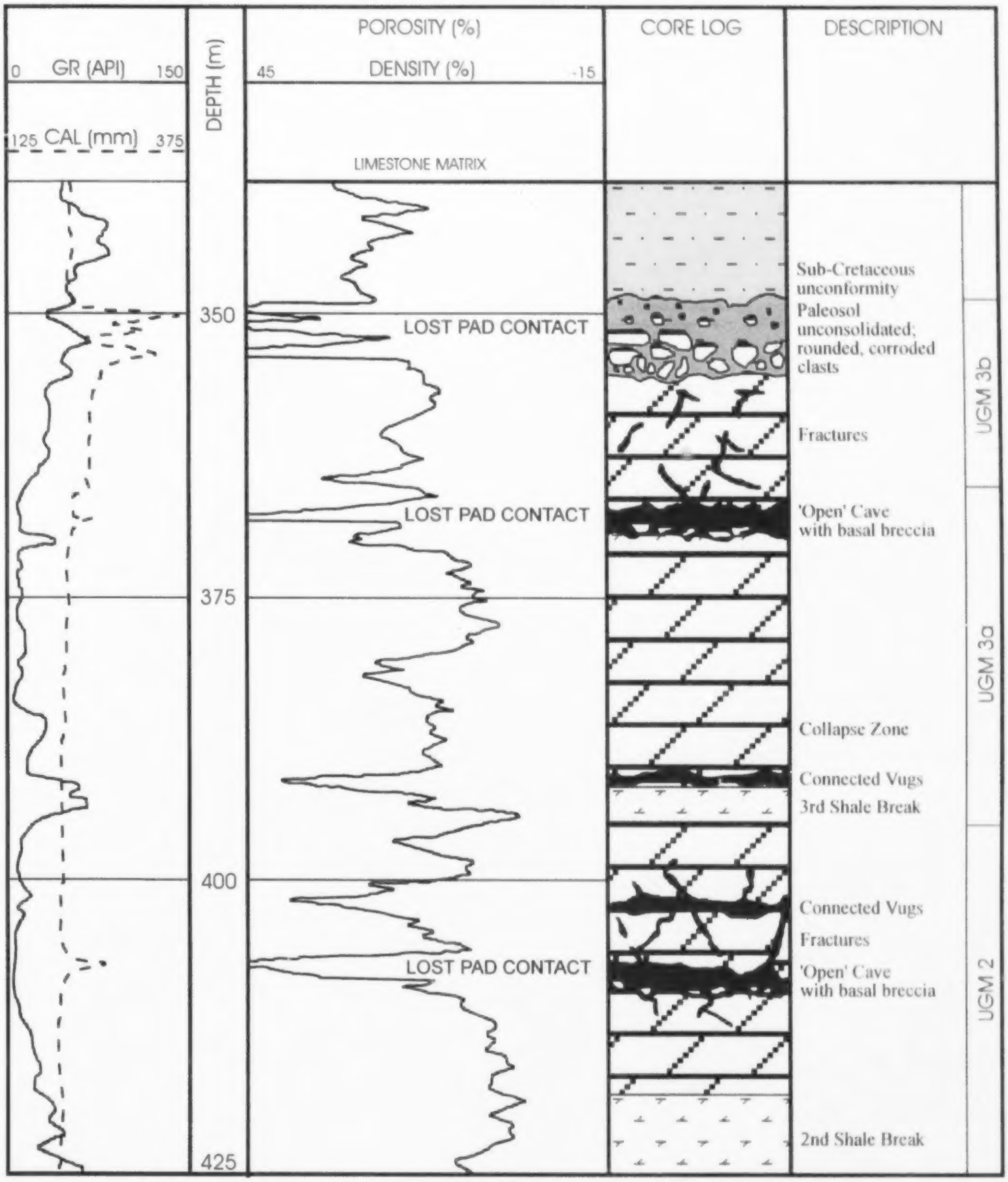

Fig. 5.10: Simplified core log through the Grosmont paleokarst at well location 10-14-84-19W4. Well log signatures of the caliper and density porosity log match well with connected vugs and caves.

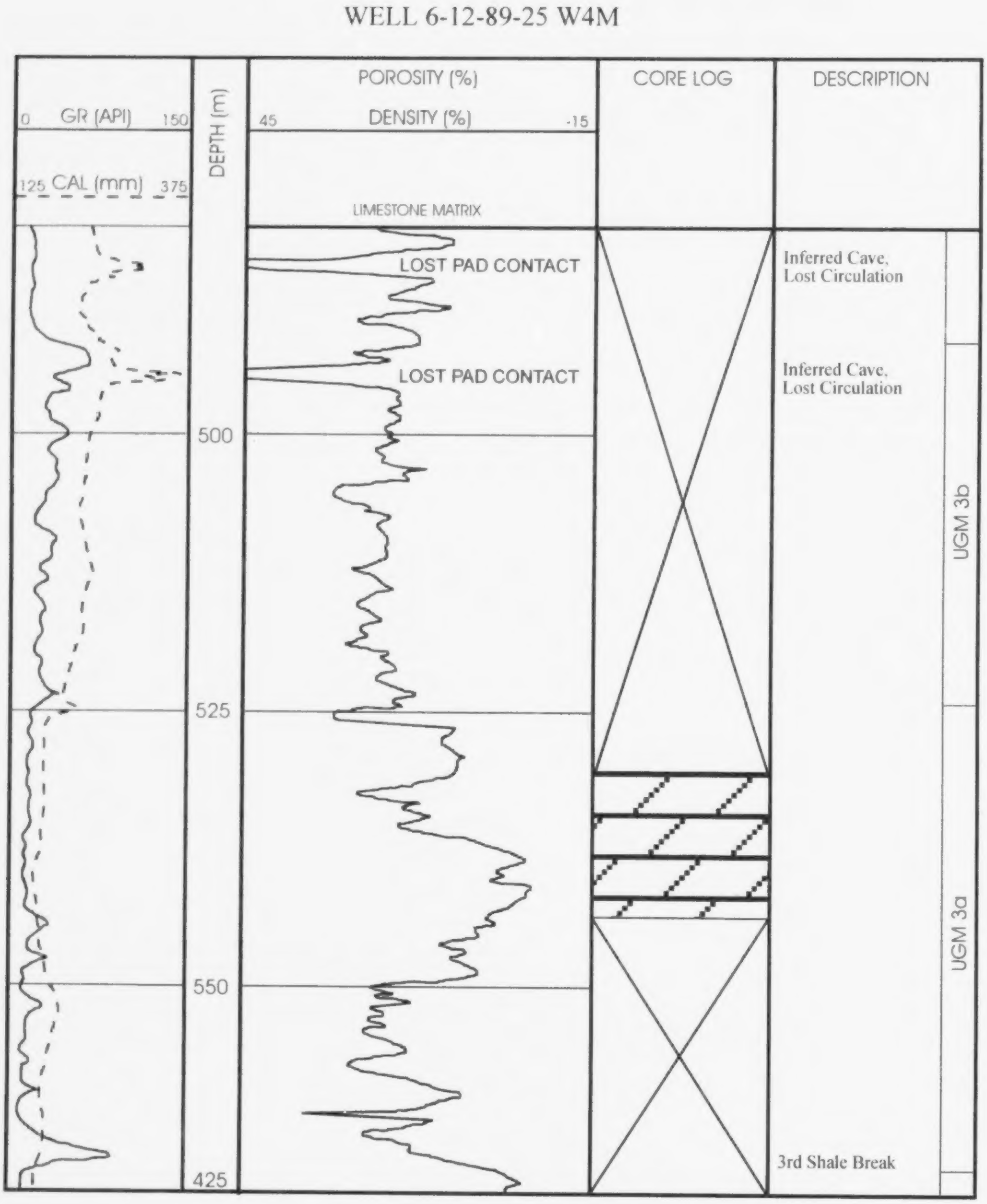

Fig. 5.11: Simplified core log and well log signatures through a possible karst zone at well location 6-12-89-25W4. Significant caliper excursions and density porosity readings greater 45 % indicate the presence of caves or other porous and unconsolidated intervals. This interpretation is further supported by lost circulation during drilling.

WELL 10-15-93-23 W4M

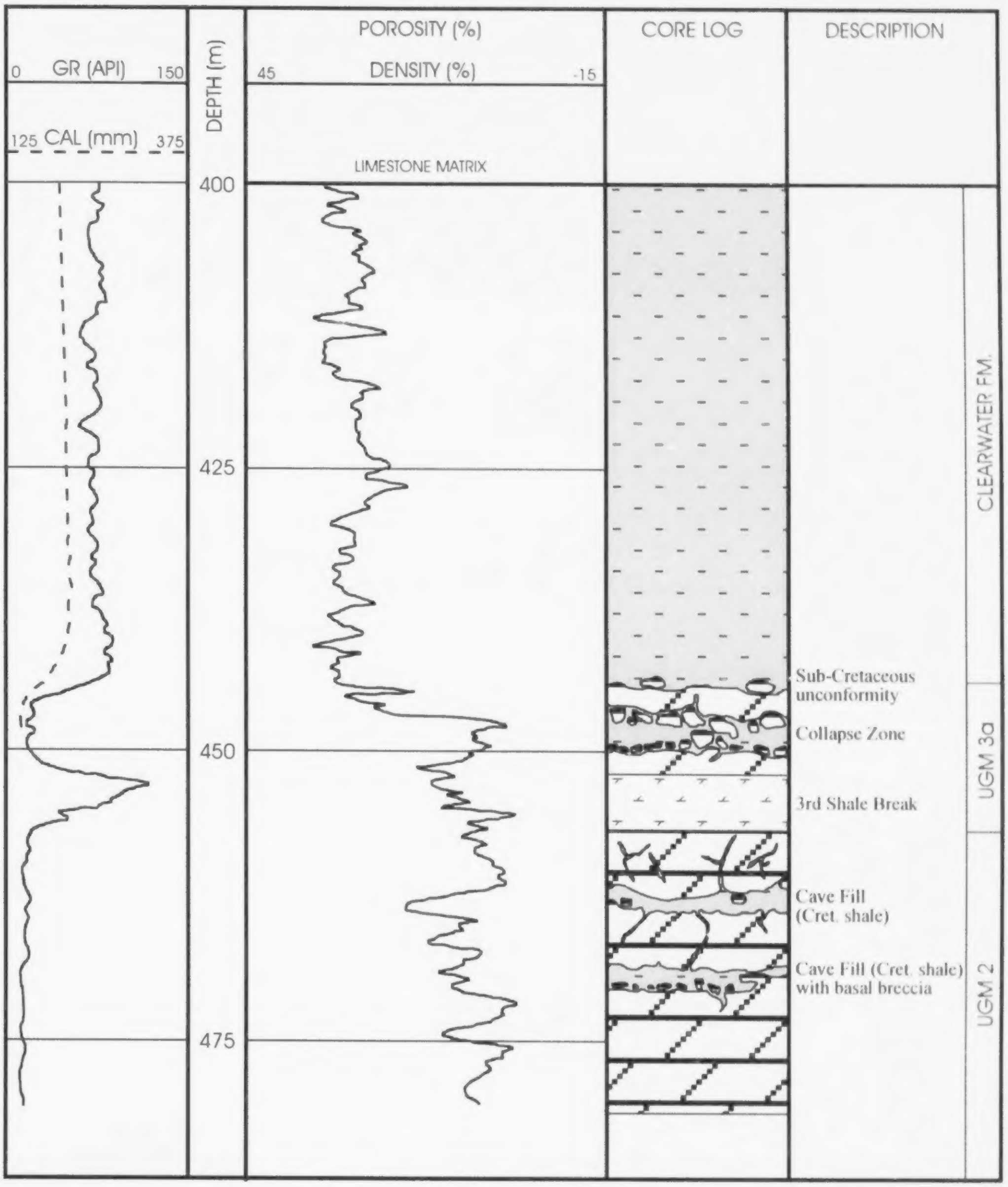

Fig. 5.12: Simplified core log of the Clearwater and Grosmont Formations at well location 10-15-93-23W4. Although the well log signatures show no deviations from 'normal' readings, several caves infilled by Cretaceous shales are present.

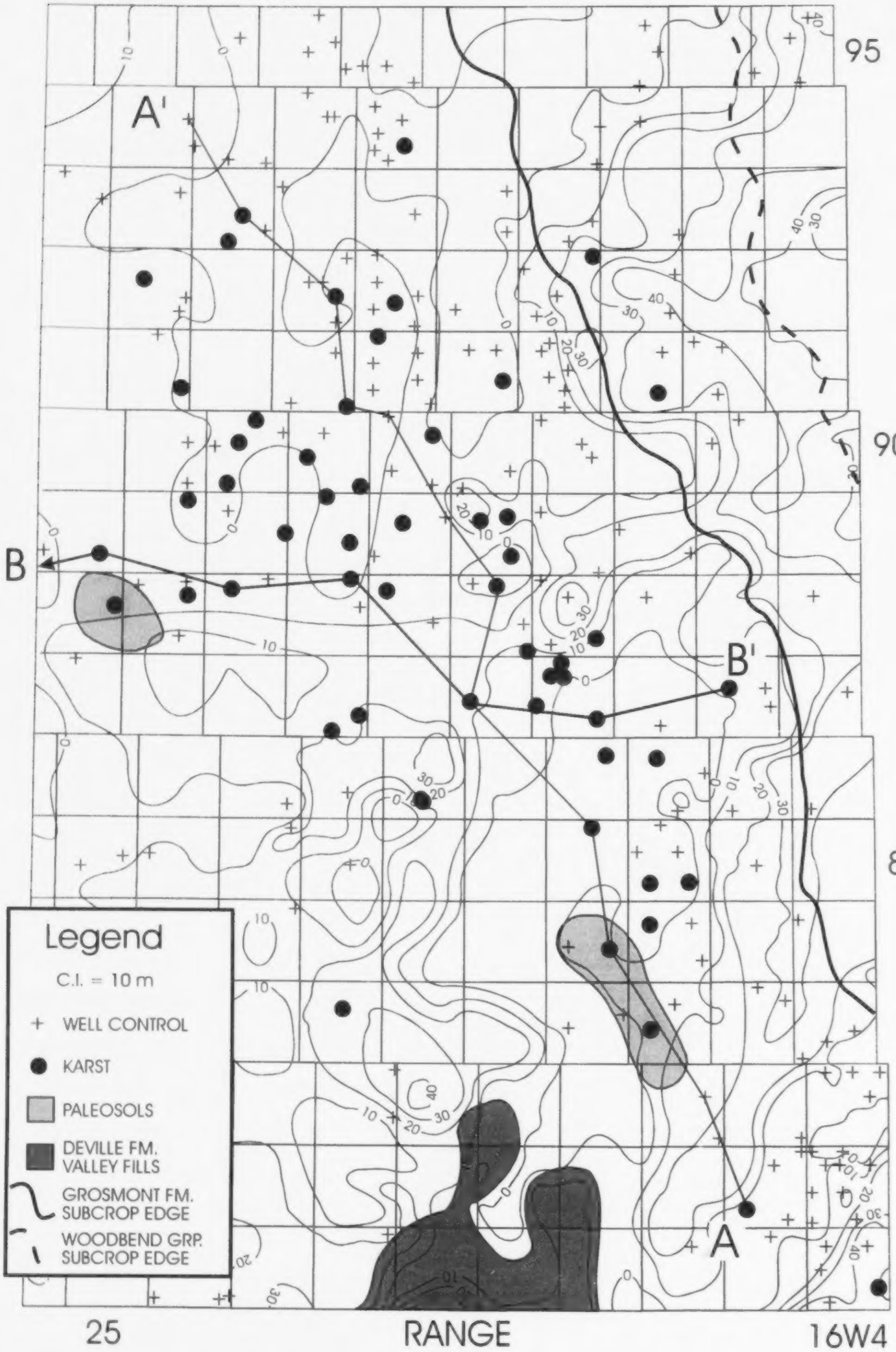
A'
B
B'
A
95
90
85
80
TOWNSHIP
25
RANGE
16W4
Legend
C.I. = 10 m
WELL CONTROL
KARST
PALEOSOLS
DEVILLE FM. VALLEY FILLS
GROSMONT FM. SUBCROP EDGE
WOODBEND GRP. SUBCROP EDGE
0
10
20
30
40

Fig. 5.13: Location of paleokarst wells, cross sections and paleosols in the study area. Distribution of Deville Formation valley fills was taken from Poulton et al. (1994).

intervals in a 5m interval, are presented in Fig. 5.14. In terms of its present structural elevation the Grosmont karst is concentrated in an interval of 200 m, between + 300 and + 100 m above present sea level (Fig. 5.14a). The karst population has a skewed distribution towards the higher elevations with the maximum at + 240 m. This distribution reflects the concentration of karst in the updip portion of the Grosmont Formation close to the subcrop underneath the sub-Cretaceous unconformity. Relative to the sub-Cretaceous unconformity all of the karst is located between 0 and 125 m below the unconformity surface (Fig. 5.14b). About half of the karstified intervals are concentrated in the upper 25 m, the second half is relatively evenly distributed between 25 and 95 m, and only few karstified intervals are present more than 95 m below the unconformity. This distribution suggests that karstification was indeed caused and controlled by exposure of the Devonian carbonates along the sub-Cretaceous unconformity.

Relating the karst distribution to a Cretaceous paleodatum (Fig. 5.14c), i.e. the top of the Lower Mannville, produces a result similar to the unconformity related distribution. One prominent maximum is present at 15 m, a second, weaker one is at around 70 m below the datum. Using this reconstruction has the advantage that the unconformity and the paleokarst are roughly restored to their Early Cretaceous position. Therefore, the data can be analyzed with respect to the paleotopographical area in which the karst occurred, i.e. Grosmont High, Wabasca and McMurray Sub-basins (Fig. 5.15).

The reconstruction of the karst distribution in the area of the Grosmont High (Fig. 5.15b) shows that karstified intervals are arranged at two main paleo-elevations. Most of the karst is focused around 15 to 25 m below the top of the Lower Mannville, but a second, minor concentration is present around 60 to 80 m below the datum. The distribution of karst around the first interval suggests that there was a stable water table at this position, which implies that the position of the water table was the main controlling factor of karst distribution (ideal water table caves as described by Ford and Ewers, 1978; Craig, 1988; Ford, 1988). This interpretation is also supported by the fact that this level can be found and correlated throughout the northern and southern ridge of the Grosmont High, crosscutting Devonian unit boundaries (Fig. 5.16). The second level (Fig. 5.15b) may also signify a water table, however, its presence beneath the Grosmont High is patchy (Fig. 5.16).

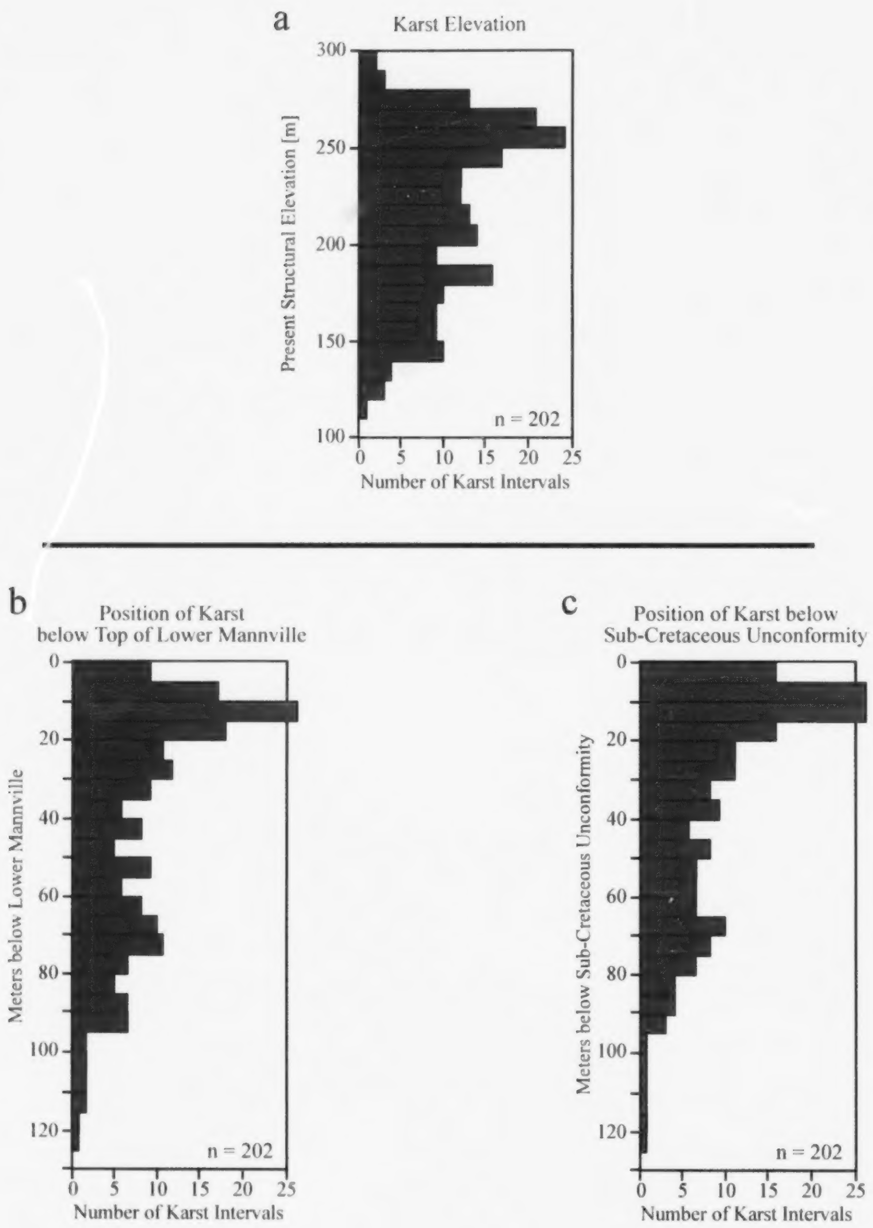

Fig. 5.14: Number of karstified intervals as a function of **(a)** their present structural elevation, **(b)** their depth below the surface of the sub-Cretaceous unconformity, and **(c)** their depth below the top of the Lower Mannville Group.

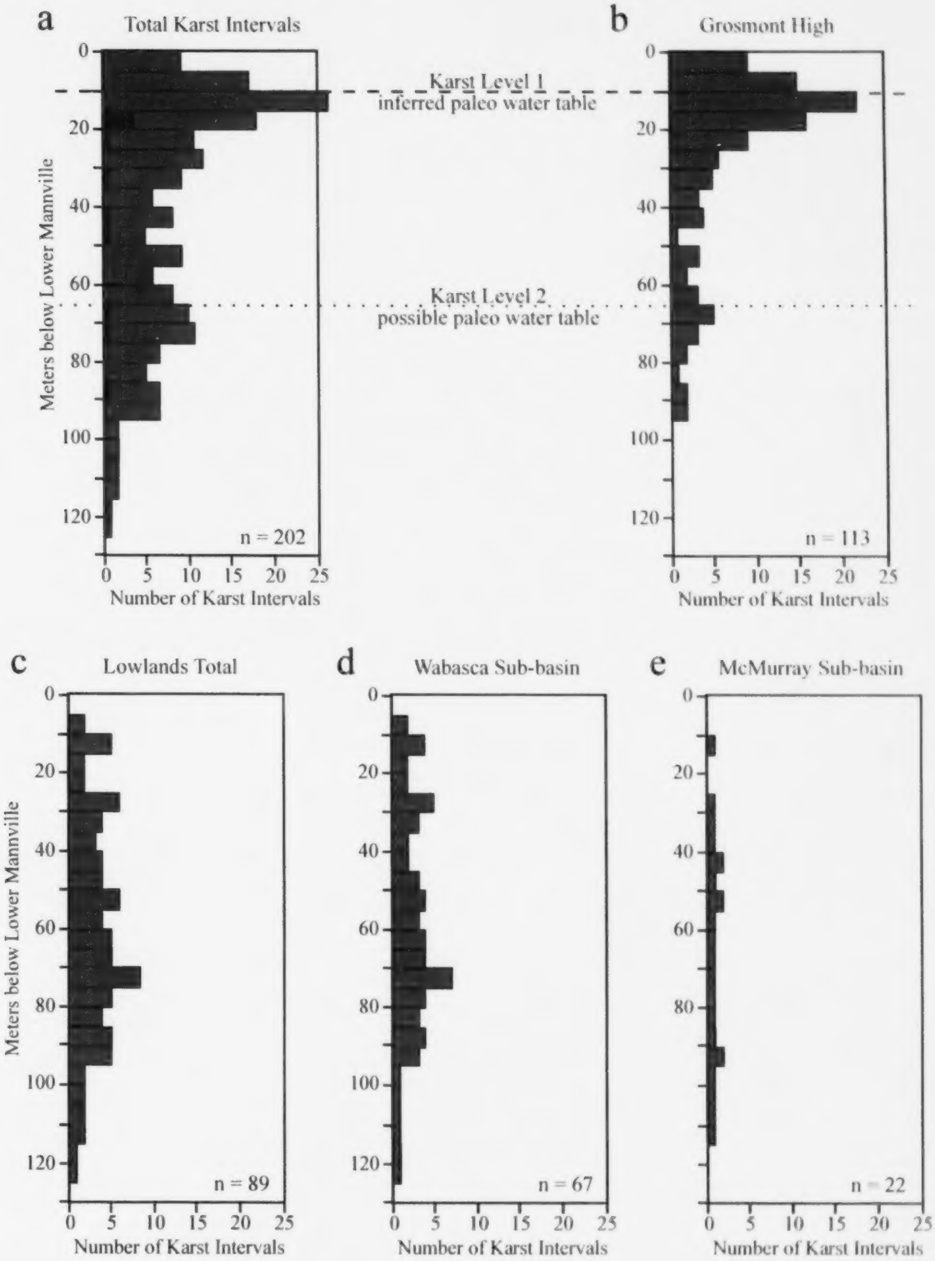

Fig. 5.15 (a to e): Number of karstified intervals versus depth below the top of the Lower Mannville. The top of the Lower Mannville Group is assumed to be a flat surface relative to the Early Cretaceous sea level and was used to reconstruct the original topography of the sub-Cretaceous unconformity (Ranger, 1994). Histograms show the distribution of karst intervals relative to the datum in the whole study area **(a)** (cored intervals are held in black), the Grosmont High **(b)**, lowlands total **(c)**, as well as the Wabasca **(d)** and McMurray Sub-basins **(e)**.

Fig 5.16: North-south cross-section A-A' across the Grosmont High. The section shows the topography of the sub-Cretaceous unconformity, the position of the two karst levels (caves) and the location of paleosol horizons. Note, that the karst levels are parallel to the top of the Lower Mannville Group and cross-cut Devonian strata. Log curves represent gamma ray logs.

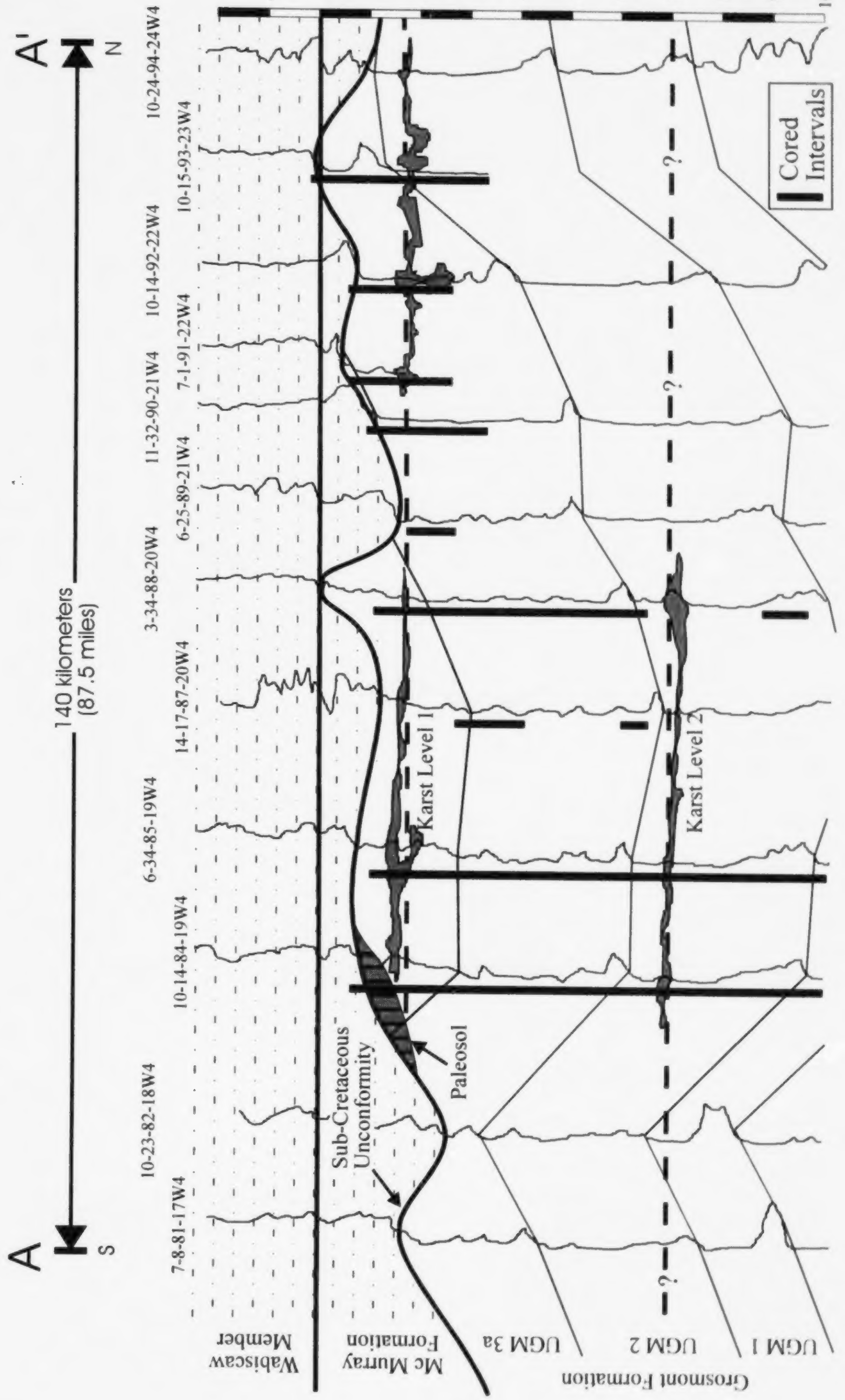
A
S
A'
N
140 kilometers
(87.5 miles)
7-8-81-17W4
10-23-82-18W4
10-14-84-19W4
6-34-85-19W4
14-17-87-20W4
3-34-88-20W4
6-25-89-21W4
11-32-90-21W4
7-1-91-22W4
10-14-92-22W4
10-15-93-23W4
10-24-94-24W4
-10 m
0 m
10 m
20 m
30 m
40 m
50 m
60 m
70 m
80 m
90 m
100 m
Wabiscaw Member
Mc Murray Formation
UGM 3a
UGM 2
UGM 1
Grosmont Formation
Sub-Cretaceous Unconformity
Paleosol
Karst Level 1
Karst Level 2
?
Cored Intervals

Karst distribution beneath the paleotopographic lows appears to be more uniform (Fig. 5.15c). The McMurray Sub-basin histogram (Fig. 5.15e) shows no significant change in karst occurrences with depth, which is probably due to the small sample population in this area. The Wabasca Sub-basin histogram (Fig. 5.15d) also shows very little variation, but has a weak maximum at 70 m below the top of the Lower Mannville, possibly indicating a weak karst/cave interval. The uniform distribution can be explained in two different ways. Firstly, the paleo-elevations between 0 and 20 m, the position of maximum karst occurrence in the Grosmont High, are eroded in the sub-basins where base levels are below the regionally correlated karst intervals. Secondly, there seems to be a strong correlation between dissolution features and certain Devonian units, particularly the UGM 3a and UGM 3b (Fig. 5.17). Incidentally, these units contain no anhydrite close to their respective subcrop area, but contain considerable amounts of anhydrite and anhydritic carbonates to the west and south of the study area, where the UGM 3a and UGM 3b are buried deeper below the unconformity. Furthermore, these units decrease somewhat in thickness to the east, although there is no evidence for collapse of these strata as observed in the southern part of the Grosmont platform (Cutler, 1983). The observed stratiform caves may, therefore, be the expression of anhydrite removal in the study area.

KARST INTERPRETATION

As previously discussed, various features indicative of paleokarst, such as breccia, caves and paleosols (Esteban and Klappa, 1983), are widely distributed throughout the study area, but are restricted to the interval from the sub-Cretaceous unconformity to a depth of 100 to 130 m below the top of the Lower Mannville Group. Most affected by karstification are the uppermost 25 m of the Grosmont Formation, just below the top of the Lower Mannville, in areas of paleotopographic highs like the Grosmont High and adjacent highlands. This, together with the fact that the sub-Cretaceous unconformity represents a major time period of weathering and erosion, strongly suggests that the Grosmont paleokarst is an example of a buried continental karst caused by carbonic acid dissolution analogous to paleokarst developed in Triassic dolostones of the Transdanubian

Fig. 5.17: East-west cross-section B-B' across the study area. The section shows the topography of the sub-Cretaceous unconformity, the position of the two karst levels (caves) and the location of solution 'caves' following bedding planes of the UGM 3a, UGM 3b and Nisku Formation. Log curves represent gamma ray logs (solid line) and caliper log (dashed line).

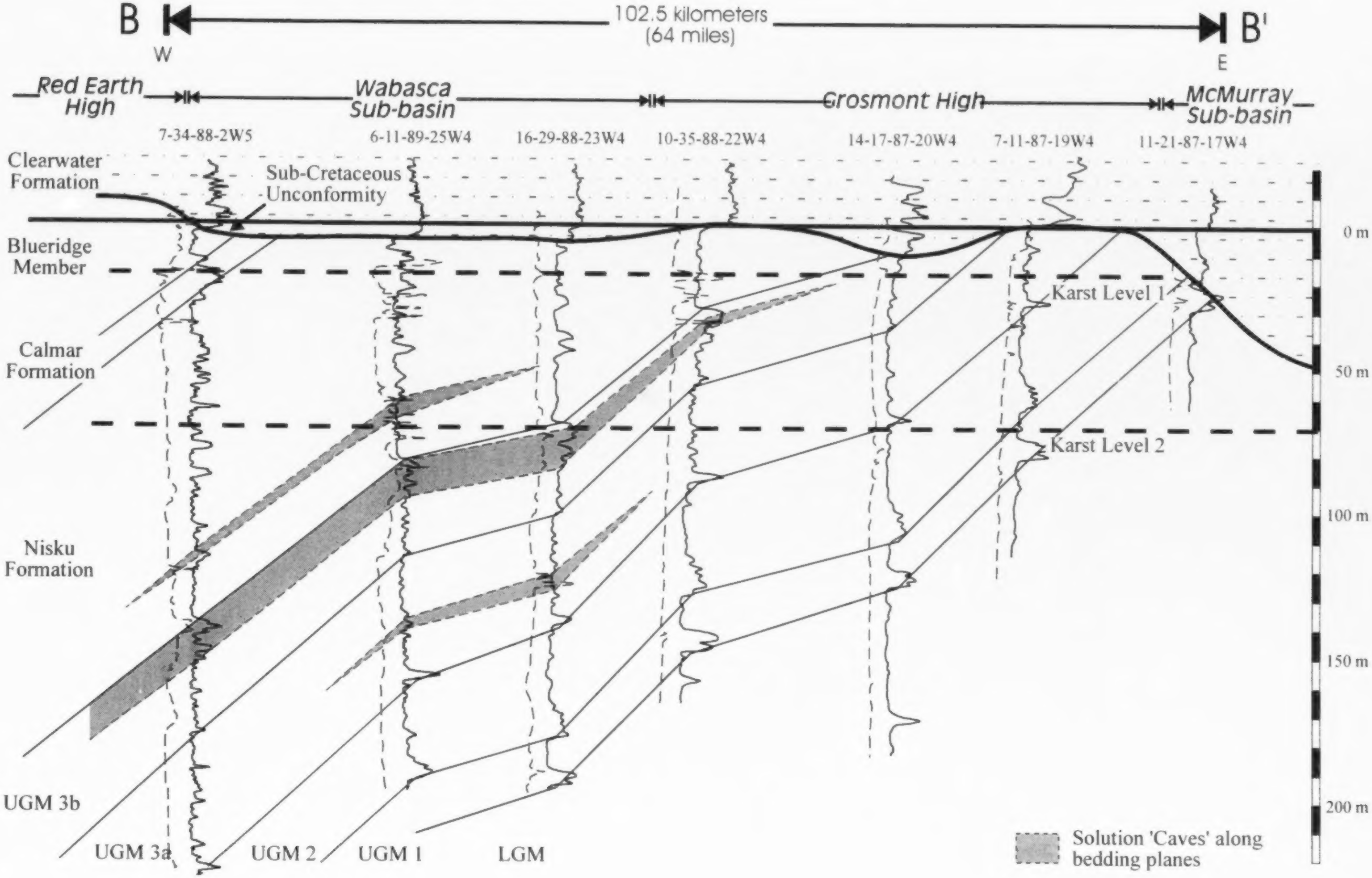

B
W
102.5 kilometers
(64 miles)
B'
E
Red Earth High
Wabasca Sub-basin
Grosmont High
McMurray Sub-basin
7-34-88-2W5
6-11-89-25W4
16-29-88-23W4
10-35-88-22W4
14-17-87-20W4
7-11-87-19W4
11-21-87-17W4
Clearwater Formation
Sub-Cretaceous Unconformity
Blueridge Member
Calmar Formation
Nisku Formation
UGM 3b
UGM 3a
UGM 2
UGM 1
LGM
Karst Level 1
Karst Level 2
0 m
50 m
100 m
150 m
200 m
Solution 'Caves' along bedding planes

Central Mountains in Hungary (Bardossy and Kordos, 1989) or to paleokarst in Mississippian dolostones of Colorado, U.S.A. (De Voto, 1988). Carbonic acid dissolution was likely continually supported by concomitant gypsum (or anhydrite) dissolution (sensu Back et al., 1983). This interpretation is further supported by the concentration of karst along well defined paleo-elevations. The histogram of karst distribution (Fig. 5.15b) and cross-section (Fig. 5.16) of the Grosmont High area show that these karst levels can be mapped over long distances. Furthermore, these karst levels are approximately parallel to the top of the Lower Mannville, but "disregard" paleo-surface topography, i.e. paleotopography of the sub-Cretaceous unconformity, and they crosscut the Devonian strata. The small dip angle of the Devonian strata of around 0.1° at the inferred time of karstification, i.e before renewed tilting during and after the Laramide orogeny, suggests that cave development probably occurred first along bedding planes. That the cave system is arranged parallel to a Cretaceous datum, furthermore, implies that cave alignment parallel to a piezometric surface was a second component. Data density is, however, not sufficient to decide whether the Grosmont caves are (1) ideal water table caves, i.e. caves solely developed along the water table, or (2) an example of a mixed phreatic-water table cave system (Ford and Ewers, 1978; Ford, 1988). The possible presence of two cave levels may suggest movement of the water table to a different position in response to lowering of the erosional base level.

The arrangement of the Grosmont karst parallel to a Lower Cretaceous datum also constrains the timing of karstification to a period between the Aptian/Albian (Early Cretaceous), the time of Mannville deposition, and the Oxfordian (Late Jurassic), the beginning of the Columbia Orogeny. This orogenic event, which initiated the transition of the Western Canada Sedimentary Basin from a passive margin setting to a foreland basin, caused regional uplift in most of Alberta, and resulted in deep erosion and the development of major valley systems in the carbonate bedrock (Poulton, 1989; Poulton et al., 1994). A Jurassic/Cretaceous origin of the Grosmont karst is further supported by the age of the earliest sediments (Deville Formation and equivalent strata) infilling its valley systems. These sediments, ranging from quartz arenites derived from an eastern, cratonic source to kaolinitic chert arenites sourced from weathering of the surrounding carbonates, are interpreted to be mostly of Barremian age with some units dating as far back as the Kimmeridgian (Hopkins, 1982; Burden, 1984; Poulton et al., 1994).

The different, stratiform distribution of paleokarst beneath the Wabasca Sub-basin suggests that this karst system may have had a different origin from paleokarst of the Grosmont High area, and was likely related to dissolution of sulfates in the subsurface. Sulfate dissolution may have been caused either by descending fluids of meteoric origin or by ascending basinal fluids (cf. Palmer and Palmer, 1995). In addition, sulfate dissolution may also have been accompanied by sulfate reduction. This process produces H_2S that, if it comes in contact with oxygen-rich waters, oxidizes to sulfuric acid (Palmer, 1995), which in turn causes strong carbonate dissolution.

EFFECTS ON RESERVOIR PROPERTIES

Karstification had a considerable impact on the reservoir characteristics as well as the seal capacity of the Grosmont Formation. Carbonate intervals not affected by karst have porosities between 5 and 20 % depending on lithology and facies (Luo et al., 1994; Luo and Machel, 1995). In comparison, porosities of 25 to 40 % are common in karstified intervals and may exceed these values in open caves. In many cases pore systems created during karstification were not occluded by later diagenetic phases. Locally, however, karst porosity was destroyed by calcite cementation of intercrystalline pores, fractures, vugs and caves as well as cave infill by sands, shales and breccia.

Reservoir permeabilities increased from 10 to 100 md in non-karstified intervals to 1,000 to 10,000 in karstified rocks (Luo et al., 1994). If connected by a system of fractures, vugs or caves these values can reach up to 30,000 md (Luo et. al., 1992).

The effectiveness of the Grosmont shale breaks as seals during steam stimulation of the reservoir is a function of karstification. As capillary pressure measurements show, the shale breaks have extremely high capillary displacement pressures and, therefore, should act as effective seals on a matrix and local scale (Luo et al., 1994). However, fracturing of the shale breaks seems not to be unusual, as observed in core. In karst zones, especially where the shale breaks crosscut the identified karst levels, breaching and fracturing, and therefore, weakening of the seals have to be expected.

CONCLUSIONS

A wide variety of distinctive dissolution related fabrics and pore occluding phases, paleotopography, and the presence of large scale porous and unconsolidated intervals that are easily recognizable in well logs testify that the Grosmont Formation and adjacent Devonian strata underwent significant karstification. Much of this karst system, especially in the Grosmont High area, is developed along well defined karst levels that are parallel to reconstructed Cretaceous paleo-elevation levels. The development of these karst levels is interpreted to reflect the position of paleo-water tables. This suggests that much of the Grosmont paleokarst developed in a continental setting via carbonic acid dissolution. The suggested timing of karstification is the Late Jurassic to Early Cretaceous based on the orientation of karst levels parallel to a Lower Cretaceous datum and the age of the oldest known karst valley infilling sediments. Stratiform "karst" in the Wabasca Sub-basin area was likely caused by sulfate dissolution. In addition, sulfate reduction and resulting H_2S production may have contributed to carbonate dissolution via oxidation of H_2S to sulfuric acid.

Karstification had a significant impact on the reservoir quality of the Grosmont Formation. Close to the sub-Cretaceous unconformity porosity and permeability are often greatly enhanced, but localized porosity reduction has occurred. Furthermore, seal quality of the Grosmont shale breaks is negatively affected by breaching near karst zones. However, since much of the karst occurs along defined karst levels, prediction of the breaching sites is possible by identifying intersection points between karst levels and potential seal beds. This method of recognition of breached seals is of potential economic importance since it helps to avoid steam loss during reservoir stimulation, therefore, aiding in choosing better sites for future enhanced recovery projects.

REFERENCES

Back, W., Hanshaw, W.W., Plummer, L.N., Rahn, P.H., Rightmire, C.T., and Rubin, M., 1983, Process and rate of dedolomitization: mass transfer and ^{14}C dating in a regional carbonate aquifer. Geological Society of America Bulletin, v. 94, p. 1415-1429.

Bardossy, G., and Kordos, L., 1989, Paleokarst of Hungary. In: Bosak, P., Ford, D.C., Glazek, J., and Horacek, I., eds., Paleokarst - a systematic and regional review, Development in Earth surface processes 1, Elsevier, Amsterdam, p. 137-153.

Bischoff, J.L., Julia, R., Shanks, W.C., III, and Rosenbauer, R.J., 1994, Karstification without carbonic acid: bedrock dissolution by gypsum-driven dedolomitization. Geology, v. 22, p. 995-998.

Brooks, P.W., Fowler, M.G., and Macqueen, R.W., 1989, Biomarker geochemistry of Cretaceous oil and tar sands and Paleozoic carbonate trend bitumens, Western Canada Basin. In: Meyer, R.F., and Wiggins, E.J., eds., Proceedings, Fourth UNITAR/UNDP International Conference on heavy crude and tar sands, Alberta Oil Sands Technology and Research Authority, Edmonton, v. 2, Geology, Chemistry, p. 594-606, Discussion, p. 629-631.

Burden, E.T., 1984, Terrestrial palynomorph biostratigraphy of the lower part of the Mannville Group (Lower Cretaceous), Alberta and Montana. In: Stott, D.F., and Glass, D.J., eds., The Mesozoic of Middle North America. Canadian Society of Petroleum Geologists, Memoir 9, p. 249-269.

Busenberg, E., and Plummer, L.N., 1982, The kinetics of dissolution of dolomite in CO_2-H_2O systems at 1.5 to 65°C and 0 to 1 atm PCO_2. American Journal of Science, v. 282, p. 45-78.

Choquette, P.W, and Pray, L.C., 1970, Geologic nomenclature and classification of porosity in sedimentary carbonates. American Association of Petroleum Geologists Bulletin, v. 54, p. 207-250.

Craig, D.H., 1988, Caves and other features of Permian karst in San Andres dolomite, Yates Field Reservoir, West Texas. In: James, N.P., and Choquette, P.W., eds., Paleokarst, Springer Verlag, New York, p. 342-363.

Cutler, W.G., 1983, Stratigraphy and sedimentology of the Upper Devonian Grosmont Formation, Alberta, Canada. Bulletin of Canadian Petroleum Geology, v. 31, p. 282-325.

De Voto, R.H., 1988, Late Mississippian paleokarst and related mineral deposits, Leadville Formation, central Colorado. In: James, N.P., and Choquette, P.W., eds., Paleokarst, Springer Verlag, New York, p. 278-305.

Dembicki, E.A., 1994, The Upper Devonian Grosmont Formation: well log evaluation and regional mapping of a heavy oil carbonate reservoir in northeastern Alberta. Unpubl. M.Sc. thesis, University of Alberta, Edmonton, 221 p.

Dembicki, E.A., and Machel, H.G., 1996, Recognition and delineation of paleokarst zones by the use of wireline logs in the bitumen-saturated Upper Devonian Grosmont Formation of northeastern Alberta, Canada. American Association of Petroleum Geologists Bulletin, v. 80, p. 695-712.

Energy Resources Conservation Board of Alberta, 1993, Alberta's reserves of crude oil, gas, natural gas liquids and sulphur. Energy Resources Conservation Board, Report ST 94-18, Calgary.

Esteban, M., and Klappa, C.F., 1983, Subaerial exposure environment. In: Scholle, P.A., Bebout, D.G., and Moore, C.H., eds., Carbonate depositional environments. American Association of Petroleum Geologists, Memoir 33, p. 1-54.

Ford, D.C., 1988, Characteristics of dissolutional cave systems in carbonate rocks. In: James, N.P., and Choquette, P.W., eds., Paleokarst, Springer Verlag, New York, p. 25-57.

Ford, D.C., 1995, Paleokarst as a target for modern karstification. Carbonates and Evaporites, v. 10, p. 138-147.

Ford, D.C., and Ewers, R.O., 1978, The development of limestone cave systems in the dimensions of length and depth. Canadian Journal of Earth Sciences, v. 15, p. 1783-1798.

Harrison, R.S., 1982, Geology and production history of the Grosmont carbonate pilot project, Alberta, Canada. In: Meyer, R.F., Wynn, J.C., and Olson J.C., eds., The future of heavy crude and tar sands. Second International Conference on heavy crude and tar sands, Caracas, Venezuela, February 7-17, 1982, v. 1, p. 199-204.

Harrison, R.S., and McIntyre, B.G., 1981, The geologic setting of the Grosmont thermal recovery project, northeastern Alberta. Seminar on Advances in Petroleum Recovery and Upgrading Technology, Calgary, Alberta, May 26-28, 1981, 11p.

Hoffmann, C.F., and Strausz, O.P., 1986, Bitumen accumulation in Grosmont platform complex, Upper Devonian, Alberta, Canada. American Association of Petroleum Geologists Bulletin, v. 70, p. 1113-1128.

Hopkins, J.C., 1982, Sedimentology of quartzose sandstones of Lower Mannville and associated units, Medicine River Area, Central Alberta. Bulletin of Canadian Petroleum Geology, v. 29, p. 12-41.

Jennings, J.N., 1971, Karst. The M.I.T. Press, Cambridge, 252 p.

Jones, B., Lockhart, E.B., and Squair, C., 1984, Phreatic and vadose cements in the Tertiary Bluff Formation of Grand Cayman Island, British West Indies. Bulletin of Canadian Petroleum Geology, v. 32, p. 382-397.

Kendall, A.C., and Broughton, P.L., 1978, Origin of fabrics in speleothems composed of columnar calcite crystals. Journal of Sedimentary Petrology, v. 48, p. 519-538.

Kerans, C., 1990, Depositional systems and karst geology of the Ellenburger Group (Lower Ordovician), subsurface of Texas. The University of Texas at Austin, Bureau of Economic Geology, Report of Investigations No. 193, 63 p.

Kerans, C., 1993, Description and interpretation of karst-related breccia fabrics, Ellenburger Group, West Texas. In: Fritz, R.D., Wilson, J.L., and Yurewicz, D.A., eds., Paleokarst related hydrocarbon reservoirs. Society for Sedimentary Geology (SEPM) Core Workshop No. 18, p. 181-200.

Luo, P., Dembicki, E.A., Machel, H.G., and Huebscher, H., 1993, Diagenesis and reservoir characteristics of the heavy-oil carbonate trend in western Canada - refined evaluation of reservoir characteristics of the Grosmont Formation. AOSTRA report 7 of 7, January 31, 1993, 170 p.

Luo, P., Huebscher, H., Dembicki, E.A., and Machel, H.G., 1992, Diagenesis and reservoir characteristics of the heavy-oil carbonate trend in western Canada - continued investigation of reservoir characteristics of the Grosmont Formation. AOSTRA report 6 of 7, July 31, 1992, 141 p.

Luo, P., and Machel, H.G., 1995, Pore size and pore throat types in a heterogeneous dolostone reservoir, Devonian Grosmont Formation, Western Canada Sedimentary Basin. American Association of Petroleum Geologists Bulletin, v. 79, p. 1698-1720.

Luo, P., Machel, H.G., and Shaw, J., 1994, Petrophysical properties of matrix blocks of a heterogeneous dolostone reservoir - the Upper Devonian Grosmont Formation, Alberta, Canada. Bulletin of Canadian Petroleum Geology, v. 42, p. 465-481.

Meijer Drees, N.C., 1994, Devonian Elk Point Group of the western Canada Sedimentary Basin. In: Mossop, G.D., and Shetsen, I., comps., Geological Atlas of the Western Canada Sedimentary Basin. Canadian Society of Petroleum Geologists and Alberta Research Counsil, p. 129-148.

Palmer, A.N., 1995, Geochemical models for the origin of macroscopic solution porosity in carbonate rocks. In: Budd, D.A., Saller, A.H., and Harris, P.M., eds., Unconformities and porosity in carbonate rocks, American Association of Petroleum Geologists, Memoir 63, p. 77-101.

Palmer, A.N., and Palmer, M.V., 1995, The Kaskaskia paleokarst of the northern Rocky Mountains and Black Hills, northwestern U.S.A., Carbonates and Evaporites, v. 10, p. 148-160.

Poulton, T.P., 1989, Upper Absaroka to Lower Zuni: the transition to the foreland basin. In: Ricketts, B.D., Western Canada Sedimentary Basin: a case history. Canadian Society of Petroleum Geologists, p. 233-247.

Poulton, T.P., Christopher, J.E., Hayes, B.J.R., Losert, J., Tittmore, J., and Gilchrist, R.D., 1994, Jurassic and lowermost Cretaceous strata of the Western Canada Sedimentary Basin. In: Mossop, G.D., and Shetsen, I., comps., Geological Atlas of the Western Canada Sedimentary Basin. Canadian Society of Petroleum Geologists and Alberta Research Counsil, p. 297-316.

Ranger, 1994, A basin study of the southern Athabasca oil sands deposits. Unpubl. Ph.D. thesis, University of Alberta, Edmonton, 290 p.

Retallack, G.J., 1990, Soils of the past: an introduction to paleopedology. Unwin Hyman, Boston, 520 p.

Richards, B.C., Barclay, J.E., Bryan, D., Hartling, A., Henderson, C.M., and Hinds, R.C., 1994, Carboniferous strata of the Western Canada Sedimentary Basin. In: Mossop, G.D., and Shetsen, I., comps., Geological Atlas of the Western Canada Sedimentary Basin. Canadian Society of Petroleum Geologists and Alberta Research Counsil, p. 221-250.

Ross, C.A., 1991, Pennsylvanian paleogeography of the western United States. In: Cooper, J.D., and Stevens, C.H., eds., Palaeozoic paleogeography of the Western United States - II. Pacific Section, Society of Economic Paleontologists and Mineralogists, v. 1, p. 137-148.

Smith, D.G., 1994, Paleogeographic evolution of the Western Canada Sedimentary Basin. In: Mossop, G.D., and Shetsen, I., comps., Geological Atlas of the Western Canada Sedimentary Basin. Canadian Society of Petroleum Geologists and Alberta Research Counsil, p. 277-296.

Stoakes, F.A., 1992, Woodbend megasequence. In: Wendte, J.C., Stoakes, F.A., and Clarence, C.V., Devonian-Early Mississippian carbonates of the Western Canada Sedimentary Basin: a sequence stratigraphic framework. Society for Sedimentary Geology (SEPM) Short Course No. 28, p. 183-206.

Theriault, F., and Hutcheon, I., 1987, Dolomitization and calcitization of the Devonian Grosmont Formation, northern Alberta. Journal of Sedimentary Petrology, v. 57, p. 955-966.

Vandermeer, J.G., and Presber, T.C., 1980, Heavy oil recovery from the Grosmont carbonates of Alberta. Seminar on Nonconventional Oil Technology. Calgary, Alberta, May 29-30, 1980, 22 p.

White, W.B., and White E.L., 1995, Correlation of contemporary karst landforms with paleokarst landforms: the problem of scale. Carbonates and Evaporites, v. 10, p. 131-137.

CHAPTER 6

SUMMARY AND CONCLUSIONS

Log marker stratigraphy, facies analysis and mapping of lithofacies distribution are used to investigate the stratigraphic evolution of the Woodbend Group in north-central Alberta *(Chapter 2)*. The results of this investigation suggest that the Woodbend shelf development proceeded in six phases: (1) carbonate platform backstepping, (2) clastic wedge sedimentation, (3) re-initiation and catch-up of carbonate platform sedimentation, (4) carbonate platform progradation, (5) mixed carbonate-siliciclastic platform sedimentation, and (6) siliciclastic basin-fill sedimentation. Carbonate platform growth appears to have been controlled by eustatic changes in sea level, input of siliciclastic sediments, the production and accumulation rate of carbonate sediment on the platform, and by the antecedent shelf topography. Input of clastic sediments was both 'detrimental' as well as 'beneficial' to carbonate platform development. Siliciclastic sedimentation terminated carbonate production and covered carbonate producing areas, but also elevated the shelf floor into the carbonate production zone. The rate of carbonate production and accumulation was largely controlled by the geographic area of the subtidal carbonate factory. The formation of areally extensive tidal flats decreased the rate of subtidal carbonate production.

Using petrography and stable isotope analysis, a paragenetic sequence for Woodbend carbonates in north-central Alberta was established and used to identify those diagenetic phases that had the greatest impact on porosity evolution *(Chapter 3)*. Woodbend reservoirs were classified into three classes (limestones, dolostones, karstified dolostones) based on diagenetic overprint and resulting porosity characteristics. Compaction and intense calcite cementation resulted in overall low porosity of Woodbend limestones. Pervasive matrix dolomitization, however, appears to have prevented extensive compaction. Consequently, dolostones have retained significantly higher porosities than limestones. In addition, significant amounts of secondary porosity were created by dissolution of anhydrite and especially by karstification. However, karstification also increased reservoir heterogeneity due to the heterogeneous distribution of fractures, breccias and caves. Greatly enhanced porosities (up to 40 %) and permeabilities (up to several Darcies) of karstified intervals of the Grosmont Formation created a local sink for formation fluids from the surrounding Devonian and Cretaceous units. Downward percolating meteoric waters were likely responsible for the extreme degree of biodegradation and waterwashing of hydrocarbons in the Grosmont heavy-oil reservoir compared to the lesser degree of degradation of heavy oils contained in the overlying Lower Cretaceous Mannville Group (Athabasca oil sands).

An analysis of petrography, stable isotopes, major and trace elements, and the regional and stratigraphic distribution, led to genetic interpretations of Woodbend replacement dolomites in north-central Alberta *(Chapter 4)*. Type 1 replacement dolomites are interpreted to have formed from, and to have been modified by, descending evaporated fluids of marine origin. Type 2 replacement dolomites are interpreted to have formed from warm, ascending, basinal fluids. Available data on the distribution of replacement dolomite types further suggest that the Cooking Lake platform margin acted as a fluid conduit for dolomitizing fluids. The warm basinal fluids appear to have ascended through the Leduc reefs of the Rimbey-Meadowbrook reef trend and its northern extension. This upward migration of basinal fluids caused dolomitization and dolomite alteration halos in parts of the Grosmont Formation that directly overly Leduc Formation reefs. Dolomitizing fluids do not appear to have descended through the Grosmont platform into the Leduc reefs.

Grosmont paleokarst can be recognized in core and caliper and neutron-density porosity logs *(Chapter 5)*. Among the karst fabrics identified in core are corroded and calcitized dolomite rhombs, fractures and breccias, vugs and caverns, as well as paleosols. Karst recognized in well logs corresponds to caves, vugs, and intensely fractured, brecciated and/or unconsolidated core intervals. The distribution of paleokarst in the Grosmont heavy-oil reservoir follows two separate patterns. In areas of Early Cretaceous paleotopographic highs, the Grosmont paleokarst is concentrated along well-defined karst levels that are parallel to Early Cretaceous paleo-elevation levels, but cross-cut Devonian strata. This distribution is interpreted to reflect the position of paleo-water tables during karstification, suggesting that much of the Grosmont paleokarst developed in a continental setting via carbonic acid dissolution, probably between the Late Jurassic to Early Cretaceous. In areas of Early Cretaceous paleotopographic lows, paleokarst is distributed parallel to Devonian bedding planes and is likely the result of anhydrite dissolution. In addition, sulfate reduction and resulting H_2S production may have contributed to carbonate dissolution via oxidation of H_2S to sulfuric acid.

The results presented in *Chapters 2* and *3* represent the first complete description of the stratigraphic and diagenetic evolution of the Woodbend Group in north-central Alberta. The outlined stratigraphic and diagenetic evolution are primarily of local importance and will serve as a base line for future stratigraphic and diagenetic studies in the area. It is suggested that future studies should focus on the recognition of potential sequence boundaries and better define systems tracts in the Woodbend Group succession. A sequence stratigraphic analysis will also allow a better characterization of the effects of exposure events on the early diagenesis and porosity evolution.

The recognition of two petrographically, geochemically and genetically different replacement dolomite types, as presented in *Chapter 4*, suggests that replacement dolomites of the Western Canada Sedimentary Basin likely represent the final product of a complex process that involved several crystallization steps and at least two dolomitization mechanisms. However, one of the main problem of pervasive dolomitization, the source of dolomitizing fluids, still remains to be solved, at least for the dolomites in the Leduc Formation. The implementation and development of additional and new analytical techniques will likely be needed to solve this outstanding question. Techniques that appear to be promising include strontium isotopes and the isotopic analysis of fluids contained in dolomite fluid inclusions.

The second contribution presented in *Chapter 4* is the recognition of platform margins and reefs as upward leaking fluid conduits. These leaking fluid conduits likely represent an underestimated control on the distribution of diagenetic phases (e.g. dolomite, calcite cements) and, consequently, on reservoir quality. The recognition of the locations of leakage should be of particular interest to hydrocarbon producers because scenarios similar to the one described in *Chapter 4* are present in many other areas and stratigraphic levels of the Western Canada Sedimentary Basin.

The results of *Chapter 5* have further immediate and long term implications for hydrocarbon production. Firstly, karstification had a significant impact on the reservoir quality of the Grosmont Formation. Close to the sub-Cretaceous unconformity porosity and permeability are often greatly enhanced, although localized porosity reduction has occurred. In addition, the seal quality of the Grosmont shale breaks, which were used to contain steam during previous heavy-oil recovery tests, is negatively affected by breaching in karsted areas. However, since much of the karst occurs along two well-defined levels, prediction of the breaching sites is possible by identifying intersection points between these karst levels and potential seal beds. This method of recognition of breached seals is of potential economic importance because it helps to avoid steam loss during reservoir stimulation, therefore, aiding in choosing better sites for future enhanced recovery projects. Finally, it appears likely that karstification along the sub-Cretaceous unconformity is a more widespread phenomenon than recognized today. For example, paleokarst may have developed beneath other Lower Cretaceous paleotopographic highs, e.g. the Wainwright or Red Earth Ridges. If this is the case, controls on karstification similar to the controls recognized in the Grosmont High area were likely in effect. Hence, the Grosmont reservoir may be an analog for other unconformity-related reservoirs and/or may be the first recognized member of an underexplored class of potential hydrocarbon reservoirs in the Western Canada Sedimentary Basin..